DEVELOPMENT OF SPECTRAL SIMPLIFICATION METHODS IN SOLID AND SOLUTION-STATE NUCLEAR MAGNETIC RESONANCE

A THESIS SUBMITTED
TO
UNIVERSITY OF HYDERABAD

FOR THE DEGREE OF
DOCTOR OF PHILOSOPHY
(IN CHEMISTRY)

BY

KAKITA VEERA MOHANA RAO

Reg. No: 09CHPH21

SUPERVISOR

Dr. BHARATAM JAGADEESH

Centre for Nuclear Magnetic Resonance and Structural Chemistry
CSIR-INDIAN INSTITUTE OF CHEMICAL TECHNOLOGY
(An Associate Institution of UNIVERSITY OF HYDERABAD)
HYDERABAD-500 007, INDIA
APRIL, 2014

Dedicate

To

My Family

DECLARATION

I hereby declare that the research work incorporated in this thesis is the result of investigations carried out by me at CSIR-Indian Institute of Chemical Technology (an associate institute of University of Hyderabad), Hyderabad, under the supervision of **Dr. Bharatam Jagadeesh**, Sr. Principal Scientist. This work is original and has not been submitted in part or full, for any degree or diploma to this or any other university.

Date: **(Kakita Veera Mohana Rao)**

CSIR-INDIAN INSTITUTE OF CHEMICAL TECHNOLOGY
HYDERABAD-500 007, INDIA
Telephone: +91- 040 - 2719 3976; Fax: +91-040 -2719 3108
E-mail: **bj@iict.res.in**

Dr. Bharatam Jagadeesh
Senior Principal Scientist
Centre for Nuclear Magnetic Resonance and Structural Chemistry,
CSIR-Indian Institute of Chemical Technology,
Uppal Road, Hyderabad - 500 007, AP, India.

CERTIFICATE

The research work embodied in this thesis entitled “***DEVELOPMENT OF SPECTRAL SIMPLIFICATION METHODS IN SOLID AND SOLUTION-STATE NUCLEAR MAGNETIC RESONANCE***” has been carried out under my supervision and is bonafied work of Mr. Kakita Veera Mohana Rao. This work is original and has not been submitted for any other degree or diploma of this or any other University.

Date:

(Dr. Bharatam Jagadeesh)
Research Supervisor

ACKNOWLEGMENTS

First of all, I would like to acknowledge ***Dr. Bharatam Jagadeesh***, supervisor of this doctoral thesis. He has tolerated my irrelevant doubts and explained me everything patiently, which helped me to improve my knowledge in NMR. His constructive analysis has improved my reading and writing skills. His liberty in the lab made me to work freely and efficiently. He has been quite helpful to me in both academic and personal fronts. He always had time for interesting and stimulating discussions, not only about NMR. Thanks for sharing his experience as a researcher and teacher. I am extremely thankful to him.

It gives me great pleasure to thank ***Dr. A. C. Kunwar***, for support in all aspects and I thank ***Dr. A. V. S. Sarma***, for helpful discussions.

My thanks go to ***Dr. S. Chandrasekhar***, ***Dr. B. Venkateswara Rao***, ***Dr. Taimur Ather*** and ***Dr. Ch. Raji Reddy*** for their constant help, suggestions and support in collaborative projects.

My special thanks to ***Dr. Mandar. V. Deshmukh***, CCMB, for his invaluable guidance in understanding theoretical NMR spectroscopy.

I would like to thank to ***Professor. V. S. S. Sastry*** and ***Dr. M. Trivikram,*** School of Physics, University of Hyderabad, for their valuable discussions in understanding the MATLAB software.

My thanks to all my colleagues ***Dr. T. Prabhakara Rao***, ***Dr. L. Satyanarayana***, ***Dr. T. V. Raju***, ***Dr. K. V. S. Rama Krishna***, ***Dr. S. Kiran Kumar***, ***Dr. M. Udaya Kiran***, ***Mrs. Sharada***, ***Dr. P. Naresh***, ***Dr. G. D. Sharma***, ***Dr. S. Jeelani Basha***, ***Dr. R. Ravi***, ***Dr. G. Srinivasulu***, ***Dr. C. Madhavi***, ***Mr. Phani***, ***Mr. D. Satya Narayana***, ***Ms. J. K. Lakshmi***, ***Mr. T. Varma***, ***Mr. Deepak***, ***Mr. Purushottam***, ***Mr. Gurava***, ***Mrs. K. Sirisha***, ***Mr. M. Kanaka Raju***, ***Mrs. N. Lakshmi Sunitha***, ***Mr. P. Ramulu***, ***Mr. P. L. Prasad***, ***Mr. U. Venkateshwarlu***, ***Mr. Narender***, ***Mrs. Rekha***, ***Mr. B. S. Rajesh***, ***Mr. Santhosh***, ***Mr. Rajendra Prasad***, ***Mr. Santha Kumar***, ***Mr. Naveen***, ***Mr. Murthy***, ***Mr. Anil***, ***Mr. Narasimha***, ***Mr. Avinash*** and ***Ms. Sirisha*** for their unreserved help and suggestions in addition to creating a beautiful working atmosphere in the lab.

This thesis would not have seen the light of the day without the moral support, love and affection from my parents ***Sri. Krishna Rao***, ***Smt. Punyawathi***, brother (***Mr. Ravi Kumar***), sister-in-law (***Mrs. Sravani***), uncles, aunts, cousin-brothers, cousin-sisters, brother-in-laws, sister-in-laws and children for their cheerful moments.

Kavitha – my wife who was once a junior in lab, I cannot thank her enough for being my support system, for constantly reminding me to take care of myself, for providing the light moments in those stressful periods, for taking her time out to listen to everything that I have to say, for making me laugh when I was nearing a breakdown… and for the countless other reasons with unconditional love which make her a huge part of this piece of work. Therefore, I would also thank ***Sri. Ramaiah Rachineni***, ***Smt. Subba Ratnamma*** and her family members for letting me takes her hand in marriage.

My special thanks to ***Mrs. Rama Lakshmi*** (wife of Dr. Bharatam Jagadeesh) for her valuable suggestions in personal fronts.

In Andhra University I got very good Professors like, ***Prof. A. Satyanarayana Rao***, ***Prof. Ramana***, ***Dr. P. Shyamala***, whose lectures I enjoyed most. I am grateful for the valuable friendship of my M.Sc. class mates ***Dr. Santosh***, ***Mr. Balu***, ***Mr. Bhaskar***, ***Mr. Lakshminarayana***, ***Mr. Laxman***, ***Mr. M. Ravi Kumar (Boss)***, ***Mr. Masthan Vali***, ***Mr. Anil***, ***Mr. Siva Ranjan, Mr. K. Raju, Mr. Vasu***, ***Mrs. Shyamala Gowri***.

I would like to thank to ***CBMR***, ***NMRS*** and ***ENC*** for their financial support to attend the ENC-2012 conference held at Miami USA.

I would like to thank my ***NMR*** and ***childhood*** friends.

My special thanks to ***Dr. C. V. Manjunath***, ***Dr. Devendra*** and ***Mr. B. Manjunath*** (Bruker, India), ***Dr. Eriks Kupce*** (Bruker, UK), ***Dr. Wolfgang Bermel*** (Bruker, Germany) and ***Dr. Vadim Zorrin*** (Agilent, UK) for their valuable analytical as well as technical services.

My special thanks to all ***contemporary colleagues*** and ***lab-mates*** for their kind coordination and maintenance of a righteous work-place environment.

I take this opportunity to express deep sense of gratitude to ***all my teachers*** who unfolded my senses to understand the knowledge in all the sciences they taught.

Last but not least, I thank ***Dr. M. Lakshmi Kantam*** (Director, CSIR-IICT), ***Dr. J. S. Yadav*** (Ex. Director, CSIR-IICT) and ***Dr. A. Kamal*** (Ex. Director, CSIR-IICT), for providing sophisticated laboratory facilities, the ***Council of Scientific and Industrial Research*** (CSIR-India) for financial support and ***University of Hyderabad*** for permitting me to submit my research work in the form of a thesis.

My sincere apologies to all those, who have helped me but are not acknowledged.

(***Veera Mohana Rao Kakita***)

TABLE OF CONTENTS

Page No

SYNOPSIS i-xv

CHAPTER-I: ***Introduction*** 1-26

I.1. Solid-state NMR Spectroscopy 1

I.2. Spin Interactions in Solids 2

I.2.1. Spin Hamiltonian 2

I.2.2. The Chemical Shift and Chemical Shift Anisotropy 3

I.2.3. Dipole – Dipole interaction 4

I.2.4. Secular Dipolar Coupling 5

I.2.5. *J*-Coupling 6

I.3. Experimental Techniques 6

I.3.1. Magic Angle Spinning (MAS) 6

I.3.2. Cross Polarization 8

I.3.3. Decoupling 9

I.3.4. Re-coupling 10

I.4. The Spin-Echo modulation of spin-spin couplings 11

I.4.1. Spin-Echo modulations in isotropic solutions 11

I.4.2. Spin-echo modulations in solids 13

I.5. Hadamard NMR 15

I.5.1. Hadamard encoded selective spin-echoes in solid-state NMR 16

I.6. Real-time pure-shift solution-state NMR spectroscopy 17

I.7. References 20

Spectral simplifications in solid-state NMR

CHAPTER-II: ***Hadamard-encoded selective spin-echoes for simultaneous measurement of multiple scalar couplings (small and large) in organic solids*** 27-54

II.1. Introduction 27

II.1.1. Basic frequency domain Hadamard NMR spectroscopy 27

II.1.2. Hadamard encoded/decoded refocusing 28

II.2. Materials 28

II.3. Experiments 29

II. 4. Results and Discussions 31

II.4.1. ***Hadamard encoded spin-echo experiments in double frequency selective refocusing mode*** 31

II.4.1.1. Hadamard encoded double frequency selective spin-echoes for different spin-pairs in $^{13}C_5$-FSAA 33

II.4.1.2. Hadamard encoded double frequency selective spin-echoes for different spin pairs in $^{13}C_6$ L-Histidine.HCl 36

II.4.1.3. Hadamard encoded double frequency selective spin-echoes for different spin pairs in $^{13}C_8$-SA 38

II.4.2. ***Hadamard encoded multiple frequency selective spin-echoes for simultaneous measurement of scalar couplings*** 40

II.4.2.1. Hadamard encoded multiple frequency selective spin-echoes for different spin combinations in $^{13}C_5$-FSAA 42

II.4.2.2. Hadamard encoded multiple frequency selective spin-echoes for different spin combinations in $^{13}C_6$ L-Histidine.HCl 46

II.4.2.3. Hadamard encoded multiple frequency selective spin-echoes for different spin combinations in $^{13}C_8$-SA 50

II.5. Conclusions 52

II.6. References 53

CHAPTER-III: ***Two-dimensional Hadamard encoded NMR spectroscopy of uniformly spin-labelled organic solids: Simultaneous and accurate measurement of multiple scalar couplings*** 55-68

III.1. Introduction 55

III.2. Materials 55

III.3. Theoretical background 56

III.3.1. Conventional spin-echo pulse sequence 56

III.3.2. Z-filtered spin-echo pulse sequence (ZFSE) 57

III.3.3. Z-Filtered *J*-Scaled Spin-Echo pulse sequence (ZFJSSE) 58

III.3.4. Hadamard Encoded Z-Filtered *J*-Scaled Selective Spin-Echo pulse sequence (HEZFJSSSE) 59

III.4. Experiments 59

III.5. Results and Discussion 60

III.5.1. *J*-scaled spin-echo of $^{13}C_2$-Glycine 60

III.5.2. *J*-scaled spin-echo of $^{13}C_5$-FSAA 61

III.5.3. *J*-scaled spin-echo of $^{13}C_8$-SA 64

III.6. Conclusion 67

III.7. References 67

CHAPTER-IV: ***Two-dimensional J-scaled Hadamard encoded DQFCOSY NMR: Accurate measurement of JCC in uniformly labelled and natural abundant clustered spin systems*** 69-88

IV.1. Introduction 69

IV.2. Theoretical background 69

IV.2.1. UC2QF-COSY or DQF-COSY (Uniform-sign cross-peak double-quantum-filtered correlation spectroscopy) 69

IV.2.2. JSDQCOSY (*J*-Scaled Double Quantum Filtered Correlation SpectroscopY) and JSHEDQFCOSY (*J*-Scaled Hadamard Encoded Double Quantum Filtered Correlation SpectroscopY) 70

IV.3. Experiments 71

Section-A

IV.A.1. Materials 72

IV.A.2. Results and Discussions 72

IV.A.2.1. *J*-scaled DQF-COSY: $^{13}C_2$-Glycine 72

IV.A.2.2. Hadamard encoded *J*-scaled DQF-COSY: mixture of $^{13}C_3$-Alanine and natural abundant amino acids 73

IV.A.2.3. Hadamard encoded *J*-scaled DQF-COSY: $^{13}C_5$-FSAA 75

IV.A.2.4. Hadamard encoded *J*-scaled DQF-COSY: $^{13}C_8$-SA 76

IV.A.2.5. Hadamard encoded *J*-scaled DQF-COSY: $^{13}C_6$ L-Histidine.2HCl 78

Section-B

IV.B.1. Results and Discussions 80

IV.B.1.1. Application of JSHEDQFCOSY: measurement of J_{CC} for polymorph-I & polymorph-II in $^{13}C_6$ L-Lysine.2HCl 81

Section-C

IV.C.1. Results and Discussions 85

IV.C.1.1. Application of JSHEDQFCOSY: natural abundant 1-Adamantanol 86

IV. 4. Conclusion 86

1V.5. References 87

CHAPTER-V: *Inter-nuclear distance measurements by using Hadamard encoded spin-echoes and Rotational Resonance echoes in uniformly labelled molecules* 89-110

V.1. Introduction 89

Section-A

V.A.1. Materials 90

V.A.2. Experiments 91

V.A.3. Results and Discussions 92

V.A.3.1. Proton Driven Spin Diffusion (PDSD) experiments of $^{13}C_5$-FSAA 92

V.A.3.2. Hadamard encoded double selective spin-echo experiments at Magic Angle Sample spinning 93

V.A.3.3. Hadamard encoded double-selective spin-echo experiments at fixed Off Magic Angle Sample spinning 93

V.A.3.4. Comparison of Hadamard encoded double frequency selective spin-echo modulations for different spin pairs in $^{13}C_5$-FSAA at MAS and OMAS 95

V.A.3.5. Comparison of Hadamard encoded double frequency selective spin-echo modulations for different spin pairs in $^{13}C_8$-SA at MAS and OMAS 98

Section-B

V.B.1. Experiments 102

V.B.2. Theory 103

V.B.3. Results and Discussion 104

V.2. Conclusion 108

V.3. References 108

CHAPTER-VI: Selective Refocused Uniform Cross-peak Signed Double Quantum Filtered Correlation Spectroscopy (SRUC2QF COSY): Enhanced efficiency and sensitivity at lower spinning speeds 111-128

VI.1.Introduction 111

VI.2.Methodology 112

VI.3.Experiments 114

VI.4. Results and Discussions 115

VI.4.1. ***Simulation of cross-peak intensities in isolated and multi-spin systems*** 115

VI.4.1.1 Simulation of cross-peak intensities for different spin-pairs in $^{13}C_6$ L-Histidine.HCl 116

VI.4.1.2. Simulation of cross-peak intensities for different spin-pairs in $^{13}C_5$-FSAA molecule 118

VI.5. Experimental results 120

VI.5.1. UC2QF-COSY NMR experiments of $^{13}C_6$ L-Histidine.HCl 120

VI.5.2. Double band-selective SRUC2QF-COSY NMR experiments of $^{13}C_6$ L-Histidine.HCl 121

VI.5.3. Hadamard encoded multiple band (or frequency) -selective refocused UC2QF-COSY of $^{13}C_6$ L-Histidine.HCl 123

VI.5.4. UC2QF-COSY experiments of $^{13}C_5$ FSAA 124

VI.5.5. Double band-selective SRUC2QF-COSY experiments of $^{13}C_5$ FSAA 124

VI.5.6. Hadamard encoded multiple band selective refocused UC2QF-COSYof $^{13}C_5$ FSAA 126

VI.6. Conclusion 127

VI.7. References 127

Spectral simplifications in solution-state NMR

CHAPTER-VII: ***Real-time Homonuclear broadband and band-selective decoupled pure-shift ROESY*** 129-148

VII.1. Introduction 129

VII.2. Concepts 130

VII.2.1. Selective excitation/refocusing during the spatial encoded gradients 130

VII.2.2. Homonuclear broadband decoupling during the slice selective gradients 131

VII.3. Results and Discussion 132

VII.3.1. HOBB-ROESY and HOBS-ROESY schemes 133

VII.3.2. Pure-shift HOBB and HOBS-decoupled ^{1}H spectra 136

VII.3.3. 2D Pure-shift HOBB-ROESY and HOBS-ROESY 140

VII.5. Conclusions 144

VII.6. References 145

CHAPTER-VIII: ***Real-time pure-shift adiabatic z-filtered spin-echo and constant time in-phase COSY*** 149-159

VIII.1. Introduction 149

Section-A

VIII.A.1. Results and discussion 151

- VIII.A.1.1. Real-time adiabatic z-filtered HOBB spin-echo pulse scheme (HOBBZFSE) 151
- VIII.A.1.2. 2D Pure-shift HOBBZF-SE of Erythromycin-A 152

VIII.A.2. Conclusions 153

Section-B

VIII.B.1. Results and discussion 154

- VIII.B.1.1. Real-time adiabatic z-filtered HOBB COSY pulse scheme (HOBBIPZFCOSY) 154
- VIII.B.1.2. Comparison of DQF-COSY, IP-COSY, IPZF-COSY and HOBBIPZFCOSY spectra of Erythromycin-A 155
- VIII.B.1.3. 2D Pure-shift HOBBIPZF-COSY of mixture of Quinine and Quinidine 157

VIII.B.2. Conclusions 157

VIII.2. References 158

Synopsis

Organization of the thesis

The present thesis reports the development of new Nuclear Magnetic Resonance (NMR) experimental methodologies to accomplish spectral simplifications and enhanced resolution, in solid-state and solution-state. The thesis is divided into 8 chapters under two sections. The chapter-1 under the first section provides a general introduction to NMR method, Hadamard NMR spectroscopy and their importance in structural chemistry. The experimental schemes developed and the results obtained are discussed in subsequent chapters.

The development of solid-state NMR experimental techniques are aimed at obtaining desired spectral information, both scalar and dipolar couplings (inter nuclear distances), by simplifying complex NMR spectra. The new 1D and 2D experimental strategies are based on selective manipulations of spin-spin interactions by means of Hadamard frequency encoding/decoding matrices. The developed techniques have been successfully applied to multi-spin systems, viz., ^{13}C-lablled organic solids for the first time. The results are presented in the first section (chapter 2 to 6).

The idea of spectral simplification has been extended to solution-state as well, for unambiguous structural elucidations and the results are presented second section. Unlike solid-state samples, the dipolar interactions are averaged to zero in solution-state, thereby yield NMR spectra representing only the features of chemical-shift and scalar (J) couplings. However, often the solution-state ^{1}H NMR spectra suffer from intense overlaps due to spread of J-multiplets. The second section of the thesis reports the techniques developed for overcoming these problems. Herein the enhanced spectral resolution has been accomplished by employing new real-time pure-shift pulse schemes that involve broadband and band-selecting homo-decoupling. The results are presented in the second section (chapter 7 and 8).

I. Hadamard solid-state NMR: Novel method developments for estimation of precise structural information

A) *Hadamard selective spin-echoes for simultaneous measurement of multiple scalar couplings (small and large) from organic solids*

Scalar spin-spin couplings (*J)* serve as powerful structural probes in NMR spectroscopy to map through-bond atomic connectivities and to gain insight into the local conformation as well as configuration of molecules. The measurements of *J*-couplings in solution-state is often straightforward from one-dimensional (1D) spectra due to the intrinsic resolution, whereas they are obscured in solid-state samples due to the dipolar and CSA-dominated line broadening, even under magic angle spinning (MAS). The DQ-based and *J*-resolved 2D-correlation techniques developed earlier for solid-state have allowed to observe *J*-multiplets in *J*-resolved dimension, for favourable cases. Alternatively, in the past few years the strategic developments in solid-state MAS NMR techniques have aptly exploited the *J*-modulation effect on spin-echoes, for precise measurement of *J*-couplings of hetero nuclear or *isolated* homo-nuclear spin-pairs.**[1]** Spectral editing methods based on only dual frequency-selective pulses are also reported for recording of pair-wise spin-spin interactions. However, these selective spin-echo schemes demand the experiments to be repeated for each spin pair of the molecules. The present sub-section discusses a versatile and conceptually different spin-echo strategy (*refocusing* scheme) based on *Hadamard encoding/decoding*,**[2]** for simultaneous recording of multiple homo-nuclear spin-spin couplings in uniformly spin-labelled solids, in *a single* experiment. In this method, the selected set of NMR resonances are encoded according to the rows of a $n\mathrm{X}n$ Hadamard matrix and the corresponding polychromatic pulse comprised of these selective frequencies is used for refocusing. Subsequently, the refocused signal (complex FID), is decoded according to the columns of the same Hadamard matrix. The resultant spectrum consists only the pre-selected resonances, and the variation of the echo-amplitude with respect to the echo-time [echo-modulation: $S(\tau) \propto \cos\{\pi J(\tau_{ev}-\tau_{sh})\}\exp(-\tau_{ev}/T_2^{J})$] yields the magnitude of the *J*-coupling with its coupled partner(s). This way, the hidden spectral information can be easily extracted, in multi-spin solids. The present approach is exemplified for measuring $^{1}J_{CC}$ and $^{3}J_{CC}$ in uniformly ^{13}C-labelled molecules. Unlike the conventional methods reported earlier, the present strategy (1) neither requires the experiments to be repeated for each spin pair in the molecule (2) nor demands a set of specially synthesized $^{13}C_2$ labelled molecules.

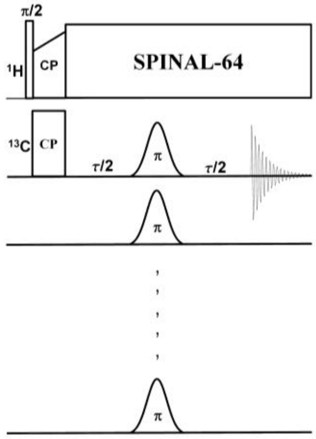

Figure 1: *Schematic representation of Hadamard encoded selective spin-echo pulse sequence in multiple frequency selective refocusing modes.*

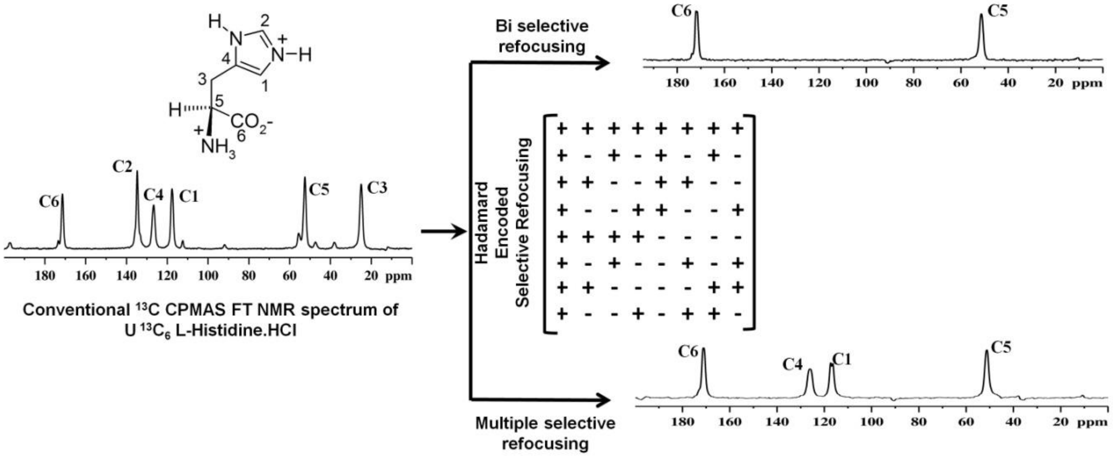

$$\begin{bmatrix} + & + & + & + & + & + & + & + \\ + & - & + & - & + & - & + & - \\ + & + & - & - & + & + & - & - \\ + & - & - & + & + & - & - & + \\ + & + & + & + & - & - & - & - \\ + & - & + & - & - & + & - & + \\ + & + & - & - & - & - & + & + \\ + & - & - & + & - & + & + & - \end{bmatrix}$$

Figure 2: *Schematic representation of Hadamard selective spin-echoes recorded for both the double and multiple selective refocusing modes on the different spin pairs/combinations of uniformly labelled L-Histidine.HCl.*

The Hadamard selective spin-echo methodology has been demonstrated for different spin combinations of same molecule and both directly bonded ($^1J_{CC}$) and long range scalar couplings ($^nJ_{CC}$) are measured in a single experiment. The experimental strategy employed herein for recording spin-spin interactions, is rather new, and it almost impossible to accomplish the same with the conventional methods. The estimated scalar couplings from all the individual echo-modulations have shown nice agreement with the values directly recorded in solution-state, which highlights the reliability of this unique approach.

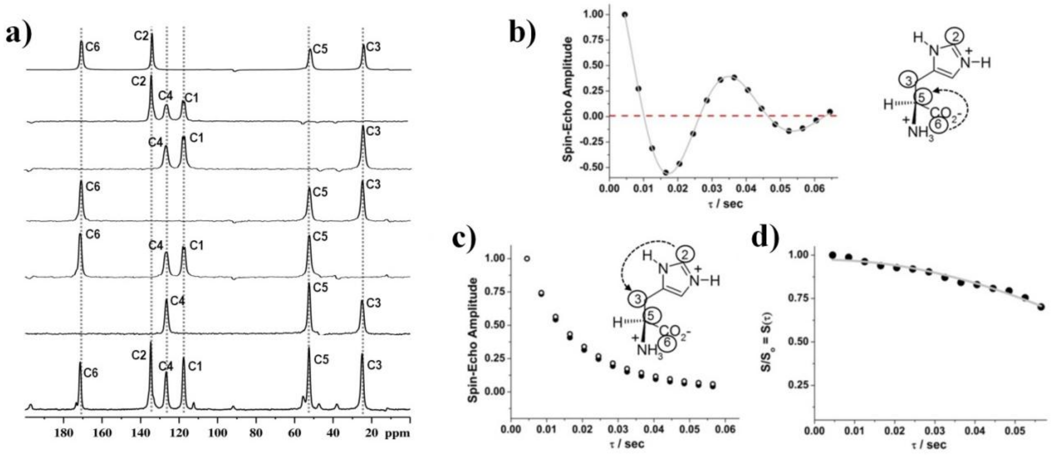

Figure 3: *Spectral simplification and the respective spin-echo modulations: (a) Comparison of* ^{13}*C-CPMAS full spectrum of* $^{13}C_6$ *L-Histidine.HCl with the Hadamard encoded multiple selective spin-echo NMR spectra of different spin-combinations. Spin-echo modulations for different spin pairs of C2-C3-C5-C6 of* $^{13}C_6$ *L-Histidine.HCl in multi frequency refocusing mode: b) C5-C6 spin-echo modulation is monitored from the C6, c) spin-echo modulation of C2, when modulating with C3 (S, closed circles) and only selection of C2 (So, open circles). d) S/So modulation of C2 results in pure frequency component equals to the* $^3J_{C2\text{-}C3}$ *of ~4.0 Hz. The corresponding J-values are determined by fitting the modulations to the equation* $S(\tau)\ \alpha \cos[\pi J_{CC}(\tau-\tau_{sh})] \exp(-\tau/T_J^2)$.

B) *Two-dimensional Hadamard encoded selective spin-echoes for uniformly spin-labelled organic solids: Simultaneous and accurate measurement of multiple scalar couplings*

As described above, Hadamard assisted multiple selective spin-echo NMR methodologies have been demonstrated in a pseudo two-dimensional method for simultaneous measurement of scalar couplings in uniformly labelled molecules. While the method is conceptually appealing and easy to implement, the disadvantages with the pseudo selective spin-echo NMR method noted are (i) for spin-pair the echo integrations to be monitored as a function of evolution times, therefore time-consuming and (ii) the performance of the selective spin-echo experiments are limited when the chemical-shift resolution is poor. However, the pseudo two-dimensional method offers basis for subsequent development of this strategy for more complex cases.

The present approach aims to triumph over these disadvantages by adopting a novel approach that relies on Hadamard assisted two-dimensional spin-echo and *J*-scaling, [3] for enhanced resolution. The *J*-scaling methodologies are well known in 1D and 2D solution-state NMR for artificially enhancing the resolution and are useful for the measurement of long-range scalar couplings. However, they are sparsely explored in solid-state NMR.

The Z-filtered *J*-scaled spin-echo (ZFJSSE) is a new pulse sequence designed from Z-filtered spin-echo, wherein the $\tau/2$ intervals are replaced by 'n' times of t1/2. In case of normal Z-filtered spin-echo pulse sequence, the *J*-coupling evolves according to $\cos(\pi J_{CC}\tau)$ term. In two-dimensional ZFJSSE, replacing the $\tau/2$ intervals with n (t1/2), the coupling evolution takes place according to $\cos(\pi J_{CC} nt1)$. While performing Fourier transformation along indirect dimension, 'n' would become a weighting factor on J_{CC}, as t1 only depends on spectral width along indirect dimension. By choosing appropriate 'n', the multiplets can be clearly resolved by 'n' times along indirect dimension of a two-dimensional spin-echo. The above described *J*-scaled pulse sequence is applicable for simple systems, where spin-spin interactions commute. On the other hand, for spin-spin interactions those do not commute with each other, as in the case of complex multi-clustered spin systems with multiplicity patterns along the indirect dimensions, a different strategy is required to overcome the difficulty. In this regard, the Hadamard encoded z-filtered *J*-scaled spin-echo (HEZFJSSE) pulse sequence is developed by replacing the conventional refocusing pulses of ZFJSSE with the Hadamard encoded pulses.

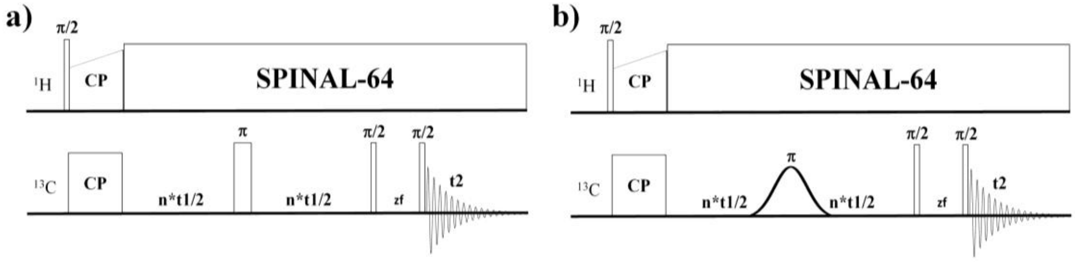

Figure 4: *Schematics representations of a) 2D Z-filtered J-scaled spin-echo and b) Hadamard encoded Z-filtered J-scaled spin-echo pulse sequences.*

Initially the pulse sequence ZFJSSE that allows the measurement of homo-nuclear spin-spin couplings is employed for a simple system, $^{13}C_2$-Glycine. The data is collected at two different *J*-scaling factors 1 (no-scaling) and 4 (Fig). The measured splitting values along the indirect dimension (F1) at scaling factors 1 and 4 are 52.2Hz and 210.5 Hz, respectively, and the average of the normalized (52.2/1 and 210.5/4 Hz) values, i.e., 52.24 Hz is found to be in good agreement with the value measured in solution-state $^{1}J_{CC}$ (53.6 Hz).

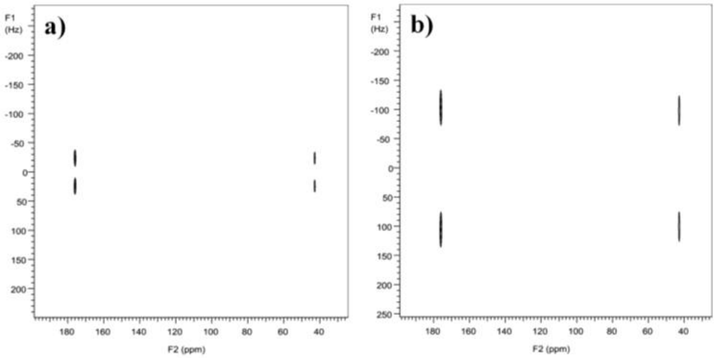

Figure 5: *Comparison of 2D Z-filtered spin-echo NMR spectra of $^{13}C_2$-Glycine without and with scaling factor of **4** is shown in a) and b), respectively.*

However, the same 2D ZFJSSE experiment could not completely resolve the multiplicity pattern along indirect dimensions of clustered spin-systems, even for 4 times *J*-scaling factor. On the other hand, by incorporating the Hadamard encoding, the pulse sequence HEZFJSSSE has greatly simplified the spectrum, resulting in a well-resolved spin-spin coupling patterns. All the J_{CC} values of are measured with the aid of Hadamard selection in Z-filtered *J*-scaled spin-echo, are found to be in good agreement with those measured in solution-state as well as in 2D pseudo Hadamard multiple selective refocusing schemes.

C) *Two dimensional J-scaled Hadamard encoded DQFCOSY SSNMR: Accurate measurement of J_{CC} from uniformly labelled and natural abundant clustered spin systems*

Herein, a new *J*-Scaled Hadamard Encoded Double Quantum Filtered COrrelation SpectroscopY (JSHEDQFCOSY) methodology is presented for accurate measurement of selective spin-spin couplings from the uniformly labelled molecules. Later the same methodology has been extended to natural abundant spin-systems.

The *J*-scaled double quantum filtered COSY (JSDQFCOSY) pulse sequence comprised of *J*-scaling has been designed by replacing the initial two τ/2 constant times of DQFCOSY with ‘n’ times of t1. Herein, data points along the indirect dimension are collected with ‘2n+1’ times of dwell time, but the data is processed with only dwell time (1/SW1, SW1 along the indirect dimension is constant), which, results in a weighting factor of 2n+1 for J_{CC}. The concept of *J*-scaling for solids has already been demonstrated in the previous section.

The *J*-scaled Hadamard encoded double quantum filtered COSY (JSHEDQCOSY) pulse sequence has been designed by replacing the hard π pulse of JSDQCOSY pulse sequence with the soft Hadamard encoded phase-ramped simultaneous refocusing pulses, for selected spins of known assignments. Hence, the commutation property can be recreated between interested spins during this selective refocusing, and scaling factors are applied as desired.

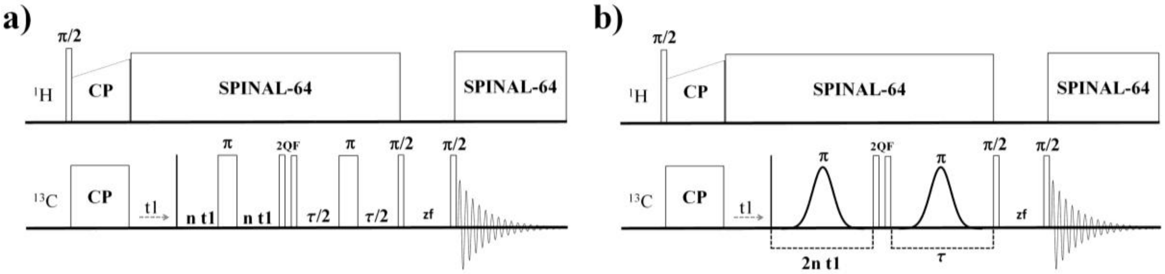

Figure 6: *Schematics of a) 2D J-scaled double quantum filtered COSY and b) Hadamard encoded 2D J-scaled double quantum filtered COSY pulse sequences.*

JSDQFCOSY and JSHEDQFCOSY experiments have been demonstrated on uniformly labelled unnatural peptido mimetic foldamer building blocks $^{13}C_5$-FSAA and $^{13}C_8$-SA molecules. Moreover, experiments are repeated for resolving the crowded resonances in $^{13}C_6$ L-Histidine.HCl, two polymorphs of $^{13}C_6$ L-Lysine.2HCl and natural abundant 1-Adamantanol, which allowed the measurement of J_{CC} for different spin-pairs.

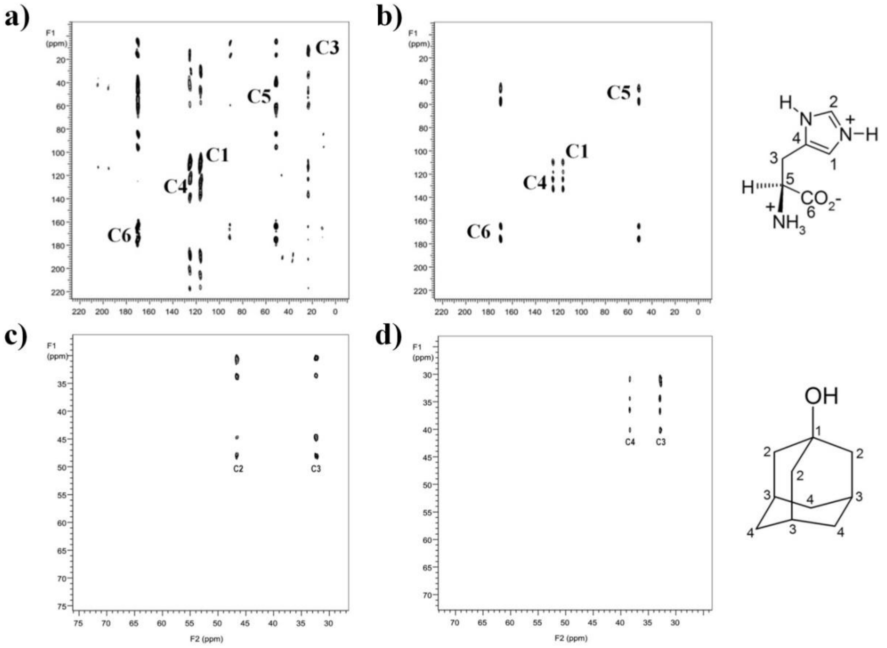

Figure 7: Comparison of J-Scaled DQFCOSY spectra of $^{13}C_6$ *L-Histidine.HCl and 1-Adamantanol recorded at 21 and 11 times scaling factors, respectively: The JSDQFCOSY (a) and the corresponding JSHEDQFCOSY spectra of C1-C4-C5-C6 selective spin combination of L-Histidine. The* ^{13}C-^{13}C *JSHEDQFCOSY spectra of different spin pairs of natural abundant 1-Adamantanol at 11 times scaling factor, (c) and (d) are the experiments recorded for C2-C3 and C3-C4 spin pairs, respectively.*

D) *Inter-nuclear Distance Measurements by using Hadamard Assisted Spin-Echoes and Rotational Resonance Echoes in Uniformly Labelled Molecules*

Selective spin-echo experiments have been developed for the measurement of Homonuclear *dipolar* couplings as well, at fixed Off-Magic Angle Sample Spinning (OMAS).**[4]** The earlier reported selective spin-echo experiments at off-magic angle are limited only for the measurement of distances up to 2.2Å; which is perhaps due to the dominant monotonic exponential decay of spin-echo modulation. Subsequently, a new spinning angle encoded (up to 4Å) and a DQ based (up to 6Å) pulse sequences have been developed for long range homonuclear distance measurements. Nevertheless, while the spinning angle encoding technique requires a special type of probe design, the DQ-based experiment demands a long time of spectral acquisition. Whereas, the present part the thesis deals with the demonstration of the measurement of long range distances by using OMAS approach for uniformly labelled molecules. While the experiments conducted at MAS yields J_{CC} values, the same experiment at OMAS resulted in $J_{CC}+D_{CC}$, from which the corresponding D_{CC} and hence inter-nuclear distance are estimated. Furthermore, the utility of long range J_{CC} facilitates to measure the long range distances at OMAS SSNMR. Conversely, OMAS destroys the ^{13}C resolution of all the resonances of spectrum even at a small angle away from the MAS.

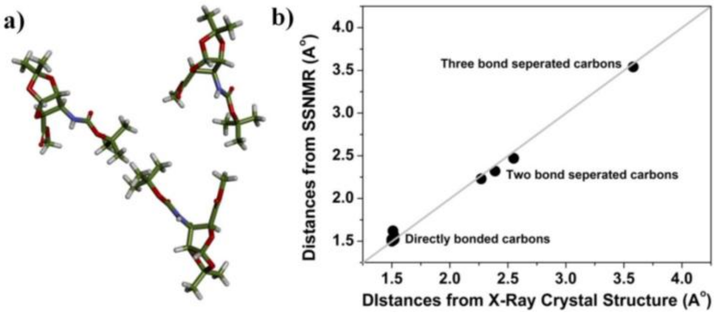

Figure 8: *(a) X-Ray Crystal structure of FSAA and (b) correlation between distances derived from X-Ray and OMAS SSNMR.*

On the other hand, a new Hadamard encoded double frequency selective zero quantum echo pulse sequence is demonstrated for selective Homonuclear dipolar coupling measurements from clustered solid spin systems. Herein, dipolar couplings between interested spin pairs are reintroduced by setting the spinning speed equal to the chemical shift difference of two spins (Rotational Resonance).**[5]** In this situation, spectral resolution may not be a problem; since, the data has been collected at MAS only. The distances thus obtained in both cases have shown excellent correlation with those determined from X-ray crystal structures.

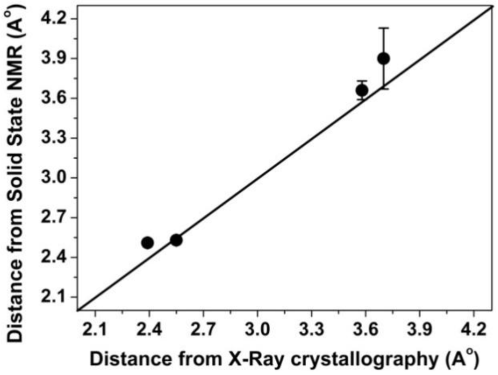

Figure 9: *Correlation between distances derived from the X-Ray crystallography and Hadamard encoded ZQ RR echo SSNMR for different spin pairs of* $^{13}C_5$*-FSAA molecule.*

E) ***Selective Refocused Uniform Cross-peak Signed Double Quantum Filtered Correlation Spectroscopy (SRUC2QF COSY) of solids: Minimize the experimental times and improves sensitivity even at the lower spinning speeds***

The chemical shift assignments of solid-state materials are established either by through bonds or through space correlation experiments. In fact, the cross-peak intensities in a spin-diffusion experiment are sensitive to the local dynamics of a considered fragment in a molecule or molecule itself. Different versions of through-bond correlated experiments have been developed over the years, such as, TOCSY, refocused-INADEQUATE, UC2QF COSY, CTUC COSY and SAR COSY, to identify the chemical shift correlations. Among these methods, TOCSY in solid-state NMR is analogous to its routine solution-state, however, the required isotropic Hamiltonian mixing at the magic angle spinning is achieved by rotor synchronized pulses, and these are suitably designed through the utilization of symmetry principles. Conversely, the isotropic mixing method heats up the RF coils and sensitive to the pulse imperfections. Alternatively, refocused-INADEQUATE with enhanced transverse relaxation times during the refocusing periods is known, which , however, has lower sensitivity compared to the two dimensional double quantum COSY (DQFCOSY). Further enhanced relaxation times by converting the faster decay double quantum signal into a single quantum signal is an advantage with the DQFCOSY.

The present SRUC2QF COSY scheme deals with the reconstruction of spinning side-band free spectra of organic solids with improved sensitivity. The sensitivity has been enhanced by recording the SRUC2QF COSY spectra either for the directly bonded spin-pairs or a long-range spin pair of uniformly labelled molecule in a small number of indirect dwell increments, which minimizes the significant experimental times. The SRUC2QF COSY spectra are acquired in a wide range of sample spinning frequencies and processed by using covariance method.**[6]** Even at very low spinning speeds, the spinning side-band free spectra are obtained. Furthermore, the experimental strategy has been extended for the multiple selective refocusing modes, as well.

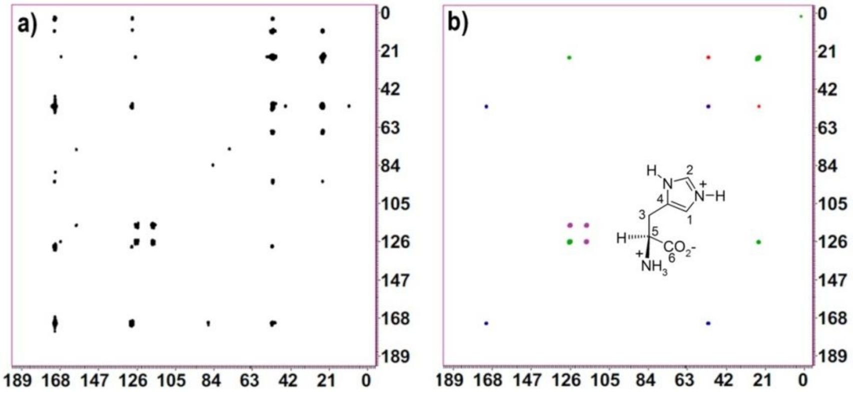

Figure 10: *Comparison of conventional 2D FT UC2QF COSY (a) and 2D Covariance processed followed by co-added SRUC2QF COSY (b) NMR spectra of $^{13}C_6$ L-Histidine.HCl. The individual spin-pairs are selected and processed by covariance method. The spectra are recorded at 4.2 kHz.*

II. Method developments for resolution enhancement and precise estimation of structural parameters in solution-state

A) ***Development of Real-time Homonuclear broadband and band-selective decoupled pure-shift ROESY in solution-state***

Unambiguous spectral assignments in ^{1}H solution-state NMR are central, for accurate structural elucidation of complex molecules, which is often hampered by signal overlap, primarily due to scalar coupling multiplets, even at typical high magnetic fields. The recent advances in homodecoupling methods have shown powerful means of achieving high resolution pure-shift ^{1}H NMR spectra by effectively collapsing the multiplet structures.[7] The present part of the thesis describes two new pure-shift ROESY pulse schemes homodecoupled broadband (HOBB)-ROESY and band-selective (HOBS)-ROESY. The advanced real-time decoupling during acquisition saves experimental time significantly. Furthermore, the adopted ROESY blocks suppress the undesired interferences of TOCSY cross-peaks and other off-sets as well. The HOBB-ROESY is particularly useful for molecules that exhibit extensive scalar coupling network spread over the entire ^{1}H chemical shift range, such as natural/synthetic organic molecules. On the other hand, the HOBS-ROESY is useful for molecules that exhibit well-separated chemical shift regions such as peptides (NH, Hα and side-chain protons). These two techniques are complimentary to each other and their combined application, wherever necessary, would provide a comprehensive approach for structural characterizations. The power of these pure-shift ROESY sequences is demonstrated for two different organic molecules, wherein complex conventional ROE cross-peaks are greatly simplified with high resolution and sensitivity. The enhanced resolution allows deriving possibly more number of ROEs with better accuracy, thereby facilitating superior means of structural characterization of medium-size molecules.

ROESY is specifically required for the analysis of mid-size molecules (ωτc~1, NOEs are close to zero or weak at typical high magnetic fields) such as Erythromycin-A and ASAS, which however is also impeded by the TOCSY and offset interferences. The very purpose of the pure-shift ROESY experiments and the accurate estimations of the cross-peak integrals reinstate the elimination of these artefacts as well.

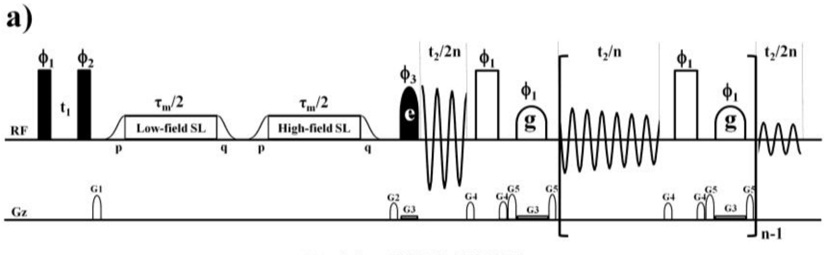
a)
ϕ1
ϕ2
t1
τm/2
Low-field SL
τm/2
High-field SL
ϕ3
e
t2/2n
ϕ1
ϕ1
g
t2/n
ϕ1
ϕ1
g
t2/2n
RF
p
q
p
q
G1
G2
G3
G4
G4
G5
G3
G5
G4
G4
G5
G3
G5
Gz
n-1

Real time HOBB-ROESY

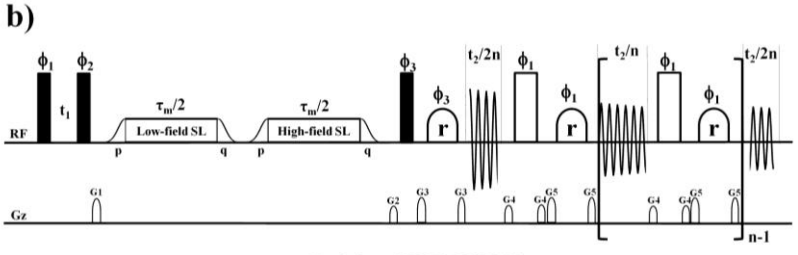
b)
ϕ1
ϕ2
t1
τm/2
Low-field SL
τm/2
High-field SL
ϕ3
ϕ3
r
t2/2n
ϕ1
ϕ1
r
t2/n
ϕ1
ϕ1
r
t2/2n
RF
p
q
p
q
G1
G2
G3
G3
G4
G4
G5
G5
G4
G4
G5
G5
Gz
n-1

Real time HOBS-ROESY

Figure 11: *Real-time pure-shift ROESY pulse sequences with Homonuclear Broadband decoupling (HOBB) and Homonuclear Band selective (HOBS) decoupling in the direct acquisition dimension.*

The Figure 12 shows the expanded regions of regular ROESY (~1 hour/ 8 scans/ 256 increments), HOBB-ROESY (~15 hours/ 96 scans/ 256 increments) and HOBS-

ROESY (~1 hour for each region / 8 scans/ 256 increments) for the Erythromycin-A. For example, the H11→H4 ROE that is important to determine the conformation of the macrolide lactone ring is severely overlapped with H14 in the regular ROESY (Figure 12.a). On the other hand, a dramatic increase in the resolution has been obtained with HOBB-ROESY (Figure 12.b) and HOBS-ROESY (Figure 12.c).

All the spectra are free from the undesired TOCSY and offset interferences. It can be seen that, expect for the signals those are scalarly coupled within the selected band, the HOBS-ROESY spectra are identical to those of HOBB-ROESY, in terms of enhanced-resolution.

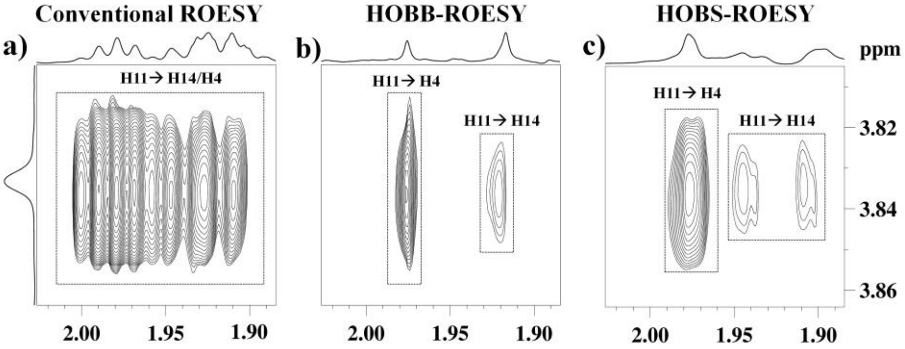

***Figure 12**: Comparison of expanded regions of conventional, HOBB and HOBS-ROESY spectra of Erythromycin-A (50mM in $CDCl_3$ solvent), recorded at 700 MHz magnetic field with 300 ms of mixing time.*

B) *Development of real-time pure-shift adiabatic z-filtered NMR methodologies: Application to spin-echo and constant time in-phase COSY*

The ${}^{n}J_{HH}$ scalar coupling information and ${}^{1}H$ chemical shift assignments of spin resonances is necessary for structural elucidation of small/medium organic molecules or large bio-macromolecules, which can be recorded from the conventional two-dimensional spin-echo (${}^{n}J_{HH}$) and COSY (${}^{n}J_{HH}$ and chemical shift assignments) NMR methods, respectively. However, as discussed in the earlier section, the spectral resolution of highly abundant ${}^{1}H$ spin-echo and COSY NMR spectra are limited to ~10 ppm and further hampered by ${}^{1}H$-${}^{1}H$ scalar couplings. To overcome these problems, the real-time HOBB pure-shift methods are added to the adiabatic z-filtered spin-echo (HOBBZF-SE) and fully in-phase adiabatic z-filtered COSY (HOBBIPZF-COSY) pulse sequences, which facilitate the unambiguous scalar coupling and chemical shift assignments, respectively. These pulse schemes are successfully demonstrated for Erythromycin-A

Figure 13 depicts the pulse sequence used for two-dimensional real-time homodecoupled broadband adiabatic z-filtered spin-echo, which operate in an instantaneous mode (no additional pseudo dimensions are required) and provide simplified spectra with enhanced resolution along with the coupling information.

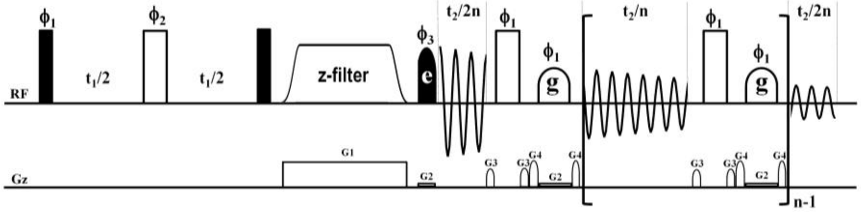

Real time HOBB z-filtered spin-echo

Figure 13: *Schematic diagram of real-time adiabatic z-filtered spin-echo pulse sequence with Homonuclear Broadband decoupling (HOBB) decoupling during the direct acquisition dimension.*

The Figure 14 shows the expanded regions of conventional adiabatic z-filtered spin-echo and HOBBZFSE for the Erythromycin-A. The crowded methyl region recorded by using conventional spin-echo, (Figure. 14a) is dramatically simplified by HOBBZFSE. Clear singlets along the direct dimension and nice doublets are observed along the indirect dimension are observed (Figure. 14b).

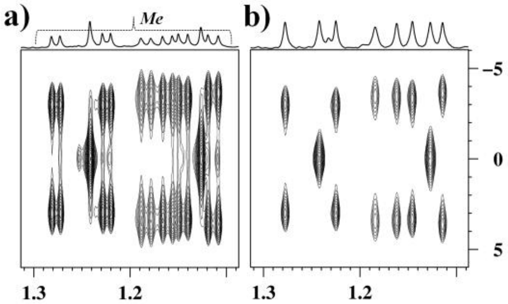

Figure 14: *Comparison of expanded region of 2D conventional spin-echo (a) and 2D HOBBZF-SE (b) spectra of Erythromycin-A (50mM in CDCl$_3$ solvent).*

Conclusions

The present thesis focuses on the development of novel NMR spectral simplification methodologies in both solid and solution-state, for enhanced resolution.

Accordingly, the Hadamard encoded selective refocusing schemes for solid-state NMR spectroscopy are reported and are employed for the first time for fully ^{13}C-labelled solids. These techniques are helpful for observing the desirable structural information viz., scalar couplings and dipolar couplings and spin-spin correlations. In the solution-state NMR real-time pure-shift SE, COSY, ROESY and NOESY methodologies are developed, which employ broadband (HOBB) and band-selective (HOBS) decoupling during the *acquisition* dimensions. Particularly, the pulse schemes are superior to the recently reported pseudo acquisition type homodecoupling schemes. The developed solid and solution-state NMR methods are highly useful for unambiguous assignments of chemical shifts and estimations of inter-nuclear distances, and may attract significant applications in structural elucidations of small/medium natural and synthetic organic molecules.

References

[1] L. Duma, W. C. Lai, M. Carravetta, L. Emsley, S. P. Brown and M. H. Levitt, Principles of Spin-Echo Modulation by J-Couplings in Magic-Angle-Spinning Solid-State NMR, Chem. Phys. Chem, 5 (2004) 815–833.

[2] E. Kupce, T. Nishida and R. Freeman, Hadamard NMR spectroscopy, Progress in Nuclear Magnetic Resonance Spectroscopy, 42 (2003) 95–122.

[3] R. V. Hosur, K. V. R. Chary and M. R. Kumar, J-scaling in two-dimensional homonuclear correlated spectroscopy for enhancement of cross peak intensities, Chem. Phys. Lett, 116 (1985) 105–108.

[4] G. Pileio, Y. Guo, T. N. Pham, J. M. Griffin, M. H. Levitt and S. P. Brown, Residual Dipolar Couplings by Off-Magic-Angle Spinning in Solid-State Nuclear Magnetic Resonance Spectroscopy, J. Am. Chem. Soc, 129 (2007) 10972–10973.

[5] D. P. Raleigh, M. H. Levitt and R.G. Griffin, Rotational Resonance in Solid-state NMR, Chem. Phys. Lett, 146 (1988) 71–76.

[6] R. Bruschweiler, Theory of covariance NMR spectroscopy, J. Chem. Phys. 121 (2004) 409–414.

[7] N. H. Meyer and K. Zangger, Simplifying proton NMR spectra by instant Homonuclear broadband decoupling, Angew. Chem. Int. Ed, 52 (2013) 7143–7146.

Chapter-I

Introduction

I.1. Solid-state NMR Spectroscopy

High resolution solution-state NMR spectroscopy has become an important part of structural chemistry and biology. The recent advances in solid-state NMR (SSNMR) theory, applications and hardware have enhanced the power of NMR spectroscopy to address the complex structural problems. For example, SSNMR has been proved as an indispensible tool for structural elucidation of membrane proteins,[1, 2] insoluble biomolecules such as amyliod fibrils [3, 4] and inorganic materials.[5] Nevertheless, there is immense need and scope for accomplishing spectral simplifications and resolution in solid-state NMR, and the present thesis focuses on these aspects.

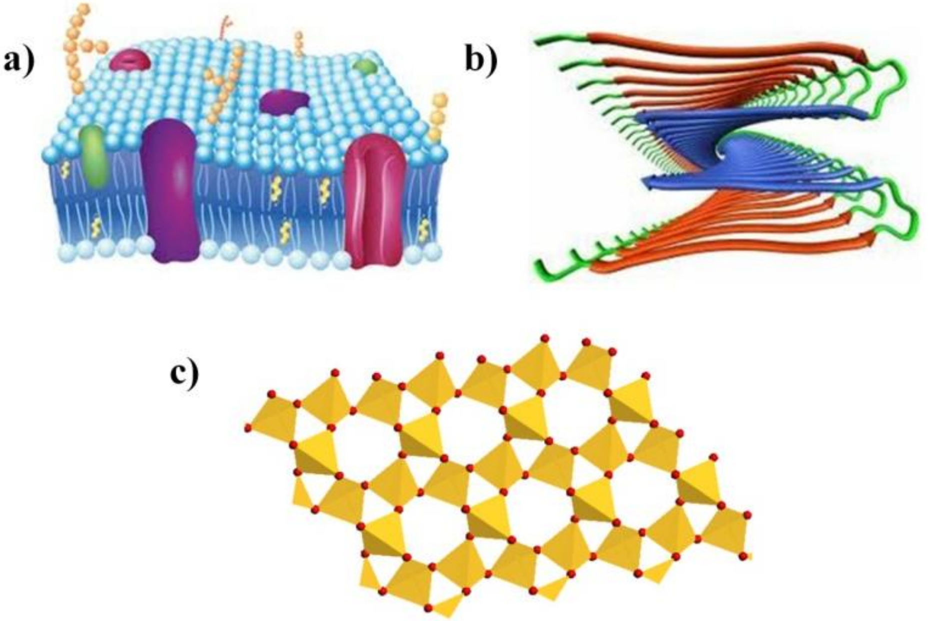

Figure I.1: *Cartoon representation of molecular structures: (a) membrane proteins, (b) amyloid fibrils and (c) aluminium silicates.*

In solution-state, the rapid tumbling of molecules average all the valuable angular and anisotropic structural parameters viz., dipolar couplings, chemical shift anisotropy (CSA) and quadrupolar interactions to zero. However, such isotropic motion is absent in solid-state, thus anisotropic structural parameters are sustained. This rich information is somewhat easily accessible in crystalline solids, whereas in the powdered samples, it is severely obscured due to many crystalline orientations that result in complex spectra with very broad lines.

In addition to CSA, a major contribution to the line broadening in solids originates from homonuclear (^{1}H-^{1}H) and hetereonuclear (^{1}H-X; X=^{13}C, ^{19}F etc.) dipolar couplings. The line broadening can be reduced to a large extent by using the radio frequency (multi-pulse sequence, high power decoupling) as well as mechanically (Magic Angle Spinning) driven spatial averaging methods. The combination of these two methods facilitates to minimize both anisotropic and dipolar interactions to a large extent, which results in a high resolution spectrum in solids.

I.2. Spin Interactions in Solids

I.2.1. *Spin Hamiltonian*

The Hamiltonian (H) of a nuclear spin system in a large static magnetic field is represented as a sum of two terms called, H_{ext} (external spin Hamiltonian) and H_{int} (internal spin Hamiltonian). **[6-9]**

$$H = H_{\text{ext}} + H_{\text{int}}$$

The Hamiltonian, H_{ext} is the sum of the contributions from external static magnetic field (H_Z) and radio frequency (H_{RF}); whereas H_{int} is the sum of the dominant and regular intrinsic contributions such as chemical shift (H_{CS}), dipole-dipole (H_{DD}) and the quadrupolar Hamiltonian (H_Q) interactions.

$$H_{\text{ext}} = H_Z+H_{RF}$$

$$H_{\text{int}} = H_{CS}+H_{DD}+H_Q$$

The rapid tumbling in solution-state leads to H_{DD} and H_Q average to zero,

the total spin Hamiltonian can be written as

$$\mathrm{H} = H_Z+H_{RF}+H_{CS}+H_{DD}+H_Q$$

I.2.2. *The Chemical Shift and Chemical Shift Anisotropy*

The chemical shift information is principally an intra-molecular interaction, which represents the indirect magnetic interaction of external magnetic field on the nuclear spins through the contribution of electrons.

The applied external magnetic field (B_o) induces a current of electrons, which produces the small magnetic fields is known as induced field, $B_j^{induced}$, and it is a vectorial quantity. The size of the induced magnetic field is much smaller than B_o and can either be added or be subtracted from B_o.

The resultant local magnetic field can be written as

$$B_j^{loc} = B_o + B_j^{induced}$$

$B_j^{induced}$ linearly depends on the B_o and can be written as

$$B_j^{induced} = \delta_j . B_o$$

where δ_j is the shielding tensor.

When a static magnetic field is applied along z-axis, the above equation can be rewritten in matrix form as shown below

$$\begin{pmatrix} B_{j,x}^{induced} \\ B_{j,y}^{induced} \\ B_{j,y}^{induced} \end{pmatrix} = \begin{pmatrix} \delta_{xz}^{j} \\ \delta_{yz}^{j} \\ \delta_{zz}^{j} \end{pmatrix} . \begin{pmatrix} 0 \\ 0 \\ Bo \end{pmatrix}$$

$$\begin{pmatrix} B_{j,x}^{induced} \\ B_{j,y}^{induced} \\ B_{j,y}^{induced} \end{pmatrix} = \begin{pmatrix} \delta_{xz}^{j}\ Bo \\ \delta_{yz}^{j}\ Bo \\ \delta_{zz}^{j}\ Bo \end{pmatrix}$$

where $\delta_{xz}^{j} B_o$ is the induced field along the x-axis.

The chemical shift Hamiltonian is a scalar product of magnetic momentum as well as the induced magnetic field and it can be written as below.

$$H_j^{CS} = - \mu_j . B_j^{induced}$$

$$\text{where } \mu_j = \gamma \hbar I$$

Therefore

$$H^{CS}_{j} = -\gamma_j \delta^{j}_{xz}(\Theta) B^0 I_{jx} - \gamma_j \delta^{j}_{yz}(\Theta) B^0 I_{jy} - \gamma_j \delta^{j}_{zz}(\Theta) B^0 I_{jz}$$

where, Θ is the angle of atomic frame with respect to the external magnetic field.

Thus the chemical shift Hamiltonian and their values depend up on Θ.

For example, the resonance frequency of carbonyl is about 160 ppm with respect to isotropic TMS, which depends upon the orientation of the C=O bond vector. Within the crystal lattice, all the atoms orient in the same direction and the chemical shift of atomic nuclei under observation can be changed by rotating the sample. However, in powdered or poly-crystalline samples, the orientations of local units are highly discrete with respect to the magnetic field, and result in a broad peak consists of an envelope of peaks, which are originated from all the orientations of the local crystallites.

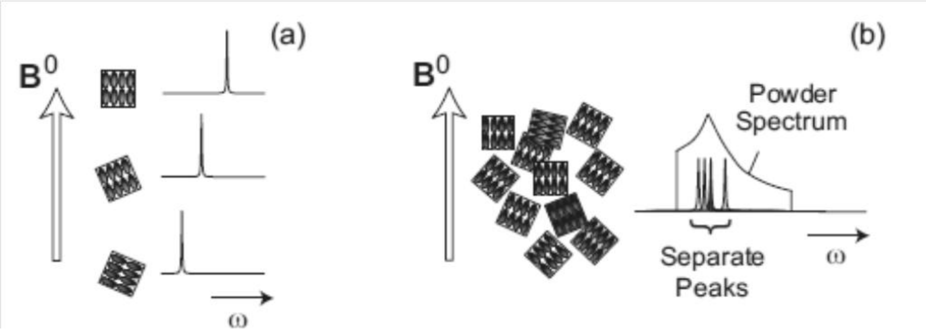

Figure I.2: *Effect of orientation of solid with respect to the magnetic field on chemical shift values in (a) a single crystal and (b) a powder molecules.*

I.2.3. *Dipole – Dipole interaction*

The nuclear spins act as tiny magnets and the through space interaction between the magnetic nuclear spins is known as dipolar or dipole-dipole (DD) coupling, which is mutual and non-zero for solids. The DD coupling can be either inter or intramolecular. The full form of the direct DD interaction between spins I_j and I_k can be written as

$$H^{DD}_{jk} = b_{jk}(3(I_j \cdot e_{jk})(I_k \cdot e_{jk}) - I_j \cdot I_k)$$

where e_{jk} is the unit vector and b_{jk} is the dipolar coupling constant

$$b_{jk} = \frac{\mu_0\, \gamma_j\, \gamma_{jk}\, h}{8\pi\, r_{ij}^3},$$

γ_j, γ_k are the gyro-magnetic ratios of the two nuclei and **r** is the inter-nuclear distance.

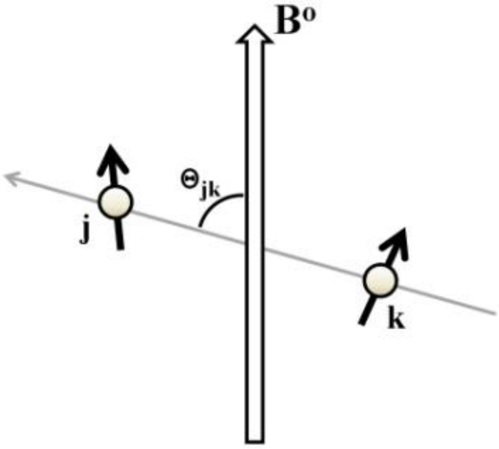

Figure I.3: *Cartoon representation of dipole-dipole coupling between spins j and k: the unit vector e_{jk} connects the spins j and k, and the Θ_{jk} is the angle made by the e_{jk} with the direction of the external magnetic field Bo.*

I.2.4. ***Secular Dipolar Coupling***

In a sample, the total dipolar interaction experienced by a nuclear spin can be written as

$$H^{DD,\,full} = \sum_k \sum_j^{k-1} H_{jk}^{DD,full}$$

The secular part of the dipolar coupling (dipole-dipole interaction is time independent in the presence of large external magnetic fields) depends upon the orientation of the spins I_j and I_k in a sample.

In the case of homonuclear interaction

$$H^{DD}_{jk}\,(\Theta_{jk}) = d_{jk}\,(3\, I_{jz}\, I_{kz} - I_j \cdot I_k)$$

where, d_{jk} is the secular DD coupling and is given as

$$d_{jk} = (½)\, b_{jk}\,(3\cos^2\Theta_{jk} - 1)$$

In the case of heteronuclear interaction

$$H^{DD}_{jk}\,(\Theta_{jk}) = d_{jk}\, 2\, I_{jz}\, I_{kz}$$

I.2.5. *J-Coupling*

J-coupling or scalar coupling is an indirect interaction between the nuclear spin pair through the bonding electrons. If two spins I_j and I_k are separated by a small number of bonds, the full form of *J*-coupling interaction may be written as

$$H_{jk}^{J,\,full} = 2\pi\, I_j .\, J_{jk} .\, I_k$$

where J_{jk} is the scalar coupling between spins I_j, I_k, which can be expressed as a 3 × 3 matrix (tensor of rank 2).

In the case of isotropic liquids, all the off-diagonal elements of the matrix average to zero and diagonal elements alone remain. The average of three diagonal elements is equal to the isotropic *J*-coupling ($J_{jk}^{isotopic}$).

The *J*-couplings and chemical shifts are field independent. The *J*-coupling values are almost positive for the homonuclear spin-1/2 pairs separated by one-bond and negative for spins with opposite gyromagnetic ratios. However, for long range scalar couplings, the sign could either be positive or be negative depending upon the molecular geometry.

For example, ^{13}C spin pairs, the observed scalar coupling values vary with the bond order and hybridization involved. The maximum observed scalar coupling value is ~150 Hz for triple bonded carbons and ~30Hz for single bonded carbons. Furthermore, in solid systems the anisotropic part of scalar coupling can be ignored due to its small magnitude, when compared to the direct dipolar couplings. While the measurements of *J*-couplings in solution-state are somewhat straight forward, the task is non-trivial in the case of solid-state, even at a high magic angle spinning (MAS).

I.3. Experimental Techniques

I.3.1. *Magic Angle Spinning (MAS)*

Experimentally, the line-broadening in solid-state NMR can be minimized by spinning the sample at an orientation of 54.74^o (magic angle) with respect to B_o.**[10, 11]** At sufficiently high spinning speeds above the DD/CSA line width, all the dipolar and CSA interactions average to zero and only the isotropic chemical shift values are retained. The recent developments of solid-state NMR probe designs allow to spin the samples up to ~110 kHz.[12]

As the spinning frequency increases, additional peaks appear at the frequencies equal to the integer multiples of spinning frequency. These additional peaks are known as spinning side-bands (Figure I.4). These side-band patterns can be suppressed by either spinning the sample at higher speeds or RF driven TOSS methods (if the experiment/sample demands lower spinning speeds). [13]

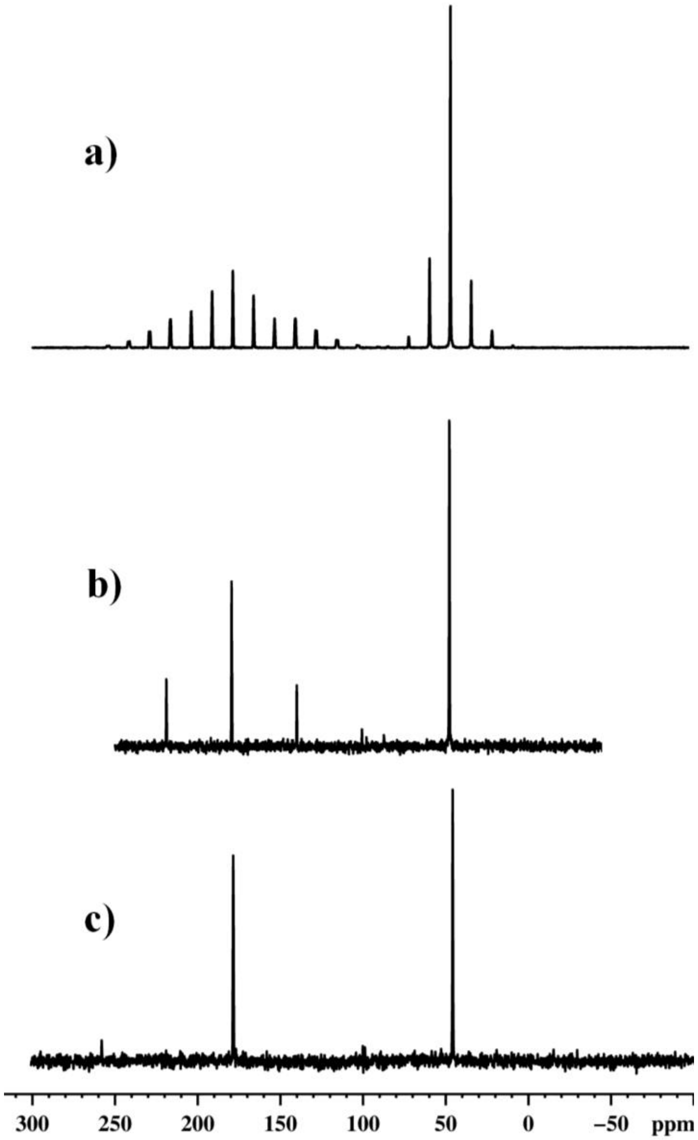

Figure I.4: *Comparison of ^{13}C CP-MAS spectra of natural abundant Glycine recorded at a spinning frequency, ωr/2π of (a) 1.5 kHz, (b) 5.0 kHz and (c) 10.0 kHz on a 9.4 T spectrometer using a proton decoupling power of 82 kHz.*

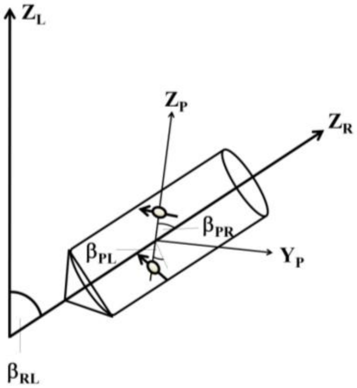

Figure I.5: *Pictorial representation of macroscopic sample rotating at an angle with respect to the applied static magnetic field B^o, where β_{PR}, β_{RL} and β_{PL} are the angles between the internuclear vector and the rotor axis, the rotor axis and the magnetic field and the magnetic field and the inter nuclear vector, respectively.*

In general, the anisotropic structural parameter CSA and dipolar couplings are directly proportional to ($3\cos^2 \beta_{PL}-1$). The rapid isotropic molecular tumbling in solution averages this numeric to zero, resulting in sharp lines. It implies that such isotropic averaging in solid samples can also be achieved at $\langle 3\cos^2 \beta_{PL}-1\rangle = 0$, which can be expressed as

$$\langle 3\cos^2 \beta_{PL}-1\rangle = (1/2)\,(3\cos^2 \beta_{RL}-1)\,(3\cos^2 \beta_{PR}-1)$$

The angular parameter β_{PR} takes all the orientations in powdered samples. Hence $\langle 3\cos^2 \beta_{PR}-1\rangle$ does not averages to zero. However, by rotating the sample at 54.74^o (magic angle) with respect to the external magnetic field, β_{RL} can be averaged out to zero.

Therefore, at MAS

$$(3\cos^2 \beta_{RL}-1) = 0$$

$$\Rightarrow \langle 3\cos^2 \beta_{PL}-1\rangle = 0$$

which result in the spectra with well resolved lines.

I.3.2. *Cross Polarization*

The sensitivity of rare spins (S) with low gyromagnetic ratios (^{13}C and ^{15}N) can be enhanced by transferring the magnetization from the abundant spins (I) with a high gyromagnetic ratio (^{1}H), this phenomenon is called as cross-polarization, which involves dipolar contact between heteronuclear spins.[14, 15] This is analogous to the transferring of heat from a high temperature object to a low temperature object. In homonuclear spins, the magnetization exchanges by mutual energy-conserving spin flip-flops. Whereas, in heteronuclear spins the flip-flopping does not allow the energy conservation and it must be established by the application of appropriate radio frequency pulses.

The Hartmann-Hahn matching condition [16] allows establishing the dipolar contact between rare spin (S) and abundant spins (I). According to the Hartmann-Hahn condition, when two independent RF pulses specifically to the resonance frequencies I and S spins are simultaneously applied and their nutation frequencies are equal, then the dipolar contact is established between the I and S spins in the rotating frame.

$$\text{Accordingly,} \qquad \gamma_I \; B^I_{rf} = \gamma_S \, B^S_{rf}$$

where, γ_I and γ_S are the gyromagnetic ratios of I and S spins, the corresponding spin-lock fields are B^I_{rf} and B^S_{rf}.

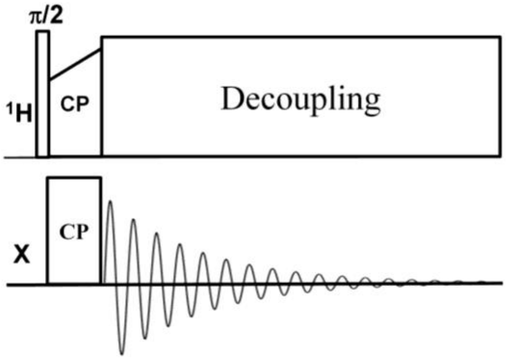

Figure I.6: *Schematic of representation of basic cross polarization pulse sequence with heteronuclear decoupling.*

I.3.3. *Decoupling*

Enhancement of spectral resolution can be achieved by minimizing the ^{1}H-mediated dipolar interactions by applying decoupling pulses on ^{1}H-channel, while observing X-nuclei (say ^{13}C). The continuous application of ^{1}H RF pulses to remove the effect of dipolar couplings in the solid-state is known as CW-decoupling, [17-19] The calculated dipolar coupling between ^{13}C and ^{1}H is equal to ~30 kHz per 1Å separation. As the ^{1}H mediated heteronuclear dipolar couplings are strong, higher decoupling powers as well as super cycled decoupling schemes (TPPM, [20] SPINAL, [21] and XIX [22]) are required to suppress the dipolar effects in solid-state NMR. In the present thesis, only SPINAL-64 (Small Phase Incremental Alternation with 64 steps) scheme has been employed, [23] which is a more efficient technique than the other TPPM and XIX schemes. The SPINAL-64 is super cycled with an 8 composite pulses, which are 8-step phase incremented.

SPINAL-64 = QQ’Q’Q Q’QQQ’

Where,

Q = 165(10^o) 165(-10^o) 165(15^o) 165(-15^o) 165(20^o) 165(-20^o) 165(15^o) 165(-15^o) and

Q’ = 165(-10^o) 165(10^o) 165(-15^o) 165(15^o) 165(-20^o) 165(20^o) 165(-15^o) 165(15^o)

The number 165 and the value in the parenthesis represent the pulse width and the phase shift of decoupling pulses, respectively.

I.3.4. *Re-coupling*

The rapid spinning of the solid sample at MAS averages all the important structural restraints viz., dipolar couplings and Chemical Shift Anisotropy (CSA). These parameters, which carry rich structural information can be reintroduced in a controlled manner by using different pulse schemes embedded with π pulses placed at half of the rotor periods (REDOR, [24] RFDR [25]).

Alternatively, the residual dipolar couplings can also be reintroduced by spinning the sample at Off-Magic Angle (OMAS),[26, 27] which is a small offset with respect to the magic angle (54.74^o). This OMAS approach makes the averaging of the DD interactions incomplete, thereby allows residual dipolar interactions to sustain. However, as DD interaction (line-broadening) is very sensitive to the OMAS angle, the spectral resolution is of main concern for the homonuclear OMAS experiments. The recent development of double quantum filters [28] and spinning angle encoding methods [29] permit to measure the distances up to ~4A^o.

Rotational Resonance (RR)[30] is an another type of re-coupling scheme. In this method the dipolar couplings are reintroduced by matching the spinning speed equal to the chemical shift difference of the interested spin pairs. However, these methods demand significant chemical shift differences between spins of interest.

I.4. The spin-echo modulation and spin-spin couplings

A versatile tool for estimating scalar and dipolar couplings

Scalar spin-spin couplings (*J)* serve as powerful structural probes in NMR spectroscopy to map through-bond atomic connectivities and to gain insight into the local conformation as well as configuration of molecules. The measurement of *J*-couplings in solution-state is often straightforward from one-dimensional (1D) spectra due to the intrinsic resolution. Thus, the readily measurable scalar couplings serve as important/central structural inputs for deriving H-C-C-H/H-C-N-H torsion angles from the Karplus equation[31] as well as useful for the chemical shift assignments from bond correlation experiments. Whereas, they are obscured in solid-state samples due to the dominant dipolar and CSA line broadening, even under magic angle spinning (MAS). The effect of *J*-coupling in spin-echoes are well known and extensively studied in solution-state multi-dimensional NMR spectroscopy and explained by using the product operator formalism (POP). [32] The *J*-resolved 2D-correlation techniques developed earlier allow measuring the *J*-multiplets in *J*-resolved dimension.[33]

I.4.1. *Spin-echo modulations in isotropic solutions*

The *J*-coupling interaction between the two spin ½ IS system is associated with sixteen product operator terms, which are comprised of four operators for each individual spin I and S.

	½ E	$\mathbf{S_x}$	$\mathbf{S_y}$	$\mathbf{S_z}$
½ E	**E**	$\mathbf{S_x}$	$\mathbf{S_y}$	$\mathbf{S_z}$
$\mathbf{I_x}$	$\mathbf{I_x}$	$\mathbf{2\,I_xS_x}$	$\mathbf{2\,I_xS_y}$	$\mathbf{2\,I_xS_z}$
$\mathbf{I_y}$	$\mathbf{I_y}$	$\mathbf{2\,I_yS_x}$	$\mathbf{2\,I_yS_y}$	$\mathbf{2\,I_yS_z}$
$\mathbf{I_z}$	$\mathbf{I_z}$	$\mathbf{2\,I_zS_x}$	$\mathbf{2\,I_zS_y}$	$\mathbf{2\,I_zS_z}$

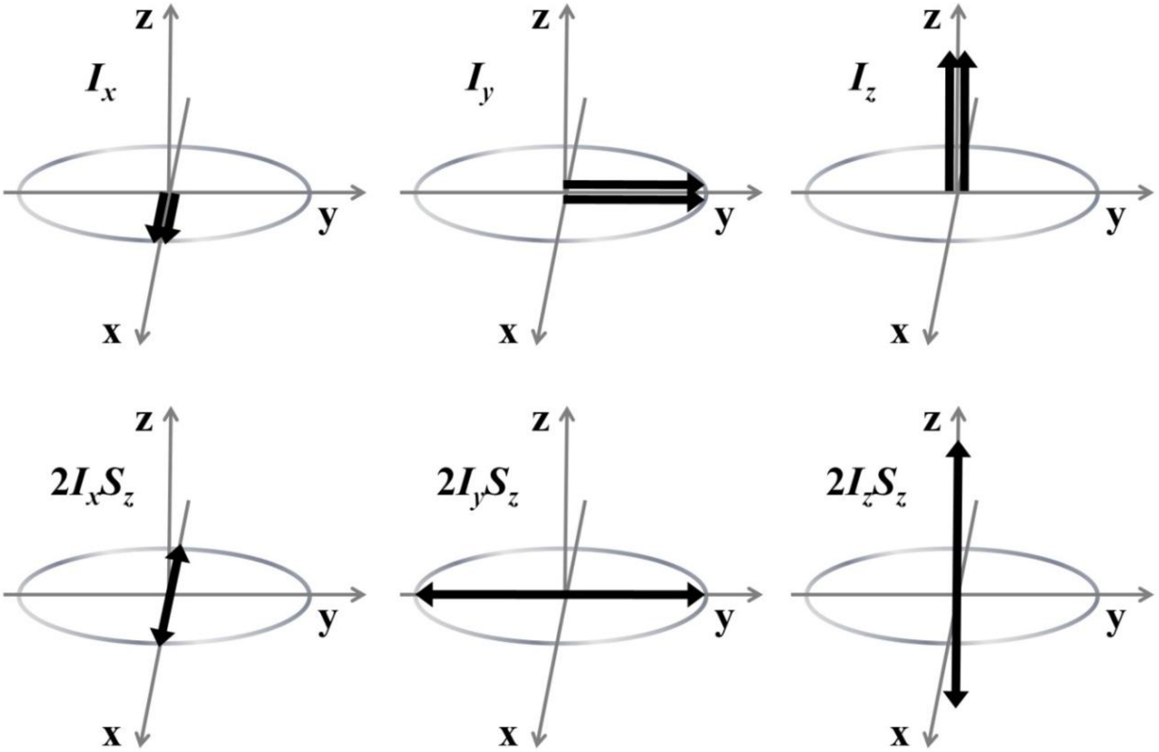
z
I_x
y
x
z
I_y
y
x
z
I_z
y
x
z
$2I_xS_z$
y
x
z
$2I_yS_z$
y
x
z
$2I_zS_z$
y
x

The resultant product operator in spin-echo pulse sequence can be written as

$$\mathrm{I_z + S_z} \xrightarrow{90\mathrm{x}-\tau/2-180\mathrm{y}-\tau/2} -(\mathrm{I_y+S_y}) \cos(\pi J_{IS}\tau) + (2\mathrm{I_xS_z}+2\mathrm{I_zS_x}) \sin(\pi J_{IS}\tau)$$

It indicates that under spin-echo, only the *J* couplings evolve at a frequency of ½ $\pi J_{IS}\tau$. The Fourier transform of the modulation directly yields the corresponding *J*-coupling.

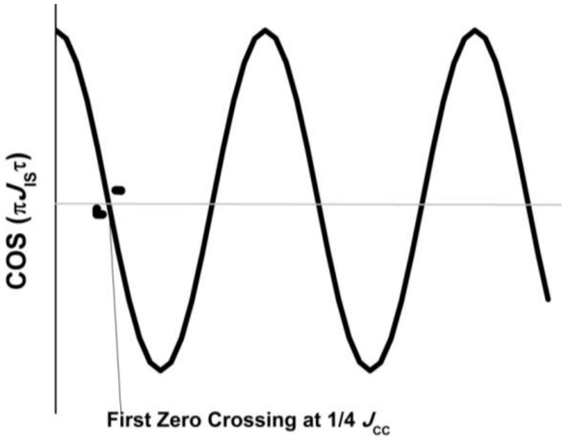

I.4.2. *Spin-echo modulations in solids*

In solid-state NMR, in addition to the *J*-coupling, spins experience comparatively large anisotropic CSA and dipolar couplings. Moreover, they may vary with the sample spinning. Hence, it is difficult to monitor the behaviour of the spin in spin-echo modulations in the solid-state. However, the recent strategic developments **[34]** in solid-state MAS NMR techniques, have aptly exploited the modulating effect of *J*-couplings on spin-echoes for precise measurement of hetero **[35]** and homonuclear **[36]** *J*-couplings and further extended for dipolar couplings **[26]** in *dilute* spin systems.

For example, in homonuclear spin systems, the experimental approaches enable the detection and accurate quantification of N-H--N hydrogen bond mediated (^{15}N-^{15}N) ($^{2}J_{NN}$) couplings in nucleic acids,**[37]** bond-order specific ^{13}C-^{13}C ($^{1}J_{CC}$) couplings for a series of selectively ^{13}C-labelled samples of retinal chromosphere in rhodopsin **[38]** and $^{2}J_{Si\text{-}O\text{-}Si}$ (^{29}Si-O-^{29}Si) couplings of layered silicates,**[39]** have added further impetus to this approach.

(i) In inorganic solids, the dipolar interactions between the low γ dilute spins are weak and the analysis is mostly based on the measurements of scalar couplings, such as $^{n}J_{Si\text{-}O\text{-}Si}$ and $^{n}J_{P\text{-}O\text{-}P}$

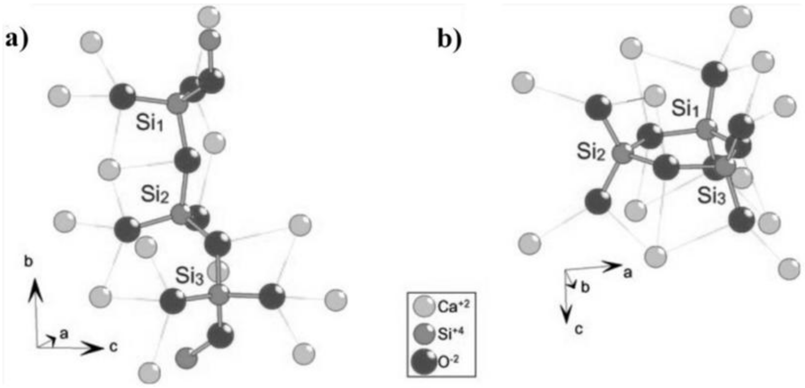

***Figure I.7:** Molecular structures of inorganic materials: (a) para wollastonite and (b) pseudo wollastonite.*

(ii) In synthetic Nucleotide bases and assemblies, hydrogen bond mediated $^{n}J_{N\text{-}N}$ couplings are helpful for identifying the bond connectivities and their strengths.

$$\text{Hydrogen bond strength} \propto {}^{n}J_{N\text{-}N}$$

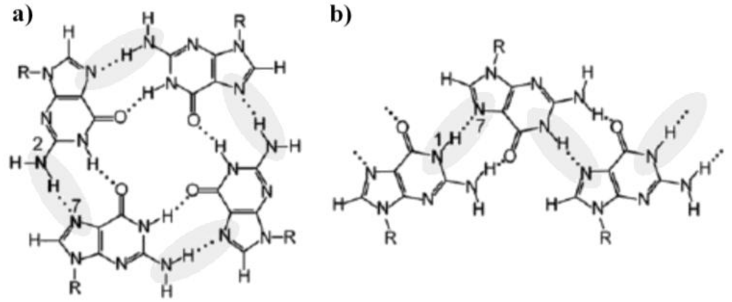

Figure I.8: *(a) Formation of quartet and ribbon like structures characterised by (a) N2–H---N7 and (b) N1-H---N7 intermolecular hydrogen-bonding patterns, respectively.*

(iii) ${}^{1}J_{C\text{-}C}$ scalar couplings are useful in calculating the bond orders in organic molecules

-C=C- ${}^{1}J_{CC}$ ~ 70 Hz (sp^2-sp^2 hybridization)
=C-C- ${}^{1}J_{CC}$ ~ 50 Hz (sp^2-sp^3 hybridization)
-C-C- ${}^{1}J_{CC}$ ~ 35 Hz (sp^3-sp^3 hybridization)

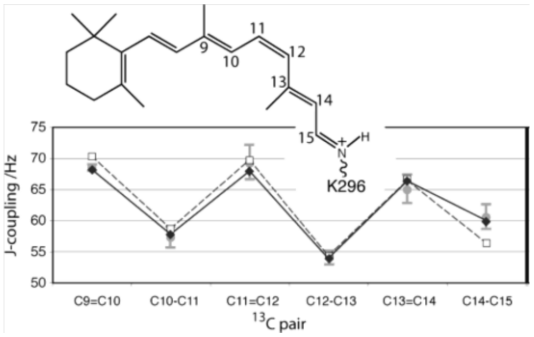

Figure I.9: *Filled circles with error bars: ${}^{1}J_{CC}$ values for the six rhodopsin isotopomers and their confidence limits. The inset shows the numbering scheme of the 11-Z-retinylidene chromophore. Diamonds and solid line: ${}^{13}C$-${}^{13}C$ J-couplings for all-E N-tert-butyl retinylidene imine triflate in solution. Open squares and dashed line: ${}^{13}C$-${}^{13}C$ J-couplings for all-E retinal in solid.* [38]

Conventional spin-echo and double selective spin-echo (two frequency-selective pulses for a specific spin-pair) modulation methods are useful for measuring homonuclear scalar couplings, which demand either a set of double selective ${}^{13}C_2$ labelled molecules or the experiments to be repeated for each spin pair of the molecule. To overcome these difficulties, new Hadamard NMR schemes are demonstrated in the thesis, which facilitate the simultaneous measurement of scalar couplings between multiple spin pairs in a single experiment.

I.5. Hadamard NMR

In solution-state NMR, the application of Hadamard matrices for data acquisition and data processing have been widely explored.[40] The Hadamard matrices in NMR are associated with the several significances such as water suppression, artefact free spectra and the sensitivities are somewhat greater than that of the routine FT-NMR. With the help of Hadamard NMR approach, the data can be acquired in a very short period of time, up to hundreds of times less than that of a routine FT data collection. However, these interesting experimental strategies are sparsely explored in solid-state NMR.[41, 42]

Conventionally, Hadamard NMR methods have been used for stochastic irradiation with a pseudo-random binary sequence of radiofrequency pulses, in order to achieve broadband excitation with a relatively low radiofrequency power.[43, 44] These are intrinsically time-domain measurements that used the Hadamard transform to derive free induction decays, and necessarily required Fourier transformation before a spectrum could be recorded. The entire range of NMR frequencies is excited in an essentially uniform manner. On the contrary, Ray Freeman and Ericks Kupce have developed a Hadamard method, which replaces the usual evolution period of two-dimensional spectroscopy with direct excitation in the frequency domain. Fourier transformation only employed in the F2 dimension, where the rate of data gathering is already near optimum.

The data acquired in the routine multidimensional Fourier transformation NMR operates by recording the FIDs at integer multiples of the dwell times. Thus, the resolution is directly proportional to the number of data points collected along the indirect dimensions. However, the prior knowledge of chemical shift values is mandatory to perform the Hadamard encoding in NMR. The data is collected along the indirect dimension by setting multiple radio frequency channels at the resonances of interest. Thus, it may not require more number of dwell increments along the indirect dimension. Although, Hadamard processing demands that the number of channels along the indirect dimension must be equal to the number of dwelling increments.

Hadamard matrices are the square matrices (H_{2n} and H_2^n) with the elements of either (+) or (-). The general form of a Hadamard matrix of 4×4 size is given below. The rows and columns in the Hadamard matrix can be treated as scans and radio frequency channels, respectively. While acquiring the data, it stores as explained here; in first scan, all the frequencies of the spectrum are in positive sign, from the second scan onwards some of them are in positive sign and others in negative sign, the same procedure continues till the last scan. Furthermore, while processing the data by Hadamard matrices, the rows undergo the algebraic addition, which results in only one column at every step of processing. Thus, the signals that are of choice can only be easily acquired with the help of Hadamard NMR.

$$\mathbf{H}_{4\times 4} = \begin{array}{lcccc} \text{Channel} & 1 & 2 & 3 & 4 \\ \text{Scan (1)} & + & + & + & + \\ \text{Scan (2)} & + & + & - & - \\ \text{Scan (3)} & + & - & + & - \\ \text{Scan (4)} & + & - & - & + \end{array}$$

I.5.1. *Hadamard encoded selective spin-echoes in Solid-state NMR*

In the present thesis, the first application of Hadamard encoding during the *refocusing periods* (evolution time of a multi-dimensional method) of spin-echoes are discussed and employed for an accurate and simultaneous measurement of homonuclear scalar couplings in multi-spin system. A set of free induction decays for pre-selected spins by Hadamard encoding, are recorded. By creating spin-spin commutation between interested spin pairs, *J*-coupling between the corresponding spins is computed from their echo-modulations. The simultaneous application of narrow band as well as low power Hadamard refocusing pulses facilitates the simultaneous measurement of scalar couplings in a single NMR experiment for the uniformly labelled spin systems.

Schematic representation of Hadamard selective refocusing pulse sequence is shown in Figure I.10. Hadamard encoding permits refocusing of “n” number of resonances with the aid of “n” number of simultaneous phase ramped soft Gaussian shaped π pulses, which generate the spectrum with “n” resonances (polychromatic). The selection of all the Hadamard resonances results in a complete spectrum that is equivalent to the conventional 1D FT-NMR spectrum. However, the power of Hadamard NMR lies with its ability to select specific resonances to be encoded/ decoded. Accordingly, the complexity/spectral overlapping can be reduced. Furthermore, a prior knowledge of the through-bond connectivity allows to selectively encode/decode multiple resonance pairs that are scalarly coupled, would facilitate precise determination of the corresponding *J*-couplings, *in a single experiment*, just by following their spin-echo modulations. The essential requirements in Hadamard encoding are the number of scans and number of channels to be greater than or equal to the number of frequencies to be refocused.

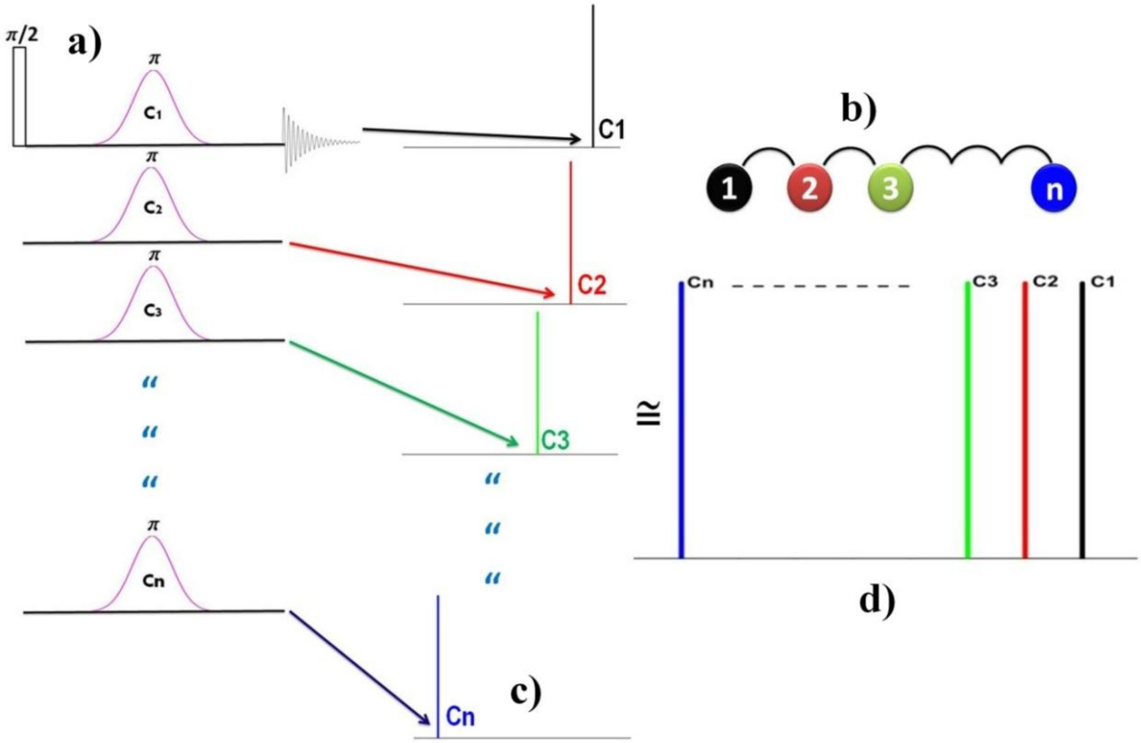

Figure I.10: *Schematic representation of Hadamard encoded NMR pulse sequence: (a) Hadamard encoded spin-echo pulse sequence with simultaneous phase ramped π pulses for selective refocusing, (b) molecule with 'n' number of spins, (c) refocused NMR spectra for individual spins and (d) sum of all the spectra yields a spectrum, which is equivalent to the routine FT NMR spectrum with 'n' resonances.*

I.6. Real-time pure-shift solution-state NMR spectroscopy

Unambiguous assignments of chemical shifts, establishment of through-bond (or dihedral angles) and through-space connectivities are central for accurate molecular structural characterizations. Solution-state ^{1}H NMR in principle carries this abundant structural information, which, however, often obscured due to the limited ^{1}H chemical shift range and poor signal resolution caused by overlapping ^{1}H-^{1}H scalar coupling (*J*) multiplets. The problem is more acute for molecules in which the nuclei are involved in multiple scalar couplings. Homo-decoupling, as a means of suppressing scalar interactions for enhanced spectral resolution, has been recognized for several years and different experimental schemes.[45-57] Most of these methods (non pulsed field gradient type) are conceptually important but lack sufficient sensitivity and/or involve complicated processing. On the other hand, isotope filtered bilinear rotational decoupling (BIRD) schemes are developed for impressive broadband decoupling. [58-60] Nevertheless, the decoupling is restricted to protons attached only to the ^{13}C atoms, therefore also suffer from poor sensitivity due to the ~1% natural abundance of ^{13}C, but eliminates problems due to strong couplings, pseudo dimension acquisitions,[60] and also advantageous for obtaining fully decoupled HSQC. [61]

Alternatively, in their seminal experimental strategy, Zangger and Sterk[56] have demonstrated an effective broadband homodecoupling, known as ZS-decoupling, which relies on a combination of a soft and a hard 180^{o} pulse in the presence of weak slice-selective z-gradient pulse. The technique offers spatially resolved (according to the slice thickness) excitation followed by the selective decoupling, which has been genesis for several significant developments of ZS-based 'pure-shift' multi-dimensional NMR experiments.[62-67] However, unfortunately, these elegant ZS-methods demand long experimental time due to two limitations viz., (i) very low sensitivity (typically only few percent of that obtained in conventional non-decoupled spectrum) as the signal originates only from a spatially encoded thin slice and (ii) require time-consuming additional pseudo 2D/3D mode data acquisition for 1D/2D spectra, respectively.

Recently, in a remarkable advancement of this method, Zangger etal., have demonstrated instantaneous (real-time) homonuclear broadband (HOBB) decoupling in 1D as well as in the direct detection dimension of TOCSY, by periodically interrupting the FID with ZS-decoupling block.[68] This smart approach eliminates the pseudo dimension acquisition and therefore greatly cuts down the long experimental time of the conventional ZS-pure-shift experiments, although the sensitivities are still limited due to the involvement of slice selection. However, in favourable cases, such as excess sample concentrations, a combination of largely available cryogenically cooled probes and faster acquisition methods, loss in the sensitivity can be minimized. [69] Subsequently, Parella and co-workers have improvised the ZS-based instant-HOBB decoupling method for full sensitive and instantaneous homodecoupled band selective (HOBS) acquisition, which involves selective decoupling pulses for the region of interest, and applied for TOCSY, HSQC and HSQMBC.[70, 71] As this strategy does not involve slice selection, the dramatic enhancement of resolution, comparable to that of regular non-decoupled spectrum, is possible.

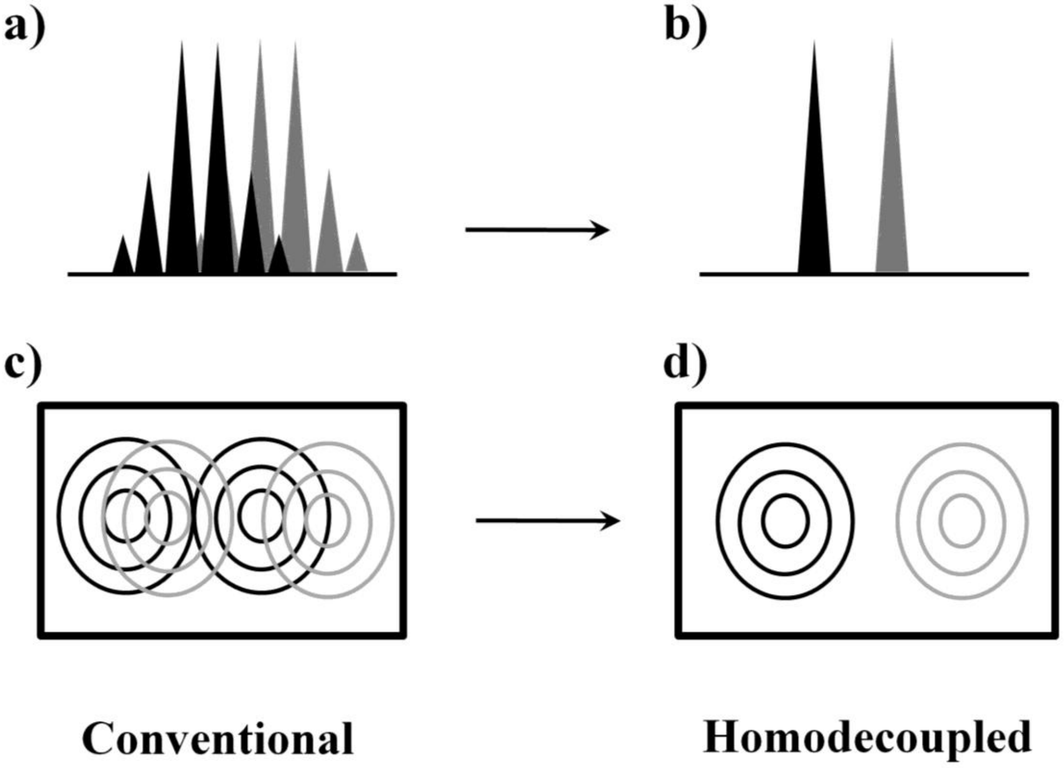

***Figure I.11: Schematic representation of resolution enhancement**: The conventional 1D and 2D spectra with crowded resonances are depicted in (a) and (c), respectively. The corresponding pure-shift homodecoupled spectra are shown in (b) and (d).*

Adopting the impressive real-time homodecoupling strategies, new pure-shift based real time HOBS (Homonuclear Band Selective)-ROESY/ HOBB (Homonuclear Broad Band)-ROESY, HOBB-spin-echo, and HOBB-COSY pulse sequences are developed in the present work (chapter-VII and VIII) and a significant enhancement in resolution is accomplished.

1.7. References

[1] S. O. Smith and O. B. Peersen, Solid-State NMR Approaches for Studying Membrane Protein Structure, Annu. Rev. Biophys. Biomol. Stru, 21 (1992) 25-47.

[2] S. J. Opella, Solid-State NMR Structural Studies of Proteins, Annu. Rev. Phys. Chem, 45 (1994) 659-683.

[3] R. Tycko, Solid-State NMR Studies of Amyloid Fibril Structure, Annu. Rev. Phys. Chem, 62 (2011) 279-299.

[4] G. Comellas and C. M. Rienstra, Protein Structure Determination by Magic-Angle Spinning Solid-State NMR, and Insights into the Formation, Structure, and Stability of Amyloid Fibrils, Annu. Rev. Biophy, 42 (2013) 515-536.

[5] A. Goldbourt and P.K. Madhu, Multiple-Quantum Magic-Angle Spinning: High-Resolution Solid-State NMR of Half-Integer Spin Quadrupolar Nuclei, Annu. Rep. NMR. Spec, 54 (2004) 81-153.

[6] M. Goldman, Quantum Description of High-Resolution NMR in Liquids, Clarendon Press, Oxford (1988).

[7] J. H. Keeler, Multinuclear Magnetic Resonance in Liquids and Solids – Chemical Applications, NATO ASI Series C, 322 (1988) 103 (Eds. P. Granger and R.K. Harris).

[8] M. H. Levitt, Spin Dynamics: Basics of Nuclear Magnetic Resonance, Second edition, John Wiley & Sons Ltd (2008).

[9] M. J. Duer, Solid-State NMR Spectroscopy Principles and Applications, Blackwell Science Ltd (2002).

[10] W. A. Anderson and J. T. Arnold, A line narrowing experiment, Phys. Rev, 94 (1954) 497–498.

[11] G. A. Williams and H. S. Gutowsky, Sample spinning and field modulation effects in nuclear magnetic resonance, Phys. Rev, 104 (1956) 278–283.

[12] R. D. Pasquale, A new benchmark for high resolution and high sensitivity analysis of micro volumes with Solid-state NMR, JEOL USA, (2012).

[13] W. T. Dixon, Spinning sideband free and spinning sideband only NMR spectra in spinning samples, J. Chem. Phys, 77 (1982) 1800-1809.

[14] N. Bloembergen, S. Shapiro, P. S. Pershan, and J. O. Artman, Cross-Relaxation in Spin Systems, Phys. Rev, 114 (1959) 445-449.

[15] A. Pines, M. G. Gibby and J. S. Waugh, Proton-Enhanced NMR of Dilute Spins in Solids, J. Chem. Phys, 59 (1973), 569-590.

[16] S. R. Hartmann and E. L. Hahn, Nuclear Double Resonance in the Rotating Frame, Phys. Rev, 128 (1962) 2042-2046.

[17] U. Haeberlen and A. Waugh, Coherent averaging effect in magnetic resonance, Phys. Rev, 175 (1968) 453–467.

[18] P. Hodgkinson, Heteronuclear decoupling in the NMR of solids, Prog. Nucl. Magn. Reson. Spec, 46 (2005) 197–222.

[19] M. H. Levitt and R. Freeman, Composite pulse decoupling, J. Magn. Reson, 43 (1981) 502–507.

[20] A. E. Bennett, C. M. Rienstra, M. Auger, K. V. Lakshmi and R. G. Griffin, Heteronuclear decoupling in rotating solids, J. Chem. Phys, 103 (1995) 6951-6958.

[21] B.M. Fung, A.K. Khitrin and K. Ermolaev, An improved broadband decoupling sequence for liquid crystals and solids, J. Magn. Reson, 142 (2000) 97–101.

[22] A. Detken, E. H. Hardy, M. Ernst and B. H. Meier, Simple and efficient decoupling in magic-angle spinning solid-state NMR: the XiX scheme, Chem. Phys. Lett, 356 (2002) 298–304.

[23] G. Comellas, J. J. Lopez, A. J. Nieuwkoop, L. R. Lemkau and C. M. Rienstra, Straightforward, effective calibration of SPINAL-64 decoupling results in the enhancement of sensitivity and resolution of biomolecular solid-state NMR, J. Magn. Reson, 209 (2011) 131–135.

[24] T. Gullion, Introduction to Rotational-Echo Double-Resonance NMR, Conc. Magn. Reson, 10 (1998) 277-289.

[25] A. E. Bennett, C. M. Rienstra, J. M. Griffiths, W. Zhen and P. T. Lansbury, Homonuclear radio frequency-driven recoupling in rotating solids, J. Chem. Phys, 108 (1998) 9463-9479.

[26] G. Pileio, Y. Guo, T. N. Pham, J. M. Griffin, M. H. Levitt and S. P. Brown, Residual Dipolar Couplings by Off-Magic-Angle Spinning in Solid-State Nuclear Magnetic Resonance Spectroscopy, J. Am. Chem. Soc, 129 (2007) 10972–10973.

[27] G. Pileio, S. Mamone, G. Mollica, I. M. Montesinos, A. Gansmuller, M. Carravetta, S. P. Brown and M. H. Levitt, Estimation of internuclear couplings in the solid-state NMR of multiple-spin systems. Selective spin echoes and off-magic-angle sample spinning, Chem. Phys. Lett, 456 (2008) 116–121.

[28] P. Thureau, A. C. Sauerwein, M. Concistre and M. H. Levitt, Selective internuclear coupling estimation in the solid-state NMR of multiple-spin systems, Phys. Chem. Chem. Phys, 13 (2011) 93–96.

[29] J. Becker-Baldus, T. F. Kemp, J. Past, A. Reinhold, A. Samoson and S. P. Brown, Longer-range distances by spinning-angle-encoding solid-state NMR spectroscopy, Phys. Chem. Chem. Phys, 13 (2011) 4514–4518.

[30] D. P. Raleigh, M. H. Levitt and R.G. Griffin, Rotational Resonance in Solid-state NMR, Chem. Phys. Lett, 146 (1988) 71-76.

[31] M. Karplus, Contact Electron-Spin Coupling of Nuclear Magnetic Moments, J. Chem. Phys, 30 (1959) 11–15.

[32] O. W. Sorensen, G. W. Eich, M. H. Levitt, G. Bodenhausen and R. R. Ernst, Product operator formalism for the description of NMR pulse experiments, Prog. Nucl. Magn. Reson. Spec, 16 (1983) 163-192.

[33] D. Massiot, F. Fayon, M. Deschamps, S. Cadars, P. Florian, V. Montouillout, N. Pellerin, J. Hiet, A. Rakhmatullin and C. Bessada, Detection and use of small J couplings in solid-state NMR experiments, Comp. Rend. Chim, 13 (2010) 117–129.

[34] L. Duma, W. C. Lai, M. Carravetta, L. Emsley, S. P. Brown and M. H. Levitt, Principles of Spin-Echo Modulation by J-Couplings in Magic-Angle-Spinning Solid-State NMR, Chem. Phys. Chem, 5 (2004) 815-833.

[35] J. Trebosc, J. P. Amoureux, L. Delevoye, J. W. Wiench, M. Pruski, Frequency-selective measurement of heteronuclear scalar couplings in solid-state NMR, Sol. State Sci, 6 (2004) 1089-1095.

[36] S. Cadars, A. Lesage, N. Hedin, B. F. Chmelka and L. Emsley, Selective NMR Measurements of Homonuclear Scalar Couplings in Isotopically Enriched Solids, J. Phys. Chem. B, 110 (2006) 16982-16991.

[37] T. N. Pham, J. M. Griffin, S. Masiero, S. Lena, G. Gottarelli, P. Hodgkinson, C. Filip and S. P. Brown, Quantifying hydrogen-bonding strength: the measurement of 2hJNNCouplings in self-assembled guanosines by solid-state ^{15}N spin-echo MAS NMR, Phys. Chem. Chem. Phys, 9 (2007) 3416–3423.

[38] W. C. Lai, N. McLean, A. Gansmuller, M. A. Verhoeven, G. C. Antonioli, M. Carravetta, L. Duma, P. H. M. Bovee-Geurts, O. G. Johannessen, H. J. M. de Groot, J. Lugtenburg, L. Emsley, S. P. Brown, R. C. D. Brown, W. J. DeGrip and M. H. Levitt, Accurate Measurements of ^{13}C-^{13}C J-Couplings in the Rhodopsin Chromophore by Double-Quantum Solid-State NMR Spectroscopy, J. Am. Chem. Soc, 128 (2006) 3878-3879.

[39] P. Florian, F. Fayon and D. Massiot, 2J Si-O-Si Scalar Spin-Spin Coupling in the Solid-state: Crystalline and Glassy Wollastonite CaSiO3, J. Phys. Chem. C, 113 (2009) 2562–2572.

[40] E. Kupce, T. Nishida and R. Freeman, Hadamard NMR spectroscopy, Prog. Nucl. Magn. Reson. Spec, 42 (2003) 95–122.

[41] J. Ashida, E. Kupce and J. P. Amoureux, Hadamard NMR spectroscopy in solids, J. Magn. Reson, 178 (2006) 129–135.

[42] T. Gopinath, K. R. Mote and G. Veglia, Proton Evolved Local Field Solid-State Nuclear Magnetic Resonance using Hadamard Encoding: Theory and Application to Membrane Proteins, J. Chem. Phys, 135 (2011) 1-8.

[43] R. Kaiser, Application of the Hadamard Transform to NMR Spectrometry with Pseudo noise Excitation, J. Magn. Reson, 15 (1974) 44-63.

[44] M. Greferath, B. Blumich, W. M. Griffith and G. L. Hoatson, Saturation in Deuteron Hadamard NMR Spectroscopy of Solids, J. Magn. Reson, 102 (1993) 73-80.

[45] A. J. Shaka, J. Keeler and R. Freeman, Separation of chemical shifts and spin coupling in proton NMR. Elimination of dispersion signals from two-dimensional spectra, J. Magn. Reson, 56 (1984) 294 – 313.

[46] W. P. Aue, J. Karhan and R. R. Ernst, Homonuclear broadband decoupling and two dimensional J-resolved NMR spectroscopy, J. Chem. Phys, 64 (1976) 4226–4227.

[47] A. Bax, A. F. Mehlkopf and J. Smidt, Homonuclear broadband-decoupled absorption spectra, with linewidths which are independent of the transverse relaxation rate, J. Magn. Reson, 35 (1979) 167 –169.

[48] Ad. Bax and R. Freeman, Investigation of Complex Networks of Spin-Spin Coupling By Two- Dimensional NMR, J. Magn. Reson, 44 (1981) 542-561.

[49] O. W. Soerensen, C. Griesinger and R. R. Ernst, Time reversal of the evolution under scalar spin-spin interactions in NMR. Application for .omega.1 decoupling in two-dimensional NOE spectroscopy, J. Am. Chem. Soc, 107 (1985) 7778-7779.

[50] R. Bruschweiler, C Griesinger, O.W Sørensen and R.R Ernst, Combined use of hard and soft pulses for ω_1 decoupling in two-dimensional NMR spectroscopy, J. Magn. Reson, 78 (1988) 178-185.

[51] M. A. McCoy and L. Mueller, Selective shaped pulse decoupling in NMR: homonuclear [carbon-13] carbonyl decoupling, J. Am. Chem. Soc, 114 (1992) 2108-2112.

[52] M. Woodley and R. Freeman, Elimination of spin–spin splittings from high resolution proton NMR spectra, J. Magn. Reson, 111 (1994) 225–228.

[53] A. Hammarstrom and G. Otting, Improved Spectral Resolution in 'H NMR Spectroscopy by Homonuclear Semiselective Shaped Pulse Decoupling during Acquisition, J. Am. Chem. Soc, 116 (1994) 8847-8848.

[54] J. Nuzillard, Time-Reversal of NMR Signals by Linear Prediction. Application to Phase-Sensitive Homonuclear *J*-Resolved Spectroscopy, J. Magn. Reson, 118 (1996) 132 – 135.

[55] S. Simova, H. Sengstschmid and R. Freeman, Proton Chemical-Shift Spectra, J. Magn. Reson, 124 (1997) 104-121.

[56] K. Zangger and H. Sterk, Homonuclear broadband-decoupled NMR spectra, J. Magn. Reson, 124 (1997) 486-489.

[57] J.C. Cobas and M. Martin-Pastor, A homodecoupled diffusion experiment for the analysis of complex mixtures by NMR, J. Magn. Reson, 171 (2004) 20–24.

[58] J. R. Garbow, D. P. Weitekamp and A. Pines, Bilinear rotation decoupling of homonuclear scalar interactions, Chem. Phys. Lett, 93 (1982) 504–509.

[59] J. A. Aguilar, M. Nilsson and G. A. Morris, Simple Proton Spectra from Complex Spin Systems: Pure Shift NMR Spectroscopy Using BIRD, Angew. Chem. Int. Ed, 50 (2011) 9716-9717.

[60] A. Lupulescu, G. L. Olsen and L. Frydman, Toward single-shot pure-shift solution ^{1}H NMR by trains of BIRD-based homonuclear decoupling, J. Magn. Reson, 218 (2012) 141-146.

[61] L. Paudel, R.W. Adams, P. Király, J.A. Aguilar, M. Foroozandeh, M.J. Cliff, M. Nilsson, P. Sándor, J.P. Waltho and G.A. Morris, Simultaneously Enhancing Spectral Resolution and Sensitivity in Heteronuclear Correlation NMR Spectroscopy, Angew. Chem. Int. Ed, 52 (2013) 1-5.

[62] J. A. Aguilar, S. Faulkner, M. Nilsson and G. A. Morris, Pure Shift 1H NMR: A Resolution of the Resolution Problem?, Angew. Chem. Int. Ed, 49 (2010) 3901-3903.

[63] G. A. Morris, J. A. Aguilar, R. Evans, S. Haiber and M. Nilsson, True Chemical Shift Correlation Maps: A TOCSY Experiment with Pure Shifts in Both Dimensions, J. Am. Chem. Soc, 132 (2010) 12770-12772.

[64] J. A. Aguilar, A. A. Colbourne, J. Cassani, M. Nilsson and G. A. Morris, Decoupling Two-Dimensional NMR Spectroscopy in Both Dimensions: Pure Shift NOESY and COSY, Angew. Chem. Int. Ed, 51 (2012) 6460-6463.

[65] S. Islam, J. A. Aguilar, M. W. Powner, M. Nilsson, G. A. Morris and J. D. Sutherland, Detection of Potential TNA and RNA Nucleoside Precursors in a Prebiotic Mixture by Pure Shift Diffusion-Ordered NMR Spectroscopy, Chem. Eur. J, 19 (2013) 4586 – 4595.

[66] M. Nilsson and G. A. Morris, Pure shift proton DOSY: diffusion-ordered 1H spectra without multiplet structure, Chem. Comm, (2007) 933–935.

[67] J. J. Koivisto, Zero-quantum filtered pure shift TOCSY, Chem. Comm, 49 (2013) 96-98.

[68] N.H. Meyer and K. Zangger, Simplifying proton NMR spectra by instant Homonuclear broadband decoupling, Angew. Chem. Int. Ed, 52 (2013) 7143-7146.

[69] P. Sakhaii, B. Haase, W. Bermel, R. Kerssebaum, G.E. Wagner and K. Zangger, Broadband homodecoupled NMR spectroscopy with enhanced sensitivity, J. Magn. Reson, 233 (2013) 92-95.

[70] L. Castanar, P. Nolis, A. Virgili and T. Parella, Full Sensitivity and Enhanced Resolution in Homodecoupled Band-Selective NMR Experiments, Chem. Eur. J, 19 (2013) 17283-17286.

[71] L. Castanar, J. Saurí, P. Nolis, A. Virgili and T. Parella, Implementing homo- and heterodecoupling in region-selective HSQMBC experiments, J. Magn. Reson, 238 (2013) 63-69.

Chapter-II

Spectral simplifications in solid-state NMR

Hadamard-encoded selective spin-echoes for simultaneous measurement of multiple scalar couplings (small and large) in organic solids

II.1. Introduction

The inherent line-broadening of resonance lines is a major concern in the solid-state NMR, which obscures the measurement of scalar couplings. In uniformly isotope labelled multi-spin systems, the dipolar network is strong and the spin-spin interactions do not commute to each other, which makes the measurement of these couplings difficult, and practically impossible in some cases. Cadars etal.,[1] have introduced a novel spin-echo pulse sequence comprised of double frequency selective pulses to selectively refocuse the desired pair of resonances. The modulation of these spin-echo amplitudes (at the magic angle spinning) with respect to the echo time facilitate the corresponding scalar coupling values.[1-6] However, this method suffers with the following disadvantages, viz., (i) experiment needs to repeat for every spin pair in the molecule, which is cumbersome and time consuming and (ii) needs to determine the resonance offset exactly at the centre of the interested resonances. The problem would be more acute in the cases of multiple spin labelled systems such as in biomolecular solids. Whereas, the conventional spin-echo is straightforward in the cases of dilute spin systems, such as molecules with only two distinctly labelled spin pairs available. To triumph over these problems, Hadamard encoded multiple selective spin-echo pulse sequences are developed in the present chapter and demonstrated for the simultaneous measurement of multiple scalar couplings in uniformly labelled molecules.

II.1.1. *Basic frequency domain Hadamard NMR spectroscopy*

In their seminal reports, Kupce and Freeman have introduced *frequency domain solution-state* Hadamard NMR spectroscopy in one and multi-dimensions[7-11] that revealed attractive features over the conventional Fourier transform NMR spectroscopy, such as, exclusion of undesired spectral regions/data-sampling and significant reduction in experimental time. The central theme of this intriguing frequency domain approach relies on direct multiplex excitation of selected resonances in either direct or indirect dimension, by an array of soft pulses (instead of a hard pulse) that are encoded according to Hadamard matrix of dimension nXn, where 'n' is the number of frequency channels. The effective frequency of each pulse is an offset from the carrier and the frequency channels/selections need not be equally spaced or continuous. The simultaneous multichannel excitation results in composite NMR signals in the receiver, which are decoded according to the corresponding Hadamard matrix. The Hadamard NMR technique has been successfully applied to diffusion studies[12,13] and imaging. [14] However, the frequency domain Hadamard encoded/decoded NMR spectroscopy has been sparsely explored in the solid-state.[15-17]

II.1.2. *Hadamard encoded/decoded refocusing*

Figure II.4 and II.18 describe the Hadamard encoded spin-echo schemes employed in the present study. The frequency encoding/decoding for refocusing is analogous to the excitation/decoding approach as discussed above. Accordingly, the conventional initial non-selective hard pulse excites all the resonances simultaneously, while the selectivity is achieved during the refocusing. Herein, the conventional refocusing π pulse in a spin-echo sequence is replaced by a polychromatic pulse comprised of several simultaneous selective pulses of different frequencies encoded according to the Hadamard matrix. The Hadamard matrices are the order of 4*n*, where *n* is an integer. For instance, in the case of Histidine, six resonances need to be encoded in the ^{13}C-spectra and the nearest hardmard matrix is of dimension 8. In this application, the six frequencies are chosen to match the known chemical shifts of Histidine and the remaining two frequencies are set dummy.

II.2. Materials

Hadamard encoded selective spin-echo experiments are performed on a set of uniformly labelled molecules (Figure II.1): (1) $^{13}C_6$ L-Histidine.HCl purchased from CIL, (2) an unnatural amino acid, $^{13}C_5$- Furanoid cis-β-Sugar-Amino Acid (FSAA), synthesized from $^{13}C_6$-Glucose as a starting material and (3) A dimer, $^{13}C_8$-SA comprised of $^{13}C_5$-FSAA and $^{13}C_3$-L-Alannine. The synthetic route for natural abundant FSAA is known;[18] and $^{13}C_8$-SA achieved by using routine peptide coupling protocols. The solid-state NMR experiments are conducted on 1:5 mixtures of isotopic labelled molecules as well as natural abundant compounds to minimize the intermolecular dipolar interactions. The mixtures are tightly filled in 4 mm Zirconia rotors.

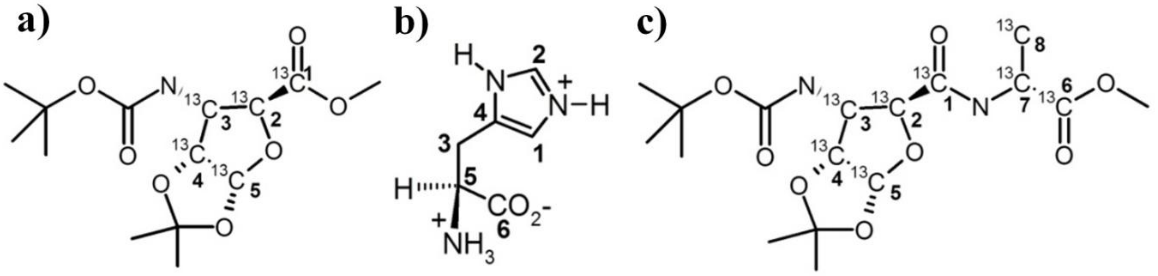

Figure II.1: *^{13}C labelled compounds studied in the present chapter: (a) $^{13}C_5$-FSAA, (b) $^{13}C_6$ L-Histidine.HCl and (c) $^{13}C_8$-SA dimer synthesized from $^{13}C_5$-FSAA and $^{13}C_3$ L-Alanine as building blocks. Numbering is given only for the isotopic labelled carbons.*

II.3. Experiments

All the SSNMR experiments are conducted on Varian Unity Inova 400 MHz spectrometer equipped with 4mm chemagnetics solid-state NMR probe, spinning speed is controlled by Varian automated MAS control unit at 8 kHz for $^{13}C_6$ L-Histidine.HCl, 10 kHz for $^{13}C_5$-FSAA and $^{13}C_8$-SA dimer. The optimized 90° pulse widths for ^{13}C and ^{1}H are 3.0 and 3.2μs, respectively. The recycle delay is 3s. The transverse magnetization is created by using ramped cross polarization from ^{1}H to ^{13}C at the contact time of 5 ms. During the pulsing and acquisition periods, the SPINAL-64 decoupling is applied at 83 KHz nutation frequency. An 8-step phase cycling is employed on ^{13}C channel, ±1 (2 steps) on $\pi/2$ pulse and ±1 (4 steps) on π pulse. Total 32 scans are acquired for each data set.

Shaped pulses are analyzed with the 'Pbox' option invoked in VNMRJ2.2D software. In the present study, Gaussian shaped pulses of length 4.5 ms are used for simultaneous refocusing of interested spins and the corresponding time shift correction**[5]** value is 1.08 ms, which is equal to the shaped pulse width at 76.69%. The resultant refocused bandwidths are equal to 200Hz. The $\tau/2$ values are incremented as the integer multiples of rotor periods. Figure II.2 represents the conventional 1D CPMAS ^{13}C spectra, which lacks the information about scalar couplings, due to the dominant line-broading mediated by residual dipolar interactions.

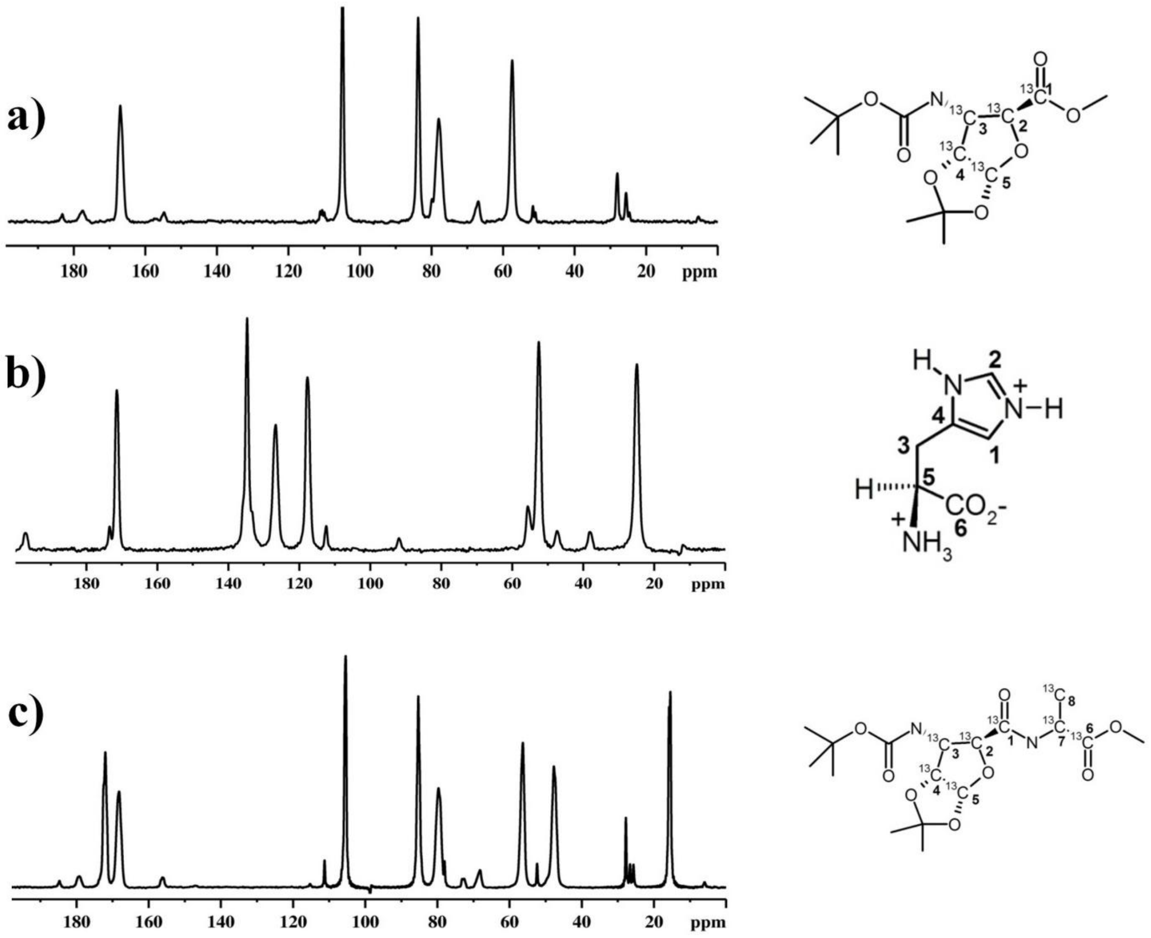

Figure II.2: *^{13}C CPMAS spectra: (a) $^{13}C_5$-FSAA, (b) $^{13}C_6$-Histidine.HCl and (c) $^{13}C_8$-SA dimer molecules.*

Initially, DQ-SQ INADEQUATE experiments are carried out to assign the ^{13}C chemical shifts of $^{13}C_5$-FSAA monomer and $^{13}C_8$-SA dimer molecules (Figure II.3). Herein, the SPC5[19] composite pulse block facilitates the efficient DQ magnetization transfer. However, for $^{13}C_6$-Histidine.HCl molecule, the assignments are already known.[5]

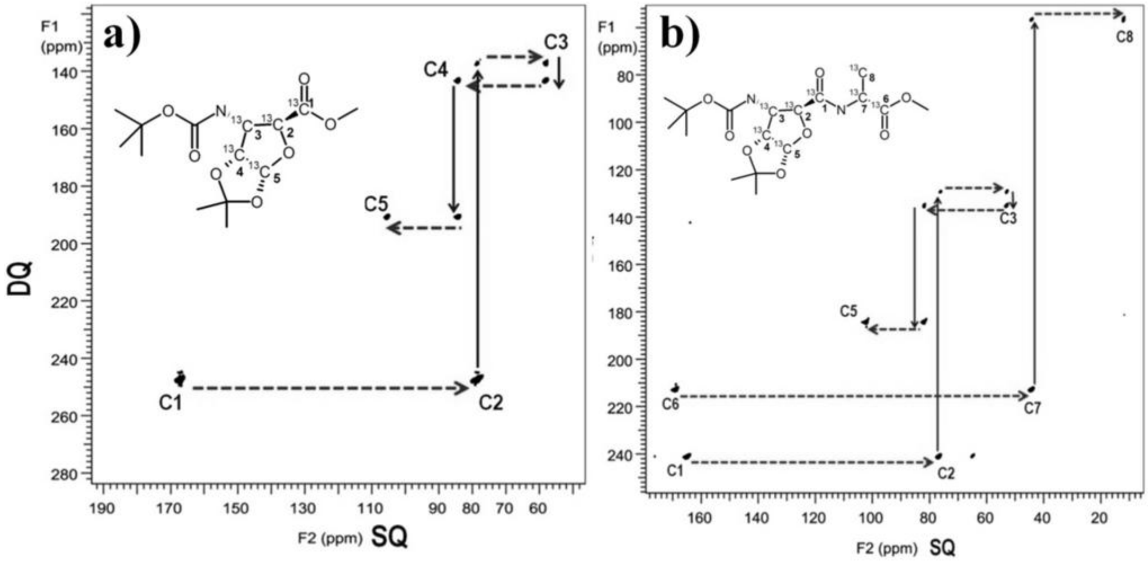

Figure II.3: *SPC5 INADEQUATE spectra of unnatural amino acids: (a) $^{13}C_5$-FSAA and (b) $^{13}C_8$-SA. Dashed arrows represent the directly bonded carbon atoms.*

Table II.1: *^{13}C Chemical shifts of $^{13}C_5$-FSAA and $^{13}C_8$-SA molecules.*

Spin	**$^{13}C_5$-FSAA chemical**	**$^{13}C_8$-SA chemical**
C1	167.0	168.3
C2	77.9	79.9
C3	57.3	56.8
C4	83.7	85.5
C5	104.9	105.7
C6	---	172.4
C7	---	47.9
C8	---	15.9

II. 4. Results and Discussions

II.4.1. *Hadamard encoded spin-echo experiments in double frequency selective refocusing mode*

As discussed in the previous sections, conventionally the earlier reports pertaining to frequency selective spin-manipulations or selective scalar coupling measurements were limited only to two frequencies. Herein, as a proof of concept and its versatility, the Hadamard encoded selective refocusing has been demonstrated initially for doubly selective frequencies, by encoding only one spin pair in each experiment and compared the results with those of conventional double frequency selective (soft Gaussian shaped π pulses) experiments. Subsequently, the Hadamard-based strategy has been extended to multiple spin pairs by simultaneous application of desired number of Hadamard encoded pulses (for each selected frequency/chemical shift) in a single experiment. The integrated spin-echoes are plotted against the spin-echo time (τ_{ev}) and fitted to a theoretical expression (1),[1] by using Levenberg-Marquardt iteration algorithm.

$$S(\tau) \propto \cos\{\pi J(\tau_{ev}-\tau_{sh})\} \exp(-\tau_{ev}/T_2^J) \rightarrow (1)$$

Where T_2^J is the empirical parameter, τ_{ev} and τ_{sh} are the spin-echo evolution time and the time shift correction of the shaped pulses, respectively.

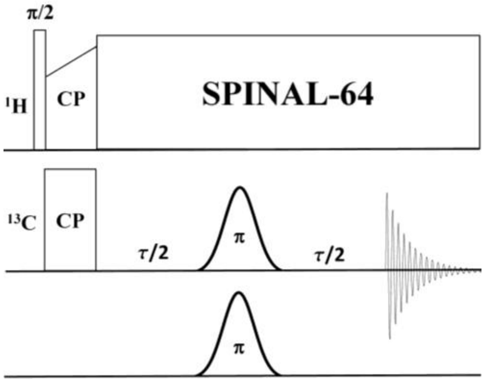

Figure II.4: *Schematic representation of Hadamard encoded selective spin-echo pulse sequence in double frequency refocusing mode.*

The scalar coupling measurements are carried out at the magic angle. The magic angle adjustment (^{79}Br FID) has been tested further by the spin-echo modulation of $^{13}C_2$ Glycine (Figure II.5), which yielded a 55.5 Hz of *J*-coupling (comparable to its value in solution-state, 53.6Hz).

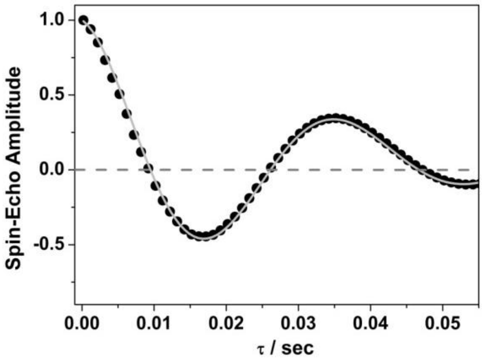

Figure II.5: *Spin-echo modulation of $^{13}C_2$-Glycine at the magic angle, yielded $^1J_{CC}$ ~ 55 Hz, which is comparable to its value in solution-state (53.6 Hz). Black filled circles and gray solid line depict the experimental data and the best fit to the equation (1), respectively.*

II.4.1.1. *Hadamard encoded double frequency selective spin-echoes for different spin-pairs in $^{13}C_5$-FSAA*

As a first example, Hadamard encoded selective spin-echoes have been demonstrated in double frequency selective on $^{13}C_5$-FSAA molecule and the selectivity of spin pairs is impressive (Figure II.6). Fourier transformation of C1-C2 Hadamard selective spin-echo modulation has yielded a clear doublet (Figure II.7), which is equivalent to the $^1J_{CC}$ of corresponding spin pair (~72Hz) in solution-state. The above described Hadamard encoding and data processing have been repeated for the other spin pairs C1-C2, C2-C3, C3-C4 and C4-C5 of $^{13}C_5$-FSAA, and the corresponding computed values of $^1J_{CC}$ are given in Table II.2. In addition to these four $^1J_{CC}$, a long range $^3J_{CC}$ is measured between C1 and C5. The results are in good agreement with the solution-state $^nJ_{CC}$ (Figure II.10).

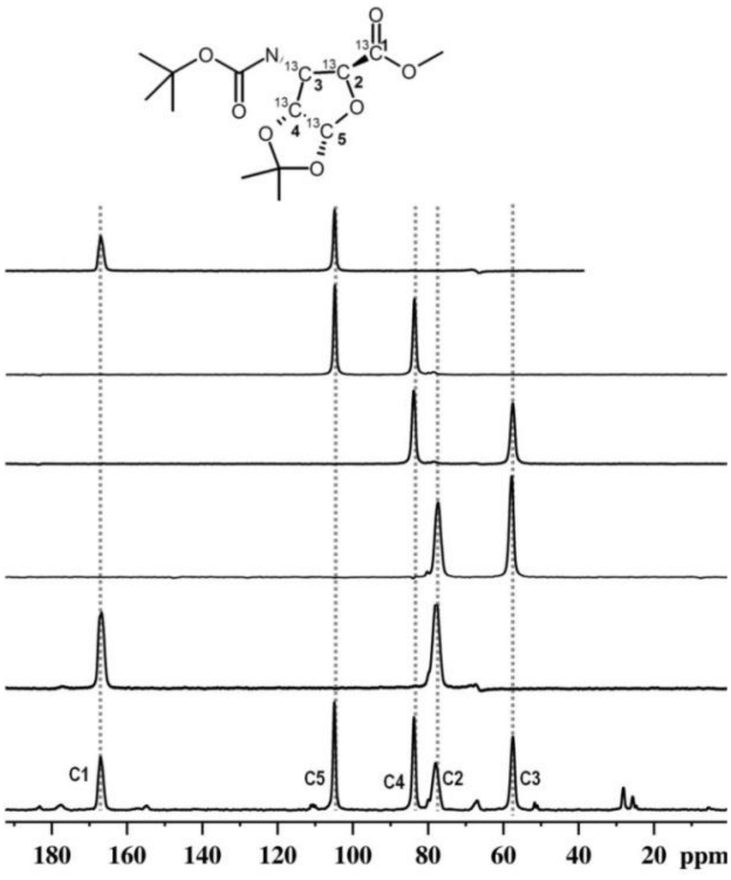

Figure II.6: *Stacked ^{13}C-CPMAS and Hadamard encoded double selective refocuing spectra for different spin-pairs of $^{13}C_5$-FSAA at $\tau/2=0$.*

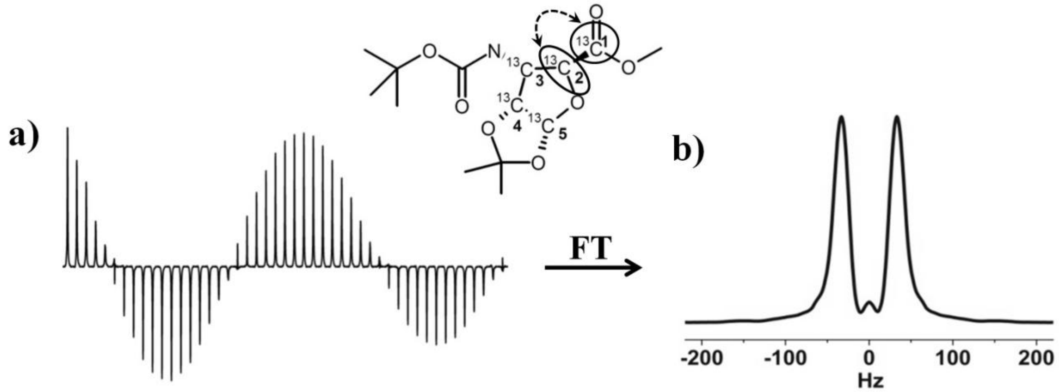

Figure II.7: *Spin-echo modulation and its Fourier transformations: (a) spin-echo modulation of spin C1 as a function of τ, while refocusing C1-C2 spin pair of $^{13}C_5$-FSAA and (b) the corresponding Fourier transformation yielded a clear doublet, which is equivalent to the solution-state $^1J_{C1\text{-}C2}$.*

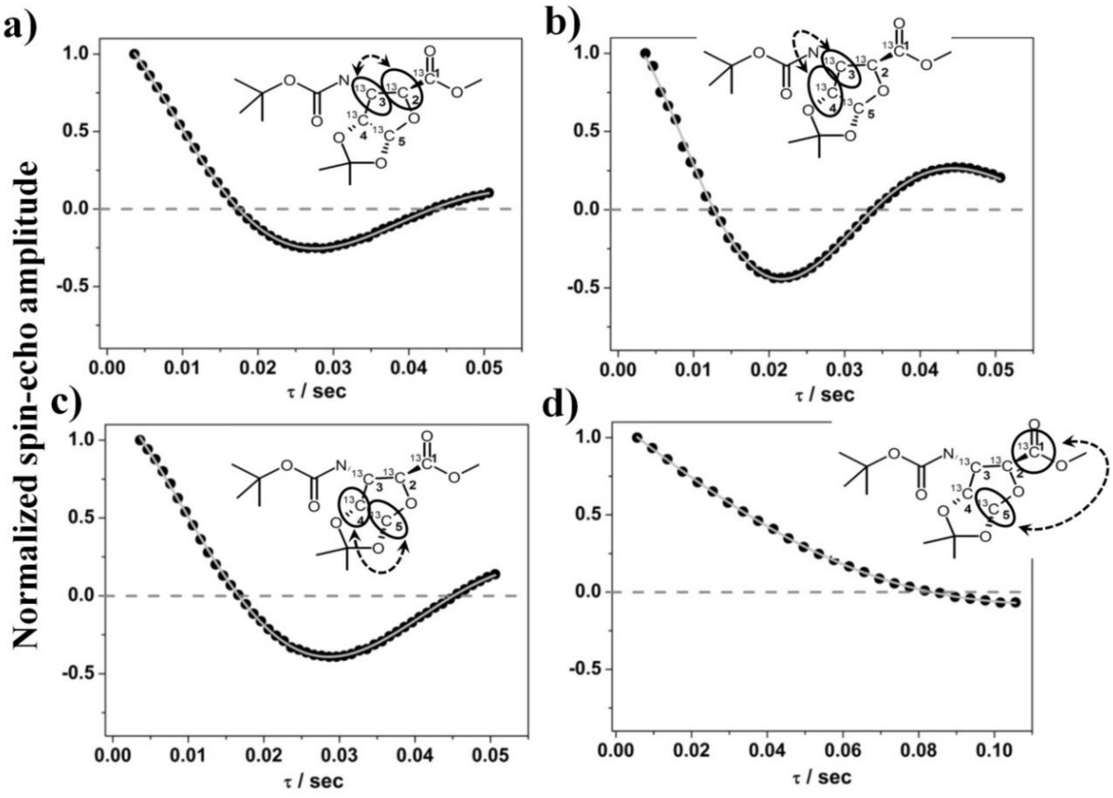

Figure II.8: *Hadamard encoded double frequency selective spin-echo modulations for different spin pairs of $^{13}C_5$-FSAA molecule: (a), (b), (c) and (d) corresponds to the C2-C3, C3-C4, C4-C5 and C1-C5 spin-echo modulations. The experimental data and best fits to the equation-1 are depicted in black circles and grey lines, respectively.*

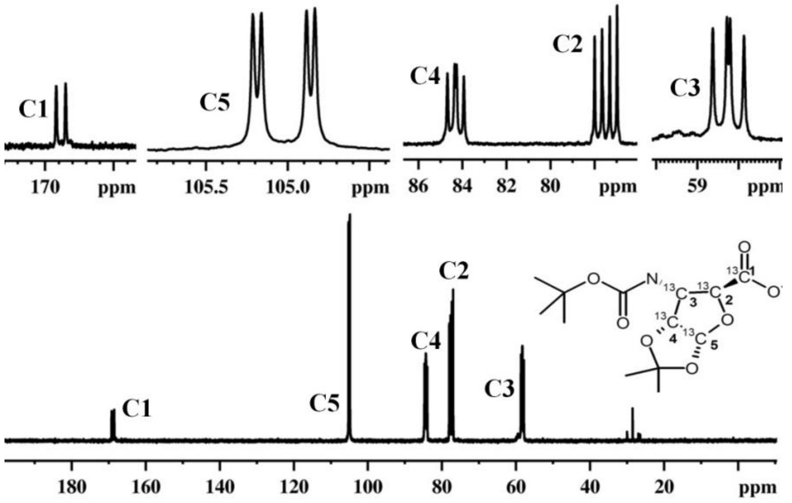

Figure II.9: *Solution-state ^{13}C spectrum of ^{13}C$_5$-FSAA dissolved in CDCl$_3$ solvent and the expanded regions for each resonance showing the scalar multiplicity.*

Table II.2: *Comparsion of $^{n}J_{CC}$ derived from solid-state and solution-state NMR for different spin pairs of ^{13}C$_5$-FSAA.*

Spin-Pair	J_{CC} derived from solid-state NMR [Hz]	J_{CC} derived from solution-state NMR [Hz]
C1-C2	72.1	71.2
C2-C3	34.1	34.1
C3-C4	43.9	41.6
C4-C5	33.9	33.1
C1-C5	8.2	5.9

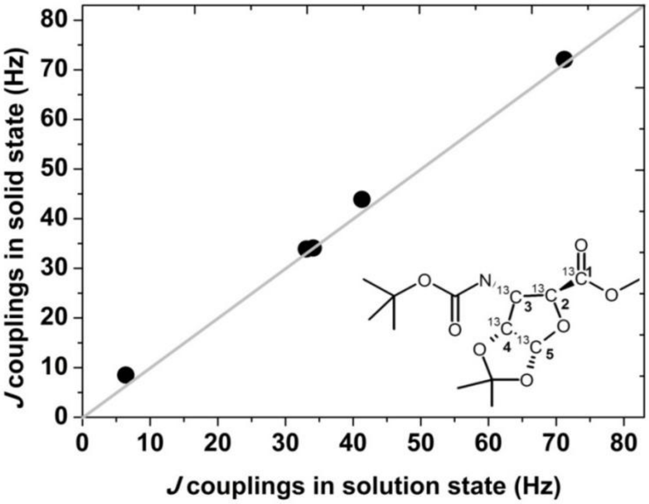

Figure II.10: *Correlation between $^{n}J_{CC}$ derived from solution-state and solid-state NMR for different spin-pairs of ^{13}C$_5$-FSAA molecule.*

II.4.1.2. *Hadamard encoded double frequency selective spin-echoes for different spin pairs in $^{13}C_6$ L-Histidine.HCl*

Figure II.11 depicts the staked Hadamard encoded refocusing spectra recorded initially in double frequency selective mode for different spin pairs of $^{13}C_6$ L-Histidine.HCl molecule. In Histidine.HCl molecule, total four selective $^1J_{CC}$ coupling constants are measured between C1-C4, C4-C3, C3-C5 and C5-C6 spin pairs (Figure II.12). Furthermore, Hadamard encoded selective spin-echo modulations for the long-range spin pairs such as C1-C2 and C2-C4 are also recorded and the corresponding spin-echo modulations resemble the pure exponential decays. The results are in good agreement with the solution-state $^nJ_{CC}$ (Figure II.13).

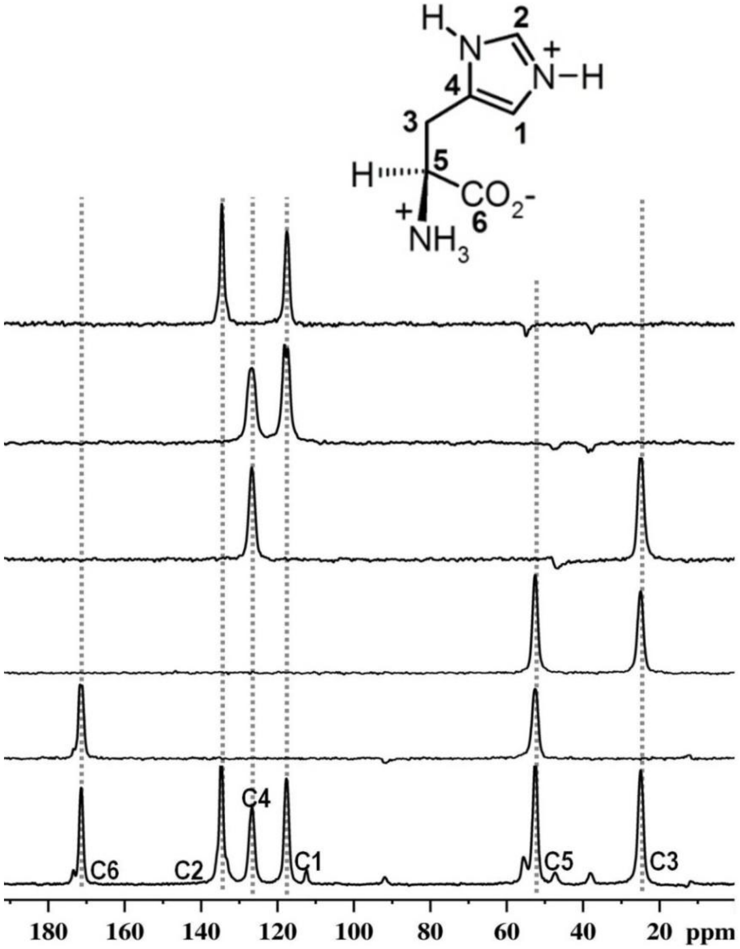

Figure II. 11: *Stacked ^{13}C-CPMAS and Hadamard encoded double selective refocuing spectra for different spin-pairs of $^{13}C_6$ L-Histidine.HCl at $\tau/2=0$.*

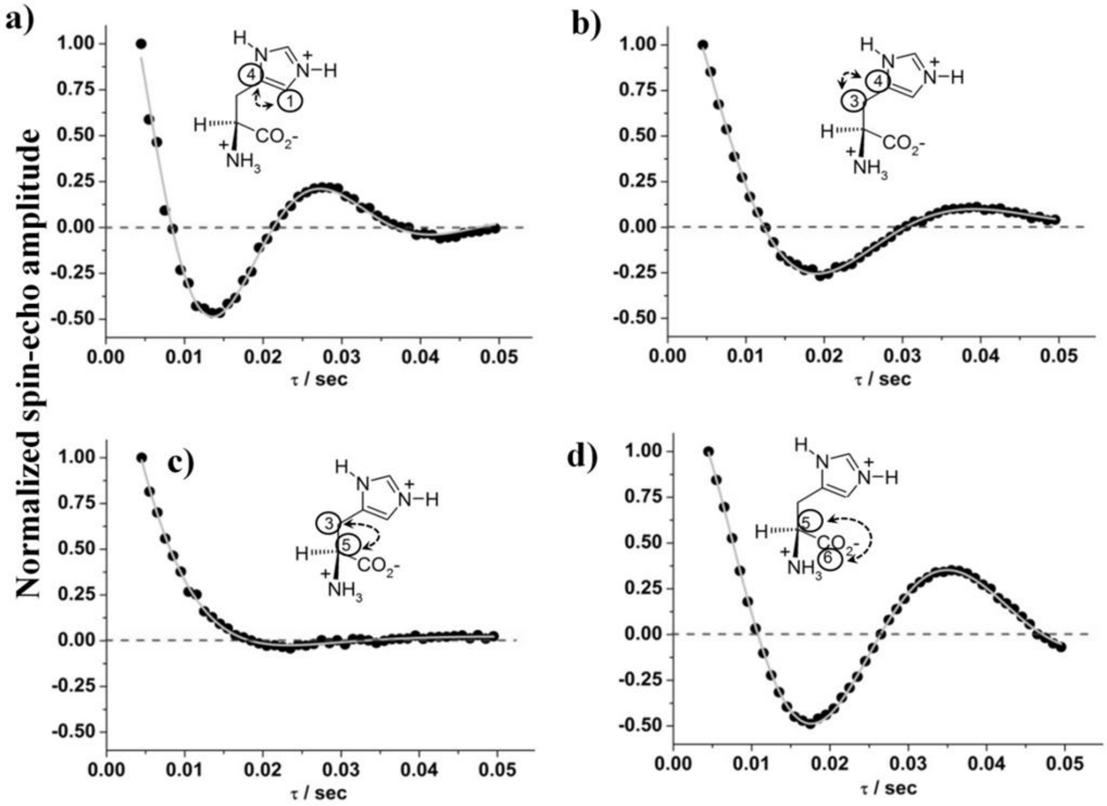

__Figure II.12:__ Hadamard encoded double selective spin-echo modulations for different spin pairs of $^{13}C_6$ L-Histidine.HCl: (a), (b), (c) and (d) corresponds to the C1-C4, C4-C3, C3-C5 and C5-C6 spin-echo modulations. The experimental data and best fits to the equation-1 are shown in black circles and the grey line, respectively.

__Table II.3:__ Comparsion of $^{n}J_{CC}$ derived from solid-state and solution-state NMR for different spin pairs of $^{13}C_6$-Histidine.HCl.

Spin-Pair	**J_{CC} derived from solid-state NMR [Hz]**	**J_{CC} derived from solution-state NMR [Hz][20]**
C5-C6	57.0±0.4	59.8
C3-C5	32.0±0.5	34.6
C3-C4	48.4±1.0	51.0
C4-C1	72.7±0.5	74.5
C1-C2	0.0	0.0
C2-C4	0.0	0.0

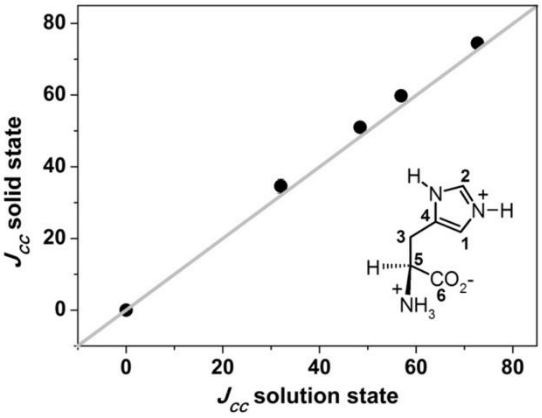

Figure II.13: *Correlation between* $^{n}J_{CC}$ *derived from solution-state and solid-state NMR for different spin-pairs of* $^{13}C_6$ *L-Histidine.HCl molecule.*

II.4.1.3. *Hadamard encoded double frequency selective spin-echoes for different spin pairs in* $^{13}C_8$*-SA*

Figure II.14 represents the staked Hadamard encoded refocusing spectra recorded in the double selective mode for different spin pairs of $^{13}C_8$-SA molecule. In this molecule also, with the support of a double selective refocusing mode, total six $^{1}J_{CC}$ coupling constants are measured between directly bonded carbons (Figure II.15). No other long range $^{n}J_{CC}$ is measured and the results are in good agreement with the $^{1}J_{CC}$ derived from the solution-state NMR (Figure II.17).

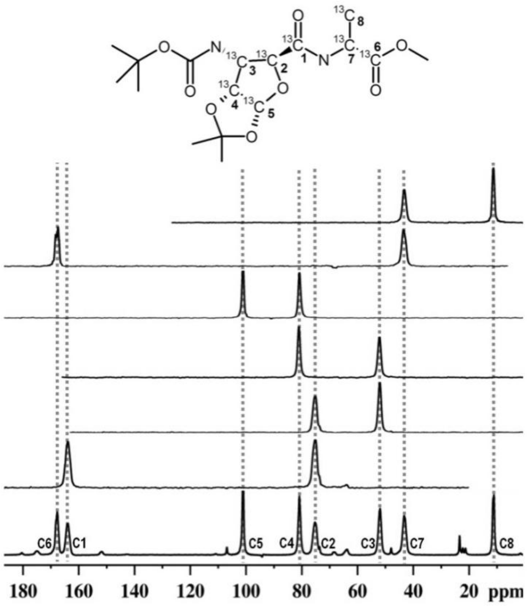

Figure II.14: *Stacked* ^{13}*C-CPMAS and Hadamard encoded double selective refocuing spectra for different spin-pairs of* $^{13}C_8$ *SA at* $\tau/2=0$.

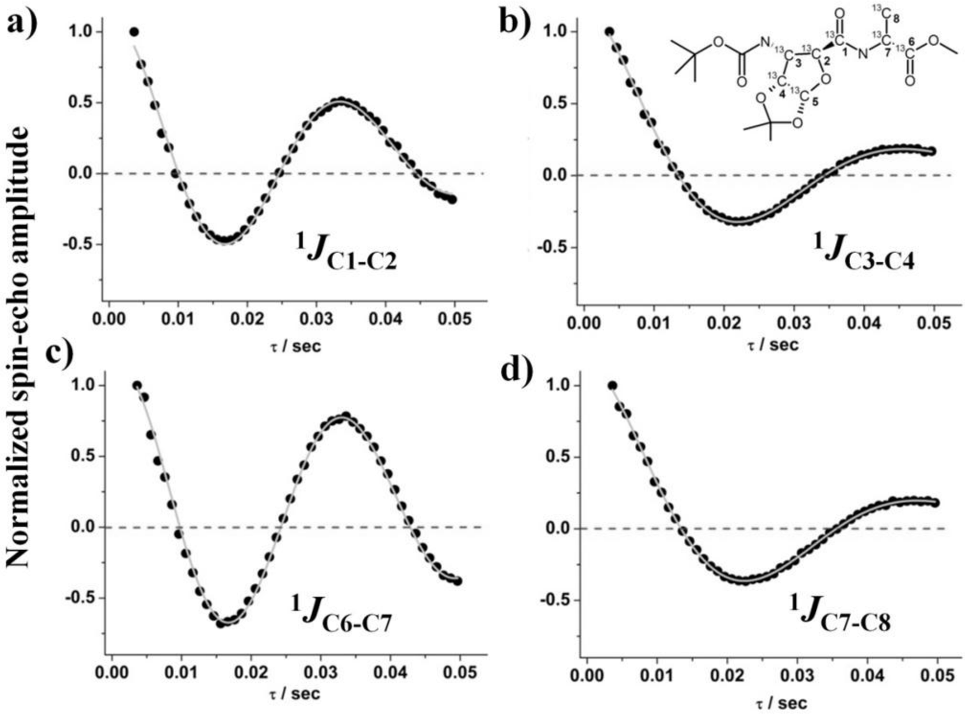

Figure II.15: *Hadamard encoded double selective spin-echo modulations for different spin pairs of $^{13}C_8$-SA: (a), (b), (c) and (d) corresponds to the C1-C2, C3-C4, C6-C7 and C7-C8 spin-echo modulations. The experimental data and best fits to the equation-1 are shown in black circles and grey lines, respectively.*

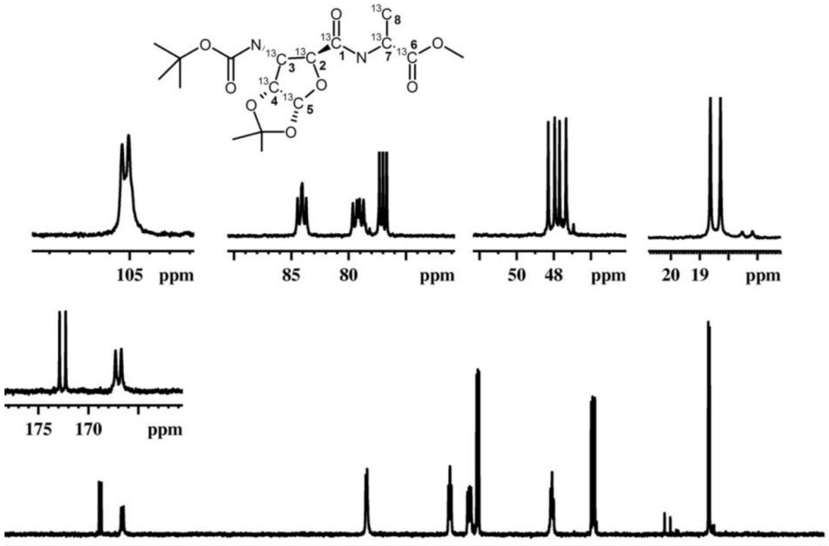

Figure II.16: *Solution-state ^{13}C spectrum of $^{13}C_8$-SA dissolved in $CDCl_3$ solvent and insets are the expanded regions.*

Table II.4: *Comparsion of* $^{n}J_{CC}$ *derived from solid-state and solution-state NMR for different spin pairs of* $^{13}C_8$*-SA molecule.*

Spin-Pair	J_{CC} derived from solid-state NMR [Hz]	J_{CC} derived from solution-state NMR [Hz]
C1-C2	60.3	60.7
C2-C3	35.4	36.9
C3-C4	42.4	42.6
C4-C5	34.7	33.3
C6-C7	61.6	62.0
C7-C8	41.4	34.8

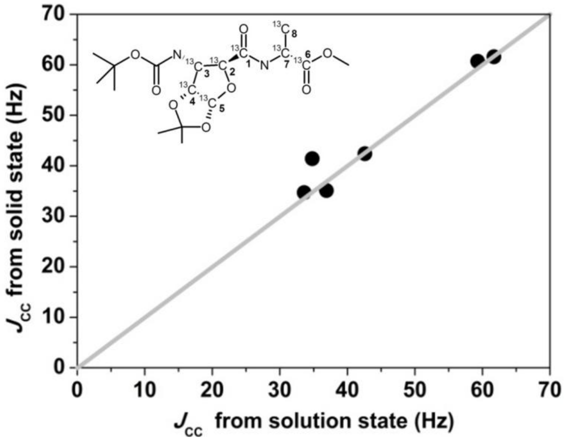

Figure II.17: *Correlation between* $^{n}J_{CC}$ *derived from solution-state and solid-state NMR for different spin-pairs of* $^{13}C_8$*-SA molecule.*

II.4.2. *Hadamard encoded multiple frequency selective spin-echoes for simultaneous measurement of scalar couplings*

In the previous section the concept of Hadamard NMR spectroscopy for measuring the scalar couplings in solid-state has been demonstrated. However, the demonstrations were limited only to the selection of two frequencies at-a-time, so that one spin-pair can only be selected in each experiment. This is analogous to the conventional double frequency selective refocusing experiments. Such experiments are repeated for each spin pair. Herein, Hadamard encoded refocusing strategy has been extended for the multiple selective spin-echoes, thereby multiple number of scalar couplings are measured in a single spin-echo experiment (directly bonded as well as long range) by creating commutation spin-spin property between interested spin pairs.

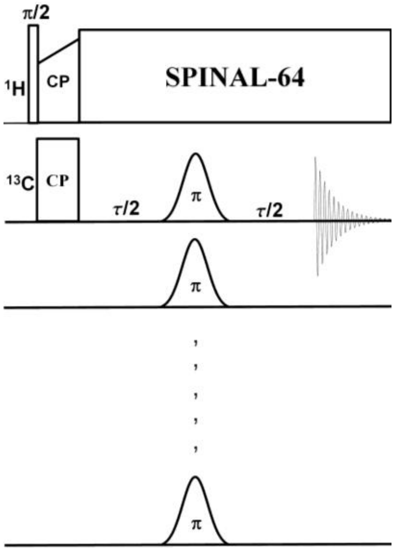

Figure II.18: *Schematic represenation of Hadamard encoded spin-echo pulse sequence in multiple frequency selective refocusing mode.*

Similar processing and fitting procedures as stated above, have been repeated for the directly bonded spin pairs. However, for long range couplings, the normalized spin-echo modulations with respect to the corresponding isolated spin-echo evolution (**So)** are used for the analysis, which removes the dominant spin-spin relaxation part of the echo-modualtion. This implies that the *J*-modulated signal amplitudes **S** are obtained in multiple frequency selective refocusing modes, while the reference signal amplitudes **So** are obtained for individual resonances (corresponding to the long-range spin-pair) in single frequency selective refocusing mode.[6]

$$S \propto \cos(\pi J\tau)\exp(T_2/\tau)$$

$$So \propto \exp(T_2/\tau)$$

$$S(\tau) = S/So \propto \cos(\pi J\tau) \rightarrow (2)$$

II.4.2.1. *Hadamard encoded multiple frequency selective spin-echoes for different spin combinations in $^{13}C_5$-FSAA*

As a first application, Hadamard encoded multiple selective refocusing experiments have been demonstrated on $^{13}C_5$-FSAA molecule and measured, two scalar couplings in a single experiment. The spin combinations C1-C2-C3, C2-C3-C4, C3-C4-C5 and C1-C4-C5 are selected for the simultaneous refocusing (Figure II.19). For the C1-C2-C3 spin combination, C1, C2 and C3 spins are selectively refocused with the help of three Hadamard encoded soft Gaussian π pulses. Herein, C2 is the common spin for both C1 and C3. Thus, $J_{C2\text{-}C3}$ and $J_{C1\text{-}C2}$ are measured from the spin-echo modulations of C1 and C3, respectively. The same procedure has been repeated for the other spin combinations C2-C3-C4 and C3-C4-C5 also, except for C1-C4-C5 (Figure II.20).

In the case of C1-C4-C5 selective spin combination, C5 is the common spin for both C1 and C4. Thus, the long range $^{3}J_{C1\text{-}C5}$ is measured by generating S/So modulation of C1. About 50 ms of spin-echo evolution time is sufficient to measure the long range J_{CC} (Figure II.21) accurately. The measured $^{3}J_{C1\text{-}C5}$ in solid-state is equal to 6.2 Hz and is in well agreement with the solution-state value (5.9Hz). Whereas, the normal spin-echo modulation demands the evolution time of 100 ms for the measurement of long range (smaller) scalar couplings. Therefore, the double frequency selective spin-echo modulation of $^{3}J_{C1\text{-}C5}$ needs a longer duration of spin-echo evolution time to observe the clear the zero-crossing and yielded the scalar coupling value of 8.4 Hz. On the other hand, the regular spin-echo modulation for C4 has directly yielded the $^{1}J_{C4\text{-}C5}$. Due to the maximum coupling value, a clear zero crossing is observed at a short spin-echo evolution time itself. Thus, for the directly bonded spins, it may not be required, collecting two sets of spin-echo modulation data sets, S and So.

Later Hadamard-encoded frequency selective refocusing pulse scheme is extended for a four spin combination C1-C2-C4-C5. Herein, C1 is the common spin for both C2 and C5. Thus, C2 and C4 spin-echo modulations are considered for the measurement of ${}^{1}J_{C1\text{-}C2}$ and ${}^{1}J_{C4\text{-}C5}$, respectively. All these measured scalar coupling values are in good aggrement with those derived from the double frequency selective refocusing modes (Figure II.22).

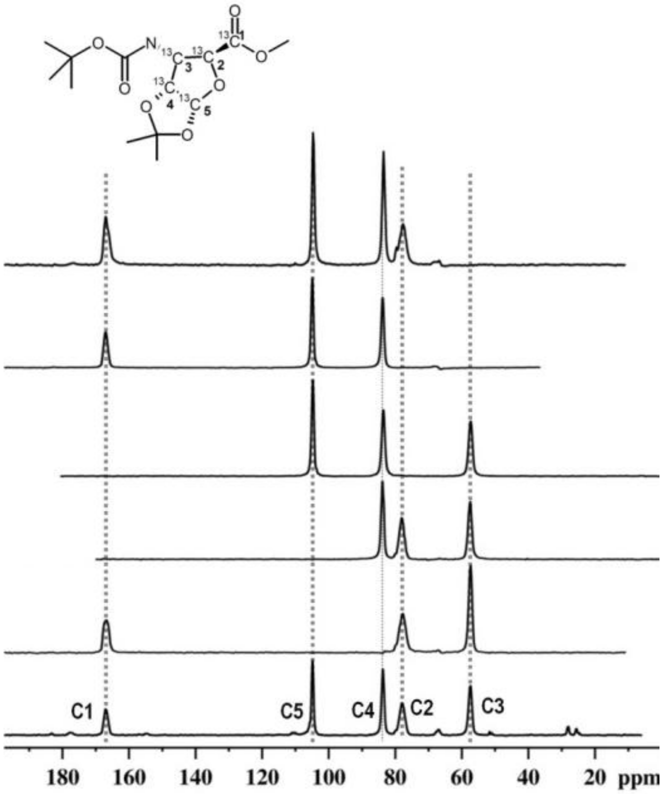

Figure II.19: *Conventional full* ^{13}*C-CPMAS and Hadamard encoded multiple selective refocusing spectra for different spin-pairs of* ${}^{13}C_5$ *FSAA at* $\tau/2=0$.

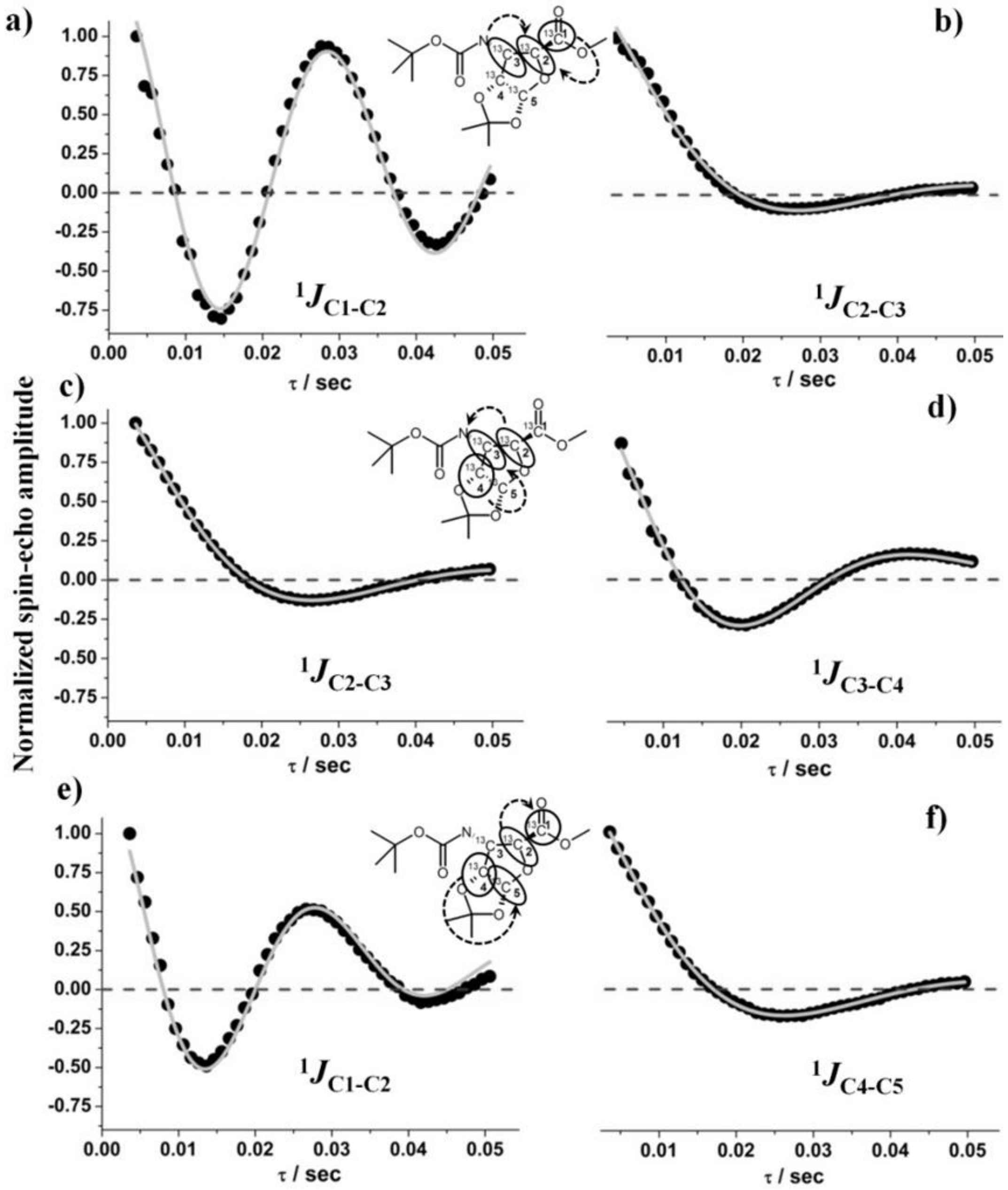

Figure II.20: *Comparison of spin-echo modulations for the different spin pairs of $^{13}C_5$-FSAA, which are recorded in Hadamard encoded multiple selective refocusing modes. The spin-echo modulations of C1 (a) and C3 (b) have yielded the $^1J_{C1-C2}$ and $^1J_{C2-C3}$, respectively, during the encoding of C1-C2-C3 spins. Similarly C2 (c) and C4 (d) spin-echo modulations are resulted in $^1J_{C2-C3}$ and $^1J_{C3-C4}$ scalar couplings, respectively, when refocusing of C2-C3-C4 spins. Whereas, four spins C1-C2-C4-C4 are refocused and the resultant C2 and C4 spin-echo modulations correspond to the $^1J_{C1-C2}$ and $^1J_{C4-C5}$ scalar couplings.*

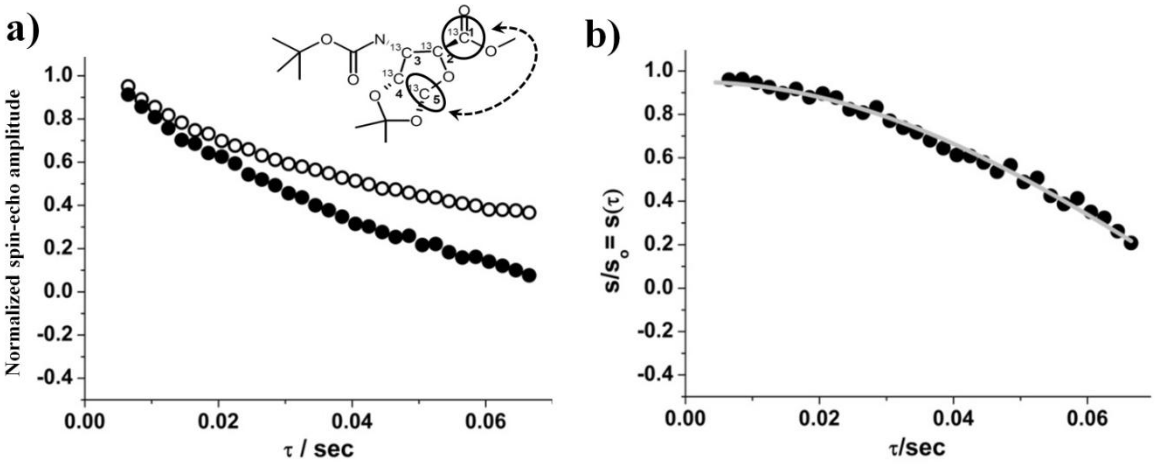

Figure II.21: Spin-echo modulations of C1 in C1-C4-C5 (**S**, closed circles) spin-combination and only the selection of C1 (**So**, open circles) (a). The **S/So** modulation of C1 results in the pure J-modulation component (b).

Table II.5: Comparsion between $^nJ_{CC}$ derived from the solution-state and Hadamard encoded multiple selective spin-echoes in the solid-state for different spin pairs of $^{13}C_5$-FSAA.

Selected spin combination	Spin pair and Scalar coupling		Spin pair and Scalar coupling	
	Observed spin	Solid-state J_{CC} (Solution-State J_{CC}) in Hz	Observed spin	Solid-state J_{CC} (Solution-State J_{CC}) in Hz
C1-C2-C3	C1 for $^1J_{C1-C2}$	70.6 (71.2)	C3 for $^1J_{C2-C3}$	34.8 (34.1)
C2-C3-C4	C2 for $^1J_{C2-C3}$	34.2 (34.1)	C4 for $^1J_{C3-C4}$	44.0 (41.3)
C3-C4-C5	C3 for $^1J_{C3-C4}$	43.9 (41.3)	C5 for $^1J_{C4-C5}$	33.0 (33.1)
C1-C2-C4-C5	C2 for $^1J_{C1-C2}$	70.0 (71.2)	C4 for $^1J_{C4-C5}$	32.4 (33.1)
C1-C4-C5	C1 for $^1J_{C1-C5}$	6.2 (5.9)	C4 for $^1J_{C4-C5}$	33.1 (33.1)

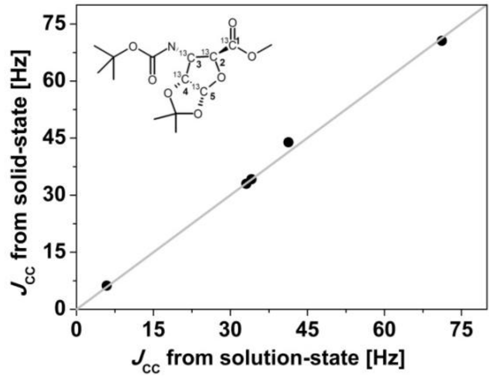

Figure II.22: Correlation between scalar couplings derived from solution-state and Hadamard encoded multiple frequency selective refocusing modes (solid-state) for different spin pairs of $^{13}C_5$-FSAA molecules.

II.4.2.2. *Hadamard encoded multiple frequency selective spin-echoes for different spin combinations in $^{13}C_6$ L-Histidine.HCl*

Hadamard encoded multiple frequency selective refocusing experiments have been repeated for different spin combinations of $^{13}C_6$ L-Histidine.HCl molecule and in a single experiment two scalar couplings are measured (either one directly bonded + one long range or two directly bonded). The spin combinations C1-C4-C3, C1-C2-C4, C3-C4-C5, C3-C5-C6, C1-C4-C5-C6 and C2-C3-C5-C6 are selected for the multiple refocusing modes (Figure II.23). In the case of C1-C4-C3 spin combination C1, C4 and C3 spins are selectively simultaneously refocused with the help of Hadamard encoded Gaussian π pulses, where C4 is the common spin for both C1 and C3. Thus, $^1J_{C3\text{-}C4}$ and $^1J_{C1\text{-}C4}$ are measured from the spin-echo modulations of C3 and C1, respectively. The same procedure has been repeated for the remaining three spin combinations such as C1-C2-C4, C4-C3-C5 and C3-C5-C6. Furthermore, in C1-C4-C5-C6 selective spin combination the C1, C4, C5 and C6 spins are selectively refocused with the help of four Hadmard encoded Gaussian π pulses. In this selection, no common spin is available, hence either the C1 or C4 spin-echo modulations can be considered for the $^1J_{C1\text{-}C4}$. Similarly $^1J_{C5\text{-}C6}$ is also measured (Figure II.24).

However, in C2-C3-C5-C6 selective spin combination, C5 is the common spin for C6 and C3, whereas C3 is the common spin for C2 and C5. Herein, $^1J_{C5\text{-}C6}$ is measured from the spin-echo modulation of C6. Furthermore, a long range $^3J_{C2\text{-}C3}$ is measured by generating S/So modulation for C2. The individual S and So spin-echo modulations for C2 resemble pure exponential decays, whereas the S/So results in the *J*-modulation component (Figure II.25). The corresponding $^3J_{C2\text{-}C3}$ (4.4 Hz) is in good agreement with 4.0 Hz, reported recently[6] (Figure II.26).

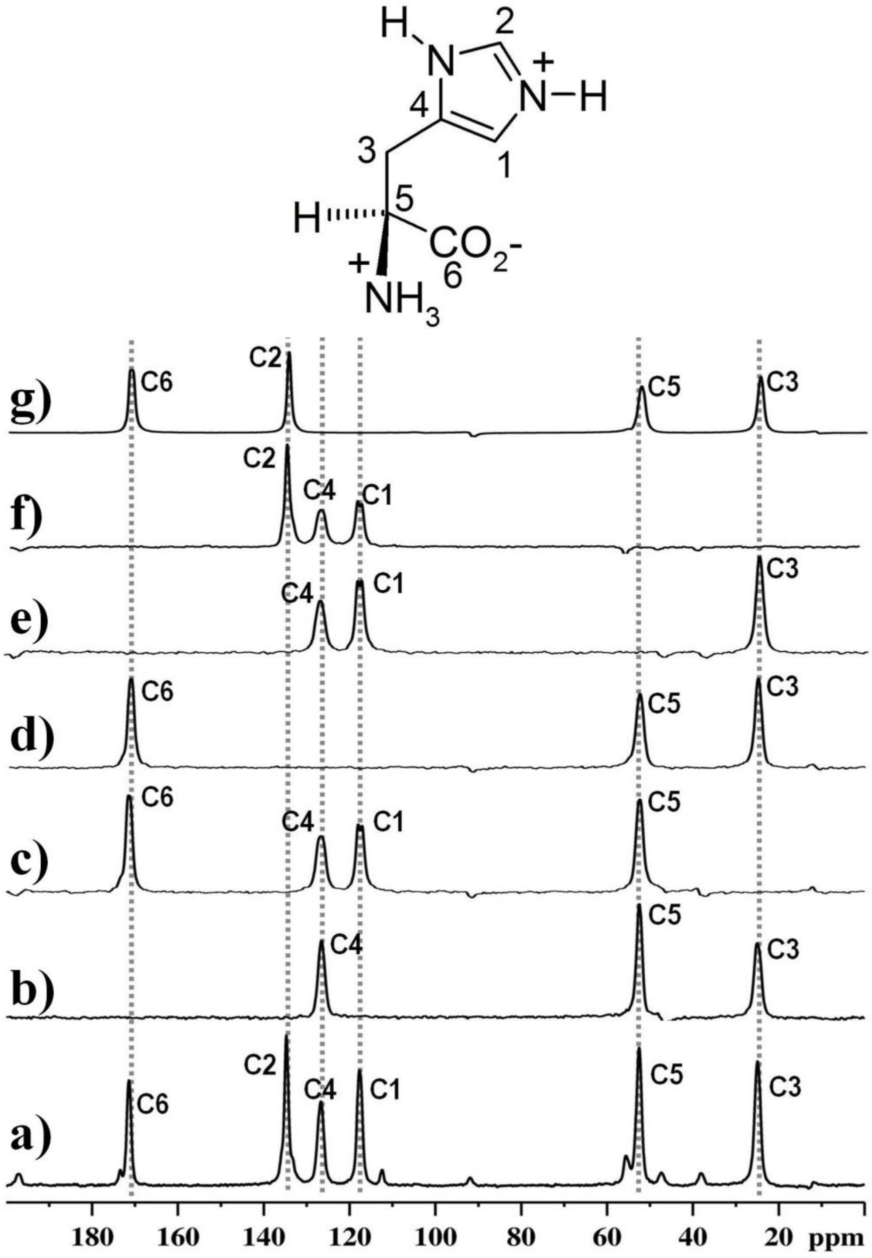

Figure II.23: *Convetnional full ^{13}C-CPMAS and the Hadamard encoded multiple selective refocuing spectra for different spin-combinations of $^{13}C_6$ Histidine.HCl recorded at $\tau/2=0$.*

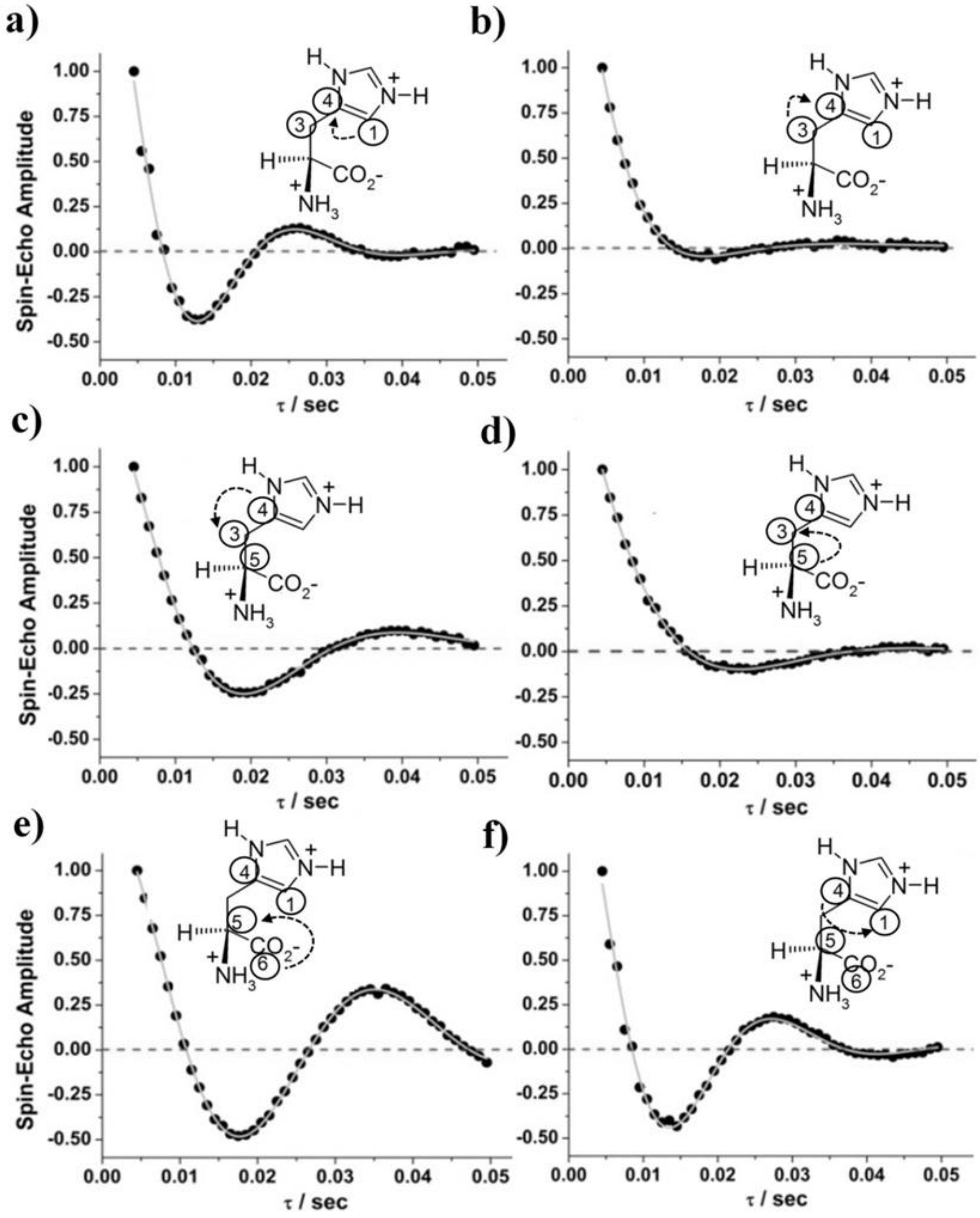

Figure II.24: *Comparison of spin-echo modulations for different spin pairs of* $^{13}C_6$ *L-Histidine.HCl, which are recorded in Hadamard encoded multiple selective refocusing modes. By encoding the C1-C4-C3 spin combination for refocusing, the spin-echo modulations C1 (a) and C3 (b) have yielded the* $^1J_{C1\text{-}C4}$ *and* $^1J_{C4\text{-}C3}$*, respectively. Similarly,* $^1J_{C3\text{-}C4}$ *(c) and* $^1J_{C3\text{-}C5}$ *(d) are measured from the selection of C4-C3-C5 spin combination. Whereas, four spins C1-C4-C5-C6 are refocused and the* $^1J_{C5\text{-}C6}$ *and* $^1J_{C1\text{-}C4}$ *scalar couplings are measured from the corresponding spin-echo modulations C6 (e) and C4 (f).*

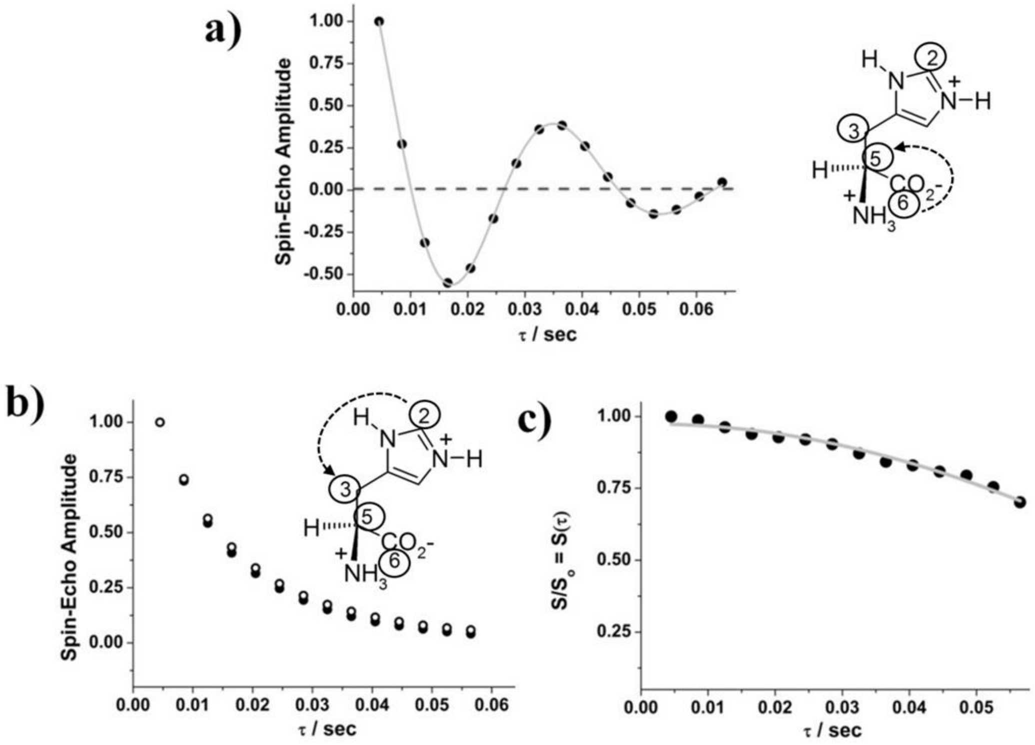

Figure II.25: *Hadamard encoded spin-echo modulations of C6 and C2 spins while encoding the C2-C3-C5-C6 spin combination for refocusing. Herein, the spin-echo modulation of C6 (a) has yielded the* $^1J_{C5\text{-}C6}$*. Whereas, the spin-echo modulations are compared for C2, when in the combined selection of C2-C3-C5-C6 (S, •) and for the selection of C2 alone (So, o) (b). The S/So modulation of C2 is resulted in the pure frequency component,* $^1J_{C2\text{-}C3}$ *(c).*

Table II.6: *Comparsion of* $^nJ_{CC}$ *derived from solution-state and Hadamard encoded multiple selective spin-echoes in solid-state for different spin pairs of* $^{13}C_6$*-Histidine.HCl.*

Selected spin combination	**Spin pair and Scalar coupling**		**Spin pair and Scalar coupling**	
	Observed spin	**Solid-state J_{CC} (solution-state J_{CC}) in**	**Observed spin**	**Solid-state J_{CC} (solution-state J_{CC})**
C1-C4-C3	C1 for $^1J_{C1\text{-}C4}$	75.4 (74.5)	C3 for $^1J_{C4\text{-}C3}$	48.9 (51.0)
C1-C2-C4	C1 for $^1J_{C1\text{-}C4}$	73.0 (74.5)	C2 for $^1J_{C1\text{-}C2}$	0.0 (0.0)
C3-C4-C5	C4 for $^1J_{C3\text{-}C4}$	48.4(51.0)	C5 for $^1J_{C3\text{-}C5}$	35.4 (34.6)
C3-C5-C6	C3 for $^1J_{C3\text{-}C5}$	33.4 (34.6)	C6 for $^1J_{C5\text{-}C6}$	56.8 (59.8)
C1-C4-C5-C6	C1 for $^1J_{C1\text{-}C4}$	72.3 (74.5)	C6 for $^1J^{C5\text{-}C6}$	56.9 (59.8)
C2-C3-C5-C6	C6 for $^1J_{C5\text{-}C6}$	55.2 (59.8)	C2 for $^3J_{C2\text{-}C3}$	4.4 (4.0)

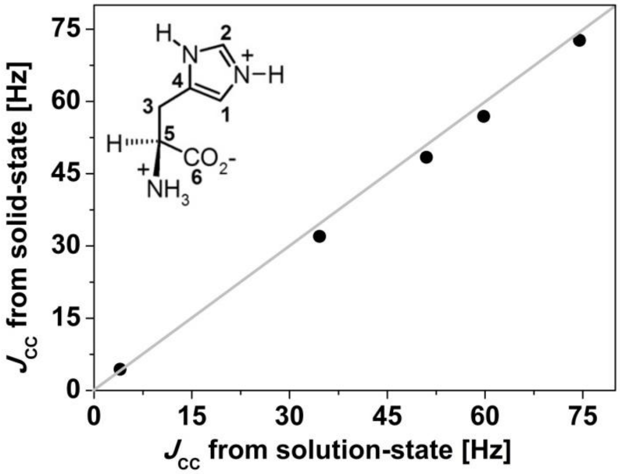

Figure II.26: *Correlation between scalar couplings derived from solution-state and Hadamard encoded multiple frequency selective refocusing modes (solid-state) for different spin pairs of* $^{13}C_6$ *L-Histidine.HCl.*

II.4.2.3. *Hadamard encoded multiple frequency selective spin-echoes for different spin combinations in* $^{13}C_8$*-SA*

Hadamard encoded simultaneous multiple frequency selective refocusing experiments have been repeated for different spin combinations (C1-C2-C3-C7-C8, C3-C4-C5-C7-C8, C4-C5-C6-C7-C8 and C1-C2-C4-C5-C7-C8) of $^{13}C_8$-SA (Figure II.27). Furthermore, in a single experiment three scalar couplings are measured. For C1-C2-C4-C5-C7-C8 spin combination, the corresponding six Hadamard encoded Gaussian shaped π pulses are used for the selective refocusing of these resonances and there is no common scalarly coupled spin is available. Therefore, $^1J_{C1\text{-}C2}$ is measured from either C1 or C2 spin-echo modulation, and the same procedure is repeated for the $^1J_{C3\text{-}C4}$ and $^1J_{C7\text{-}C8}$ couplings as well (Figure II.28).

Nevertheless, in the case of C1-C2-C3-C7-C8, total five spins are selectively refocused with the five Hadamard encoded Gaussian pulses. Herein, C2 is the common spin of C1 and C3. Therefore, C1 and C3 spin-echo modulations are considered for $^1J_{C1\text{-}C2}$ and $^1J_{C2\text{-}C3}$, respectively. The remaining $^1J_{C7\text{-}C8}$ is measured from either C7 or C8 spin-echo modulations (Figure II.28). The measured scalar couplings are in good agreement with those derived from the double frequency selective refocusing modes (Figure II.29).

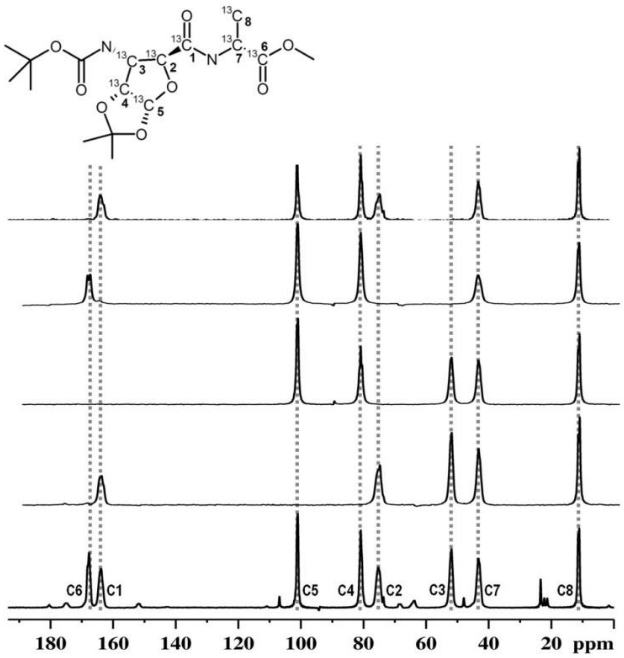

Figure II.27: *Convetnional full ^{13}C-CPMAS and the Hadamard encoded multiple selective refocuing spectra for different spin combinations of ^{13}C8-SA recorded at $\tau/2=0$.*

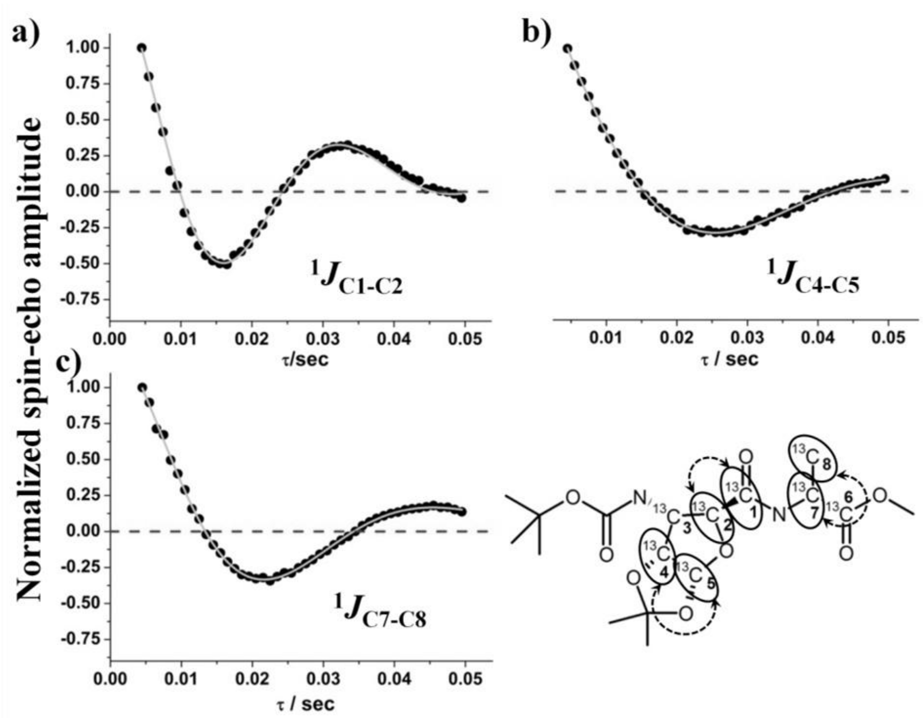

Figure II.28: *Hadamard encoded spin-echo modulations for different spin pairs of $^{13}C_8$-SA, which are recorded in multiple refocusing modes. By encoding the C1-C2-C4-C5-C7-C8 spin combination, the spin-echo modulations for C1 (a), C4 (b) and C7 (c) have yeilded the $^1J_{C1-C2}$, $^1J_{C4-C5}$ and $^1J_{C7-C8}$, respectively.*

Table II.7: *Comparsion of* $^{n}J_{CC}$ *derived from solution-state and Hadamard encoded multiple selective spin-echoes in the solid-state for different spin pairs of* $^{13}C_8$*-SA*

Selected spin combination	Spin pair and Scalar coupling		Spin pair and Scalar coupling		Spin pair and Scalar coupling	
	Observed spin	**Solid-state J_{CC} (Solution-state J_{CC}) in Hz**	**Observed spin**	**Solid-state J_{CC} (Solution-state J_{CC}) in Hz**	**Observed spin**	**Solid-state J_{CC} (Solution-state J_{CC}) in Hz**
C1-C2-C3-C7-C8	C1 for $^{1}J_{C1-C2}$	61.4 (60.7)	C3 for $^{1}J_{C2-C3}$	35.4 (36.9)	C8 for $^{1}J_{C7-C8}$	42.0 (34.8)
C3-C4-C5-C7-C8	C3 for $^{1}J_{C3-C4}$	43.1 (42.6)	C5 for $^{1}J_{C4-C5}$	35.6 (33.3)	C8 for $^{1}J_{C7-C8}$	42.4 (34.8)
C4-C5-C6-C7-C8	C5 for $^{1}J_{C4-C5}$	35.0 (33.3)	C6 for $^{1}J_{C6-C7}$	61.9 (61.7)	C8 for $^{1}J_{C7-C8}$	41.5 (34.8)
C1-C2-C4-C5-C7-C8	C1 for $^{1}J_{C1-C2}$	61.5 (60.7)	C5 for $^{1}J_{C4-C5}$	36.1 (33.3)	C8 for $^{1}J_{C7-C8}$	42.6 (34.8)

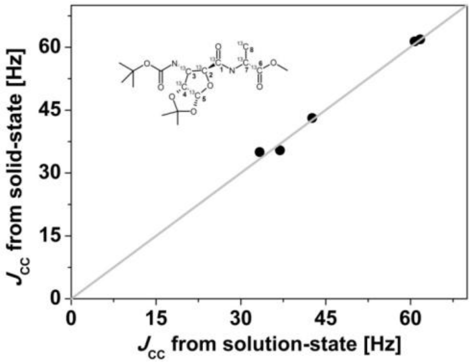

Figure II.29: *Correlation between scalar couplings derived from solution-state and Hadamard encoded multiple frequency selective refocusing modes (solid-state) for different spin pairs of* $^{13}C_8$*-SA molecule.*

II.5. Conclusions

Chapter-II introduces a conceptually different approach, Hadamard encoded refocusing for measuring multiple ^{13}C-^{13}C scalar couplings in solid-state has been demonstrated for uniformly ^{13}C labelled spin systems in a single experiment. The novel approach facilitates an efficient way to record multiple spin-spin scalar couplings and also dipolar couplings (as shown in the chapter-v). Unlike the conventional methods, the demonstarted technique does not require (1) the experiments to be repeated for each spin pair present in the molecule, and (2) a set of specially synthesized $^{13}C_2$ labelled molecules.

Furthermore, the observed results are in well agreement with those obtained from solution-state NMR. The same methodology has been extended to the two-dimensional NMR experiments as well (shown in chapter-iii and iv), which can be extended to the 3D NMR methods for refocusing the required selective resonance bands to edit the *J*-couplings information.

II.6. References

[1] S. Cadars, A. Lesage, N. Hedin, B. F. Chmelka and L. Emsley, Selective NMR Measurements of Homonuclear Scalar Couplings in Isotopically Enriched Solids, J. Phys. Chem. B, 110 *(*2006) 16982-16991.

[2] L. Duma, W. C. Lai, M. Carravetta, L. Emsley, S. P. Brown and M. H. Levitt, Principles of Spin-Echo Modulation by J-Couplings in Magic-Angle-Spinning Solid-State NMR, Chem. Phys. Chem, 5 (2004) 815-833.

[3] W. C. Lai, N. McLean, A. Gansmuller, M. A. Verhoeven, G. C. Antonioli, M. Carravetta, L. Duma, P. H. M. Bovee-Geurts, O. G. Johannessen, H. J. M. de Groot, J. Lugtenburg, L. Emsley, S. P. Brown, R. C. D. Brown, W. J. DeGrip and M. H. Levitt, Accurate Measurements of ^{13}C-^{13}C J-Couplings in the Rhodopsin Chromophore by Double-Quantum Solid-State NMR Spectroscopy, J. Am. Chem. Soc, 128 (2006) 3878-3879.

[4] G. Pileio, Y. Guo, T. N. Pham, J. M. Griffin, M. H. Levitt and S. P. Brown, Residual Dipolar Couplings by Off-Magic-Angle Spinning in Solid-State Nuclear Magnetic Resonance Spectroscopy, J. Am. Chem. Soc, 129 (2007) 10972–10973.

[5] G. Pileio, S. Mamone, G. Mollica, I. M. Montesinos, A. Gansmuller, M. Carravetta, S. P. Brown and M. H. Levitt, Estimation of internuclear couplings in the solid-state NMR of multiple-spin systems. Selective spin echoes and off-magic-angle sample spinning, Chem. Phys. Lett, 456 (2008) 116–121.

[6] P. Thureau, G. Mollica, F. Ziarelli and S. Viel, Selective measurements of long-range homonuclear *J*-couplings in solid-state NMR, J. Magn. Reson, 231 (2013) 90-94.

[7] E. Kupce and R. Freeman, Frequency-domain Hadamard spectroscopy, J. Magn. Reson, 162 (2003) 158–165.

[8] E. Kupce, T. Nishida and R. Freeman, Hadamard NMR spectroscopy, Prog. Nucl. Magn. Reson. Spec, 42 (2003) 95–122.

[9] E. Kupce and R. Freeman, Two-dimensional Hadamard spectroscopy, J. Magn. Reson, 162 (2003) 300–310.

[10] E. Kupce and R. Freeman, Molecular structure from a single NMR sequence (fast-PANACEA), J. Magn. Reson, 206 (2010) 147–153.

[11] E. Kupce and R. Freeman, Fast multi-dimensional NMR of proteins, J. Biomol. NMR, 25 (2003) 349–354.

[12] C. A. Steinbeck and B. F. Chmelka, Rapid 1H{13C}-Resolved Diffusion and Spin-Relaxation Measurements by NMR Spectroscopy, J. Am. Chem. Soc, 127 (2005) 11624-11635.

[13] S. P. Viel and S. Caldarelli, Improved 3D DOSY-TOCSY experiment for mixture analysis, Chem. Commun, 17 (2008) 2013-2015.

[14] C. H. Cunningham and M. L. Wood, Method for Improved Multiband Excitation Profiles Using the Shinnar–Le Roux Transform, Magn. Reson. Med, 42 (1999) 577–584.

[15] J. Ashida, E. Kupce and J. P. Amoureux, Hadamard NMR spectroscopy in solids, J. Magn. Reson, 178 (2006) 129–135.

[16] T. Gopinath, K. R. Mote and G. Veglia, Proton Evolved Local Field Solid-State Nuclear Magnetic Resonance using Hadamard Encoding: Theory and Application to Membrane Proteins, J. Chem. Phys, 135 (2011) 1-8.

[17] M. Greferath, B. Blumich, W.M. Griffith and G.L. Hoatson, Saturation in Deuteron Hadamard NMR Spectroscopy of Solids, J. Magn. Reson, 102 (1993) 73-80.

[18] S. C. sekhar, M. S. Reddy, B. Jagadeesh, A. Prabhakar, M. H. V. R. Rao and B. Jagannadh, Formation of a Stable 14-Helix in Short Oligomers of Furanoid *cis*-β-Sugar-Amino Acid, J. Am. Chem. Soc, 126 (2004) 13586–13587.

[19] M. Hohwy, C. M. Rienstra, C. P. Jaroniec and R. G. Griffin, Fivefold symmetric homonuclear dipolar recoupling in rotating solids, J. Chem. Phys, 110 (1999) 7983-7992.

[20] S. T. Dinh, S. Fermandjian, E. Sala, R. M. Bouvier and P. Fromageot, Geminal and Vicinal ^{13}C-^{13}C Coupling Constants of 85% ^{13}C-Enriched Amino Acids, J. Am. Chem. Soc, 75 (1974) 1267-1269.

Chapter-III

Spectral simplifications in solid-state NMR

Two-dimensional Hadamard encoded NMR spectroscopy of uniformly spin-labelled organic solids: Simultaneous and accurate measurement of multiple scalar couplings

III.1. Introduction

In chapter-II, Hadamard encoded multiple selective spin-echo NMR methodologies in pseudo two-dimensional mode have been demonstrated for the simultaneous measurement of scalar couplings in uniformly labelled solids. The inconveniences involved in such pseudo selective spin-echo NMR method are i) it necessitates that for each spin-pair, the spin-echo integrations to be monitored as a function of evolution times and (ii) the performance of the selective spin-echo experiments are limited, when the chemical-shift resolution is poor. However, the pseudo two-dimensional method offers the basis for the subsequent development for more complex cases.

The present chapter aims to overcome these disadvantages, by adopting a novel combination of two-dimensional *J*-resolved solid-state NMR spectroscopy and Hadamard encoded spin-echoes. As the resolution along the indirect dimension is not sufficient to observe the well defined doublets, the adopted method features with *J*-scaling for enhanced resolution.

The *J*-scaling methodologies are well known in solution-state NMR and useful for the measurement of long-range scalar couplings in one, two-dimensional experiments.**[1-7]** However, *J*-scaling schemes are sparsely explored in solid-state NMR.**[8]** The present chapter deals with the development of two-dimensional spin-echo pulse sequences viz., (1) Z-filtered *J*-scaled spin-echo (ZFJSSE) and (2) Hadamard encoded Z-filtered *J*-scaled selective spin-echo (HEZFJSSSE) NMR experiments for accurate measurement of scalar couplings in isotopic ^{13}C labelled organic solids.

III.2. Materials

The *J*-scaled methodologies are demonstrated for ^{13}C labelled molecules: Boc protected unnatural β-amino acid monomer, Furanoid cis-*β*-Sugar-Amino Acid (FSAA) and dimer $^{13}C_8$-SA are shown in Figure III.1.

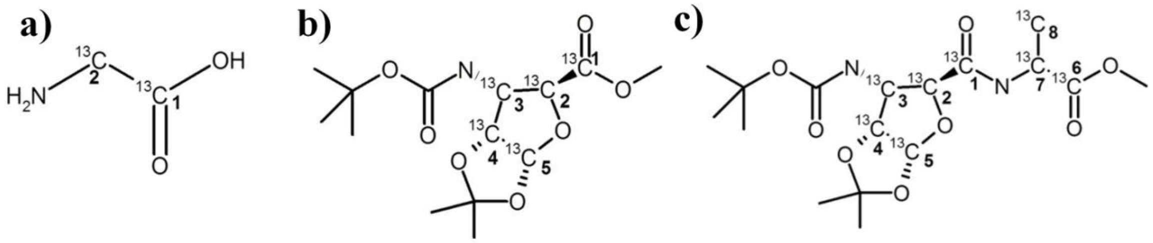

Figure III.1: *Schematic representation of molecular structures: (a)* $^{13}C_2$*-Glycine, (b) un-natural* $^{13}C_5$*-Furanoid cis-β-Sugar-Amino Acid (FSAA) and (c)* $^{13}C_8$*-SA. Numbering has been given only for the isotopic* ^{13}C *labelled carbons.*

III.3. Theoretical Background

III.3.1. *Conventional spin-echo pulse sequence*

Spin-echo experiment (Figure III.2) plays an important role for the suppression of inhomogeneous line broadening during the refocusing period and facilitates the measurement of *J*-couplings in the solid-state. The conventional pseudo 2D spin-echo experiment demands recording the peak integration as a function of spin-echo evolution time (Figure III.3), which results in cancellation of anti-phase components (I_xS_z and I_zS_x) (Figure III.3) of spin-echo modulation.

The spin-echo modulation terms for the homonuclear spins I and S may be written as

$$\mathbf{I_z + S_z \xrightarrow{90x-\tau/2-180y-\tau/2} -(I_y+S_y)\cos(\pi J_{IS}\tau) + (2I_xS_z+2I_zS_x)\sin(\pi J_{IS}\tau)}$$

Thus, the modulation of a pseudo two-dimensional spin-echo is in the pure cosine form (anti phase terms get cancelled).

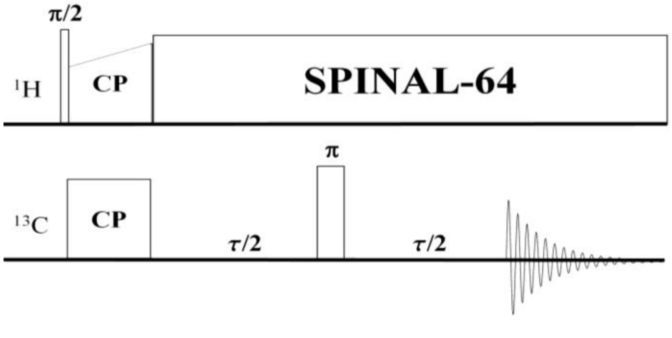

Figure III.2: *Schematic representation of basic spin-echo pulse sequence with cross-polarization block.*

However, a two-dimensional spin-echo experiment requires automated amplitude mode processing; thus the peak amplitude (both in-phase and anti-phase components together) needs to be taken into the account for processing. In general, it is appropriate to process the data in in-phase mode to measure the accurate J_{CC}.

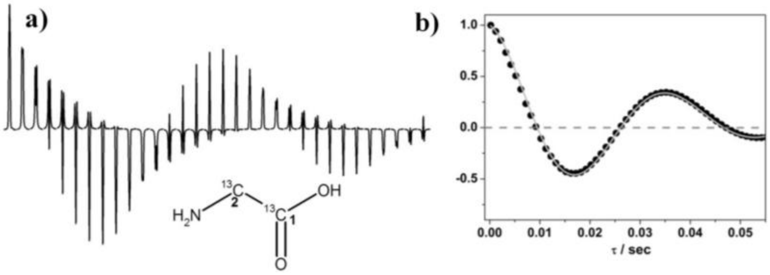

Figure III.3: *Spin-echo profile of $^{13}C_2$-Glycine as a function of τ and its integrated spin-echo modulations are shown in (a) and (b), respectively.*

III.3.2. *Z-filtered spin-echo pulse sequence (ZFSE)*

Figure III.4 depicts the conventional 2D Z-filtered pseudo spin-echo pulse sequence,[9] which results in complete in-phase as well as a pure cosine form of spin-echo modulation and the resultant product operator can be written as

$$\mathbf{I_z + S_z \xrightarrow{90x-\tau/2-180y-\tau/2-90y-zf-90y} -(I_y + S_y)\cos(\pi J_{IS}\tau)}$$

In two-dimensional version of ZFSE pulse sequence, spin-echo evolution takes place only through in-phase (I_y) term of magnetization, and it can simply be processed in phase-sensitive mode (Figure III.5). However, in the case of clustered spins, this approach may suffer from the spectral crowding/ poor resolution that hampers the measurement of *J*cc from the multiplicity patterns.

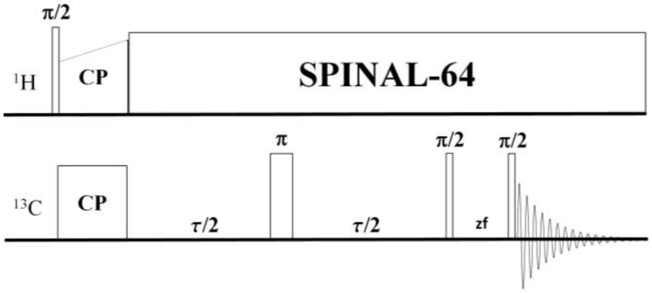

Figure III.4: *Schematic representation of two-dimensional Z-filtered spin-echo pulse sequence with cross-polarization block.*

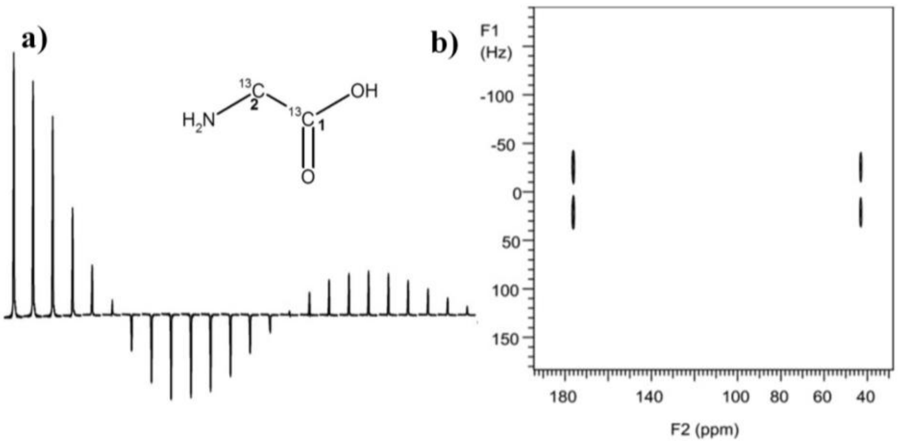

Figure III.5: *ZFSE of $^{13}C_2$-Glycine recorded at 2 ms of z-filter time: (a) spin-echoes as a function of τ and (b) 2D ZFSE spectrum.*

III.3.3. *Z-Filtered J-Scaled Spin-Echo pulse sequence (ZFJSSE)*

ZFJSSE is a new pulse sequence designed from ZFSE, herein τ/2 intervals are replaced with ‘n’ times of t1/2. In the case of normal Z-filtered spin-echo pulse sequence (Figure III.6), *J*-coupling evolution takes place according to the cos ($\pi J_{CC}\tau$) term. Whereas, in two-dimensional ZFJSSE, by replacing the τ/2 intervals with n(t1/2), the coupling evolution takes place according to cos(πJ_{CC}nt1). While performing the Fourier transformation along the indirect dimension, ‘n’ would become a weighting factor on the J_{CC}, since the t1 depends only on spectral width along the indirect dimension. By choosing appropriate ‘n’; the multiplets can be clearly resolved by ‘n’ times along indirect dimension of a two-dimensional spin-echo.

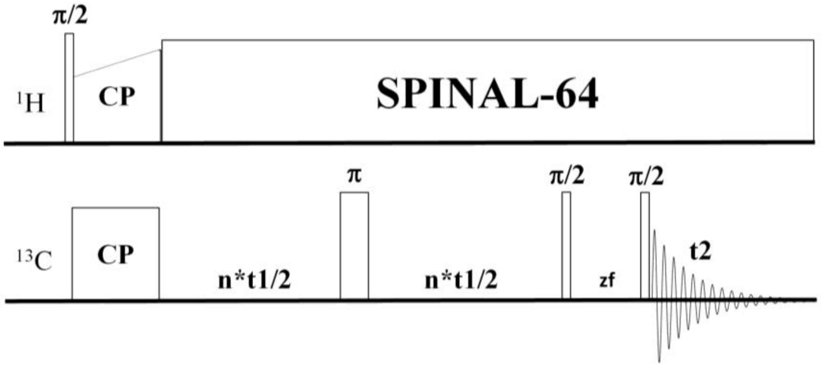

Figure III.6: *Schematic representation of two-dimensional Z-filtered J-scaled spin-echo pulse sequence with cross-polarization block.*

III.3.4. *Hadamard Encoded Z-Filtered J-Scaled Selective Spin-Echo pulse sequence (HEZFJSSSE)*

The above described *J*-scaled pulse sequence is applicable for the simple systems, where, the spin-spin interactions commute. On the other hand, for spin-spin interactions those do not commute with each other, as in the case of complex multi-clustered spin systems, a different strategy is required to overcome this difficulty.

This chapter introduces a new pulse sequence, HEZFJSSSE, which is developed on the basis of ZFJSSE. The Figure III.7 describes the replacement of hard π pulses with the phase ramped Hadamard encoded selective π pulses, which allow to recreate the commutation property between interested spins and useful to measure the multiple selective spin-spin couplings from two-dimensional NMR spectra.

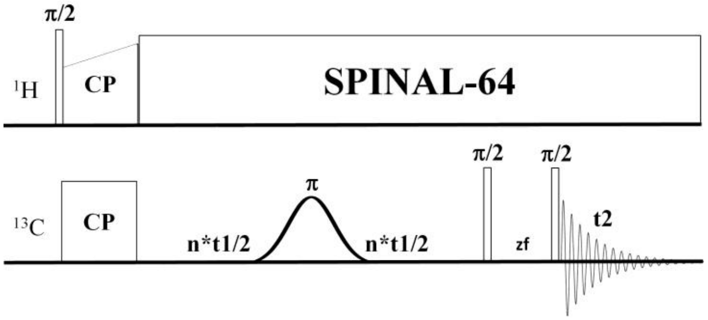

Figure III.7: *Schematic representation of two-dimensional Hadamard encoded Z-filtered J-scaled spin-echo pulse sequence with cross-polarization.*

III.4. Experiments

All the solid-state NMR experiments are performed on Varian Unity Inova 400 MHz spectrometer equipped with 4mm chemagnetics solid-state NMR probe at 10 kHz sample spinning speed, and spinning speed is controlled by Varian automated MAS control unit. The calibrated pulse widths for ^{13}C and ^{1}H are 3.15us and 2.9us, respectively. During the pulsing and acquisition, SPINAL-64 decoupling is employed. The *J*-scaled spin-echo experiments are conducted at different scaling factors. Number of transients is 16. The number of increments acquired along the indirect dimension is 64 for ZFSE and 32 for both ZFJSSE and HEZFJSSSE experiments, respectively.

III.5. Results and Discussion

In the following, the importance of Hadamard encoding combined with *J*-scaling in accurate measurement of spin-spin couplings of multiple-spin systems, has been discussed, and exemplified with specific spin-systems and pulse-sequences.

III.5.1. *J-scaled spin-echo of $^{13}C_2$-Glycine*

Initially the pulse sequence ZFJSSE that allows the measurement of homonuclear spin-spin couplings is employed for a simple system, $^{13}C_2$-Glycine to demonstrate the effect of *J*-scaling. The Figure III.8 depicts the comparison of ZFJSSE that recorded at two different *J*-scaling factors 1 (no-scaling) and 4. The measured splitting values along the indirect dimension (F1) at scaling factors 1 and 4 are 52.2Hz and 210.5 Hz, respectively, and the average of the normalized (52.2/1 and 210.5/4 Hz) value, i.e., 52.2 Hz is found to be in good agreement with the value measured in solution-state $^{1}J_{CC}$ (53.6 Hz). These findings suggest that molecules like simple $^{13}C_2$- isotopic labelled do not require a *J*-scaling. Furthermore, the Figure III.9 examines the effect of indirect increments on the spectral resolution; the expanded regions of Figure III.9a, Figure III.9b and Figure III.9c correspond to the data recorded in 32, 48 and 64 indirect dwelling increments, respectively. In all the cases, the observed normalized J_{CC} are comparable, suggesting increments of 32 along the indirect dimension are sufficient.

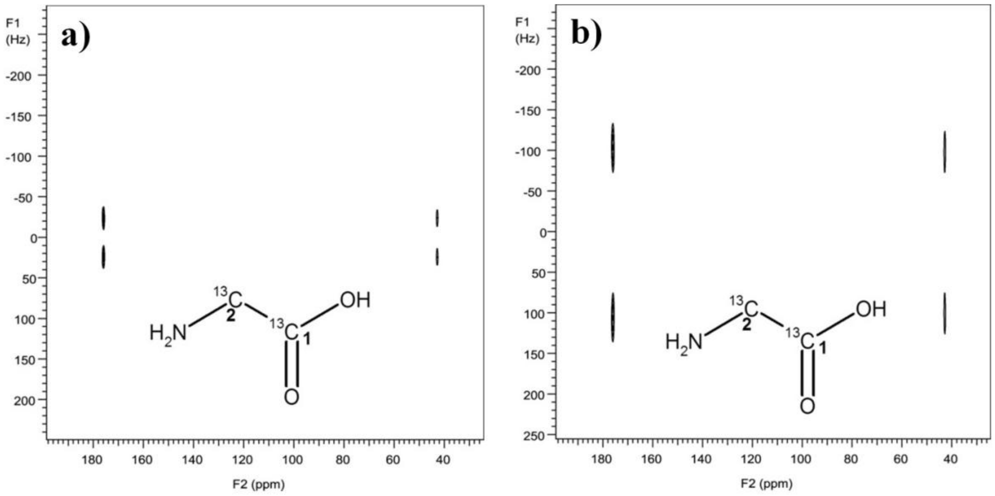

Figure III.8: *Comparison between the 2D Z-filtered spin-echo spectra of $^{13}C_2$-Glycine (a) without and (b) with scaling factor of* ***4.***

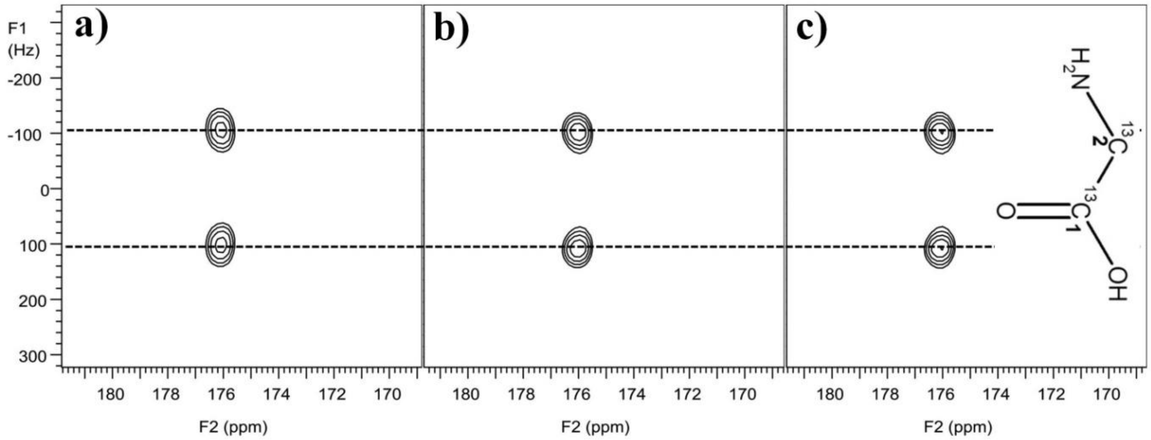

***Figure III.9**: Comparison of expanded 2D ZFJSSE spectra of $^{13}C_2$-glycine at four times scaling: (a), (b) and (c) are recorded in 32, 48 and 64 increments along the indirect dimension, respectively.*

III.5.2. *J-scaled spin-echo of $^{13}C_5$-FSAA*

On the other hand, the same 2D ZFJSSE experiment could not completely resolve the multiplicity patterns along the indirect dimensions for $^{13}C_5$-FSAA, even at 4 times of the *J*-scaling factor (Figure III.10a). The expected multiplicity patterns for IS2 spin-systems must be either doublet of doublets (if the coupling constants are different) or triplets (if the coupling constants are comparable). The 2D ZFJSEE spectrum of $^{13}C_5$-FSAA recorded at 4 times scaling factor is useful to measure the scalar couplings between C1-C2, C2-C3 and C4-C5. Moreover, the observed multiplicity patterns for C3 and C4 spins are not well resolved and still they are ambiguous. These findings indicate, that the ZFJSSE method also does not allow the measurement of all the J_{CC} couplings of $^{13}C_5$-FSAA molecule; which could be because of the dominant exponential damping (T_2-relaxation) or comparable J_{CC} couplings of other spins.

Alternatively, by incorporating the Hadamard encoding, the pulse sequence HEZFJSSSE has impressively resulted in well resolved spin-spin coupling patterns. The Figure III.10b represents the HEZFJSSSE spectrum recorded at 4 times scaling factor for the C1-C2-C4-C5 spin combination of $^{13}C_5$-FSAA, which is achieved by using four Hadamard encoded Gaussian shaped pulses for selective refocusing. Furthermore, the observed coupling patterns for all the spins are found to be clear doublets. By deselecting the spin C3 from the encoding, the commutation between the selected spins C1-C2 and C4-

C5 is set, which allows the measurement of J_{C1-C2} and J_{C4-C5} coupling constants in a single experiment. In another combination C1, C2, C3 and C4 spins are selectively refocused by four Hadamard encoded π pulses, which yielded J_{C1-C2} and J_{C2-C3} coupling constants (Figure III.10c). All the J_{CC} values of $^{13}C_5$-FSAA molecule that are measured with the aid of Hadamard selection in Z-filtered *J*-scaled spin-echo, are found to be well in agreement with the J_{CC} measured from solution-state NMR as well as from pseudo two-dimensional Hadamard multiple selective refocusing schemes (Chapter-II) (Figure III.11).

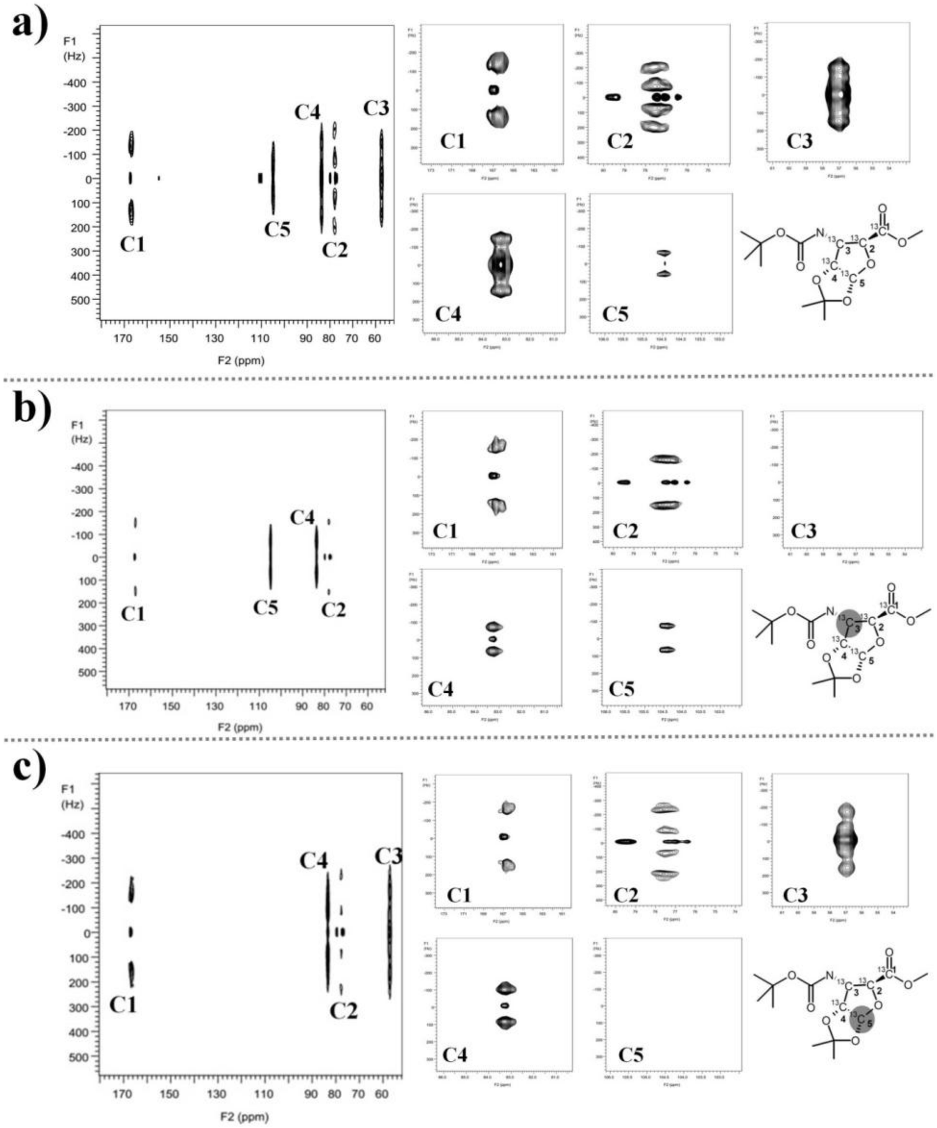

***Figure III.10**: Full and expanded regions of spin-echoes recorded at four times J-scaling factor for different spin-combinations of $^{13}C_5$-FSAA: two-dimensional ZFJSSE (a), HEZFJSSSE for the two spin combinations C1-C2-C4-C5 and C1-C2-C3-C4 are shown in (b) and (c), respectively. The expanded regions are represented by carbon numbers and the deselected carbons are highlighted with semi-transparent black filled circles.*

Table III.1: *Comparison of $^{1}J_{CC}$ derived from solution-state and different solid-state spin-echo experimental methods for different spin-pairs of $^{13}C_5$-FSAA molecule.*

Spin Pair	$^{1}J_{CC}$ derived from different spin-echo experimental methods						
	Double Selective spin-echoes (solution-state) [Hz]	ZFJSSE		HEZFJSSSE C1-C2-C4-C5		HEZFJSSSE C1-C2-C3-C4	
		At 4 times scaling (Hz)	Normalized value (Hz)	At 4 times scaling (Hz)	Normalized value (Hz)	At 4 times scaling (Hz)	Normalized value (Hz)
C1-C2	72.1 (71.2)	279.0	69.8	289.0	72.3	288.0	72.0
C2-C3	34.1 (34.1)	136.0	34.0	138.0	34.5	136.0	34.0
C3-C4	43.9 (41.6)	Not resolved		Not selected		180.0	45.0
C4-C5	33.9 (33.1)	128.0	32.0	137.0	34.3	Not selected	

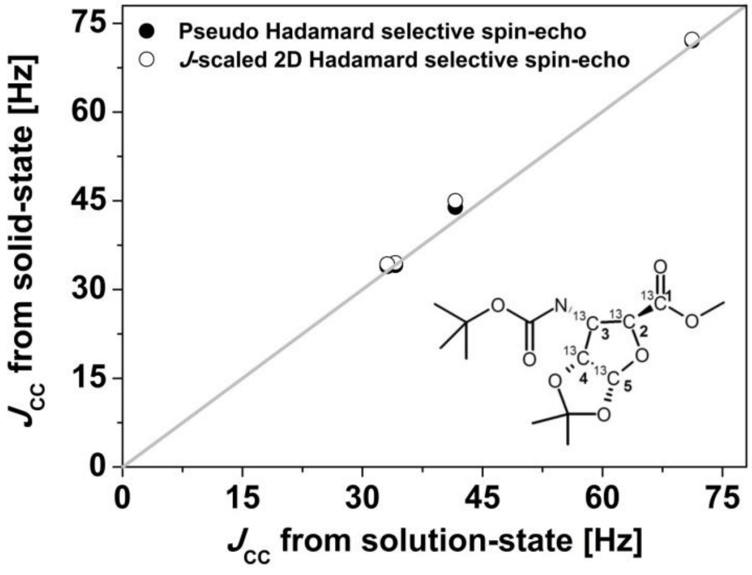

Figure III.11: *Correlation between $^{1}J_{CC}$ derived from solution-state and Hadamard selective spin-echoes in solid-state (pseudo 2D and various two dimensional J-scaled methodologies) for different spin-pairs of $^{13}C_5$-FSAA molecule.*

III.5.3. *J-scaled spin-echo of $^{13}C_8$-SA*

Analysis of 2D ZFJSSE spectrum of $^{13}C_8$-SA molecule (Figure III.12a) is rather complex compared that of $^{13}C_5$-FSAA. Furthermore, without the use of Hadamard selection for refocusing, the $^1J_{CC}$ between C1-C2 is measured from either C1 doublet or C2 doublet of doublets. Similarly, a doublet of C5 enables the measurement of $J_{C4\text{-}C5}$. Moreover, the doublets of C6 and C8 result the remaining scalar couplings $J_{C6\text{-}C7}$ and $J_{C7\text{-}C8}$, too. Hence, all the $^1J_{CC}$ are measured for $^{13}C_8$-SA molecule in the ZFJSSE experiment, except $J_{C3\text{-}C4}$ coupling constant.

Alternatively, Figure III.12b, Figure III.12c and Figure III.12d depict the Hadamard encoded 2D ZFJSSSE spectra of different spin combinations of $^{13}C_8$-SA, viz., C1-C2-C4-C5-C6-C7, C2-C3-C7-C8 and C3-C4, respectively. At these selective combinations, all the coupling patterns along indirect dimension resemble the clear doublets, which permit to measure the accurate J_{CC} between C1-C2, C2-C3, C3-C4, C4-C5, C6-C7 and C7-C8. The results are in well agreement with $^1J_{CC}$ derived from the Hadamard selective spin-echoes (Figure III.13).

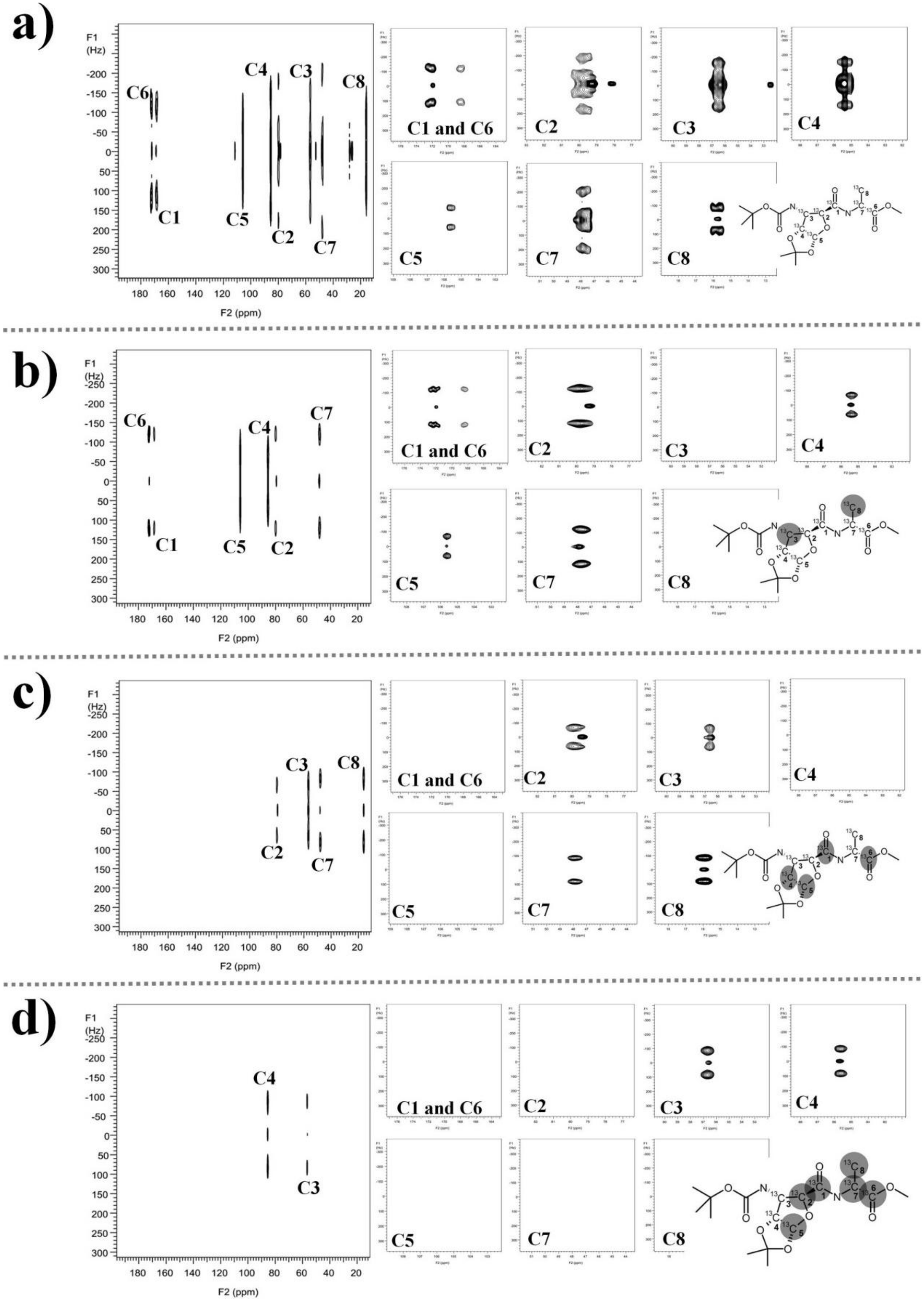

Figure III.12: *Full and expanded regions of spin-echoes recorded at four times J-scaling factor for the different spin-combinations of* $^{13}C_8$*-SA: (a) usage of hard pulses. The HEJZFSSSE spectra of interested spin combinations C1-C2-C4-C5-C6-C7, C2-C3-C7-C8 and C3-C4 are shown in (b), (c) and (d), respectively. The expanded regions are represented by carbon numbers and the deselected carbons are highlighted with semi-transparent black filled circles.*

Table III.2: *Comparison of $^{1}J_{CC}$ derived from solution-state and different solid-state spin-echo experimental methods for different spin-pairs of $^{13}C_8$-SA molecule.*

Spin Pair	Selective spin-echoes (solution-state) [Hz]	$^{1}J_{CC}$ derived in different experimental spin-echo methods							
		ZFJSSE		HEZFJSSSE C1-C2-C4-C5-C6-C7		HEZFJSSSE C2-C3-C7-C8		HEZFJSSSE C3-C4	
		At 4 times scaling (Hz)	Normalized value (Hz)	At 4 times scaling (Hz)	Normalized value (Hz)	At 4 times scaling (Hz)	Normalized value (Hz)	At 4 times scaling (Hz)	Normalized value (Hz)
C1-C2	60.3 (60.7)	232.0	58.0	240.0	60.0	Not selected		Not selected	
C2-C3	35.4 (36.9)	143.0	35.8	Not selected		138.4	34.6	Not selected	
C3-C4	42.4 (42.6)	Not resolved		Not selected		Not selected		170.0	42.5
C4-C5	34.7 (33.3)	131.6	32.9	135.6	33.9	Not selected		Not selected	
C6-C7	61.6 (62.0)	244.0	61.0	246.0	61.5	Not selected		Not selected	
C7-C8	41.4 (34.8)	158.0	39.5	Not selected		161.6	40.4	Not selected	

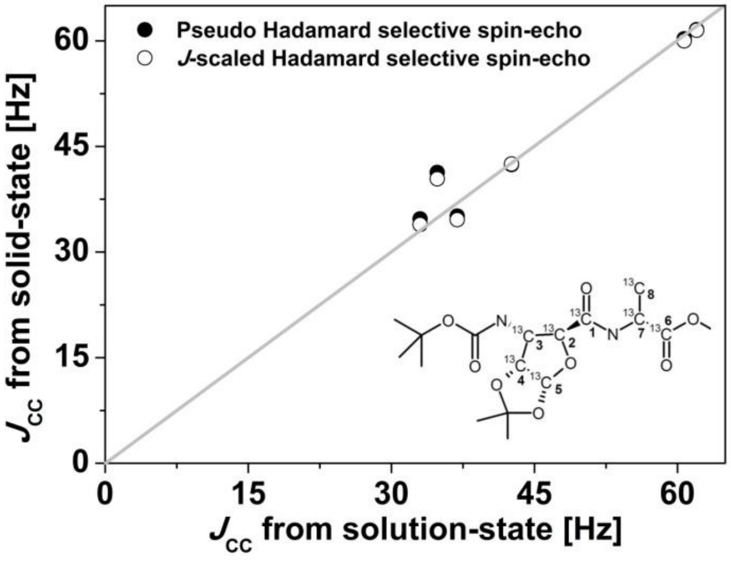

Figure III.13: *Correlation between $^{1}J_{CC}$ derived solution-state and Hadamard selective spin-echoes (pseudo 2D and various two dimensional J-scaled methodologies) for different spin-pairs of $^{13}C_8$-SA molecule.*

III.6. Conclusion

In the present chapter-III, new two-dimensional NMR experimental methods, ZFJSSE and HEZFJSSSE, have been developed for the simultaneous and accurate measurement of J_{CC} in uniformly labelled molecules. The superiority of Hadamard encoded NMR experiments over the conventional methods and the versatility of *J*-scaling in combination with Hadamard encoding, has been demonstrated. Furthermore, the same *J*-scaled spin-echo pulse block can be extended to the DQFCOSY pulse sequences to measure *J*-scaled scalar couplings by suppressing the natural abundant background signals (discussed in chapter-vi).

III.7. References

[1] L. R. Brown, Differential Scaling along w1 in COSY Experiments, J. Magn. Reson, 57 (1984) 13-18.

[2] P. Gundhi, K. V. R. Chary and R.V. Hosur, Direct observation of (H8, H6)-HI' *J*-coupling correlations in oligonucleotides for unambiguous resonance assignments, Use of *J*-scaling in two-dimensional correlated spectroscopy, FEBS. Lett, 191 (1985) 92-96.

[3] R. V. Hosur, K. V. R. Chary and M. R. Kumar, J-scaling in two-dimensional homonuclear correlated spectroscopy for enhancement of cross peak intensities, Chem. Phys. Lett, 116 (1985) 105-108.

[4] A. Majumdar and R. V. Hosur, ω_1-Scaling pulse sequences for two-dimensional homonuclear multiple-quantum spectroscopy, Chem. Phys. Lett, 138 (1987) 431-435.

[5] R. V. Hosur, Scaling in one and two dimensional spectroscopy in liquids, Prog. Nucl. Magn. Reson. Spec, 22 (1990) 1–53.

[6] K. E. Kover and P. Forgo, J-modulated ADEQUATE (JM-ADEQUATE) experiment for accurate measurement of carbon–carbon coupling constants, J. Magn. Reson, 166 (2004) 47–52.

[7] J. K. Furihata and H. Seto, J-Resolved HMBC, a new NMR technique for measuring heteronuclear long-range coupling constants, Tetr. Lett, 40 (1999) 6271–6275.

[8] W. Kolodziejski, P. J. Barrie, H. He and J. Klinowski, Two-dimensional J-scaled 29Si NMR COSY of Highly Siliceous Mordenite, J. Chem. Soc, Chem. Commun, (1991) 961-962.

[9] J. Becker-Baldus, T. F. Kemp, J. Past, A. Reinhold, A. Samoson and S. P. Brown, Longer-range distances by spinning-angle-encoding solid-state NMR spectroscopy, Phys. Chem. Chem. Phys, 13 (2011) 4514–4518.

Chapter-IV

Spectral simplifications in solid-state NMR

Two-dimensional J-scaled Hadamard encoded DQFCOSY NMR: Accurate measurement of J_{CC} in uniformly labelled and natural abundant clustered spin systems

IV.1. Introduction

DQF-COSY/INADEQUATE pulse sequences are useful for the chemical shift assignments in solid-state NMR.[1,2] Nevertheless, DQFCOSY variant with two refocusing periods along with the z-filter (UC2QF-COSY),[3] exhibits better sensitivity over the refocused-INADEQUATE[1] and also enhances the relaxation times by converting the faster decay double quantum signal into a single quantum signal. While some other variants of COSY schemes viz., CTUC[4, 5] and SAR-COSY[6] are known; however, the UC2QF-COSY scheme is a versatile method in terms of implementation of *J*-scaling**.**[3] In the light of the proven advantages and superiority of the Hadamard encoded pulse schemes over the conventional methods (chapter-II and III), the present chapter extends this strategy to DQFCOSY based experiments in solid-state NMR.

The section-A of this chapter deals with the development of new *J*-Scaled Hadamard Encoded Double Quantum Filtered COrrelation SpectroscopY (JSHEDQFCOSY) methodologies, which facilitate the accurate measurement of selective spin-spin scalar couplings in uniformly labelled molecules. Furthermore, the same methodology has been extended to the measurement of scalar couplings for the different polymorphs of L-Lysine.2HCl (section-B) and also to the natural abundant spin-systems (section-C).

IV.2. Theoretical background

IV.2.1. *UC2QF-COSY* or *DQF-COSY (Uniform-sign cross-peak double-quantum-filtered correlation spectroscopy)*

The UC2QF-COSY[3] technique (Figure IV.1) with two refocusing pulses and z-filter allows the chemical shift assignments in the conventional manner. The data acquisition and processing takes place as a function of dwelling increments (1/SW1, SW1 is the sweep width along the indirect F1dimension).

The spin-spin coupling evolution along the indirect dimension can be expressed as

$$S(\tau) \propto \sin^2(\pi J_{CC} t1)$$

where, J_{CC} is the spin-spin coupling constant and t1 is the dwell time (1/SW1).

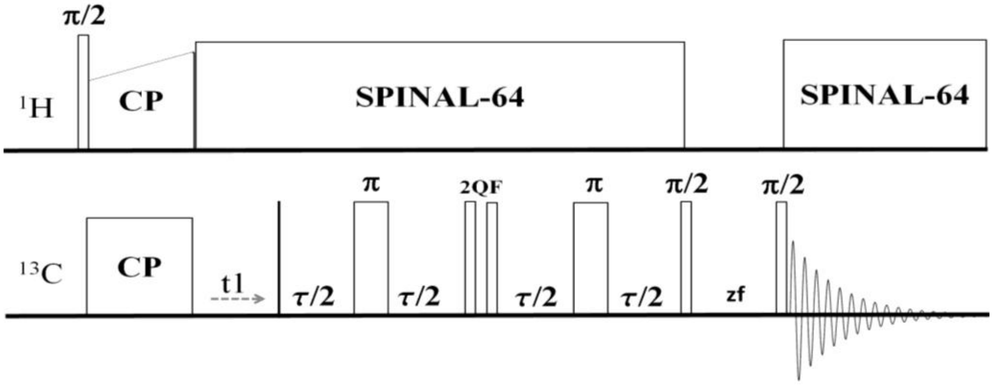

Figure IV.1: *Schematic representation of UC2QF-COSY pulse sequence, where, τ =1/4J for optimum cross-peak intensities.*

IV.2.2. *JSDQFCOSY (J-Scaled Double Quantum Filtered Correlation SpectroscopY)* and *JSHEDQFCOSY (J-Scaled Hadamard Encoded Double Quantum Filtered Correlation SpectroscopY)*

The JSDQFCOSY is an improvised version of the conventional DQFCOSY pulse sequence (Figure IV.2), wherein the *J*-scaling is introduced by replacing the initial two τ/2 constant times of DQFCOSY with 'n' times of t1. Thereby, the data points along the indirect dimension are acquired according to the multiples of '2n+1' dwell time, but the data processing uses only the dwell time (1/SW1, SW1 along the indirect dimension is a constant), which results in a weighting factor of '2n+1' for J_{CC}. The concept of *J*-scaling for solids has already been demonstrated in the previous chapter.

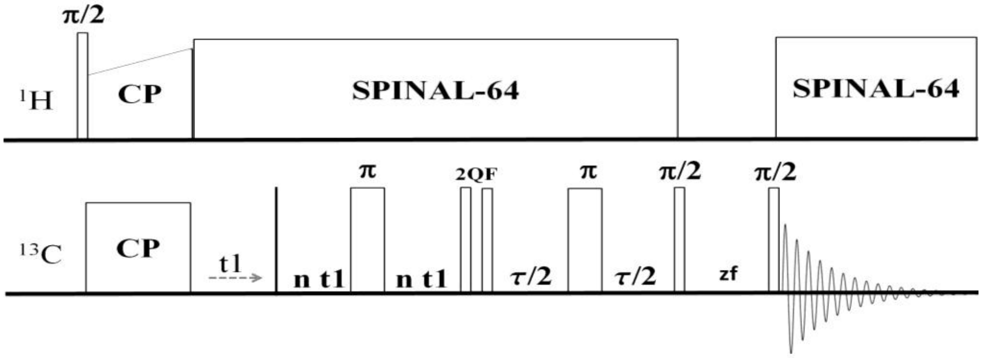

Figure IV.2: *Schematic representation of JSDQFCOSY NMR pulse sequence, with (2n+1) times of J-scaling factor.*

JSHEDQFCOSY pulse sequence (Figure IV.3) designed by replacing the hard π pulse of JSDQFCOSY with the Hadamard encoded simultaneous refocusing pulses.

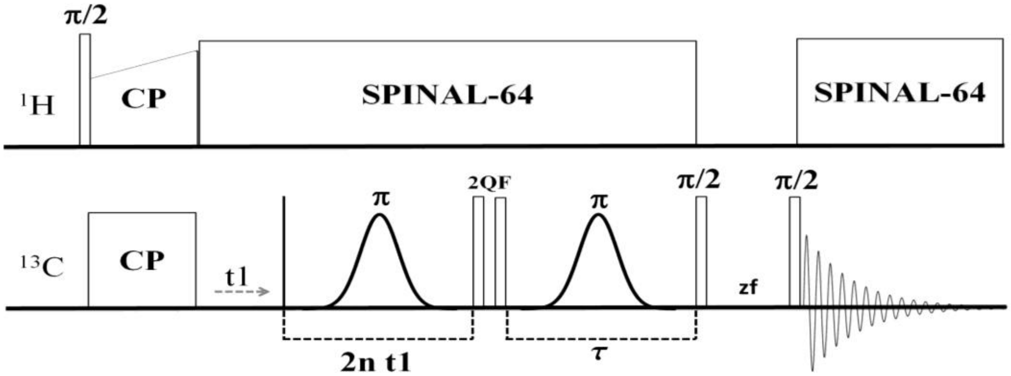

Figure IV.3: *Schematic representation of JSHEDQFCOSY with (2n+1) J-scaling factor.*

IV.3. Experiments

The isotopic labelled compounds are spin diluted with the natural abundant analogues in the ratio of 1:5 to minimize the intermolecular interactions. The DQFCOSY, JSDQFCOSY and JSHEDQFCOSY experiments with desirable scaling factors are conducted on Varian Unity Inova 400 MHz spectrometer equipped with 4mm chemagnetics solid-state NMR probe at MAS of 10 kHz. The optimized pulse widths are 3.15us and 2.9us for ^{13}C and ^{1}H, respectively. During the pulsing and acquisition, the SPINAL-64 decoupling is employed. Total 64 and 512 transients are collected for the isotopic labelled and the natural abundant spin systems, respectively.

Section-A

IV.A.1. Materials

The JSDQFCOSY and JSHEDQFCOSY methodologies are demonstrated on uniformly isotopic ^{13}C labelled compounds (Figure IV.A.1), (a) $^{13}C_2$-Glycine, (b) $^{13}C_3$ L-Alanine (2 mg) in a mixture of natural abundant Glycine and L-Lysine (60 mg), (c) $^{13}C_5$-FSAA monomer, (d) $^{13}C_8$-SA dimer, and (e) $^{13}C_6$ L-Histidine.

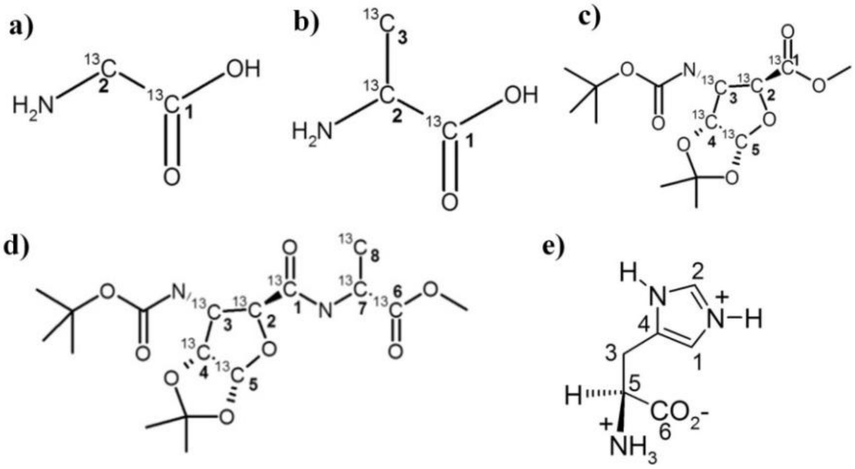

Figure IV.A.1: *Molecules studied in the present chapter: (a) $^{13}C_2$-Glycine, (b) $^{13}C_3$-Alanine, (c) $^{13}C_5$-FSAA, (d) $^{13}C_8$-SA and (e) $^{13}C_6$ L-Histidine.HCl, numbering is given only for the isotopic labelled carbon atoms.*

IV.A.2. Results and Discussions

IV.A.2.1. *J-scaled DQF-COSY: $^{13}C_2$-Glycine*

Figure IV.A.2 compares the conventional and *J*-scaled two-dimensional DQFCOSY spectra of $^{13}C_2$-Glycine. The resolution of the cross-peaks of conventional DQFCOSY (Figure IV.A.2a) is not sufficient to measure the important scalar couplings. Whereas, the JSDQFCOSY spectrum (Figure IV.A.2b) recorded at 21 times *J*-scaling factor has yielded well resolved doublets along the indirect dimensions, that enabled the doublet splitting measurement of J_{CC} (normalized value 1155/21 =55 Hz), which is in good agreement with the J_{CC} value measured in the solution-state (53.6Hz).

The present example reveals that the isolated/independent IS spin systems do not require any soft selective pulses for refocusing purpose, since the spin-spin interactions are commuted. On the other hand, the measurement of scalar couplings for clustered spin-systems (ISn) is rather difficult.

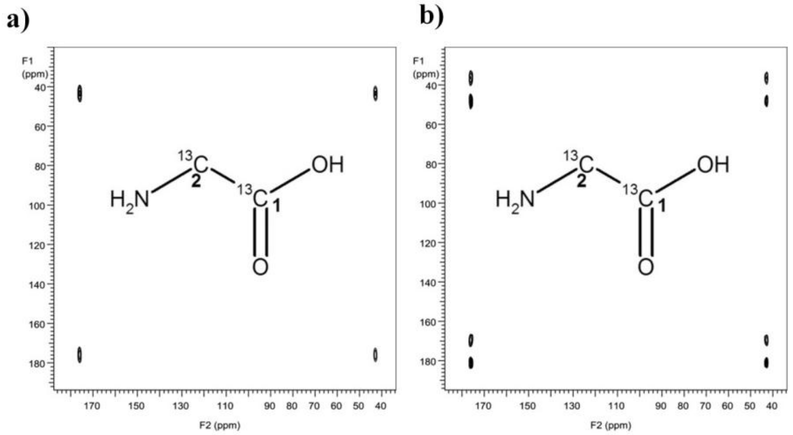

Figure IV.A.2: *Comparison of 2D conventional (a) and J-scaled (b) DQFCOSY spectra of $^{13}C_2$-Glycine. Clear doublets at scaling factor 21 are observed along the indirect dimension permit to measure the scalar couplings directly.*

IV.A.2.2. *Hadamard encoded J-scaled DQF-COSY: mixture of $^{13}C_3$-Alanine and natural abundant amino acids*

This study is aimed at analyzing the specific labelled residues of very low concentrations, in the presence of large amount of natural abundant amino acids. Such complex mixtures are difficult to analyze by using conventional SSNMR methods, as they exhibit resonances of natural abundant and isotopic labelled spins have comparable intensity (Figure IV.A.3). Furthermore, the signal overlappings resist to conduct the pseudo 2D selective spin-echo experiments.

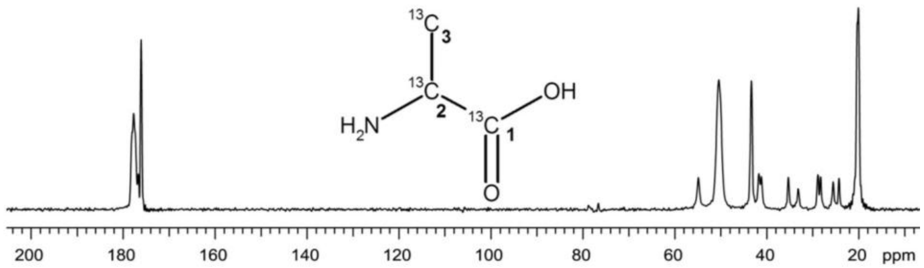

Figure IV.A.3: *^{13}C CPMAS spectrum of mixture of a natural abundant amino acids (60 mg of Glycine and L-Lysine) and $^{13}C_3$-Alanine (2 mg). Sample spinning:10 kHz and number of scans:64.*

Figure IV.A.4a shows the ^{13}C-^{13}C DQFCOSY spectrum of $^{13}C_3$ L-Alanine, which is simple and the double quantum filter suppresses the signals of natural abundant contribution in the mixture. But, this method is not useful for the measurement of J_{CC}, as the obscured signals are not resolved along the indirect dimension. These signals are resolved by employing the JSDQFCOSY at 21 times scaling factor, which exhibit well-resolved doublets along the indirect dimension (Figure IV.A.4b). However, the C2 spin in L-Alanine (IS2 spin system) has developed artefacts due to the combined coupling modulations of spins along the indirect dimension. On the contrary, upon introducing Hadamard encoding, JSHEDQFCOSY of C1-C2 (Figure IV.A.4c) and C2-C3 (Figure IV.A.4d) spin-pairs have yielded artefact free spectra and the normalized J_{CC} are well in agreement with the solution-state J_{CC}.

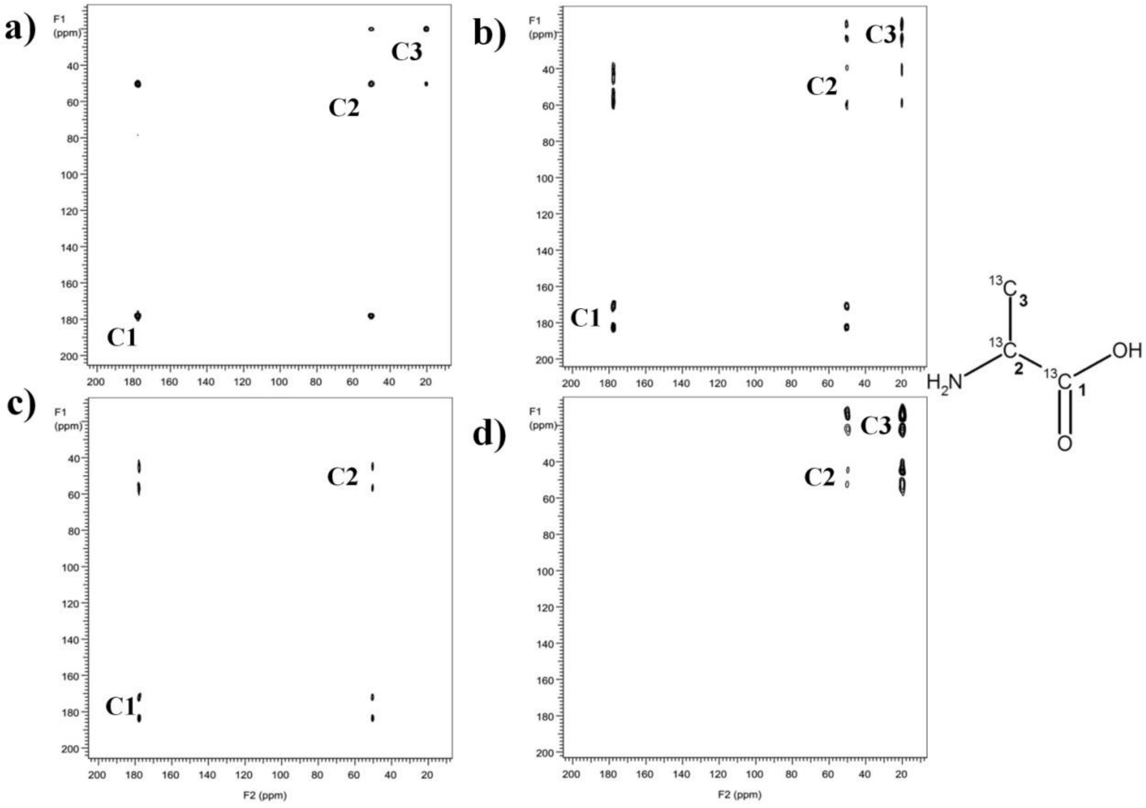

Figure IV.A.4: *2D conventional (a) and J-scaled (b) DQFCOSY spectra of mixture of natural abundant amino acids and $^{13}C_3$-Alanine recorded at 21 times scaling. The blocks (c) and (d) are the JSHEDQFCOSY spectra of C1-C2 and C2-C3 spin pairs of $^{13}C_3$-Alanine, respectively.*

IV.A.2.3. *Hadamard encoded J-scaled DQF-COSY: $^{13}C_5$-FSAA*

One-bond and long-range couplings: $^{13}C_5$-FSAA is rather a complex molecule compared to $^{13}C_2$-Glycine and $^{13}C_3$ L-Alanine. The Figure IV.A.5a represents the JSDQFCOSY spectrum recorded at 21 times scaling factor. Except $J_{C1\text{-}C2}$ and $J_{C4\text{-}C5}$, the rest of the spectrum exhibits ambiguous multiplicity patterns. However, the JSHEDQFCOSY with 21 times *J*-scaling factor has yielded four resolved $^1J_{CC}$ couplings. (Figure IV.A.5c, IV.A.5d and IV.A.5e). In addition to these directly bonded scalar couplings, a long range $^3J_{CC}$ is also measured (7.2 Hz) between C1-C5 at 41 times scaling factor (Figure IV.8f). The spin-spin commutation property is recreated between two pairs by using Hadamard encoded selective refocusing pulses (C1-C2-C4-C5), which yielded two $^1J_{CC}$ couplings in a single experiment.

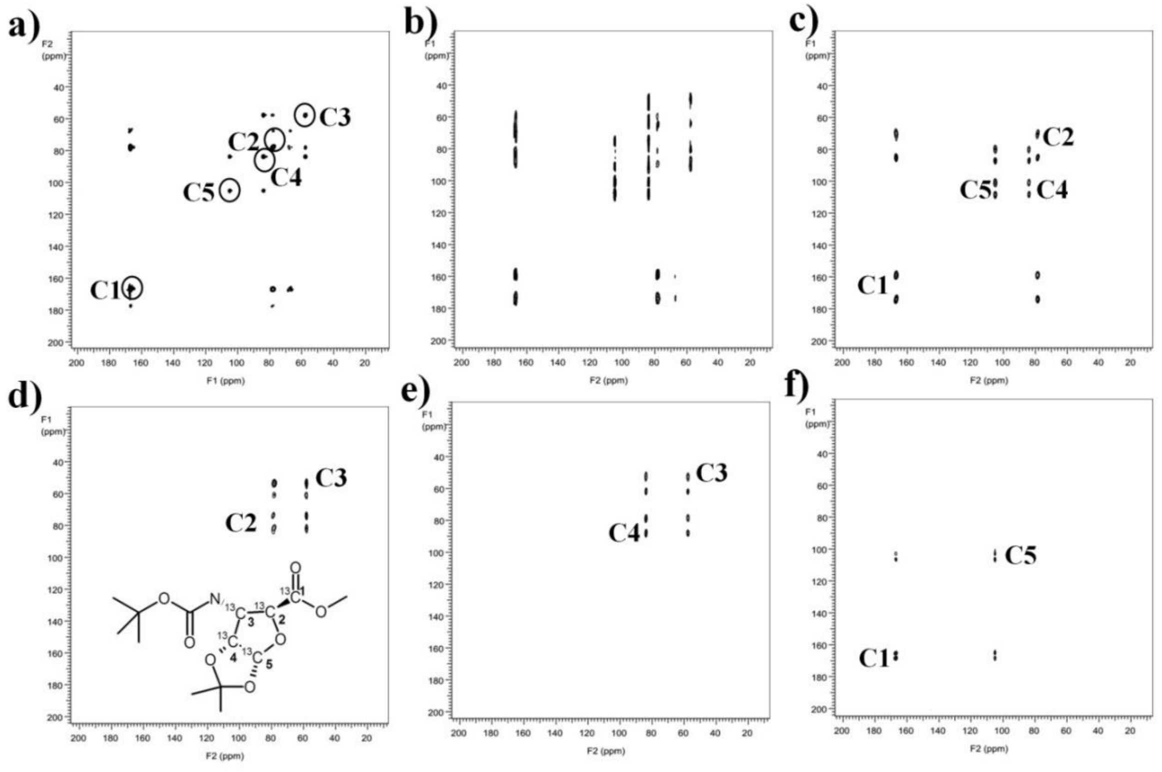

Figure IV.A.5: *Comparison of 2D conventional (a) and J-scaled (b) DQFCOSY spectra of $^{13}C_5$-FSAA recorded at 21 times J-scaling. The spin-combinations C1-C2-C4-C5, C2-C3 and C3-C4, which are selected for JSHEDQFCOSY experiment at the scaling factor 21 are shown in (c), (d) and (e), respectively. The JSHEDQFCOSY of C1-C5 is selected for the measurement of long range $^3J_{C1\text{-}C5}$ at 41 times scaling factor (f).*

Table IV.A.1: *Comparison of* $^{n}J_{CC}$ *derived from JSHEDQCOSY and 2D pseudo spin-echo pulse sequences for different spin pairs of* $^{13}C_5$*-FSAA.*

Spin-pair	Scaling factor	Observed coupling (Hz)	Normalized coupling constant (Hz)	$^{n}J_{CC}$ derived from 2D pseudo spin-echo (Hz)
C1-C2	21	1520	**72.4**	**72.1**
C2-C3	21	749	**35.6**	**34.1**
C3-C4	21	890	**42.4**	**43.9**
C4-C5	21	748	**35.6**	**33.9**
C1-C5	41	327	**8.0**	**8.2**

IV.A.2.4. *Hadamard encoded J-scaled DQF-COSY:* $^{13}C_8$*-SA*

For $^{13}C_8$-SA dimer molecule also, same procedure has been repeated at 17 times of scaling factor. The accessibility of more number of spins in the present molecule allows to measure, three $^{1}J_{CC}$ viz., C1-C2, C4-C5 and C6-C7 in a single experiment with the application of six simultaneous Hadamard encoded phase ramped selective refocusing pulses (Figure IV.A.6a). The Figure IV.A.6b shows the selective refocusing of C2-C3-C7-C8, which permits to measure, two $^{1}J_{CC}$ between C2-C3 and C7-C8, at the same scaling factor value of 17 times. The normalized scalar couplings are in excellent agreement with $^{1}J_{CC}$ derived in Hadamard pseudo selective spin-echo experiments.

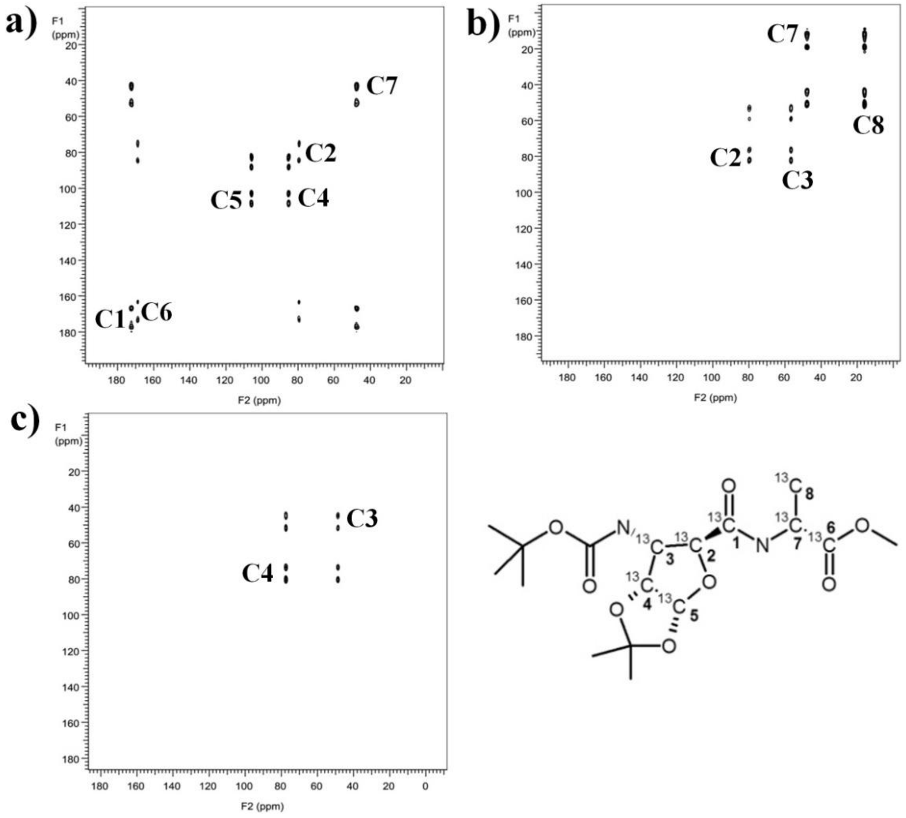

Figure IV.A.6: JSHEDCOSY spectra of $^{13}C_8$-SA at 17 times scaling factor. The spin-combinations C1-C2-C4-C5-C6-C7, C2-C3-C7-C8 and C3-C4 are shown in (a), (b) and (c), respectively.

Table IV.A.2: *Comparison of $^{n}J_{CC}$ derived from JSHEDQCOSY and 2D pseudo spin-echo pulse sequences for different spin pairs of $^{13}C_8$-SA.*

Spin-pair	**Scaling factor**	**Observed coupling (Hz)**	**Normalized coupling constant (Hz)**	**$^{n}J_{CC}$ derived from 2D pseudo spin-echo (Hz)**
C1-C2	17	1054	**62.0**	**62.0**
C2-C3	17	590	**34.7**	**35.1**
C3-C4	17	701	**41.2**	**42.4**
C4-C5	17	566	**33.3**	**34.8**
C6-C7	17	1020	**60.0**	**60.7**
C7-C8	17	716	**42.1**	**41.3**

IV.A.2.5. *Hadamard encoded J-scaled DQF-COSY: $^{13}C_6$ L-Histidine.2HCl*

The Figure IV.A.7a describes the JSDQFCOSY NMR spectrum of $^{13}C_6$ L-Histidine.HCl at 21 times scaling. Herein, the observed artefacts resist to measure the scalar couplings, which is due to the problem in spin-spin commutation. Thus, the studies have been extended to JSHEDQFCOSY experiments, which facilitate measuring the selective scalar couplings between interested spins (Figure IV.A.7b, Figure IV.A.7c and Figure IV.A.7d). A total four $^{1}J_{CC}$ selective scalar couplings are measured in three individual experiments. The normalized values of scalar couplings are in good agreement with scalar couplings derived from the solution-state as well as from the solid-state Hadamard encoded selective refocusing schemes.

Table IV.A.3: *Comparison of $^{n}J_{CC}$ derived from JSHEDQCOSY and 2D pseudo spin-echo pulse sequences for different spin pairs of $^{13}C_6$-L-Histidine.HCl.*

Spin-pair	**Scaling factor**	**Observed coupling (Hz)**	**Normalized coupling constant (Hz)**	**$^{n}J_{CC}$ derived from 2D pseudo spin-echo (Hz)**
C5-C6	21	1137	**54.1**	**57.0**
C3-C5	21	718	**34.2**	**32.0**
C3-C4	21	1102	**52.5**	**48.4**
C4-C1	21	1482	**70.6**	**72.7**

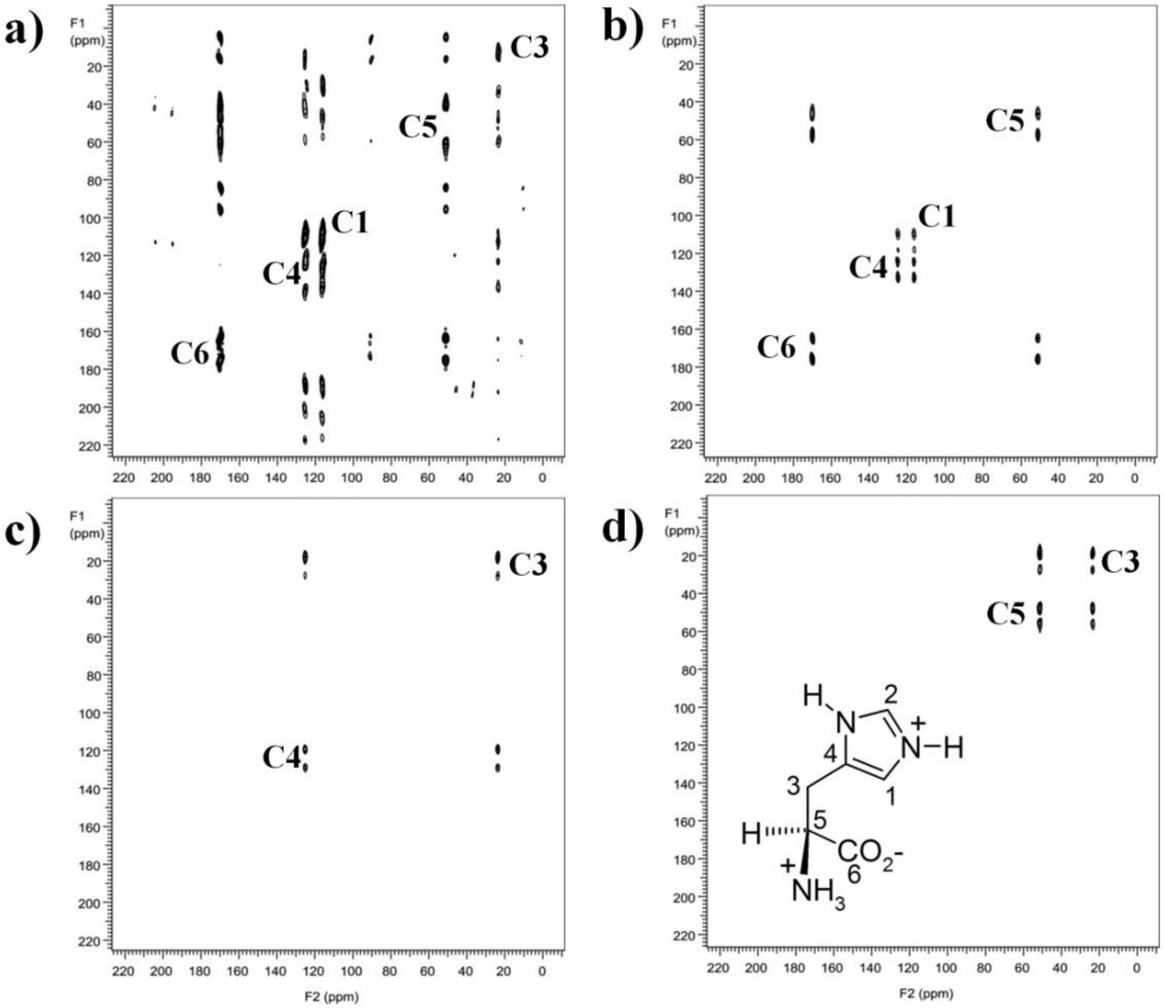

Figure IV.A.7: *Comparison of J-Scaled DQFCOSY spectra of* $^{13}C_6$ *L-Histidine.HCl at 21 times scaling factor: (a) JSDQFCOSY. On the other hand, the selective spin-combinations C1-C4-C5-C6, C3-C4, C3-C5 are shown in (b), (c) and (d), respectively.*

Section-B

The present section-B deals with the exemplification of *J*-scaled Hadamard encoded DQFCOSY experiments to measure the selective scalar couplings for two polymorphs of $^{13}C_6$ L-Lysine.2HCl.

IV.B.1. Results and Discussions

Figure IV.B.1 shows the ^{13}C CPMAS NMR spectrum of $^{13}C_6$ L-Lysine.2HCl recorded at 10 kHz sample spinning speed, which has only six carbons. However, ^{13}C CPMAS spectrum shows total 12 lines. This is an unexpected behaviour and may be due to the plausibility of two dominant polymorphs for L-Lysine.2HCl molecule. Furthermore, DQFCOSY (Figure IV.B.2) facilitates the chemical shift assignments for all the 12 resonances of two polymorphs (Table IV.B.1).

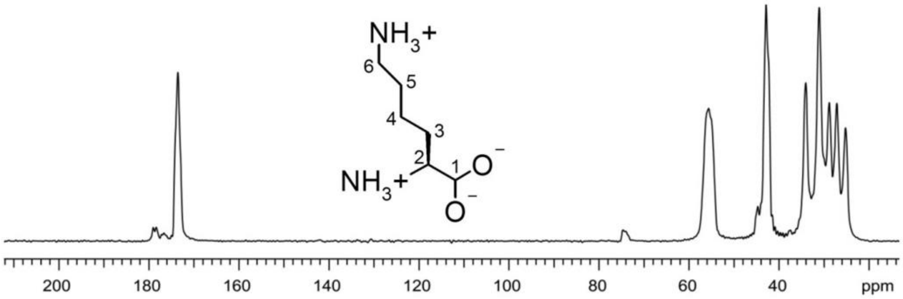

Figure IV.B.1: *^{13}C CPMAS spectrum of $^{13}C_6$ L-Lysine.2HCl at 10 kHz sample spinning.*

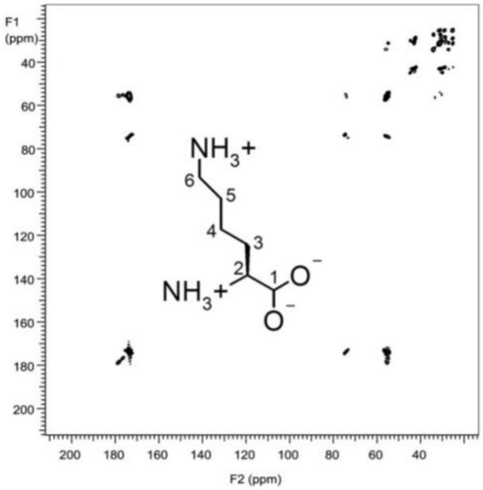

Figure IV.B.2: *DQFCOSY spectrum of $^{13}C_6$ L-Lysine.2HCl at 10 kHz sample spinning.*

Table IV.B.1: *^{13}C chemical shifts (in ppm units) of two polymorphs of L-Lysine.2HCl.*

Spin	Polymorph-I	Polymorph-II
C1	173.6	173.6
C2	56.0	54.7
C3	33.8	31.0
C4	26.9	25.0
C5	30.8	28.4
C6	42.7	42.2

Due to the poor ^{13}C chemical shift resolution of 12 crowded resonance lines, Hadamard encoded pseudo spin-echo 2D experiments cannot be performed on $^{13}C_6$ L-Lysine.2HCl for the measurement of selective scalar coupling. Furthermore, spin-echo modulation requires peak volume as a function of evolution time; in the present case efficient spin state selectivity is the main problem. Alternatively, the double quantum filter of JSHEDCOSY suppresses the non scalar coupled magnetization, which allows measuring all the 12 scalar couplings for two polymorphs of $^{13}C_6$ L-Lysine.2HCl molecule.

IV.B.1.1. *Application of JSHEDQFCOSY: measurement of J_{CC} for polymorph-I & polymorph-II in $^{13}C_6$ L-Lysine.2HCl*

The chemical shifts of C1 and C2 are assigned as 173.6 ppm and 56.0 ppm for polymorph-I; 173.6 ppm and 54.7 ppm for polymorph-II. The carbon chemical shift values are exactly overlapped for C1, but not for C2. The observed 1.3ppm chemical shift separation value for C2 is not sufficient to conduct the two separate pseudo spin-echo experiments for these two polymorphs. However, 2D JSHEDQFCOSY permits to measure the J_{CC} at appropriate 41 times *J*-scaling factor is applied for these spin selections. A clear contrast has been observed between Hadamard encoded selective spin-echo and DQ filtered spectra, which are recorded at $\tau/2 = 0$ (Figure IV.B.3). Therefore, DQ spin-echo suppresses the non scalar coupled signals and results in clear doublets along the indirect dimension of JSHEDQFCOSY for C1-C2 spin pairs of $^{13}C_6$ L-Lysine.2HCl

Similarly, eight separate JSHEDQFCOSY experiments are repeated at different scaling factors for the remaining spin pairs C2-C3, C3-C4, C4-C5 and C5-C6, as well. The observed chemical shift differences of 1.3ppm for C2, 2.8ppm for C3, 1.9ppm for C4, 2.4ppm for C5 and 0.5ppm for C6 of two polymorphs, facilitate to conduct the separate experiments. The Figure IV.B.4 shows the JSHEDQFCOSY spectra of different spin pairs for two polymorphs of $^{13}C_6$ L-Lysine.2HCl. The normalized $^{1}J_{CC}$ are in nice agreement with the $^{1}J_{CC}$ reported in the solution-state (Table IV.B.2).

Table IV.B.2: *$^{n}J_{CC}$ derived from JSHEDQCOSY pulse sequence and reported in the isotropic solution-state for different spin pairs of $^{13}C_6$ L-Lysine.2HCl.*

Spin-pair (polymorph)	**Scaling factor**	**Observed coupling (Hz)**	**Normalized coupling constant (Hz)**	**$^{n}J_{CC}$ values reported in solution-state (Hz)[15]**
C1-C2 (I)	41	2244	**54.7**	**53.6**
C1-C2 (II)	41	2244	**54.7**	
C2-C3 (I)	21	727	**34.7**	**34.2**
C2-C3 (II)	21	701	**33.4**	
C3-C4 (I)	11	377	**34.3**	**34.5**
C3-C4 (II)	11	364	**33.1**	
C4-C5 (I)	5	183	**36.6**	**34.0**
C4-C5 (II)	5	182	**36.5**	
C5-C6 (I)	11	389	**35.4**	**35.8**
C5-C6 (II)	11	395	**35.9**	

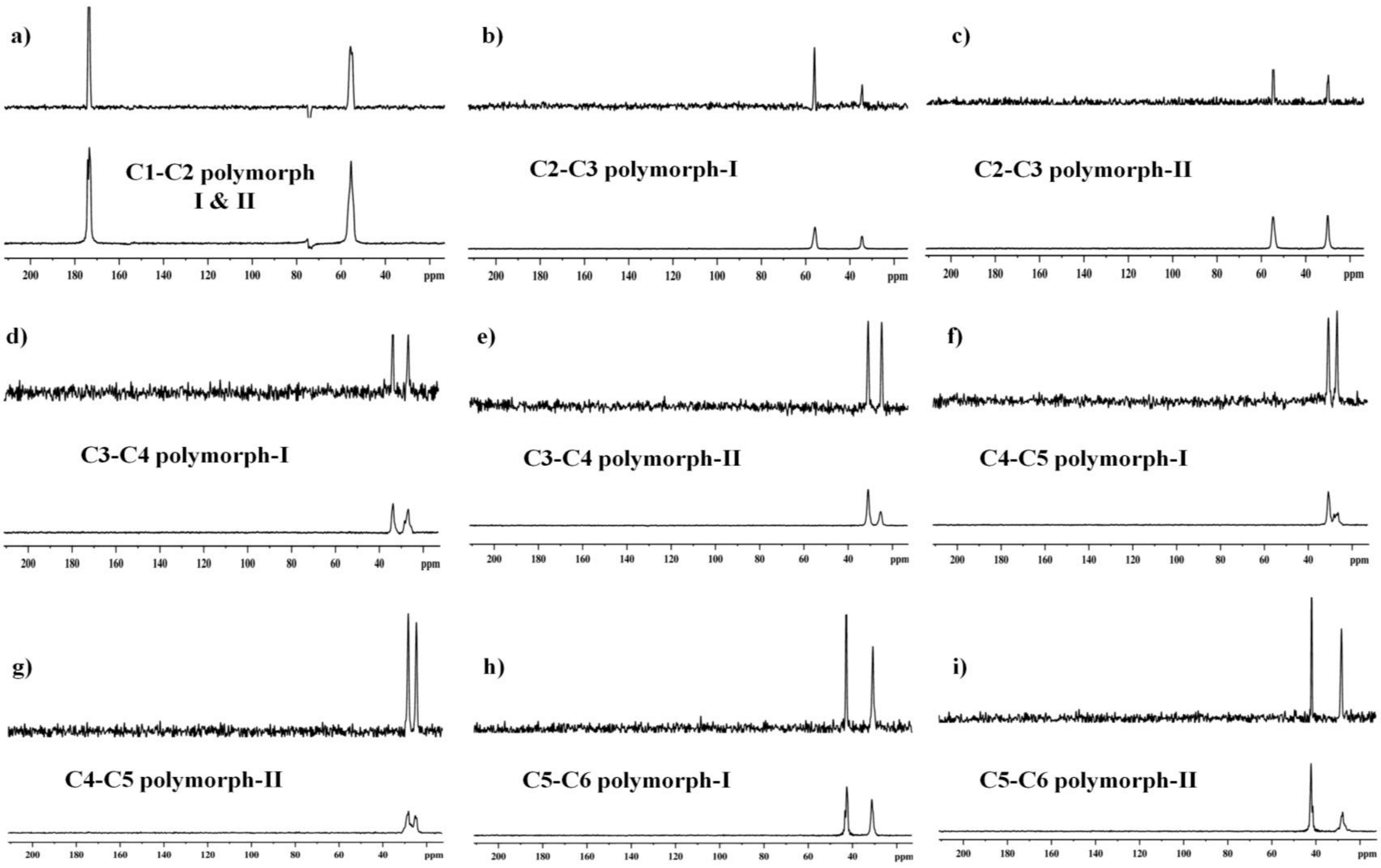

Figure IV.B.3: *Comparison between Hadamard encoded selective spin-echoes (lower traces) and double quantum spin-echoes (upper traces) for different spin pairs of $^{13}C_6$ L-Lysine.2HCl at 10 kHz sample spinning.*

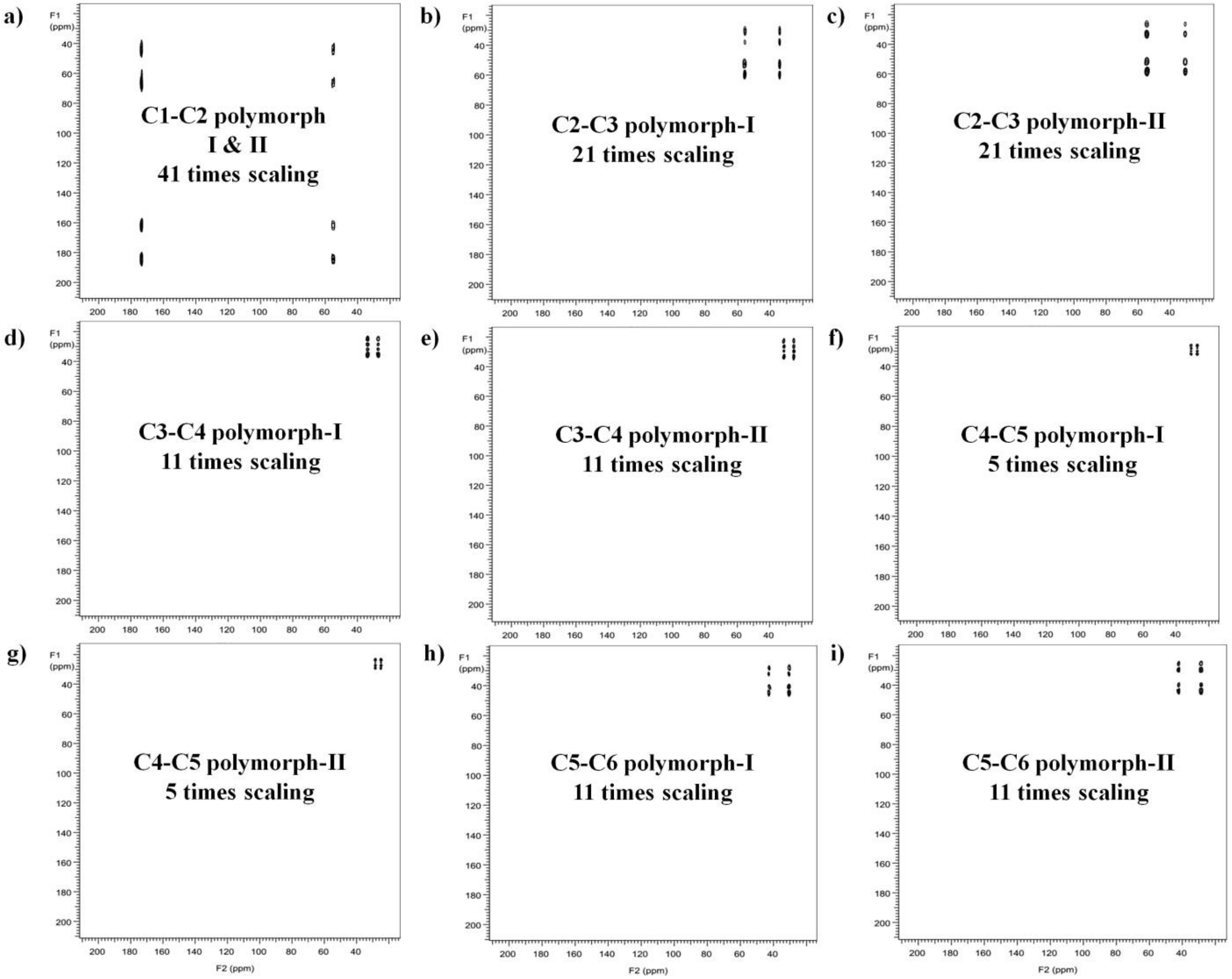

Figure IV.B.4: *JSHEDQCOSY spectra for different spin pairs of* $^{13}C_6$ *L-Lysine.2HCl recorded at various appropriate scaling factors (depicted in the individual figures).*

Section-C

The present section-C describes the applicability of Hadamard encoded *J*-scaled DQFCOSY experiments for natural abundant, in this regard, 1-Adamantanol is studied.

IV.C.1. Results and Discussions

In addition to the isotopic labelled molecules, the JSHEDQFCOSY pulse sequence has been explored for the measurement of ^{13}C-^{13}C scalar couplings at natural abundance levels. The 1-Adamantanol molecule is selected as a model compound to perform these experiments. The Figure IV.C.1 depicts the ^{13}C CPMAS spectrum of 1-Adamantanol recorded at 10 kHz sample spinning. Furthermore, the DQFCOSY spectrum of 1-Adamantanol facilitates the chemical shift assignments (Figure IV.C.2).

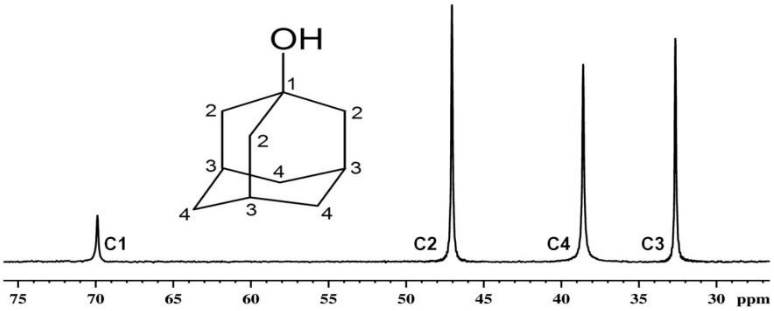

Figure IV.C.1: *^{13}C CPMAS spectrum of 1-Adamantanol recorded at 10 kHz sample spinning speed.*

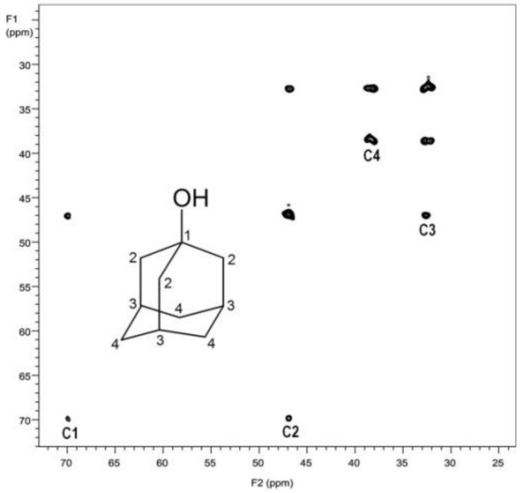

Figure IV.C.2: *The ^{13}C-^{13}C DQFCOSY spectrum of 1-Adamantanol recorded at 10 kHz sample spinning speed.*

IV.C.1.1. *Application of JSHEDQFCOSY: natural abundant 1-Adamantanol*

The Figure IV.C.3 represents the Hadamard encoded *J*-scaled DQFCOSY of two different spin pairs C2-C3 and C3-C4 of 1-Adamantanol, which are acquired at a scaling factor of 11. The normalized values of ^{13}C-^{13}C scalar couplings derived at natural abundance levels are equal to 30Hz and 31.1 Hz for C2-C3 and C3-C4 spin pairs, respectively. Finally, these values are in good agreement with the corresponding solution-state scalar couplings ($J_{C2\text{-}C3}$ = 29.2 Hz and $J_{C3\text{-}C4}$ = 30.1 Hz), which are measured from the INADEQUATE experiment.

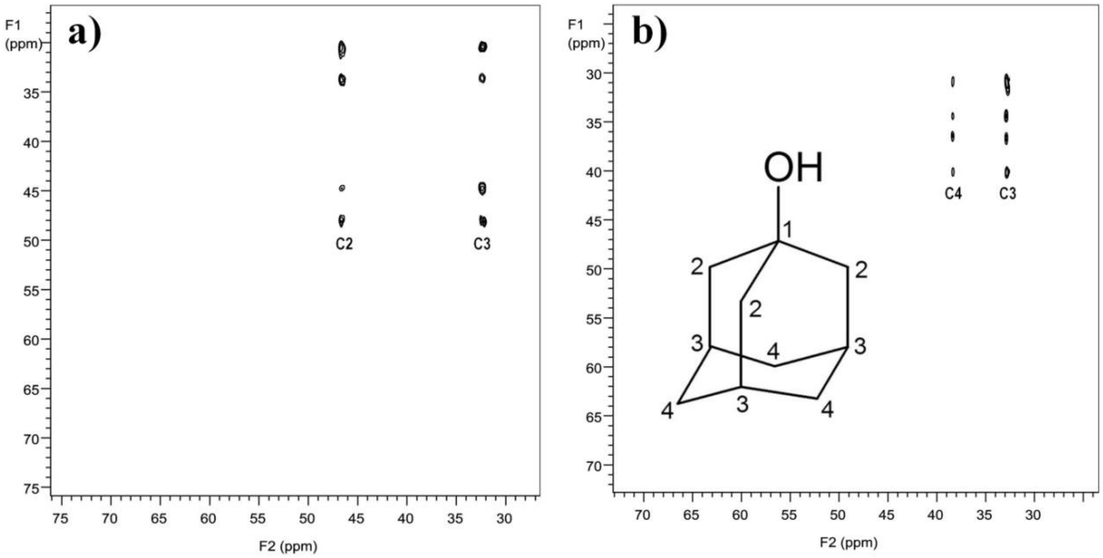

Figure IV.C.3: *^{13}C-^{13}C JSHEDQFCOSY spectra of C2-C3 and C3-C4 spin pairs of 1-Adamantanol recorded at 11 times scaling factor, which are shown in (a) and (b), respectively.*

IV. 4. Conclusion

In the present chapter-IV, a novel *J*-scaled Hadamard Encoded Double Quantum Filtered Correlation SpectroscopY (JSHEDQFCOSY) pulse sequence has been demonstrated to measure the accurate ^{13}C-^{13}C scalar couplings in uniformly labelled spin systems with crowded resonances. Moreover, the effective spin-state selection can be created by using the double quantum filter, which facilitates the determination of scalar couplings for two different polymorphs of $^{13}C_6$ L-Lysine.2HCl. Finally, the same methodology has been extended to measure the J_{CC} at natural abundance levels. The normalized scalar couplings are in good agreement with the solution-state and J_{CC} measured in pseudo-selective 2D spin-echo methods. In favourable cases, the present method can be further extended to highly complex spin systems.

1V.5. References

[1] A. Lesage, M. Bardet and L. Emsley, Through-Bond Carbon-Carbon Connectivities in Disordered Solids by NMR, J. Am. Chem. Soc, 121 (1999) 10987-10993.

[2] R. A. Olsen, J. Struppe, D. W. Elliott, R. J. Thomas and L. J. Mueller, Through-Bond 13C-13C Correlation at the Natural Abundance Level: Refining Dynamic Regions in the Crystal Structure of Vitamin-D3 with Solid-State NMR, J. Am. Chem. Soc, 125 (2003) 11784-11785.

[3] L. J. Mueller, D. W. Elliott, G. M. Leskowitz, J. Struppe, R. A. Olsen, K. Kim and C. A. Reed, Uniform-sign cross-peak double-quantum-filtered correlation spectroscopy, J. Magn. Reson, 168 (2004) 327–335.

[4] L. Chen, R. A. Olsen, D. W. Elliott, J. M. Boettcher, D. H. Zhou, C. M. Rienstra and L. J. Mueller, Constant-Time Through-Bond 13C Correlation Spectroscopy for Assigning Protein Resonances with Solid-State NMR Spectroscopy, J. Am. Chem. Soc, 128 (2006) 9992-9993.

[5] L. Chen, J. M. Kaiser, J. Lai, T. Polenova, J. Yang, C. M. Rienstra and L. J. Mueller, *J*-based 2D homonuclear and heteronuclear correlation in solid-state proteins, Magn. Reson. Chem, 45 (2007) S84–S92.

[6] D. Lee, J. Struppe, D. W. Elliott, L. J. Mueller and J. J. Titman, Sensitive absorptive refocused scalar correlation NMR spectroscopy in solids, Phys. Chem. Chem. Phys, 11 (2009) 3547–3553.

[7] L. R. Brown, Differential Scaling along w1 in COSY Experiments, J. Magn. Reson, 57 (1984) 13-18.

[8] P. Gundhi, K. V. R. Chary and R.V. Hosur, Direct observation of (H8, H6)-HI' J-coupling correlations in oligonucleotides for unambiguous resonance assignments, Use of J-scaling in two-dimensional correlated spectroscopy, FEBS. Lett, 191 (1985) 92-96.

[9] R. V. Hosur, K. V. R. Chary and M. R. Kumar, J-scaling in two-dimensional homonuclear correlated spectroscopy for enhancement of cross peak intensities, Chem. Phys. Lett, 116 (1985) 105-108.

[10] A. Majumdar and R. V. Hosur, ω_1-Scaling pulse sequences for two-dimensional homonuclear multiple-quantum spectroscopy, Chem. Phys. Lett, 138 (1987) 431-435.

[11] R. V. Hosur, Scaling in one and two dimensional spectroscopy in liquids, Prog. Nucl. Magn. Reson. Spec, 22 (1990) 1–53.

[12] K. E. Kover and P. Forgo, J-modulated ADEQUATE (JM-ADEQUATE) experiment for accurate measurement of carbon–carbon coupling constants, J. Magn. Reson, 166 (2004) 47–52.

[13] J. K. Furihata and H. Seto, J-Resolved HMBC, a new NMR technique for measuring heteronuclear long-range coupling constants, Tetra. Lett, 40 (1999) 6271–6275.

[14] W. Kolodziejski, P. J. Barrie, H. He and J. Klinowski, Two-dimensional J-scaled 29Si NMR COSY of Highly Siliceous Mordenite, J. Chem. Soc, Chem. Commun, (1991) 961-962.

[15] S. T. Dinh, S. Fermandjian, E. Sala, R. M. Bouvier and P. Fromageot, Geminal and Vicinal ^{13}C-^{13}C Coupling Constants of 85% ^{13}C-Enriched Amino Acids, J. Am. Chem. Soc, 75 (1974) 1267-1269.

Chapter-V

Spectral simplifications in solid-state NMR

Inter-nuclear distance measurements by using Hadamard encoded spin-echoes and Rotational Resonance echoes in uniformly labelled molecules

V.1. Introduction

Accurate measurement of dipolar couplings is essential for estimating the inter-nuclear distances. These rich structural parameters are averaged to zero in the isotropic solution-state due to the rapid molecular tumbling, whereas they are sustained in solid-state, yet their measurement is not straight forward. During the past two decades, a variety of techniques have been reported for the measurement of homonuclear dipolar couplings (RFDR: Radio Frequency driven Dipolar Re-coupling,[1] RR: Rotational Resonance,[2] PDSD: Proton Driven Spin Diffusion and its variants[3-6]) and heteronuclear dipolar couplings (REDOR: Rotational Echo Double Resonance,[7] TEDOR:[8] Transverse Echo Double Resonance and its variants) in the solid-state. Indeed, the measurement of homonuclear dipolar couplings is difficult, when compared to the hetereonuclear dipolar couplings due to the spectral overlap, particularly in uniformly labelled spin systems.

While the PDSD variants offer qualitative information useful to correlate the spatial connectivity of long range spins,[9] the RFDR methods[1] require a set of experiments to be recorded at different mixing times. On the other hand, many variants of rotational resonance (RR) pulse sequences have been developed such as (i) zero-quantum relaxation[2] that requires a set of $^{13}C_2$ labelled molecules, (ii) constant mixing time 2D RR experiments,[10] which require collecting the data at different spinning speeds, (iii) constant spinning speed 2D RR methods, which require collecting the data at different mixing times[11] and (iv) the methods those involve the processing of data on the knowledge of individual homonuclear dipolar coupling in the clustered spin systems.[12] All these methods are either involved with expensive isotope enrichments (bi-selective labelling) or time consuming (2D experiments at different mixing times or different spinning speeds).

Alternatively, selective spin-echo experiments have been developed (as discussed in earlier chapters) for the measurement of homonuclear dipolar couplings at fixed Off Magic Angle Sample Spinning,[13-14] which are suitable only for the measurement of distances < 3Å. Subsequently, a new spinning angle encoded and DQ based pulse sequences have been developed[15] and demonstrated for homonuclear distance up to 6Å. Nevertheless, while the spinning angle encoding technique warrants a special type of probe design,[16] the DQ-based experiments demand long spectral acquisitions. The present chapter deals with novel experimental strategies that employ selective spin-echoes for the measurement of long range D_{CC} /distances in uniformly labelled organic solids.

The chapter-v comprises of two parts. The section-A deals with the selective spin-echo experiments at fixed off-magic angle sample spinning (OMAS) for the measurement of homonuclear dipolar couplings in $^{13}C_5$-FSAA and $^{13}C_8$-SA molecules. By setting up the spinning axis of the sample slightly away from the magic angle, the dipolar interactions do not average to zero and allow to measure the residual dipolar couplings along with the corresponding scalar couplings. Hence, the resultant spin-echo modulation is according to the $J+D$, from which the D can be computed with the prior knowledge of J (measured at MAS). However, these OMAS experiments are carried out at the cost of spectral resolution for favourable cases. Care must be taken to set up the small offset angles for retaining the required spectral information.

The section-B discusses the first demonstration of a new Hadamard encoded double frequency selective zero-quantum echo pulse sequence for selective homonuclear dipolar coupling measurements in clustered solid spin systems. Herein, the dipolar couplings between interested spin pairs have been reintroduced by setting the spinning speed equal to the chemical shift difference of two spins (Rotational Resonance). In this situation, as the data is always collected only at MAS, spectral resolution may not be a problem.

Section-A

V.A.1. Materials

^{13}C-^{13}C selective spin-echo experiments are conducted for two unnatural peptides, to derive homonuclear distance measurements at Off Magic Angle Sample Spinning (OMAS) condition. Crystallization of $^{13}C_5$-FSAA (cis- Furanoid Sugar Amino Acid) monomer and $^{13}C_8$-SA dimer are carried out in 1:1 mixture of methanol and water at 25^oC. Solid-state NMR experiments are conducted in 1:5 mixtures of isotopic labelled and the corresponding natural abundant compounds to minimize the intermolecular dipolar interactions.

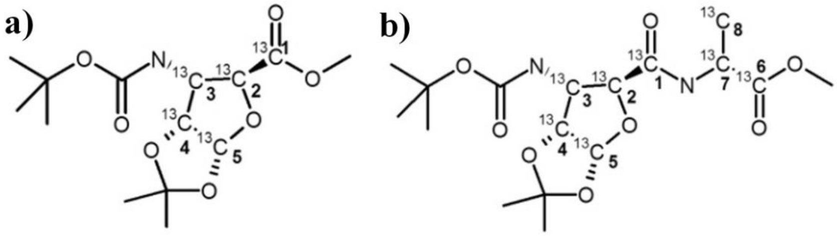

Figure V.A.1: *Schematic representations of molecular structures of unnatural peptides: (a)* $^{13}C_5$*-FSAA and (b)* $^{13}C_8$*-SA.*

V.A.2. Experiments

All the experiments are performed on Varian Unity Inova 400 MHz spectrometer equipped with 4mm chemagnetics solid-state NMR probe. The spinning speed (10 kHz) is controlled by Varian automated MAS control unit. The optimized 90° pulse widths are 2.75µs and 2.91µs for ^{13}C and ^{1}H, respectively. Contact time of 5 ms for cross polarization and 3s recycle delays is used.

Shaped pulses are analyzed with the Pbox option invoked in VNMRJ2.2D software. In the present case Gaussian shaped pulses of 3.62ms duration are used for the simultaneous refocusing of the specified spins, and the resultant bandwidths are equal to the 249 Hz. Since the simultaneous application of shaped pulses may introduce the multi quantum artefacts in the spin-echo modulations. A shift correction**[14]** of 869 µs is applied to the Gaussian pulses, which is equal to the shaped pulse width at 76.69%. The $\tau/2$ values are incremented as integer multiples of rotor periods, where, τ_{ev} is the total interval during the shaped pulses (τ_p) and τ.

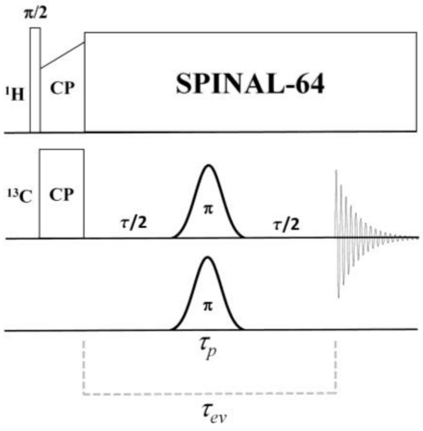

Figure V.A.2: *Schematic representation of Hadamard encoded pulse sequence in double frequency selective refocusing.*

V.A.3. Results and Discussions

V.A.3.1. *Proton Driven Spin Diffusion (PDSD) experiments of $^{13}C_5$-FSAA*

Figure V.A.3 depicts the comparison of PDSD spectra of $^{13}C_5$-FSAA recorded at two different mixing times, 5 ms and 50 ms. The PDSD spectrum at 5 ms mixing time shows only correlation between nearby spins, whereas, all the correlations are observed at 50 ms mixing time. Figure V.A.4 illustrates the magnetization build-up curves for the different spin pairs in $^{13}C_5$-FSAA, which exhibit A.exp (-k/t_{mix}) form.[4] However, they give only semi-quantitative information, which is not sufficient for accurate measurement of distances.[9]

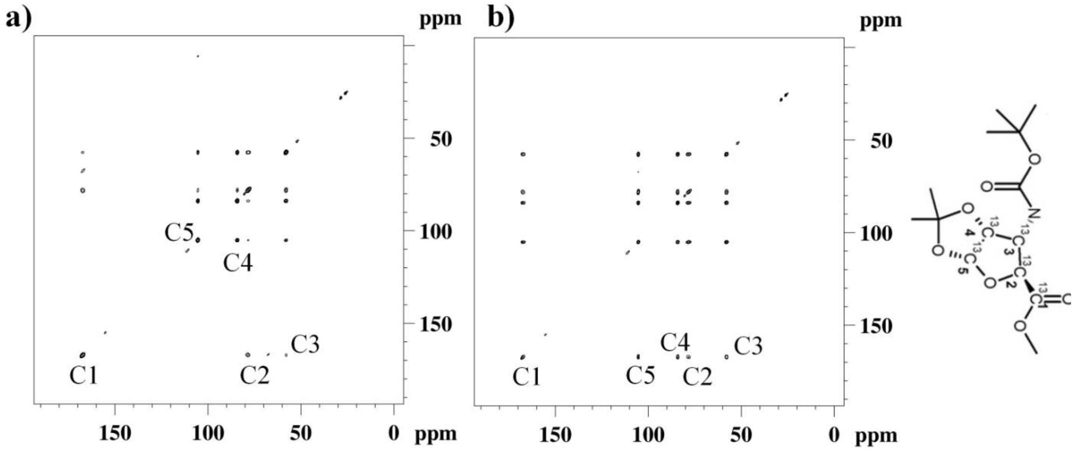

Figure V.A.3: *Comparison of PDSD spectra of $^{13}C_5$-FSAA recorded at 5 ms (a) and 50 ms (b) mixing times.*

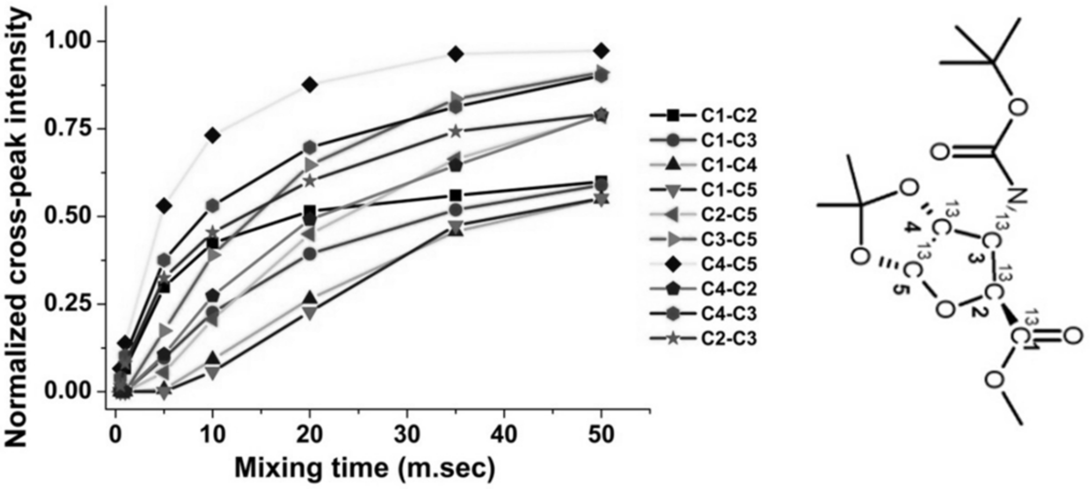

Figure V.A.4: *PDSD cross-peak intensity profiles for different spin-pairs of $^{13}C_5$-FSAA.*

V.A.3.2. *Hadamard encoded double selective spin-echo experiments at Magic Angle Sample spinning*

As discussed in chapter-II, the *J*-coupling measurements are carried out at the magic angle adjusted by ^{79}Br. Further, the ^{13}C spin-echo modulation of Glycine is used to confirm the magic angle adjustment, which yielded 55.5 Hz of *J*-coupling that is comparable to the value in the solution-state (53.6Hz). Initially, Hadamard encoded double frequency selective refocusing experiments are conducted at MAS on both $^{13}C_5$-FSAA and $^{13}C_8$-SA molecules to obtain $^{1}J_{cc}$ and $^{3}J_{cc}$ scalar couplings. The resultant spin-echoes are integrated and plotted against the τ_{ev}. Later, the experimental spin-echo modulations are fitted by using Levenberg-Marquardt iteration algorithm for the theoretical expression (1).**[13, 14]**

$$S\,(\tau) \propto \cos\{\pi J\,(\tau_{ev}-\tau_{sh})\}\,\exp\,(-\tau_{ev}/T_2^{J}) \rightarrow (1)$$

Where p, T_2^J is the empirical parameters, τ_{ev} *is* the spin-echo evolution time and τ_{sh} is the time shift associated with the shaped pulses.

For $^{13}C_5$-FSAA molecule, total five J_{CC} couplings (4 $^{1}J_{CC}$ and 1 $^{3}J_{CC}$) are measured. On the other hand, in $^{13}C_8$-SA molecule all the available seven $^{1}J_{CC}$ coupling constants are measured, whereas no long-range J_{CC} is observed.

V.A.3.3. *Hadamard encoded double-selective spin-echo experiments at fixed Off Magic Angle Sample spinning*

The dipolar couplings are measured for different spin pairs of $^{13}C_5$-FSAA and $^{13}C_8$-SA molecules by using Hadamard encoded double frequency selective refocusing spin-echoes at fixed off-magic angle sample spinning condition. The Figure V.A.5 represents the spin-echo modulation of $^{13}C_2$-Glycine at fixed off magic angle spinning axis, which facilitates the calibration of rotor angle offset. In the present case, the calculated angle offset value is -1.924 ± 0.003^{o}. The ^{13}C CPMAS spectrum of $^{13}C_5$-FSAA is well resolved at this off-set angle, whereas it is ambiguous for $^{13}C_8$-SA (Figure V.A.6). The selective spin-echo experiments at OMAS have been carried out by the same procedure as described for J_{CC} couplings at MAS. Herein, the equation (2) allows fitting the spin-echo amplitude modulations, which are recorded at fixed *off-magic angle*.

$$S(\tau) \sim p \exp(-\tau/T_2^{0}) + (1-p)\, S_{mod}(\tau,\Delta) \exp(-\tau/T_2^{J}) \rightarrow (2)$$

where, **p** represents the population

$$S_{mod}(\tau,\Delta) = x^{-1}\{F_c(x)\cos(\theta) + F_s(x)\sin(\theta)\}$$

is the modulation part comprised of Fresnel integral terms, $F_c(x)$ and $F_s(x)$ and

$$\theta(\tau,\Delta) = (\pi J + 2^{-1/2}\, b\Delta)\tau$$

$$x(\tau) = (6b\tau/\pi\sqrt{2})^{1/2}$$

θ and x are the parameters depend on dipole-dipole coupling constant **b,** whereas Δ is the angle offset.

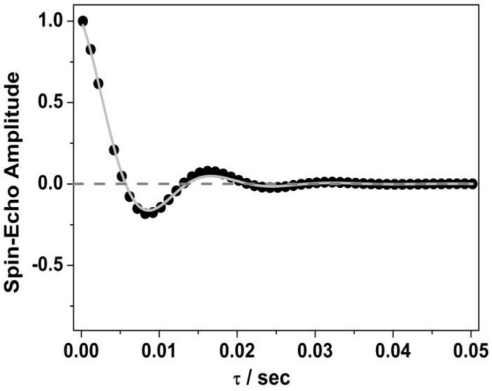

Figure V.A.5: *The spin-echo modulation of $^{13}C_2$-Glycine at off magic angle sample spinning, which allows to calculate the angle offset away from the MAS with the prior knowledge of $^{1}J_{CC}$ ~ 55 Hz at MAS as well as ^{13}C-^{13}C distance parameters. Black filled circles and gray solid line depict the experimental data and the theoretical fit for expression-2, respectively.*

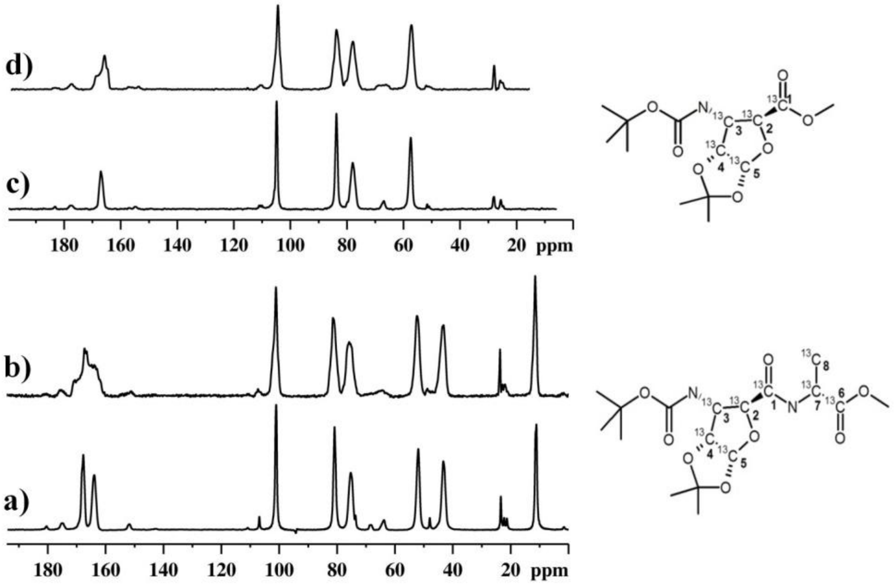

Figure V.A.6: *Comparison of ^{13}C CPMAS spectra acquired at MAS and OMAS for $^{13}C_5$-FSAA and $^{13}C_5$-SA molecules: (a) and (c) are ^{13}C CPMAS spectra collected at MAS for $^{13}C_8$-SA and $^{13}C_5$-FSAA, respectively. The corresponding OMAS spectra are shown in (b) and (d). As explained in the text at larger offset angles, the reintroduction of the dominant dipolar and CSA interactions spoil the spectral resolution. Accordingly, the spectral resolution for these two compounds is reduced (relatively more for $^{13}C_8$-SA) at OMAS due to the increased line broadening.*

V.A.3.4. ***Comparison of Hadamard encoded double frequency selective spin-echo modulations for different spin pairs in $^{13}C_5$-FSAA at MAS and OMAS***

Table.V.A.1 represents the comparison of Hadamard double-frequency selective spin-echo modulations recorded at MAS and OMAS conditions, for different spin pairs of $^{13}C_5$-FSAA. The measured ^{13}C-^{13}C homo-nuclear dipolar couplings are divided into three groups. (i) -2500 to -2100 Hz for the directly bonded carbons (~ 1.45 – 1.52 Å), the modulations are strong enough to observe the coupling information at MAS as well as OMAS conditions. (ii) -700 to -500 Hz for the two bond separated carbons (~ 2.2 to 2.4 Å), no modulations are observed at MAS, whereas, at OMAS generates weak modulations. (iii) -150 Hz for the three bond separated carbons (~ 3.55 Å) C1-C5, which is the maximum distance measured in $^{13}C_5$-FSAA, by using this technique. Herein, the inherently available $^3J_{CC}$ coupling of 6.2 Hz strongly supports the spin-echo modulation between 1 and 5 at OMAS; hence the modulation is not a simple monotonic decay at OMAS, as well. However, spin-echo modulation for C1 and C4 is a pure monotonic decay at MAS and OMAS also. Levitt and co-workers have indicated in their study, that the OMAS spin-echo technique is limited to accessing the distances only up to 2.2 Å, as the spin-echo modulation for far apart spins is mainly of simple exponential decay that is predominantly governed by T_2-relaxation. On the other hand, as a special case, distances up to ~3.6 Å are measured due to significant long range J_{CC} between C1 and C5 in FSAA.

Table V.A1: *Comparison of selective spin-echo modulations for different spin-pairs of $^{13}C_5$-FSAA, recorded at MAS and OMAS conditions.*

Spin Pair	Hadamard encoded double selective spin-echo modulation **at magic angle:** Black filled circles and grey line depict the experimental data and best fit to the equation (1), respectively.	Hadamard encoded double selective spin-echo modulation **at off magic angle:** Black filled circles and grey line depict the experimental data and best fit to the equation (2), respectively.	J_{CC} coupling in Hz; L for solution-state, S for solid-state	b, X and N represent the dipolar coupling constant in Hz, inter nuclear distances (Å) derived from X-ray and SS NMR derived distances, respectively
$^{13}C_2$-Glycine	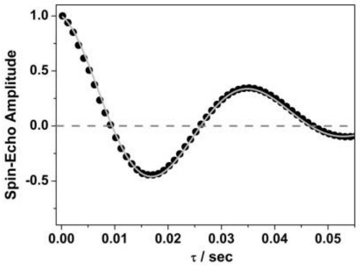	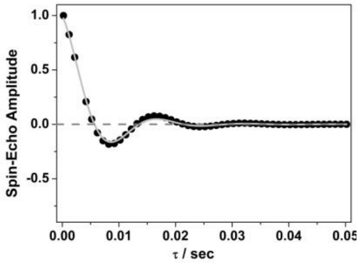	**L=53.6** **S=55.5**	**b = -2135** **X = 1.52** **N = 1.50**
1,2 of FSAA	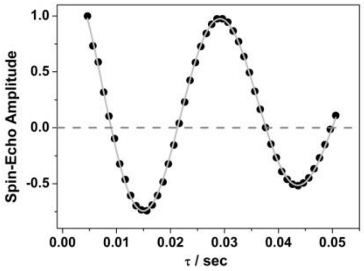	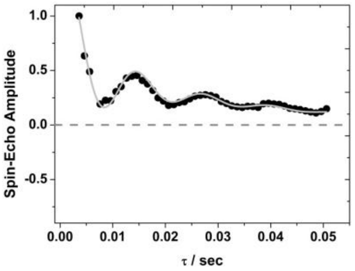	**L = 71.2** **S = 72.1**	**b = -2514±7.5** **X = 1.50** **N = 1.44**
2,3 of FSAA	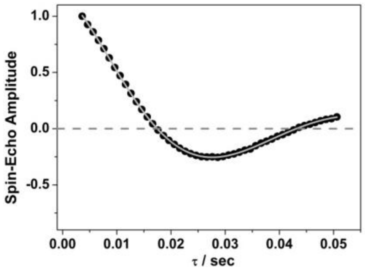	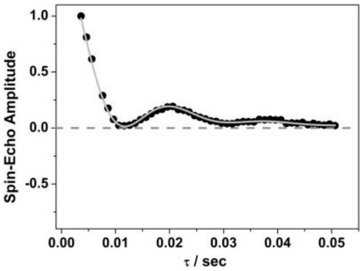	**L = 34.1** **S = 34.3**	**b = -2171±3.2** **X = 1.51** **N = 1.51**

3,4 of FSAA	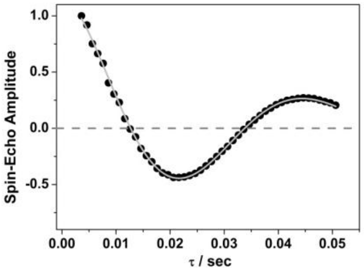	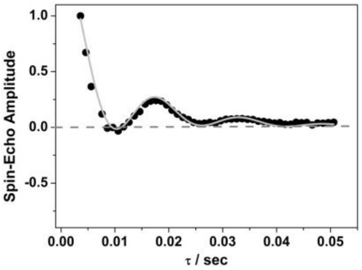	**L = 41.3** **S = 43.9**	**b = -2370±2.2** **X = 1.50** **N = 1.47**
4,5 of FSAA	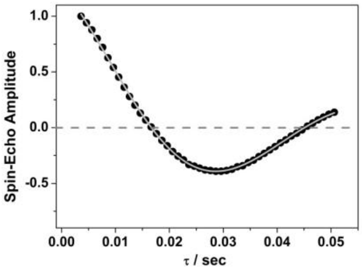	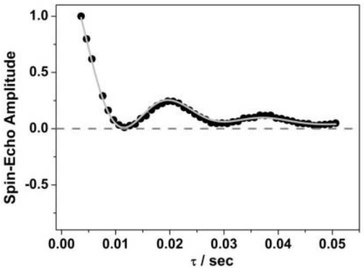	**L = 33.1** **S = 33.9**	**b = -2266±4.5** **X = 1.52** **N = 1.49**
1,3 of FSAA	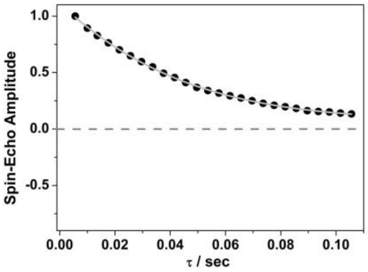	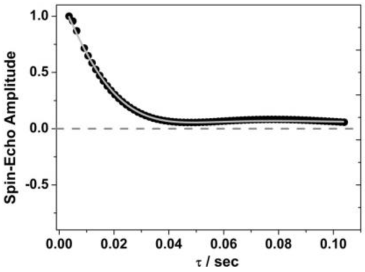	**L = obscured** **S = monotonic decay**	**b = -538±4** **X = 2.55** **N = 2.41**
1,4 of FSAA	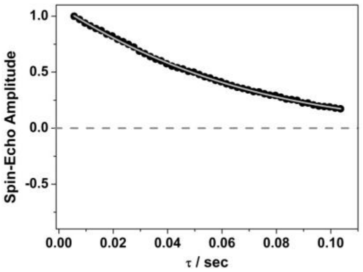	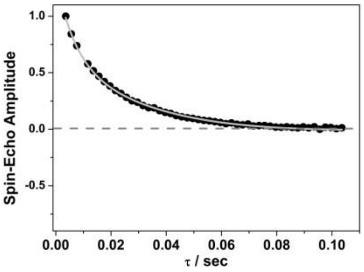	**L = 0.0** **S = monotonic decay**	**b = monotonic decay** **X = 3.72** **N = obscure**
1,5 of FSAA	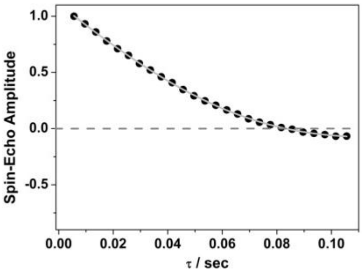	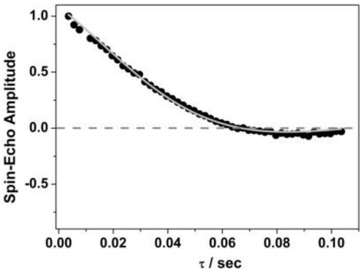	**L = 6.4** **S = 6.4+/-1.0**	**b = -169±5.3** **X = 3.58** **N = 3.54**

2,5 of FSAA	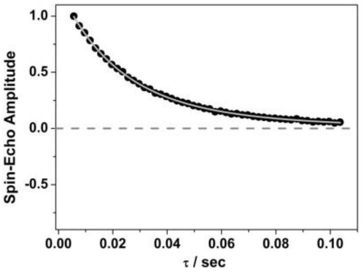	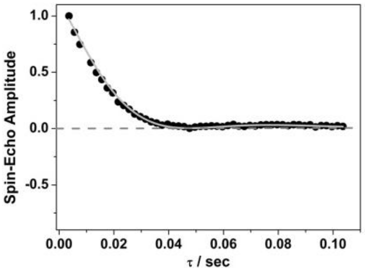	L = 0.0 S = monotonic decay	b = -699±6 X = 2.27 N = 2.21
3,5 of FSAA	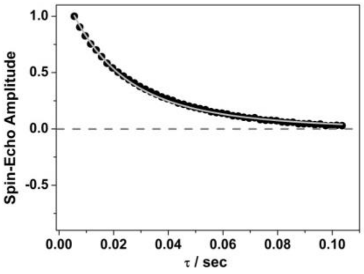	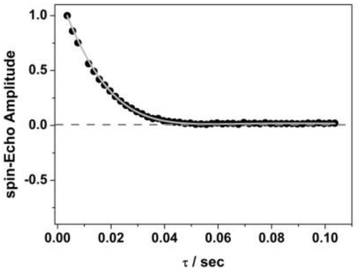	L = 0.0 S = monotonic decay	b = 560±3 X = 2.39 N = 2.38

Interestingly, distances derived for the different spin pairs of $^{13}C_5$-FSAA at OMAS NMR are in excellent agreement with distances derived from X-ray crystallographic structure (Figure V.A.7).

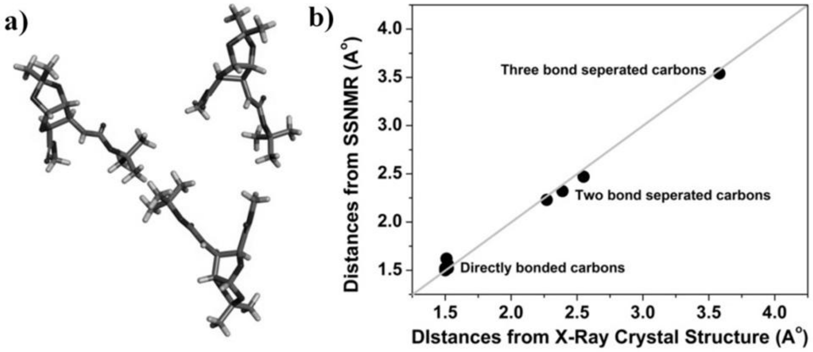

Figure V.A.7: *(a) X-Ray crystal structure of FSAA and (b) correlation between distances derived from X-Ray and OMAS SSNMR.*

V.A.3.5. *Comparison of Hadamard encoded double selective spin-echo modulations for different spin pairs in $^{13}C_8$-SA at MAS and OMAS*

Table V.A.2 described the comparison of Hadamard encoded double selective spin-echo modulations for different spin pairs of $^{13}C_8$-SA, which are generated at MAS and OMAS conditions. The measured ^{13}C-^{13}C Homonuclear dipolar couplings are divided in three groups. (i) -2500 to -2100 Hz for directly bonded carbons (~ 1.45 – 1.52 Å), modulations are strong enough at both MAS and OMAS also, (ii) -700 to -500 Hz for the two-bond separated carbons (~ 2.2 to 2.4 Å), whereas, only very week modulations are observed at OMAS condition and (iii) for the present molecule no long-range dipolar couplings are measured.

Table V.A.2: *Comparison of selective spin-echo modulations for different spin-pairs of* $^{13}C_8$*-SA, recorded at MAS and OMAS conditions.*

Spin Pair	Hadamard encoded double selective spin-echo modulation **at magic angle:** Black filled circles and grey line depict the experimental data and best fit to the equation (1), respectively.	Hadamard encoded double selective spin-echo modulation **at off magic angle**: Black filled circles and grey line depict the experimental data and best fit to the equation (2), respectively.	J_{CC} coupling in Hz; L for solution-state, S for solid-state	b, X and N represent the dipolar coupling constant in Hz, inter nuclear distances (Å) derived from X-ray and SS NMR derived distances, respectively
1,2 of SA	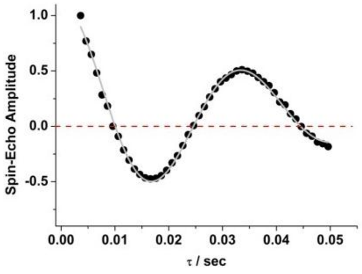	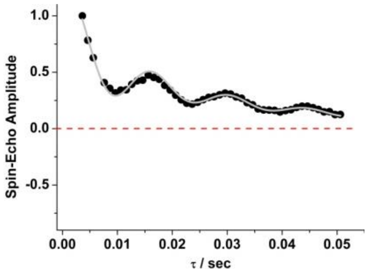	**L=59.3** **S=60.3**	**b = -2413** **X = 1.52** **N=1.46**
2,3 of SA	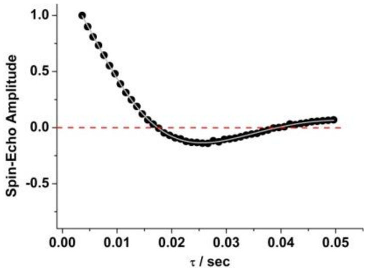	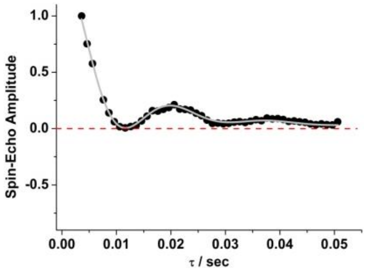	**L=36.9** **S=35.4**	**b = -2125** **X = 1.52** **N=1.52**

3,4 of SA	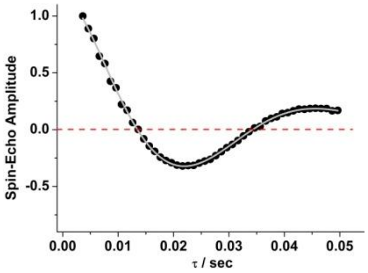	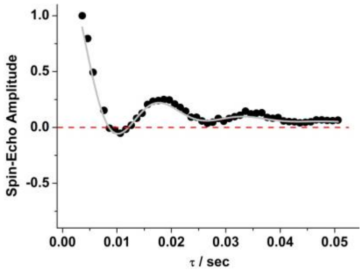	L=42.6 S=42.4	b = -2437 X = 1.52 N=1.46
4,5 of SA	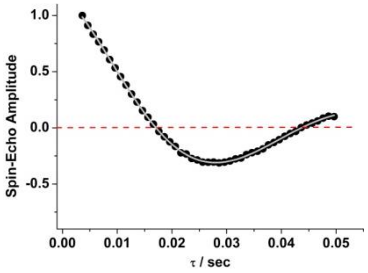	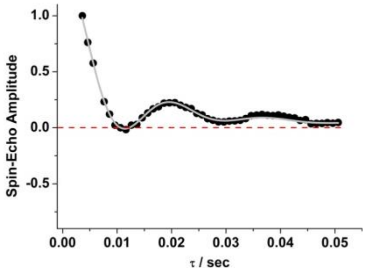	L=33.3 S=34.7	b = -2312 X = 1.52 N=1.48
6,7 of SA	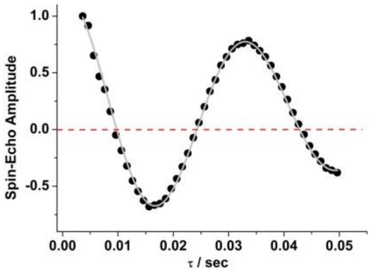	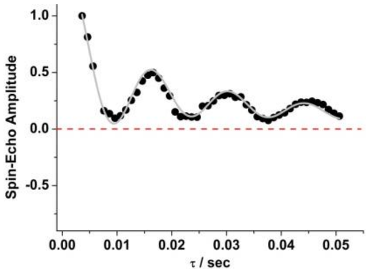	L=61.7 S=62.0	b = -2364 X = 1.52 N=1.47
7,8 of SA	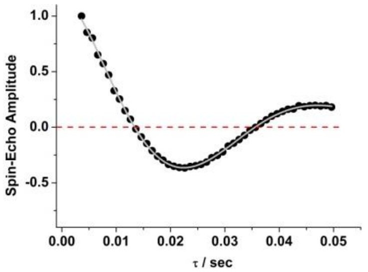	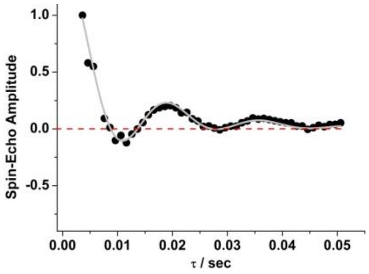	L=34.8 S=41.3	b = -2245 X = 1.52 N=1.50
1,3 of SA	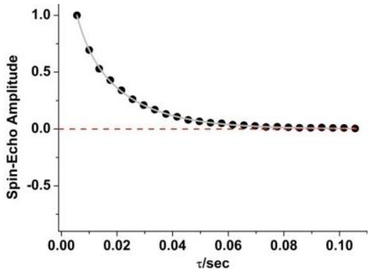	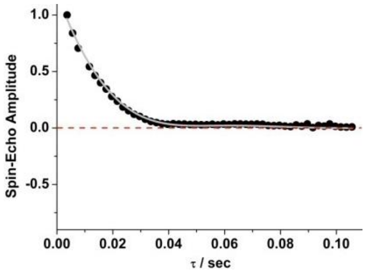	L=0.0 S= monotonic decay	b = -509 X = 2.56 N=2.45

<table>
<tr>
<td>1,4 of SA</td>
<td>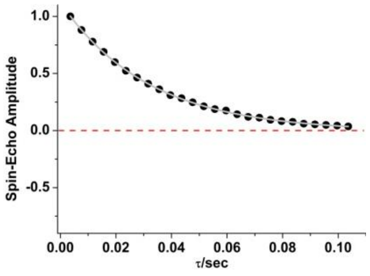
</td>
<td>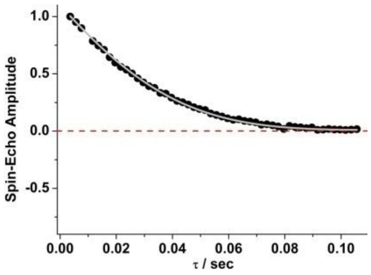
</td>
<td>L=0.0
S= monotonic decay</td>
<td>b = monotonic decay
X = 3.61
N= obscured</td>
</tr>
<tr>
<td>1,5 of SA</td>
<td>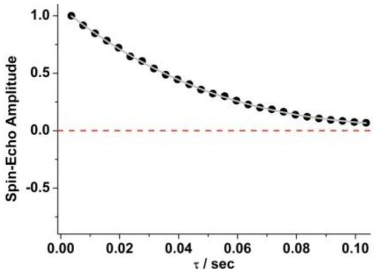
</td>
<td>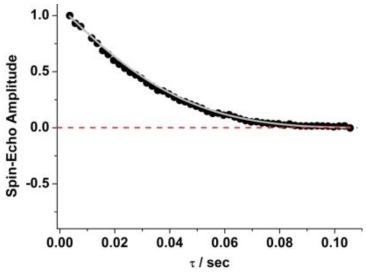
</td>
<td>L=0.0
S= monotonic decay</td>
<td>b = monotonic decay
X = 3.73
N= obscured</td>
</tr>
<tr>
<td>2,5 of SA</td>
<td>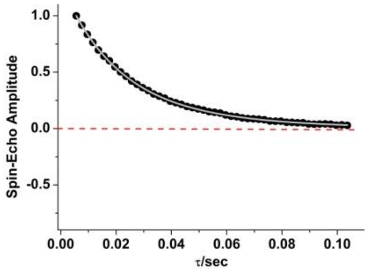
</td>
<td>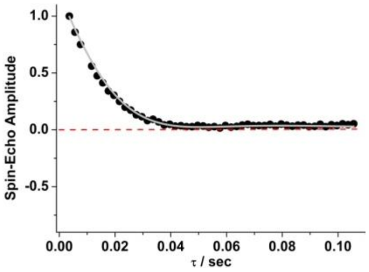
</td>
<td>L=0.0
S= monotonic decay</td>
<td>b = -663
X = 2.31
N=2.25</td>
</tr>
<tr>
<td>3,5 of SA</td>
<td>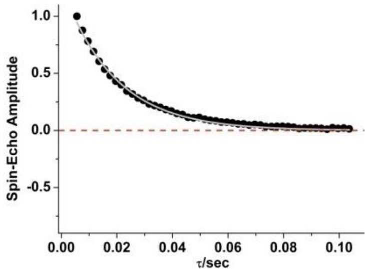
</td>
<td>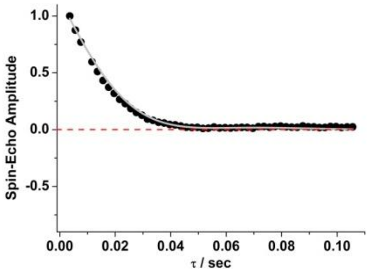
</td>
<td>L=0.0
S= monotonic decay</td>
<td>b = -633
X = 2.42
N=2.28</td>
</tr>
</table>

Distances derived from OMAS NMR are found to be fair in agreement with those obtained from X-ray crystal structure of $^{13}C_8$-SA (Figure V.A.8).

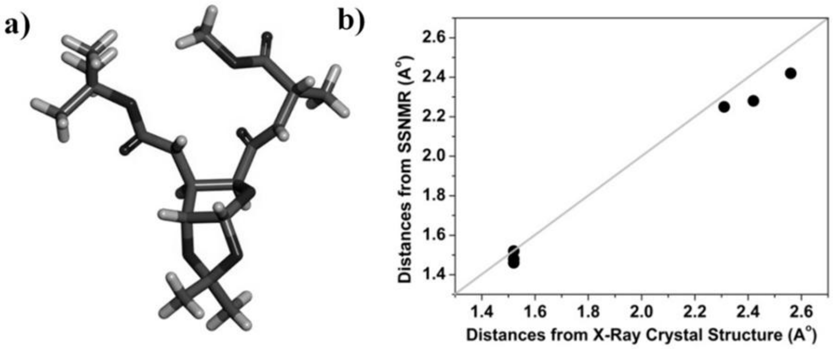

Figure V.A.8: *(a) X-Ray crystal structure of $^{13}C_8$-SA and (b) correlation between distances derived from X-Ray and OMAS SSNMR.*

Section-B

V.B.1. Experiments

Figure V.B.1 depicts the Hadamard encoded zero-quantum Rotational Resonance pulse scheme, which is an analogous version of zero-quantum selective spin-echo method.[15] In this pulse scheme, the bi-selective Gaussian refocusing pulses are replaced by the Hadamard encoded phase ramped Gaussian pulses. A total 64 step phase cycling is required and this is a more sensitive technique than the DQ method. All the experiments are performed on the Varian Unity Inova 400 MHz spectrometer equipped with 4mm chemagnetics solid-state NMR probe. Spinning speed is controlled by Varian automated MAS control unit at rotational resonance condition. The 90^{o} pulse widths are 2.75µs and 2.91µs for ^{3}C and ^{1}H, respectively. The contact time of 5s and 3s recycle delay is used. During the pulsing and acquisition periods, the SPINAL64 decoupling is employed.

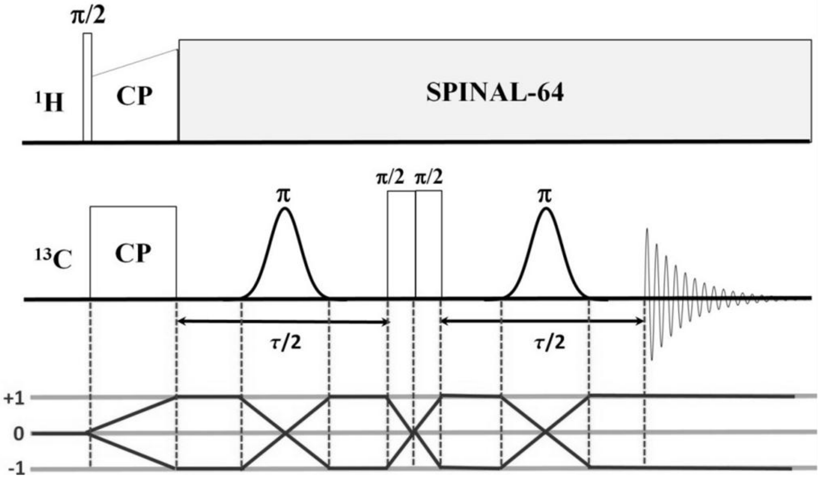

Figure V.B.1: *Schematic representation of Hadamard encoded zero-quantum spin-echo pulse sequence used for the present study with phase ramped shaped pulses.*

V.B.2. Theory

The zero-quantum echo modulation of a spin pair, far away from the rotational resonance condition may be written as

$$S(\tau) = A \exp(-0.5\tau/T_2) \cos(\pi J \tau/2)^2 \quad \rightarrow \textbf{(1)}$$

where, A is the spin population, T_2 is the spin-spin relaxation time and J is the scalar coupling constant.

The equation (2) represents the zero-quantum selective echo modulation (with shift correction for the shaped pulses) of a spin pair at away from the rotational resonance condition.

$$S(\tau) = A \exp(-0.5\tau/T_2) \cos(\pi J \tau_{eff}/2)^2 \quad \rightarrow \textbf{(2)}$$

where $\tau_{eff} = \tau - 2\tau_{sh}$

Furthermore, the zero-quantum selective echo modulation of a spin pair, at rotational resonance condition can be written as

$$S(\tau) = A \exp(-0.5\tau/T_2) \cos(\pi \varphi \tau_{eff}/2)^2 \quad \rightarrow \textbf{(3)}$$

$$\text{where } \varphi = J + D \quad \rightarrow \textbf{(4)}$$

$$= J + b/2\pi \quad \rightarrow \textbf{(5)}$$

where **b** is the dipolar coupling constant of the selected spin-pair.

From the equations (3) and (5)

$$S\,(\tau) = A\,exp\,(-0.5\,\tau/T_2)\,cos\,\{(1/4)\,(2\pi J+b)\;\tau_{eff}\}^2 \quad \rightarrow \quad \textbf{(6)}$$

V.B.3. Results and Discussions

Figure V.B.2 compares the Hadamard encoded double selective zero-quantum echo spectra for different spin pairs of $^{13}C_5$-FSAA, which are recorded at rotational resonance and away from the rotational resonance conditions.

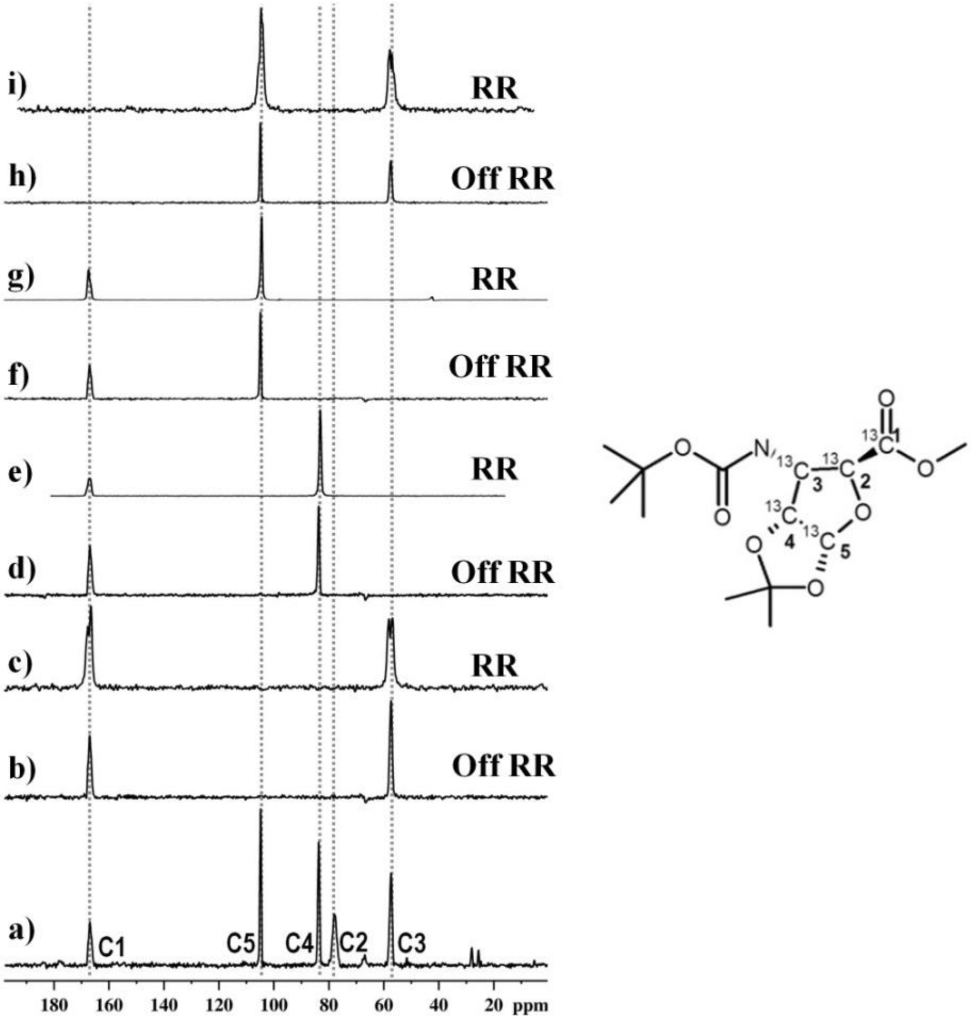

__Figure V.B.2:__ Comparison of (a) ^{13}C CPMAS spectra and the corresponding Hadamard encoded zero-quantum selective echoes for different spin pairs of $\boldsymbol{^{13}C_5}$*-FSAA at away from RR (b, d, f, h) condition and at the exact RR condition (c, e, g, i).*

(i) C1-C3 dipolar coupling:

In $^{13}C_5$-FSAA molecule C1 and C3 resonances are separated by 11025 Hz on the chemical shift scale. The sample spinning at 11025 Hz matches to the rotational resonance condition. The Figures V.B.2a and V.B.2b depict the Hadamard encoded double selective zero-quantum spectra of C1-C3 at off-RR and RR conditions, respectively. The observed line-widths at RR condition have a slightly higher value than the line-widths of spectrum recorded at off RR condition, which is due to the re-introduction of the small amount of dipolar couplings. Nevertheless, no great changes in line broadening have been identified, when compared with the OMAS spectrum. Figure V.B.3 represents the double selective zero-quantum echo modulation for C1-C3 of $^{13}C_5$-FSAA, which yields the ^{13}C-^{13}C dipolar coupling (-463 Hz and 2.54Å) between C1 and C3 by fitting the data to the theoretical equation (6).

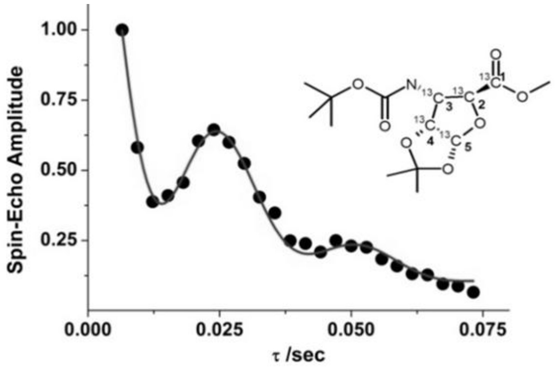

Figure V.B.3: *Hadamard encoded ZQ-selective echo modulation for C1-C3 spin pair of* $^{13}C_5$*-FSAA at 11025 Hz of sample spinning speed.*

(ii) C1-C4 dipolar coupling:

The C1 and C4 resonances of $^{13}C_5$-FSAA are separated by 8380Hz on the chemical shift scale. The sample spinning at 8380 matches the RR condition and introduces the dipolar coupling between selected spin pair C1 and C4. Herein, no scalar coupling is observed between C1 and C4 from the spin-echo modulation at MAS. The Figure V.B.4 shows the zero-quantum echo modulation for C1-C4 at RR condition and the fitted dipolar coupling value is -121 Hz (3.7Å). The distance derived from the estimated dipolar coupling is fairly comparable to the X-ray crystallographic data. Furthermore, line-widths of the spectra recorded at RR and off RR are well comparable (Figure V.B.2d and Figure V.B.2e).

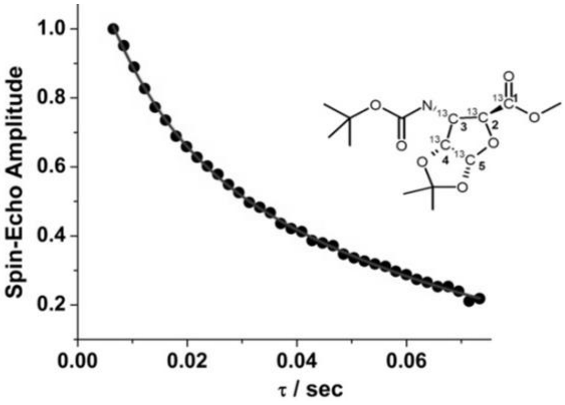

Figure V.B.4: *Hadamard encoded zero-quantum selective echo modulation for C1-C4 spin pair of $^{13}C_5$-FSAA at 8380 Hz of sample spinning speed.*

(iii) C1-C5 dipolar coupling:

The C1 and C5 resonances are separated by 6250Hz on the chemical shift scale. The sample spinning at 6250Hz reintroduces the dipolar coupling for C1-C5 spin pair of $^{13}C_5$-FSAA molecule by matching the RR condition. The Figure V.B.5 depicts the zero-quantum echo modulation for C1 and C5 at RR condition, and the fitted dipolar coupling value is -153 Hz (3.63Å), which is strongly supported by inherently available scalar coupling (6.2 Hz) between the selected spin-pair. Furthermore, line-widths are comparable for RR and off-RR spectra of C1-C5, which are shown in Figures V.B.2f and V.B.2g, respectively.

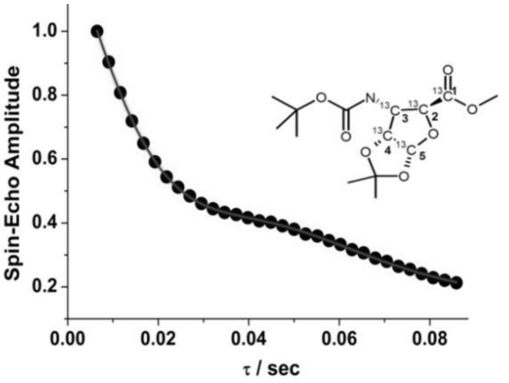

Figure V.B.5: *Hadamard encoded ZQ selective spin-echo modulation for C1-C5 spin pair of $^{13}C_5$-FSAA at 6250 Hz of sample spinning speed.*

(iv) C3-C5 dipolar coupling:

The C3 and C5 resonances of $^{13}C_5$-FSAA are separated by 4775Hz on the chemical shift scale. The sample spinning at 4775 Hz matches the rotational resonance condition for the selected C3-C5 spin pair, which introduces the dipolar coupling. The Figure V.B.6 shows the zero-quantum spin-echo modulation of the C3-C5 spin pair, which yields a dipolar coupling value of -475 Hz (2.51Å). The comparison of Figure V.B.2h and Figure V.B.2i describes the change in line-widths of C3 and C5 resonances, while introducing the full amount dipolar couplings for 2.51Å separation.

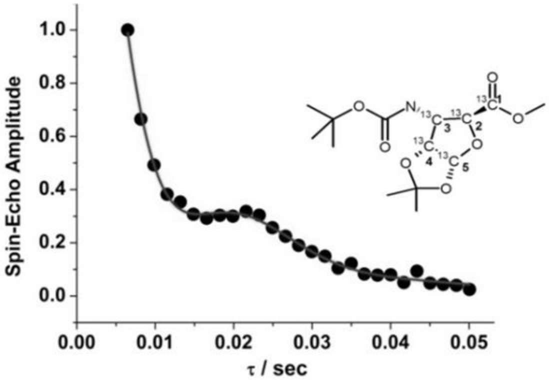

Figure V.B.6: *Hadamard encoded zero-quantum selective spin-echo modulation for C3-C5 spin pair of $^{13}C_5$-FSAA at 4775 Hz of sample spinning speed.*

The inter-nuclear distances thus estimated from the experimentally derived dipolar couplings have shown a nice correlation with the distances derived from the X-Ray crystal structure (Figure V.B.7).

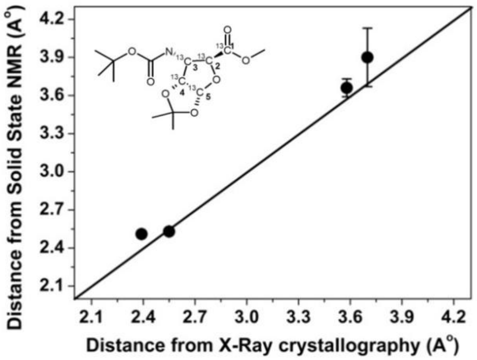

Figure V.B.7: *Correlation between distances derived from the X-Ray crystallography and Hadamard encoded zero-quantum RR echo SSNMR for different spin pairs of $^{13}C_5$-FSAA molecule.*

V.2. Conclusion

In conclusion, the conventional PDSD build-up curves are recorded for the $^{13}C_5$-FSAA molecule, which helps in monitoring the long-range spin-spin correlations, but provide only the semi-qualitative information. On the other hand, a new set of Hadamard encoded selective spin-echo experiments are demonstrated, which allow to measure the accurate distances between selected spin-pairs in uniformly labelled molecules. The distances derived from the spin-echoes at off-magic angle sample spinning are in good agreement with the X-ray crystallographic data. However, the spectral resolution is rather poor at off-magic angle sample spinning condition, since the dominant CSA and dipolar contributions introduce a huge line-broadening. Herein, a long-range distance up to 4Å is measured, where the echo modulation is strongly supported by the inherently available $3J_{CC}$ coupling between C1 and C5 of $^{13}C_5$-FSAA. Alternatively, to overcome these resolution issues due to the off-magic angle spinning experiments, rotational-resonance zero-quantum spin-echo experiments are presented. The measured line-widths of the spectra, which are recorded at RR condition, have shown additional broadening, since the dipolar couplings are reintroduced. However, the measured distances are well comparable with the distances derived from the x-ray crystallographic data. The described methodologies can be extended to the isotope labelled complex biological solids.

V.3. References

[1] A. E. Bennett, C. M. Rienstra, J. M. Griffiths, W. Zhen and P. T. Lansbury, Homonuclear radio frequency-driven recoupling in rotating solids, J. Chem. Phys, 108 (1998) 9463-9479.

[2] D. P. Raleigh, M. H. Levitt and R.G. Griffin, Rotational Resonance in Solid-State NMR, Chem. Phys. Lett, 146 (1988) 71-76.

[3] N. Bloembergen, On the interaction of nuclear spins in a crystalline lattice, Physica, 15 (1949) 386–426.

[4] K. Takegoshi, S. Nakamura and T. Terao, ^{13}C-^{1}H dipolar-assisted rotational resonance in magic-angle spinning NMR, Chem. Phys. Lett, 344 (2001) 631–637.

[5] J. R. Lewandowski, G. D. Paepe, M. T. Eddy and R. G. Griffin, ^{15}N-^{15}N Proton Assisted Recoupling in Magic Angle Spinning NMR, J. Am. Chem. Soc, 131 (2009) 5769–5776.

[6] A. Lange, S. Luca and M. Baldus, Structural Constraints from Proton-Mediated Rare-Spin Correlation Spectroscopy in Rotating Solids, J. Am. Chem. Soc, 124 (2002) 9704-9705.

[7] T. Gullion, Introduction to Rotational-Echo Double-Resonance NMR, Conc. Magn. Reson, 10 (1998) 277-289.

[8] C. P. Jaroniec, C. Filip and R. G. Griffin, 3D TEDOR NMR Experiments for the Simultaneous Measurement of Multiple Carbon-Nitrogen Distances in Uniformly ^{13}C, 15N-Labeled Solids, J. Am. Chem. Soc, 124 (2002) 10728-10742.

[9] A. Egawa, T. Fujiwara, T. Mizoguchi, Y. Kakitani, Y. Koyama and H. Akutsu, Structure of the light-harvesting bacteriochlorophyll-c assembly in chlorosomes from Chlorobium limicola determined by solid-state NMR, 104 (2007) 790–795.

[10] R. Ramachandran, V. Ladizhansky, V. S. Bajaj, and R. G. Griffin, ^{13}C-^{13}C Rotational Resonance Width Distance Measurements in Uniformly ^{13}C-Labeled Peptides, J. Am. Chem. Soc, 125 (2003) 15623-15629.

[11] L. Sonnenberg, S. Luca and M. Baldus, Multiple-spin analyses of chemical-shift-selective (13C, 13C) transfer in uniformly labeled biomolecules, J. Magn. Reson, 166 (2004) 100–110.

[12] P. T. F. Williamson, A. Verhoeven, M. Ernst and B. H. Meier, Determination of Internuclear Distances in Uniformly Labeled Molecules by Rotational-Resonance Solid-State NMR, J. Am. Chem. Soc, 125 (2003) 2718-2722.

[13] G. Pileio, Y. Guo, T. N. Pham, J. M. Griffin, M. H. Levitt, S. P. Brown, Residual Dipolar Couplings by Off-Magic-Angle Spinning in Solid-State Nuclear Magnetic Resonance Spectroscopy, J. Am. Chem. Soc, 129 (2007) 10972–10973.

[14] G. Pileio, S. Mamone, G. Mollica, I. M. Montesinos, A. Gansmuller, M. Carravetta, S. P. Brown and M. H. Levitt, Estimation of internuclear couplings in the solid-state NMR of multiple-spin systems. Selective spin echoes and off-magic-angle sample spinning, Chem. Phys. Lett, 456 (2008) 116–121.

[15] P. Thureau, A. C. Sauerwein, M. Concistre and M. H. Levitt, Selective internuclear coupling estimation in the solid-state NMR of multiple-spin systems, Phys. Chem. Chem. Phys, 13 (2011) 93–96.

[16] J. Becker-Baldus, T. F. Kemp, J. Past, A. Reinhold, A. Samoson and S. P. Brown, Longer-range distances by spinning-angle-encoding solid-state NMR spectroscopy, Phys. Chem. Chem. Phys, 13 (2011) 4514–4518.

Chapter-VI

Spectral simplifications in solid-state NMR

Selective Refocused Uniform Cross-peak Signed Double Quantum Filtered Correlation Spectroscopy (SRUC2QF COSY): Enhanced efficiency and sensitivity at lower spinning speeds

VI.1.Introduction

The chemical shift assignments of solid-state samples can be established either by through bond or through space correlation experiments, wherein an accurate identification of the cross-peaks are crucial. The cross-peak intensities of double quantum techniques are governed by the scalar coupling network specific to the molecule as well as the corresponding spin-spin relaxation times. Different experimental methods: TOCSY,[1] refocused-INADEQUATE,[2] UC2QF-COSY (uniform cross peak sign double quantum filtered COSY),[3] CTUC-COSY[4] (constant time uniform cross-peak sign COSY) and SAR-COSY[5] (sensitive absorptive refocused COSY) have been developed over the years, to identify the chemical shift correlations.

Among the other methods, solid-state TOCSY is analogous to its routine solution-state version and the required isotropic mixing at the magic angle spinning is achieved by rotor synchronized pulses. But, the described scheme results in heating up of RF coils and is sensitive to the pulse imperfections. Alternatively, refocused-INADEQUATE with enhanced transverse relaxation times during the refocusing periods is known, [2] which has lower sensitivity with respect to the two dimensional double quantum COSY (DQCOSY).

On the other hand, UC2QF-COSY is a versatile technique and has better efficiency for double quantum filtration over the CTUC-COSY. However, these methods suffer from (i) longer acquisitions times and (ii) cumbersome determination of the evolution times (based on the spin system; IS and IS_n) for attaining optimum cross-peak intensities. These problems can be addressed by selective refocusing of interested resonance bands in either double or Hadamard encoded multiple selective refocusing modes. Based on the choice of the spin-pairs for selective refocusing, the UC2QF-COSY facilitates commutation between spin-spin interactions,[6] thereby the damping components are limited to the spin-spin couplings and to the corresponding relaxation times. To this effect, in the present chapter, a selective refocused UC2QF-COSY (SRUC2QF-COSY) is introduced.

The present chapter demonstrates the reconstruction of spinning side-band free DQFCOSY of organic solids, which is fast and shows improved sensitivity. The sensitivity has been enhanced by recording the SRUC2QF-COSY spectra for the commuted spin-pairs (directly bonded or long-range) by choosing appropriate mixing times those are computed from simulations. Furthermore, the utility of covariance processing [7] significantly minimizes the experimental times, and a small number of indirect dwell increments are sufficient. The SRUC2QF-COSY spectra are acquired in a wide range of sample spinning frequencies and permit to observe the spinning sideband free spectra, even at low sample spinning speeds.

The covariance processing has been well explored in solution-state NMR, [8-11] whereas, it is sparsely used in solid-state NMR.[12-14] In contrast to the regular 2D-FT, in a 2D covariance spectrum, resolution along the indirect dimension is determined by the resolutions of the direct dimensions. The mathematical form of covariance NMR is straightforward and it may be as defined by the following equation

$$C = (XX^{T})^{1/2}$$

where C is the symmetric covariance matrix, X and X^T are the real and transpose of the regular 2D FT spectrum, respectively.

VI.2.Methodology

Solid-state UC2QF-COSY[3] is a similar to its solution-state DQFCOSY pulse sequence. However, the diagonal and cross-peak anti-phase signals of solution-state DQFCOSY are converted to in-phase signals in the UC2QF-COSY pulse scheme, by using the additional refocusing pulses and z-filter. While the mixing time or evolution time 2τ, during the refocusing periods for IS type of spin systems is $1/2J$, its value ranges from $1/8J$ to $1/4J$ for clustered spin systems.

The dependences of spin evolution times on the cross-peak intensities for IS and IS_n spin-systems are given in equation (1) and (2), respectively. The spin-spin interactions of IS_n spin-system can be converted to IS type by using selective refocusing pulses, which has been reported for the sensitivity enhancement of Cα-Cβ cross-peaks by deselecting the -C=O resonance bands in CTUC-COSY of bio-molecules.[4] In the present chapter, the same strategy has been explored for the selection of different spin-pairs or spin combinations by using either normal bi-selective or Hadamard encoded refocusing pulses. The theoretical expressions for mixing time dependent cross-peak intensities of *IS* and IS_n spin-systems are given below.

For *IS* spin-system, the cross-peak intensity can be written as,

$$T_{1,2} = \tfrac{1}{2} \sin^2 (2\pi J_{1,2}\tau) \exp(-4\tau/T_2^*) \quad \rightarrow \ (1)$$

Similarly, for IS_n spin-system, the cross-peak intensity can be written as

$$T_{m,n} = \tfrac{1}{2} \sin^2 (2\pi J_{m,n}\tau)\, \Pi\cos(2\pi J_{m-1,m}\tau)\, \Pi\cos(2\pi J_{n,n+1}\tau) \exp(-4\tau/T_2^{*\,m,n})\, \Pi\exp(-4\tau/T_2^{*\,m-1,m})\, \Pi\exp(-4\tau/T_2^{*\,n,n+1}) \rightarrow \ (2)$$

where, $T_{m,n}$ and $T_2^{*\,m,n}$ are the intensity of the cross-peaks and homogeneous spin-spin relaxation times of spin pair $-C_{m-1}-\underline{\boldsymbol{C_m-C_n}}-C_{n+1}-$, respectively.

In the case of *IS* spin-system (ex: $^{13}C_2$-Glycine), $T_{1,2}$ is optimum at τ = 5ms, which is calculated from the measured scalar coupling $J_{CO\text{-}C\alpha}$ (~50 Hz). The required total mixing time during the refocusing period of UC2QF-COSY is equal to 10 ms, which is considerably large for the transverse de-phasing of magnetization in solid-state samples. The estimation of cross-peak intensities are governed by the spin-spin relaxation time and scalar couplings. Accordingly, the intensities for a combination of smaller scalar couplings (< 50 Hz, $J_{C\alpha\text{-}C\beta}$ ~30 Hz) with short spin-spin relaxation times are lower with respect to the combination of maximum coupling constant and considerably large spin-spin relaxation times.

The commutation between spin-spin interactions is achieved by replacing the refocusing hard π pulses of UC2QF-COSY, either by the bi-selective or Hadamard encoded selective refocusing pulses as described in the earlier chapters. The schematic representation of UC2QF-COSY and SRUC2QF-COSY pulse sequences are depicted in Figure VI.1, and are demonstrated for uniformly labelled molecules, $^{13}C_6$ L-Histidine.HCl and $^{13}C_5$-FSAA.

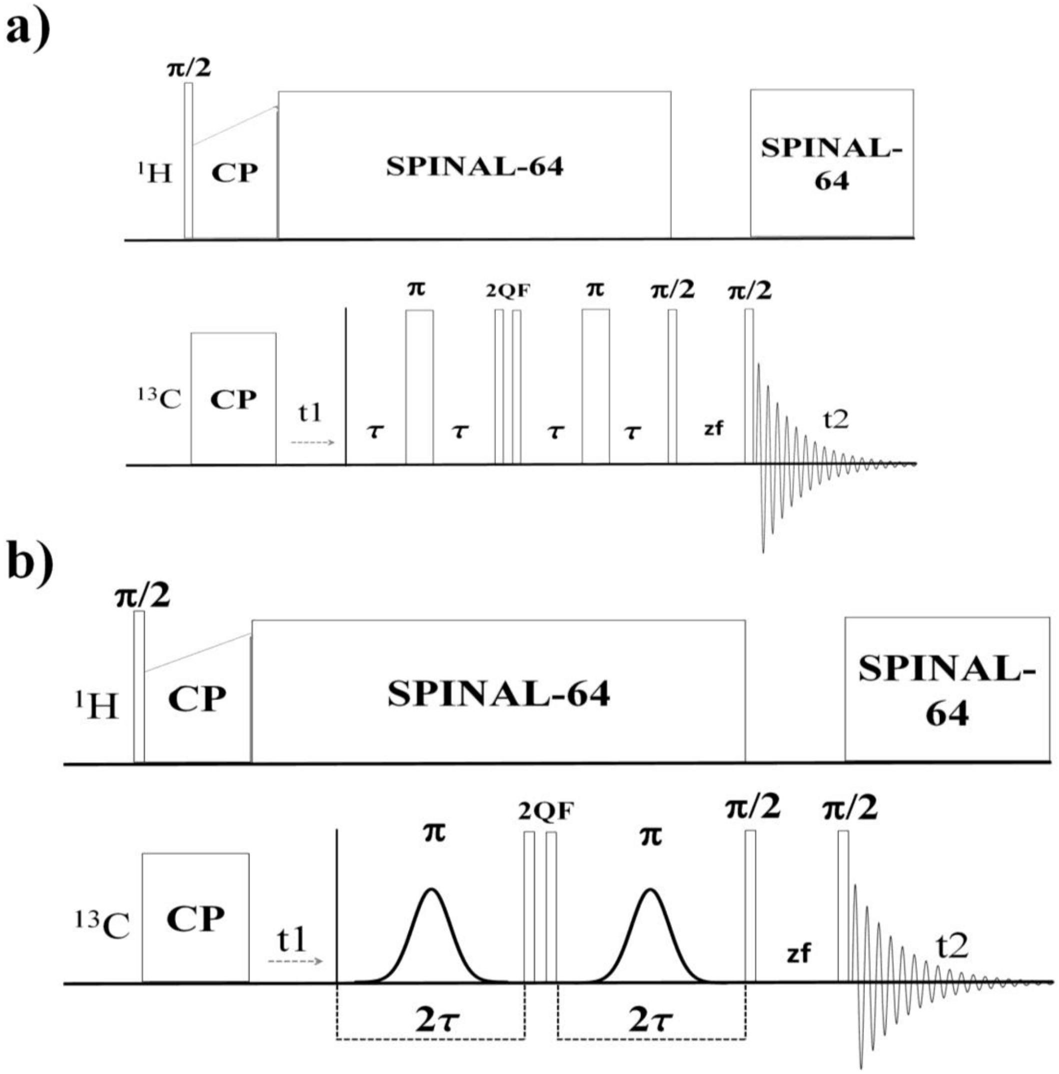
a)
π/2
¹H
CP
SPINAL-64
SPINAL-64
π
2QF
π
π/2
π/2
¹³C
CP
t1
τ
τ
τ
τ
zf
t2
b)
π/2
¹H
CP
SPINAL-64
SPINAL-64
π
2QF
π
π/2
π/2
¹³C
CP
t1
zf
t2
2τ
2τ

Figure VI.1: *Schematic representation of double quantum filtered pulse sequences: (a) UC2QF-COSY and (b) SRUC2QF-COSY.*

VI.3.Experiments

All the Hadamard selective spin-echo, UC2QF-COSY and SRUC2QF-COSY are performed on Varian UNITY INOVA 400 MHz spectrometer equipped with 4mm chemagnetics probe. The sample spinning frequencies are controlled at 4.2 kHz, 8.0 kHz, and 13.0 kHz for $^{13}C_6$ L-Histidine.HCl and 10.0 kHz for $^{13}C_5$-FSAA. The optimized pulse widths are 3.1 μs and 3.5 μs for ^1H and ^{13}C, respectively. Contact times of 1.0, 2.0, 3.0 and 3.0 ms are used for 4.2, 8.0, 10 and 13.0 kHz spinning speeds, respectively. Total 64 step phase cycling is applied. The sweep-widths 24, 24, 20 and 26 kHz are used for 4.2, 8.0, 10, and 13.0 kHz spinning speeds, respectively. The Gaussian shaped pulse of 4.5 ms is used for double and multiple selective refocusing modes, which is equal to 200 Hz of bandwidth. The SRUC2QF-COSY experiments are acquired with 16 complex points along the indirect dimensions; whereas, UC2QF-COSY experiments are acquired with the 256 complex increments.

VI.4. Results and Discussions

VI.4.1. *Simulation of cross-peak intensities in isolated and multi-spin systems*

Initially, the optimum evolution times required for obtaining the maximum DQ cross-peak intensities of UC2QF-COSY (clustered spin system) and SRUC2QF-COSY (commuted spin pairs) are computed for each spin pair in uniformly labelled molecules ($^{13}C_6$ L-Histidine.HCl and $^{13}C_5$-FSAA) by using equations (1) and (2), respectively. Subsequently, these optimum values are employed in UC2QF-COSY and SRUC2QF-COSY experiments at different sample spinning speeds. The selective scalar couplings and spin-spin relaxation times ($J_{m,n}$ and $T_2{*}^{\,m,n}$) are the essential input parameters for these simulations, which are obtained from the selective spin-echo modulations recorded for different spin pairs at altered spinning speeds, as discussed in chapter-II.

The measured selective J_{CC} values for $^{13}C_6$ L-Histidine.HCl molecule, at higher spinning speeds are in good agreement with the solution-state J_{CC}. However, at the lower spinning speed 4.2 kHz, a considerable difference in J_{CC} is observed, especially for the CH_2 carbons, which may be due to the introduction of small magnitude of dipolar couplings. The relaxation times of CH_2 carbons measured at 13.0 kHz spinning speed are about twice to the values measured at 4.2 kHz spinning speed. The scalar couplings and spin-spin relaxation times, which are experimentally measured from the selective spin-echoes for different spin pairs of $^{13}C_6$ L-Histidine.HCl and $^{13}C_5$-FSAA at different spinning speeds, are given in Table VI.1.

***Table VI.1:** $^nJ_{CC}$ and spin-spin relaxation times derived from the 2D pseudo selective spin-echo modulations for different spin pairs of $^{13}C_6$ L-Histidine.HCl and $^{13}C_5$-FSAA at altered spinning frequencies.*

Spin pair	$^{13}C_6$ Histidine.HCl							$^{13}C_5$-FSAA			
	4.2 kHz sample spinning		8.0 kHz sample spinning		13.0 kHz sample spinning		Solution-state scalar coupling	Spin pair	10.0 kHz sample spinning		Solution-state scalar coupling
	$^1J_{CC}$ (Hz)	T_2 (m s)	$^1J_{CC}$ (Hz)	T_2 (m s)	$^1J_{CC}$ (Hz)	T_2 (m s)	$^1J_{CC}$ (Hz)		$^1J_{CC}$ (Hz)	T_2 (m s)	$^1J_{CC}$ (Hz)
C6-C5	57.9	**13.5**	57.0	**23.6**	58.3	**39.0**	59.8	**C1-C2**	72.1	**78.8**	71.2
C5-C3	24.7	**6.4**	32.0	**7.3**	34.3	**12.5**	34.6	**C2-C3**	34.1	**25.4**	34.1
C3-C4	34.8	**8.9**	48.4	**13.2**	52.2	**20.7**	51.0	**C3-C4**	43.9	**27.0**	41.3
C4-C1	75.1	**9.3**	72.7	**12.5**	75.6	**23.6**	74.5	**C4-C5**	33.9	**39.8**	33.9
								C1-C5	8.2	**108.8**	6.4

VI.4.1.1 *Simulation of cross-peak intensities for different spin-pairs in $^{13}C_6$ L-Histidine.HCl*

For clustered spin system, the cross-peak intensity profiles for different spin pairs of $^{13}C_6$ L-Histidine.HCl are simulated by using equation-2 and are shown in Figure VI.2. As expected, the intensity of the cross-peak enhances with the spinning speed, which is due to the increased spin-spin relaxation times (decreased line width). The cross-peak intensities of C5-C3 (red line) and C3-C4 (green line) spin pairs are about 10 to 20 times larger at different spinning speeds with respect to the cross-peak intensities of C6-C5 (blue line) and C4-C1 (magenta line). The peak maxima are observed at mixing times 1.0, 1.25, and 1.8 for 4.2, 8.0, and 13.0 kHz spinning speeds, respectively.

On the other hand, the cross-peak intensity profiles for commuted spin pairs of $^{13}C_6$ L-Histidine.HCl molecule are simulated by using equation-1. Here also the C5-C3 (red line) and C3-C4 (green line) spin pairs exhibit around 6 times lower intensity at 4.2 kHz spinning speed and ~3 times lower intensity at 13.0 kHz spinning speed, when compared to the C6-C5 (blue line) and C4-C1 (magenta line) spin pairs. Furthermore, interestingly, the simulated cross-peak intensities for commuted spin pairs (SRUC2QF-COSY) at 4.2 kHz are relatively higher with respect to those in clustered system (UC2QF-COSY), at 13 KHz spinning speed.

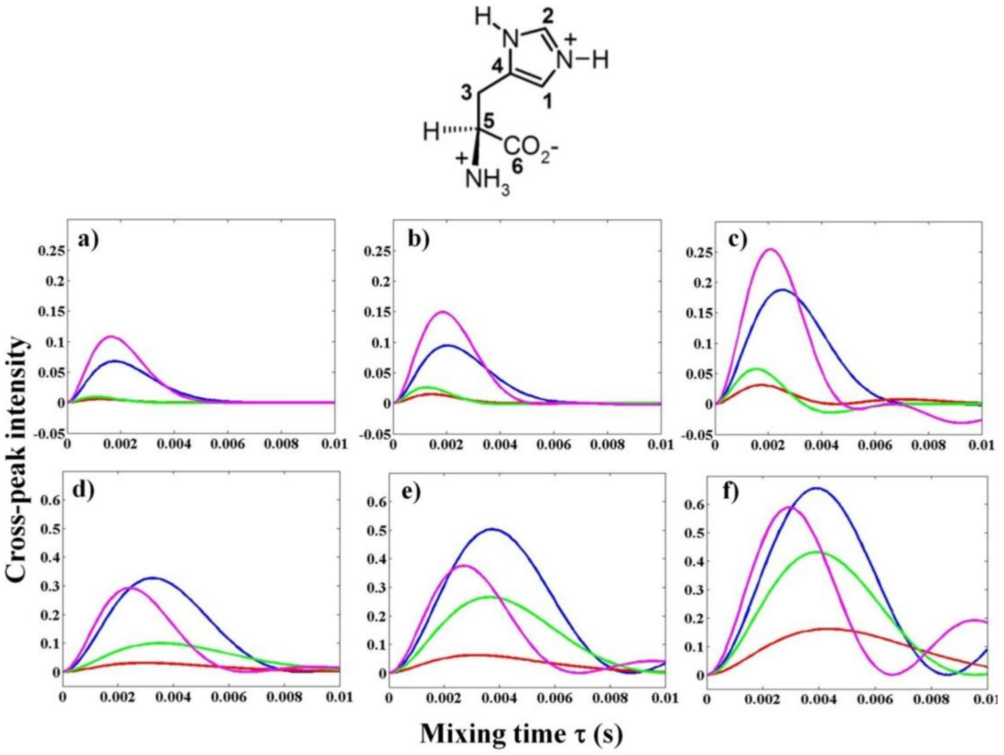

Figure VI.2: *The simulated UC2QF-COSY (for the clustered spin system) cross-peak intensity profiles for different spin pairs (C6-C5 (•), C5-C3 (•), C3-C4 (•) and C4-C1 (•)) of* $^{13}C_6$ *L-Histidine.HCl are shown in (a), (b) and (c) at altered spinning speeds 4.2, 8.0 and 13.0 kHz, respectively. The corresponding cross-peak intensity profiles of SRUC2QF-COSY (for individual spin-pairs) are shown in (d), (e) and (f).*

In the light of the observed sensitivity enhancement, the SRUC2QF-COSY experiments are extended to the multiple selective refocusing modes, which can be experimentally implemented by using Hadamard encoded selective refocusing pulses. Herein, the variation in cross-peak intensities is simulated for the two different spin combinations: C6-C5-C4-C1 and C5-C3-C4 of $^{13}C_6$ L-Histidine.HCl (Figure VI.3) by using equation-2. The J_{CC} and relaxation times, which are measured at 13.0 kHz sample spinning speed are used for the simulation. For commuted C6-C5-C4-C1 spin combination, no loss in the cross-peak intensities is observed with respect to these cross-peak intensities in double selective refocusing mode. Whereas, in C5-C3-C4 spin-combination, a threefold increase in the cross-peak intensities of C5-C3 (red line) and C3-C4 (green line) is observed at 3.0 ms of evolution time with respect to the cross-peak intensities in the clustered spin system.

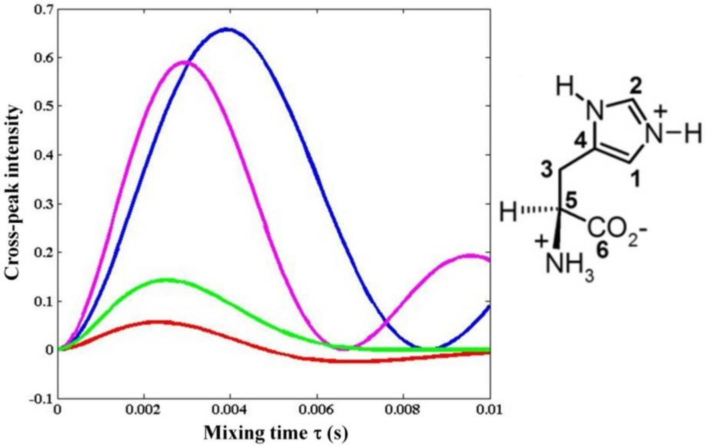

Figure VI. 3: *The simulated SRUC2QF-COSY cross-peak intensity profiles (~10 kHz) for different spin pairs (C6-C5 (●), C5-C3 (●), C3-C4 (●) and C4-C1 (●)) of $^{13}C_6$ L-Histidine.HCl. The spin combinations C6-C5-C4-C1 and C5-C3-C4 can be selected with the Hadamard multiple selective refocusing modes.*

VI.4.1.2. *Simulation of cross-peak intensities for different spin-pairs in $^{13}C_5$-FSAA molecule*

Similarly, the cross-peak intensities at 10 kHz sample spinning speed are simulated for individual spin-pairs of $^{13}C_5$-FSAA molecule by considering (i) clustered spin-system (UC2QF-COSY) and (ii) commuted spin-pairs (SRUC2QF-COSY). A considerable enhancement in SRUC2QF-COSY (equation-1) cross-peak intensities are observed, with respect to those in UC2QF-COSY (equation-2). The simulated SRUC2QF-COSY cross-peak maxima (Figure VI.4) for directly bonded spin pairs and the long range C1-C5 spin pair, are observed at ~4.0 ms and ~10 ms, respectively. Whereas, in the case of UC2QF-

COSY, the average simulated peak maxima are observed at ~2 ms for all the spin pairs (Figure VI.4). Furthermore, the dominant J_{CC} and spin-spin relaxation values of directly bonded spin-pairs of clustered spin systems do not allow to observe the long range correlations. However, the SRUC2QF-COSY method overcomes this difficulty, since the effect of dominant relaxations and scalar coupling information is suppressed during the selective refocusing.

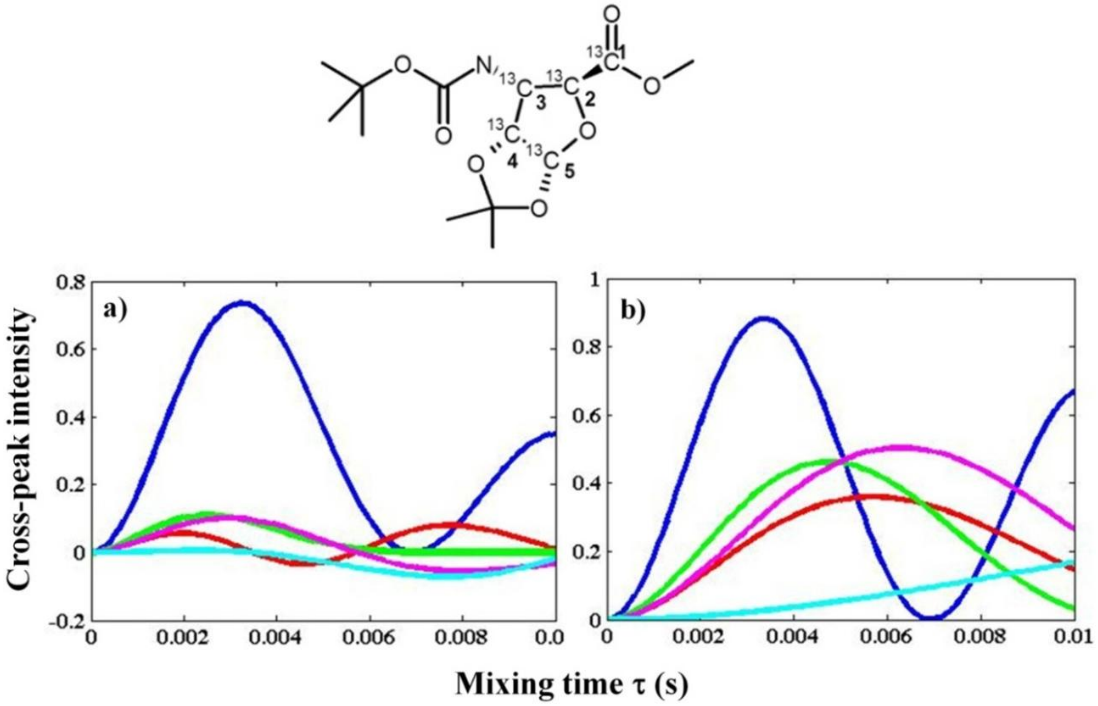

Figure VI.4: *The simulated UC2QF-COSY (for complete spin system) cross-peak intensity profiles for different spin pairs (C1-C2 (•), C2-C3 (•), C3-C4 (•), C4-C5 (•) and C1-C5 (•)) of* $^{13}C_5$*-FSAA is shown in (a) at 10.0 kHz sample spinning speed. The corresponding cross-peak intensity profiles of SRUC2QF-COSY (for individual spin-pairs) are shown in (b).*

The SRUC2QF-COSY cross-peak intensities are also simulated for three different spin combinations of $^{13}C_5$-FSAA, at 10 kHz sample spinning speed. In case of C1-C2-C4-C5 spin combination, no loss in the cross-peak intensities is observed, which is due to the spin-spin commutation. Furthermore, for C2-C3-C4 spin combination, a considerable increase in the cross-peak intensities for C2-C3 and C3-C4 spin pairs is observed with respect to the corresponding intensities in the clustered spin system. The third combination: long range C1-C5 spin pair, requires relatively long mixing time, due to the small spin-spin coupling. For directly bonded spin pairs, the mixing time is around ~3 ms, seems to be optimum cross-peak intensities, whereas its value is ~10 ms for the long range ${}^{3}J_{C1\text{-}C5}$ (Figure VI.5).

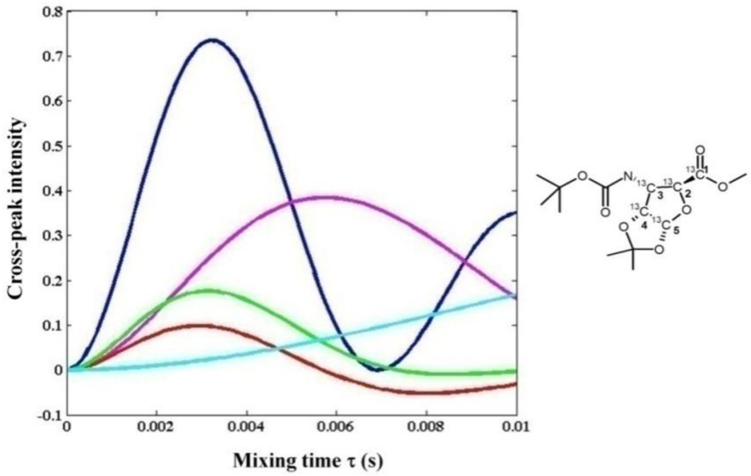

Figure VI.5: *The simulated SRUC2QF-COSY cross-peak intensity profiles for different spin pairs* ***(C1-C2 (●), C2-C3 (●), C3-C4 (●), C4-C5 (●)*** *and* ***C1-C5 (●))*** *of* $^{13}C_5$*-FSAA recorded at 10 kHz sample spinning speed. The different spin combinations C1-C2-C4-C5, C2-C3-C4 and C1-C5 can be selected with the Hadamard multiple selective refocusing modes.*

VI.5. Experimental results

VI.5.1. *UC2QF-COSY NMR experiments of* $^{13}C_6$ *L-Histidine.HCl*

The UC2QF-COSY spectra of $^{13}C_6$ L-Histidine.HCl are recorded at 4.2 kHz (Figure VI.6a), 8.0 kHz (Figure VI.6b) and 13.0 kHz (Figure VI.6c) with the optimized mixing time (τ) values 1.0, 1.25 and 1.8 ms, respectively. The acquired UC2QF-COSY spectrum at 4.2 kHz is difficult to analysis due to the poor cross-peak intensities. Furthermore, the less sensitive cross-peaks are severely overlapped by the spinning side-bands of sp2 carbons (C6, C4 and C1). However, the data collected at higher spinning speeds viz., 8.0 and 13.0 kHz exhibit relatively better intensity, but each UC2QF-COSY spectrum requires ~ 9 Hrs of acquisition time. Therefore, the conventional UC2QF-COSY demands more acquisitions and the spectra exhibit inferior cross-peak sensitivities. Nevertheless, the re-introduction of spin-spin commutation facilitates the acquisition of 2D spectra with the optimum cross-peak intensity.

VI.5.2. *Double band-selective SRUC2QF-COSY NMR experiments of $^{13}C_6$ L-Histidine.HCl*

The SRUC2QF-COSY spectra are recorded at 4.2 kHz (Figure VI.7d), 8.0 kHz (Figure VI.7e) and 13.0 kHz (Figure VI.7f) of sample spinning with the corresponding optimized mixing time (τ) values 3.0, 3.0 and 4.0 ms, respectively. The choice of selective refocusing of two resonance bands in each experiment facilitates the minimization of acquisition times. Herein, 16 complex increments are collected along the indirect dimension and processed with the covariance method (Figure VI. 6) and the number of increments is sufficient to observe the chemical shift connectivity along the indirect dimensions. The required spectral acquisition time for each double band selective experiment (SRUC2QF-COSY) is only ~30 min. In the present case, total four double band selective experiments are recorded for $^{13}C_6$ L-Histidine.HCl in ~ 2Hrs. The spin pairs C6-C5, C5-C3, C3-C4 and C4-C1 are selected based on the known knowledge of resonance bands of natural amino acids. The same methodology can be adopted for unnatural amino acids as well. Subsequently, the double band selective SRUC2QF-COSY spectra of the individual spin-pairs are co-added to yield a spectrum equivalent to that of a full UC2QF-COSY spectrum with the improved sensitivity and free from the spinning sidebands (Figure VI.7). The cross-peak intensities observed for SRUC2QF-COSY spectra are equal to the diagonal peaks of individual spin-pairs. Independent spectra that are free from spinning side bands can be observed for each spin pair, even at lower spinning speeds. The experimental strategy can be conveniently applied to other samples and also for the cases that require lower spinning speeds.

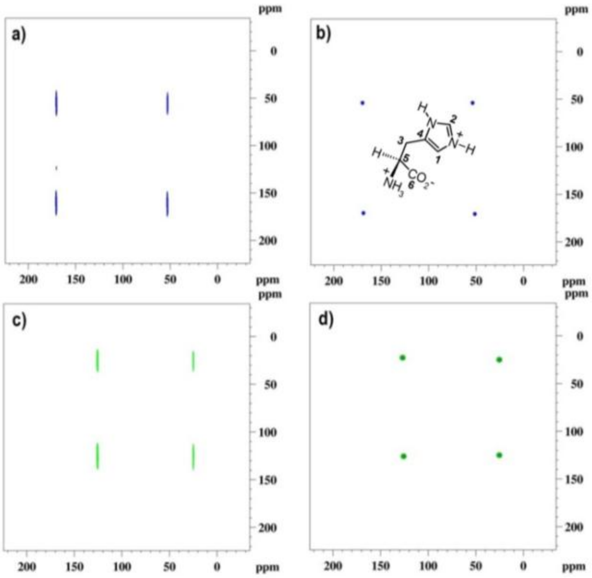

Figure VI.6: *Comparison of 2D-FT and 2D-covariance processed spectra of individual spin-pairs of $^{13}C_6$ L-Histidine.HCl recorded with 16 indirect dwell increments, in a total ~30 min of experimental time. The 2D-FT processed NMR spectra of C6-C5 and C3-C4 are shown in (a) and (c), respectively. Their corresponding 2D-COV processed NMR spectra are shown in (b) and (d).*

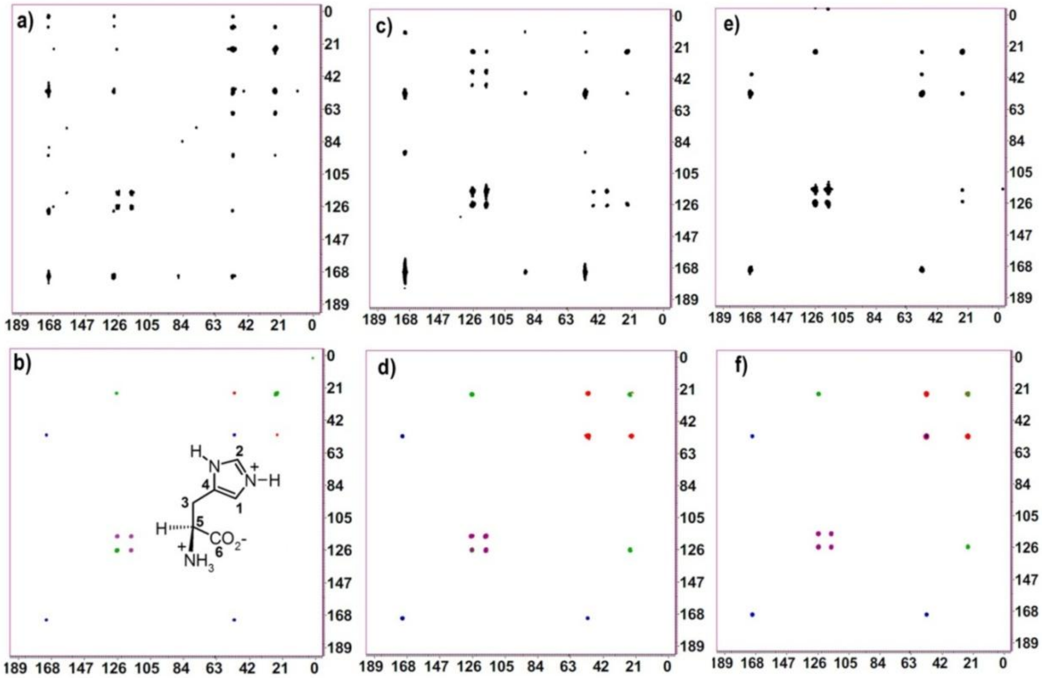

Figure VI. 7: *Comparison of 2D FT UC2QF-COSY and 2D co-added Covariance-processed SRUC2QF-COSY spectra of individual spin-pairs of $^{13}C_6$ L-Histidine.HCl. The UC2QF-COSY NMR spectra of $^{13}C_6$ L-Histidine.HCl recorded at 4.2 kHz, 8.0 kHz and 13.0 kHz are shown in (a), (c) and (e), respectively. Their corresponding, co-added, covariance-processed spectra of individual spin-pairs are shown in (b), (d) and (f).*

VI.5.3. Hadamard encoded *multiple band (or frequency) -selective refocused UC2QF-COSY of $^{13}C_6$ L-Histidine.HCl*

The SRUC2QF-COSY experiments are repeated at 13.0 kHz sample spinning speed for the $^{13}C_6$ L-Histidine.HCl molecule in multiple band (frequency) selective refocusing modes with the optimized evolution time (3.0 ms). As demonstrated earlier, Hadamard encoding facilitates the simultaneous selection of multiple spin pairs in a single experiment. Accordingly, only one experiment is conducted (~ 30 minutes) for the two spin pairs, C6-C5 and C4-C1 by selecting four resonances (C1-C4-C5-C6), instead of recording two separate SRUC2QF-COSY experiments.

In another spin combination, C5-C3-C4 spins are selectively refocused with the three band-selective Hadamard encoded selective π pulses. Herein, C3 is common spin for both the C5 and C4, thus the cross-peaks are of relatively low intensity, when compared to the double selective SRUC2QF-COSY experiments (Figure VI.8 and Figure VI.9). *The total experimental time required for the above two Hadamard encoded spin combinations is ~1 Hrs, whereas the corresponding double band-selective SRUC2QF-COSY and UC2QF-COSY are recorded in ~2Hrs and ~ 9 Hrs, respectively.*

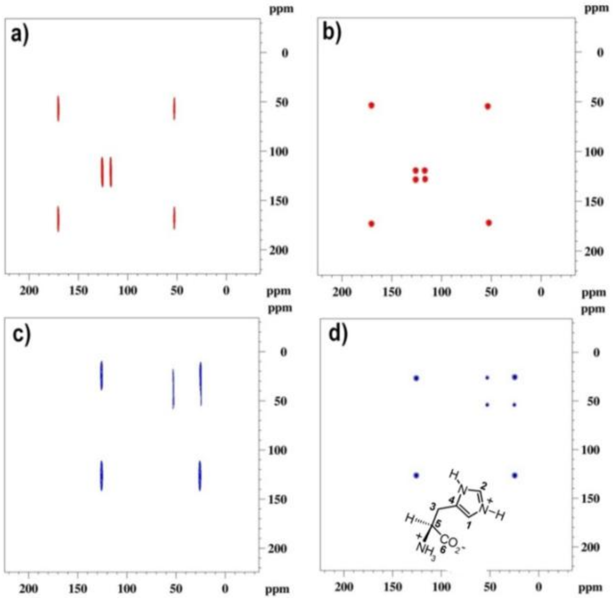

Figure VI.8: *Comparison of 2D-FT and 2D-covariance processed spectra of different spin combinations of $^{13}C_6$ L-Histidine.HCl recorded with 16 indirect dwell increments, in a total ~30 min of experimental time. The 2D-FT processed spectra of C6-C5-C4-C1 and C5-C3-C4 are shown in (a) and (c), respectively. Their corresponding 2D-COV processed spectra are shown in (b) and (d).*

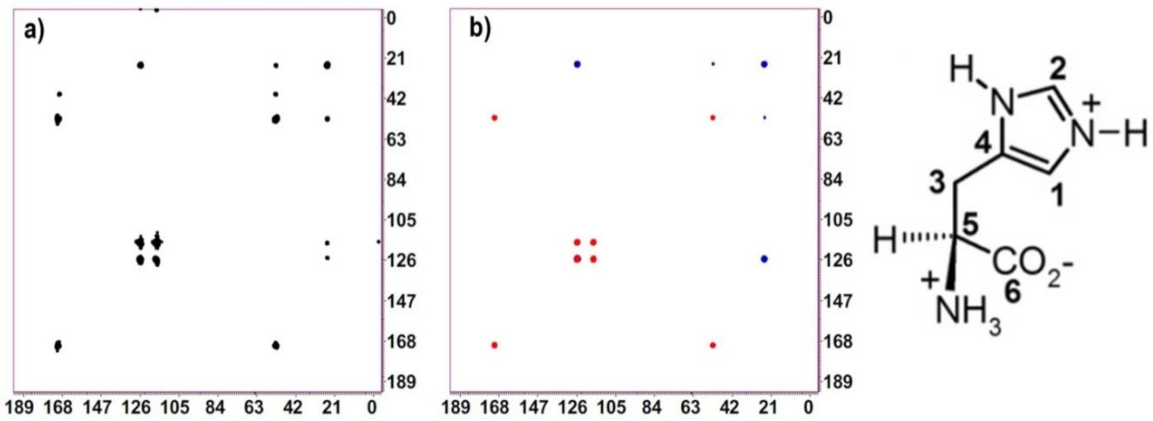

Figure VI.9: *Comparison of 2D UC2QF-COSY (a) and 2D co-added covariance processed SRUC2QF-COSY (b) spectra of two different spin combinations of $^{13}C_6$ L-Histidine.HCl are recorded at 13.0 kHz of sample spinning speed. Hereby, the spin combinations C6-C5-C4-C1 and C5-C3-C4 are depicted in red and blue colours, respectively.*

VI.5.4. *UC2QF-COSY experiments of $^{13}C_5$ FSAA*

The UC2QF-COSY experiment of $^{13}C_5$-FSAA is recorded at 10.0 kHz of sample spinning speed with the mixing time (τ) value of 2.0 ms and the required acquisition time is ~ 9 Hrs (Figure VI.11). Thus, UC2QF-COSY of $^{13}C_5$-FSAA demands a longer acquisition and the recorded spectrum is inferior in the sense of cross-peak intensity at higher spinning speeds, as well. However, as described for $^{13}C_6$ L-Histidine.HCl molecule, re-introduction of spin-spin commutation facilitates the acquisition of spectrum in relatively short times, with optimum cross-peak sensitivity.

VI.5.5. *Double band-selective SRUC2QF-COSY experiments of $^{13}C_5$ FSAA*

The SRUC2QF-COSY spectra are recorded for commuted spin pairs of $^{13}C_5$ FSAA, at 10.0 kHz of sample spinning with the optimized mixing time (τ) values 4.0 ms and 7.0 ms for the directly bonded and long-range spin pairs, respectively. The selective refocusing of two resonance bands in each experiment requires only minimal acquisition times, by recording a less number of complex data points along the indirect dimensions. Herein, 16 complex increments are acquired along the indirect dimension followed by covariance processing. The number of increments is sufficient to ascertain the chemical shift connectivity along the indirect dimensions. The long range correlation between C1-C5 has also been established, which is not possible in the conventional UC2QF-COSY experiment (Figure VI.10). The required spectral acquisition time for these each double band-selective experiment (SRUC2QF-COSY) is only 30 min. Total five double band selective experiments (spin pairs C1-C2, C2-C3, C3-C4, C4-C5 and C1-C5) are recorded for $^{13}C_5$ FSAA molecule in ~ 2.5 Hrs. Later, all the double band-selective COSY spectra are co-added to yield a spectrum equivalent to the full UC2QF-COSY with improved sensitivity (Figure VI.11).

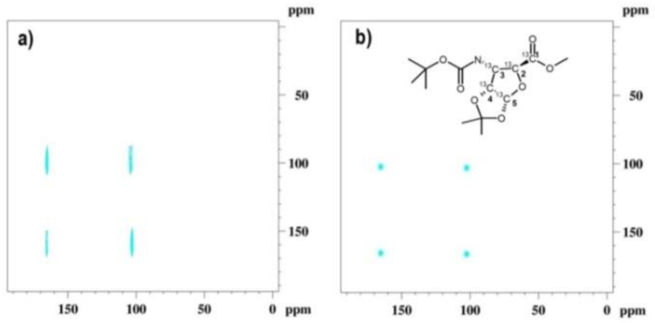

Figure VI. 10: *Comparison of 2D-FT and 2D-covariance processed spectra of C1-C5 spin-pair of $^{13}C_5$-FSAA are shown in (a) and (b), respectively. The spectra are recorded with 16 indirect dwell increments, in a total ~30 min of experimental time.*

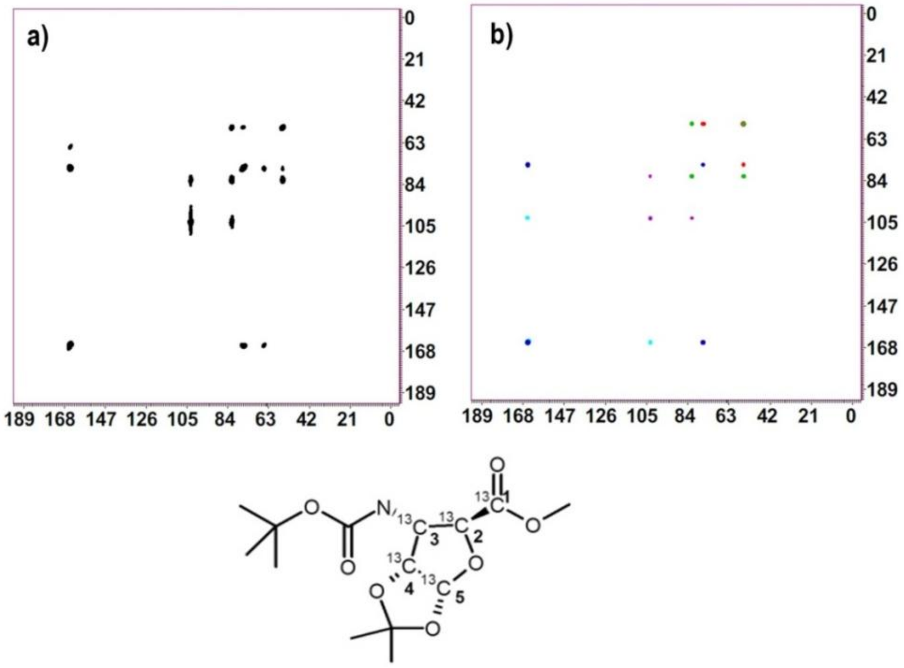

Figure VI.11: *Comparison of 2D FT UC2QF-COSY (a) and 2D co-added covariance-processed SRUC2QF-COSY spectra of individual spin-pairs of $^{13}C_5$-FSAA (b).*

VI.5.6. *Hadamard encoded multiple band selective refocused UC2QF-COSY of $^{13}C_5$ FSAA*

Hadamard encoded multiple band-selective experiments are conducted for the three independent spin combinations of $^{13}C_5$ FSAA. In first spin combination, C1-C2-C4-C5 spins are selectively refocused with the corresponding four Hadamard encoded frequency selective π pulses by creating spin-spin commutation between the two spin-pairs, C1-C2 and C4-C5. Thus, no signal loss is observed in the cross-peaks with respect to the corresponding spin pairs in double selective refocusing method. *Furthermore, only one experiment is recorded for the four resonance bands in a ~30 minutes, instead of recording two separated SRUC2QF-COSY experiments for these two spin-pairs.*

In another spin combination, C2-C3-C4 spins are selectively refocused with the three band-selective Hadamard encoded selective π pulses. Herein, C3 is a common spin for both the C2 and C4, thus the cross-peak intensities are comparatively lower than that of corresponding cross-peaks in the double selective refocusing UC2QF-COSY experiments (Figure VI.12). This is due to the enhanced damping of the magnetization among the selected multiple spins. *The total time required for the three spin combinations, including the long-range spin-pair is ~1.5 hours, whereas the time taken for the double band selective SRUC2QF-COSY and UC2QF-COSY is ~2.5 Hrs and ~ 9 Hrs, respectively.*

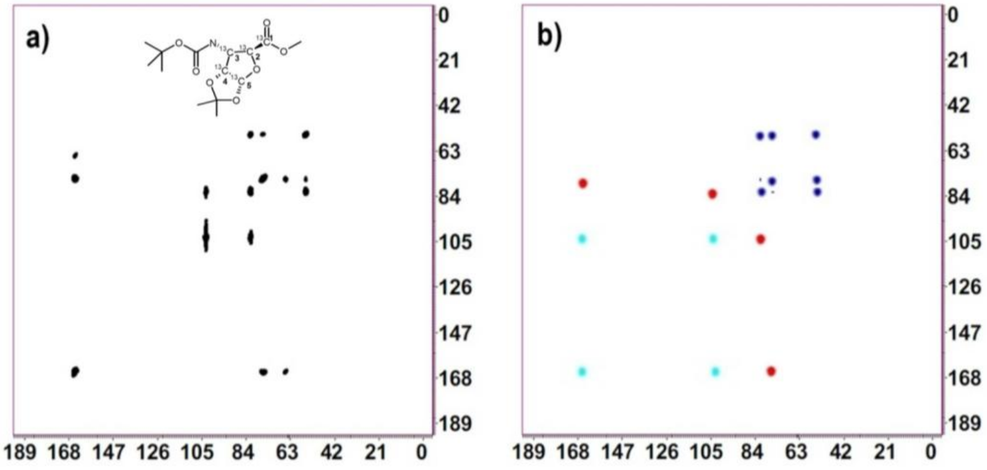

Figure VI.12: *Comparison of 2D FT UC2QF-COSY (a) and its 2D co-added covariance processed SRUC2QF-COSY (b) spectra of the different spin combinations of $^{13}C_5$-FSAA recorded at 10.0 kHz of sample spinning speed. Hereby, the three spin combinations C1-C2-C4-C5, C2-C3-C4 and C1-C5 are depicted in red, blue and cyan colours, respectively.*

VI.6. Conclusion

A new pulse scheme, Hadamard encoded Selective Refocused Uniform Cross-peak Singed Double Quantum Filtered COSY (SRUC2QF-COSY) is developed and demonstrated its importance for the identification chemical shift assignments for solid-state samples. The cross-peak intensities of UC2QF-COSY and SRUC2QF-COSY are simulated at different spinning speeds for various spin-pairs in different spin-combinations, to find the optimum evolution times. The experiments are conducted on a natural amino acid residue ($^{13}C_6$ L-Histidine.HCl) and an important foldamer building block $^{13}C_5$-FSAA. Sideband free and sensitivity improved spectra are recorded even at lower spinning speeds, by restricting the damping terms (spin-spin coupling and spin-spin relaxations) only to the directly bonded spin-pairs. Moreover, data is acquired in a small number of indirect dwell increments and processed with the covariance method, which reduces the experimental time significantly. These experimental strategies may have significant potential in Biomolecular solid-state NMR.

VI.7. References

[1] M. Baldus and B. H. Meier, Broadband Polarization Transfer under Magic-Angle Spinning: Application to Total Through-Space Correlation NMR Spectroscopy, J. Magn. Reson, 128 (1997) 172-193.

[2] A. Lesage, M. Bardet and L. Emsley, Through-Bond Carbon-Carbon Connectivities in Disordered Solids by NMR, J. Am. Chem. Soc, 121(1999) 10987-10993.

[3] L. J. Mueller, D. W. Elliott, G. M. Leskowitz, J. Struppe, R. A. Olsen, K. Kim and C. A. Reed, Uniform-sign cross-peak double-quantum-filtered correlation spectroscopy, J. Magn. Reson, 168 (2004) 327–335.

[4] L. Chen, R. A. Olsen, D. W. Elliott, J. M. Boettcher, D. H. Zhou, C. M. Rienstra and L. J. Mueller, Constant-Time Through-Bond ^{13}C Correlation Spectroscopy for Assigning Protein Resonances with Solid-State NMR Spectroscopy, J. Am. Chem. Soc, 128 (2006) 9992-9993.

[5] D. Lee, J. Struppe, D. W. Elliott, L. J. Mueller and J. J. Titman, Sensitive absorptive refocused scalar correlation NMR spectroscopy in solids, Phys. Chem. Chem. Phys, 11 (2009) 3547–3553.

[6] S. Cadars, A. Lesage, N. Hedin, B. F. Chmelka and L. Emsley, Selective NMR Measurements of Homonuclear Scalar Couplings in Isotopically Enriched Solids, J. Phys. Chem. B, 110 (2006) 16982-16991.

[7] R. Bruschweiler, Theory of covariance NMR spectroscopy, J. Chem. Phys, 121 (2004) 409–414.

[8] F. Zhang, L. Bruschweiler-Li and R. Brüschweiler, Simultaneous de novo identification of molecules in chemical mixtures by doubly indirect covariance NMR spectroscopy, J. Am. Chem. Soc, 132 (2010) 16922-16927.

[9] D. A. Snyder and R. Brüschweiler, Multi-dimensional correlation spectroscopy by covariance NMR, Encyclopedia of Magnetic Resonance (editors D. M. Grant and R. K. Harris), Wiley (2009)

[10] D. A. Snyder and R. Brüschweiler, Generalized indirect covariance NMR formalism for establishment of multidimensional spin correlations, J. Phys. Chem. A, 113 (2009) 12898-12903.

[11] D. A. Snyder, Y. Xu, D. Yang and R. Brüschweiler, Resolution-enhanced 4D 15N/13C NOESY protein NMR spectroscopy by application of the covariance transform, J. Am. Chem. Soc, 129 (2007) 14126 – 14127.

[12] M. Weingarth, P. Tekely, R. Brüschweiler and G. Bodenhausen, Improving the quality of 2D solid-state NMR spectra of microcrystalline proteins by covariance analysis, Chem. Comm, 46 (2010) 952-954.

[13] H. A. Scheidt, I. Morgado and D. Huster, Solid-state NMR Reveals a Close Structural Relationship between Amyloid-β Protofibrils and Oligomers, J. Bio. Chem, 287 (2012) 22822-22826.

[14] L. Olivier, H. Bingwen, A. Jean-Paul and L. Philippe, Fast and High-Resolution Stereo chemical Analysis by Nonuniform Sampling and Covariance Processing of Anisotropic Natural Abundance 2D 2H NMR Datasets, Chem. Euro. J, 17 (2011) 6716-6724.

Chapter-VII

Spectral simplifications in solution-state NMR

Real-time homonuclear broadband and band-selective decoupled pure-shift ROESY

VII.1. Introduction

The ^{1}H-^{1}H through-space distances estimated from nuclear Overhauser effect (NOE/ROE) cross-peak intensities serve as important structural (distance) restraints and are routinely used for conformational/configurational analysis of variety of synthetic/natural organic molecules and biopolymers in solution-state. However, this abundant structural information is often obscured due to overlapping ^{1}H-^{1}H scalar coupling (J) multiplets spread over the limited chemical shift range.

Homodecoupling, as a means of suppressing scalar interactions for enhanced spectral resolution, has been recognized for several years.[1-13] Subsequent seminal developments of broadband homodecoupling techniques to achieve complete collapse of multiplets to *pure-shift* singlets, include: Zangger-Sterk (ZS)-decoupling scheme [12] and its refined variants for multi-dimensional NMR [14-19] that rely on spatially encoded excitation in the presence of slice-selective z-gradient pulse. On the other hand, ^{13}C-isotope filtered bilinear rotational decoupling (BIRD) [20] based schemes are reported, which particularly eliminate strong coupling effects [21, 22] and are also advantageous for obtaining fully decoupled pure-shift HSQC.[23-26] All these methods are fundamentally important and genesis for developmental evolutions, but lack sufficient sensitivity and demand prolonged experimental times and/or complicated acquisition/processing. The BIRD-based decoupling is restricted to protons attached only to the ^{13}C atoms, therefore the sensitivity is limited to the ~1% natural abundance of ^{13}C. The sensitivity of the elegant ZS-methods also limited to the signals originating only from the spatially encoded thin slice and to the time-consuming additional pseudo 2D/3D mode data acquisition for 1D/2D spectra. Alternatively, despite some loss in the sensitivity, Keeler and co-workers have shown a unique way of achieving broadband decoupling by simply taking the 45° projection of the diagonal-peak multiplets of anti z-COSY spectra [27] or the chemical-shift dimension of *J*-resolved spectra.[28] Similarly, pattern recognition approach is also proposed [29] which involves an additional processing of the data.

Very recently, in a remarkable advancement, Zangger et al., have revived their original ZS- method to an instantaneous (real-time) homonuclear broadband (HOBB) decoupling [30] suitable for direct detection dimension, by periodically interrupting the FID

[9] with ZS-decoupling block. This smart approach eliminates the pseudo dimension acquisition and therefore greatly cuts down the long experimental time, although the sensitivities are still limited due to the involvement of slice-selection. However, with the largely available high-field NMR spectrometers, sufficient sample concentrations and faster acquisition methods, [31] the sensitivity loss can be minimized. Followed by this, Parella and co-workers [32, 33] have improvised the HOBB method for full sensitive and instantaneous homodecoupled band-selective (HOBS) acquisition sequence that applies selective BURP [34] excitation /refocusing pulses for the region of interest. As this strategy does not involve slice-selection, high sensitivity comparable to that of regular non-decoupled spectrum, is possible. These two techniques are complimentary to each other and their combined application would provide a comprehensive approach for structural characterizations, which have so far been utilized only for through-bond correlation experiments, TOCSY, HSQC and HSQMBC.[30, 32, 33]

VII.2. Concepts

VII.2.1. *Selective excitation/refocusing during the spatial encoded gradients*

The ZS-method employs the concept of slice-selective excitation by a weak magnetic gradient field to decouple all spins: Different parts of the NMR sample experience different magnetic field strengths when a linear gradient is applied. Therefore, a location-dependent frequency shift $\Delta\omega=\gamma*G*s$ across the sample volume over a length of s is established, with the gyromagnetic ratio of the observed nucleus γ and the gradient strength G. While the gradient is active, a selective pulse thus excites the whole spectrum. However, different signals are excited in different parts of the sample, so that a spatially resolved excitation is achieved (Figure VII.1)

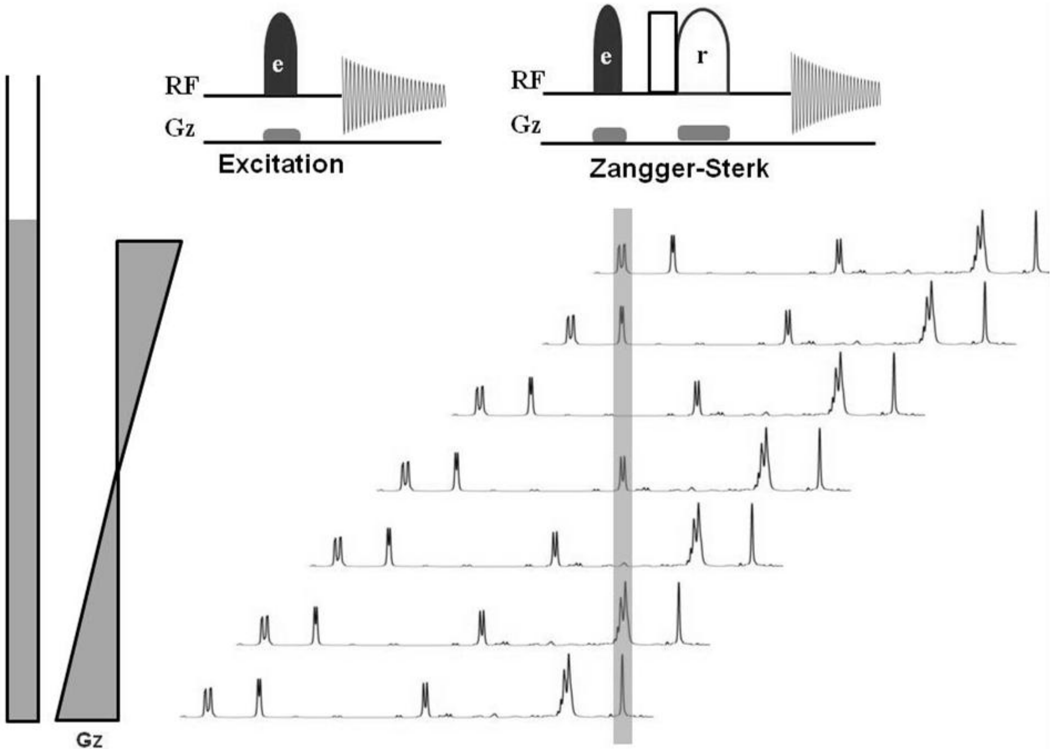

Figure VII. 1: *Schematic of slice selective excitation: The use of selective excitation during a weak field gradient excites the whole spectrum, herein each signal is irradiated from the different parts of the sample.*

VII.2.2. *Homonuclear broadband decoupling during the slice selective gradients*

Figure VII.2 represents the pulse sequence used for the broadband decoupling as well as the magnetizations of the observed and decoupled spins. The decoupling is achieved by using a combination of soft and hard π pulses. If the semi-selective pulse is applied in a region A of the spectrum, the multiplet structure of *J* coupled signals resonating in a different region B appear simplified while they are detected. This results in a complete homonuclear broadband (HOBB) decoupled spectrum. It has to be taken into consideration that decoupling during acquisition is only possible if no chemical shift evolution occurs, while the acquisition is interrupted (~1/3 ($^3J_{HH}$)).

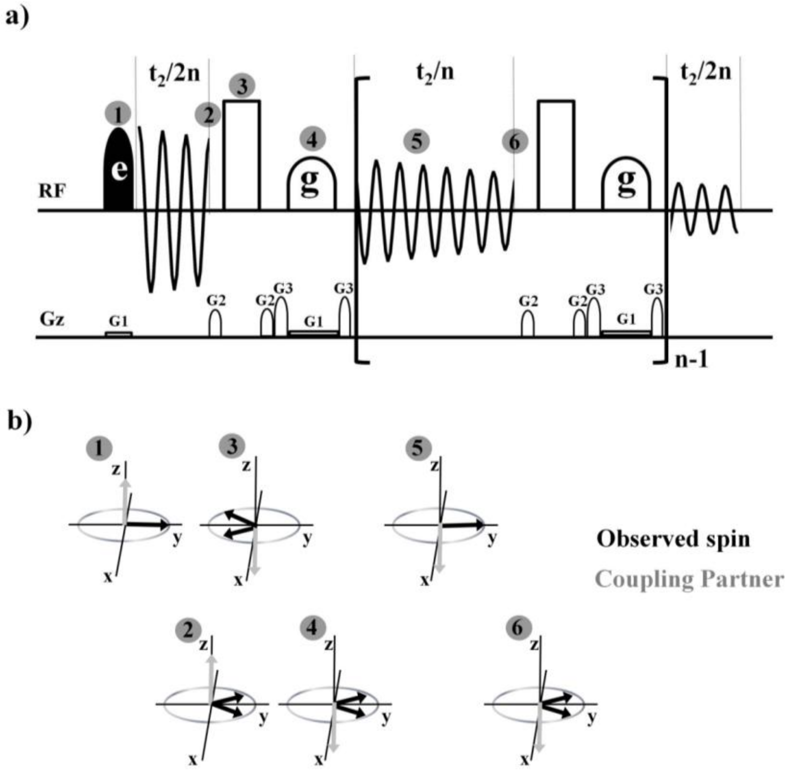

Figure VII.2: *1D HOBB pulse-sequence and the magnetization vectors for slice-selective decoupling during acquisition are shown in a) and b), respectively.*

VII.3. Results and Discussion

It is very essential to extend these advanced homo-decoupling strategies for through-space correlation studies as well. Moreover, pure-shift band-selective NOESY sequence is reported by the research group of Bax, [35] which is suitable for large molecules. However, for medium-size molecules (~ 1 kDa), ROESY is more appropriate. Particularly, the target-specific activity of synthetic / natural organic molecules and small secondary structures is often related to their specific conformations, which have to be established by accurate means. In this regard ROESY serves as indispensible tool for medium-size molecules in solution-state, and the *real-time* pure-shift ROESY schemes, that do not involve time-consuming pseudo-dimension acquisitions and special processing, have not been reported so far. The present work fulfils this immense requirement.

Herein, new *real-time* pure-shift HOBB-ROESY, and HOBS-ROESY pulse sequences (with decoupling during direct acquisition dimension-F2) are developed for broadband and band-selective applications, respectively, which provide enhanced resolution. The HOBB-ROESY facilitates full-decoupling over the entire spectrum, but with low sensitivity. Whereas, the HOBS-ROESY yields high sensitivity over the selected band, which is comparable or even higher to that of the conventional non-decoupled spectrum. It is known that the coherence magnetization transfer by TOCSY causes undesired interferences/overlaps in ROESY, [36, 37] which have to be suppressed for accurate determinations of through-space connectivities. The proposed pure-shift ROESY schemes are essentially hybrids of the advanced HOBB/HOBS and the jump-symmetrised (JS) ROESY blocks [37, 38] that provide optimal suppression of possible TOCSY-transfer and resonance offsets as well. The importance and versatility of these schemes are exemplified for two different types of organic molecules. The first sample, Erythromycin-A, [39] is a three-domain molecule that exhibits a complex ^{1}H spectrum with extensive scalar couplings. The second sample is a four-residue hybrid peptidic oligomer comprised of 1:1 natural α- and rigid unnatural β-Furanoid Sugar amino acids (β-FSAA, with additional carbon atom along the backbone).[40] The later referred to as ASAS, represents the class of 'foldamers', [41] that adopt well-defined secondary structures and hydrogen-bond patterns akin to proteins, even at oligomer level and can also serve as antagonists for protein-protein interactions.[42] Unambiguous assignments of ^{1}H resonances and estimation of ROE-cross-peak integrals, particularly for the crowded non-amide regions, are crucial to establish the actual folding pattern and the relative positions of side-chain groups. Multiplet-free pure-shift ROESY would be of great advantage for such interesting molecules.

VII.3.1. ***HOBB-ROESY and HOBS-ROESY schemes***

Figure VII.3a and 3b depict the pulse sequences used for *real-time* homodecoupled broadband (HOBB) and homodecoupled band-selective (HOBS) ROESY, respectively. They operate in the instantaneous mode (no additional pseudo dimensions are required) and provide simplified spectra with enhanced resolution. The initial part of the sequence contains an improvised JS-ROESY block [37] with spin-lock pulses bracketed by adiabatic ramps, [38] which is also referred as EASY-ROESY, to facilitate a high sensitive spectra with successfully minimized offset dependences and TOCSY cross-peaks. Herein the mixing time τ_m is divided into two equal parts, during which continuous wave spin-lock fields corresponding to low and high field regions of the spectrum, respectively, are applied sequentially. This significantly averages out the offset dependences of the cross-peak intensities. Further, the spin-lock fields are set outside of the spectral region to facilitate an optimal Hartman-Hahn mismatch and hence to effectively suppress the TOCSY transfer. However, the direction of the spin-lock axis undergoes a change during the switching from low to high spin-lock field, which has to be compensated. The adiabatic ramps **p** and **q** provide the necessary correction by rotating the magnetization from the z-axis to spin-lock axis and back. Finally, the conventional 90° observe pulse at the end of the ROESY block is replaced by HOBB or HOBS decoupling block.

Accordingly, in the resultant HOBB-ROESY sequence (Figure VII.3a), the ROESY-filtered z-magnetization is subjected to slice-selective excitation by 90° EBURP (**e**) in the presence of gradient G3. The broadband decoupling is accomplished through interrupting the acquisition in **n** number of intervals (30 for ASAS and 20 for Erythromycin-A) with a combination of hard 180° and soft 180°slice-selective Gaussian (**g**) refocusing pulses.[6, 7] Similarly, the HOBS-ROESY sequence is constructed for band-selective decoupling (Figure VII. 3b), by essentially replacing the slice-selective 90° EBURP of HOBB with a combination of hard 90° and band-selective REBURP refocusing pulses. Subsequently, the band-selective decoupling in the direct observe dimension is achieved through interrupting the acquisition in **n** number of intervals (30 for ASAS and 20 for Erythromycin-A) with a combination of hard 180° and soft 180° band-selective REBURP (**r**) refocusing pulses. Importantly, contrary to HOBB, this scheme does not involve slice-selective gradient pulses at any stage of excitation/refocusing and hence the sensitivity is not limited by the signal arising only from a narrow selected slice. However, it is important to note that, although the HOBS provides a well-simplified and high-sensitive spectrum, the residual scalar couplings *within* the selected band of frequencies cannot be eliminated, which may not be a limiting factor for favourable cases. The HOBB-ROESY provides complete pure-shift spectrum in a single experiment, whereas the HOBS-REOSY has to be conducted for each region of interest. If necessary, for complex molecules, the HOBS-ROESY analysis can be easily verified with the full broadband decoupling scheme, HOBB-ROESY, at the expense of time.

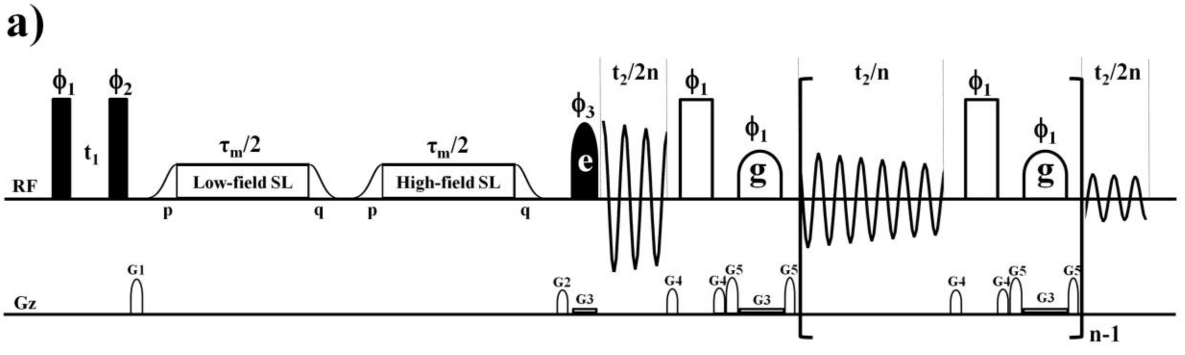
a)
φ1
φ2
t1
τm/2
Low-field SL
τm/2
High-field SL
φ3
e
t2/2n
φ1
φ1
g
t2/n
φ1
φ1
g
t2/2n
RF
p
q
p
q
G1
G2
G3
G4
G4
G5
G3
G5
G4
G4
G5
G3
G5
Gz
n-1

Real time HOBB-ROESY

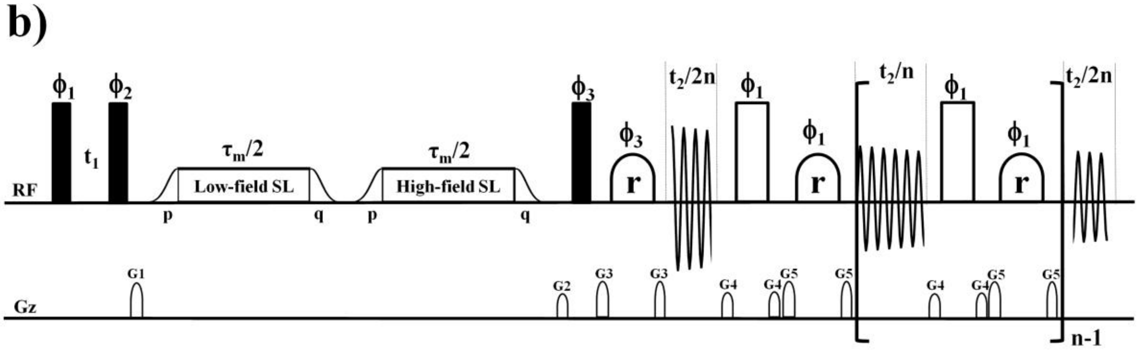
b)
φ1
φ2
t1
τm/2
Low-field SL
τm/2
High-field SL
φ3
φ3
r
t2/2n
φ1
φ1
r
t2/n
φ1
φ1
r
t2/2n
RF
p
q
p
q
G1
G2
G3
G3
G4
G4
G5
G5
G4
G4
G5
G5
Gz
n-1

Real time HOBS-ROESY

Figure VII.3. *Real-time pure-shift ROESY pulse sequences with Homonuclear Broadband decoupling (HOBB) and Homonuclear Band selective (HOBS) decoupling in the direct acquisition dimension: The corresponding pulse-schemes for recording HOBB-ROESY and HOBS-ROESY are shown in (a) and (b), respectively. The filled and open rectangles represent the 90° and 180° pulses, respectively. The* ***p*** *and* ***q*** *are half Gaussian shaped pulses of 1 ms length. The* ***p*** *pulses rotate the magnetization from Z-axis to spin-lock field and* ***q*** *pulses flip back the magnetization from spin-lock field to Z-axis. The filled semi ellipsoid, '****e****', represents the 90° EBURP* [34] *shape pulse (53.5 ms) applied during the slice-selective gradient that corresponds to 100 Hz bandwidth. The open semi ellipsoids, '****g****' and '****r****' represent Gaussian and REBURP* [34] *shapes, respectively. Herein, Gaussian 180° pulse of 8.8 ms (bandwidth of 100 Hz) is applied during slice-selection gradient. For a given sample, the applied EBURP and Gaussian pulse lengths are same in all the experiments. Specific to the sample and the corresponding bandwidth of interest, the REBURP pulse lengths have to be optimized, which is simple. The REBURP pulse lengths of 9.0, 11.7 and 1.9 ms are used to refocus the methyl (~1.6 to 0.7 ppm), CH_2 (~2.1 to 1.4 ppm) and the rest of the spectral (~5.3 to 1.9 ppm) regions of Erythromycin-A, respectively. Similarly, REBURP pulse of 4.2 and, 3.7 ms duration, are used to refocus the $H\alpha+H\beta+H\gamma$ (~4.2 to 2.9 ppm) and NH (~9.0 to 6.3 ppm) regions of ASAS, respectively. The number of dwelling points/sweep-width along the direct dimensions are equal to 4096/3.5 kHz, 8192/7.0 kHz are used for Erythromycin-A and ASAS, respectively. The corresponding acquisition time is ~585 ms. The number of decoupling interruptions* ***n*** *equals to 30 and 20 for ASAS and*

Erythromycin-A, respectively. Specific parameters for pulse sequence (a): Phase cycling: ϕ_1 *= x, -x;* ϕ_2 *= x;* ϕ_3 *= -x, -x, x, x, -y, -y, y, y;* ϕ_{rec} *= x, -x, -x, x, y, -y, -y, y; Pulsed field gradients:* $G_{1,}$ *= 31%,* G_2*=11%,* G_3*= 1% (Erythromycin-A) or 2% (ASAS),* G_4*=11%;* G_5*=11(Erythromycin-A) or 31% (ASAS), respectively, of 53.5G/cm gradient strength in 1 ms duration. Specific parameters for pulse sequence (b): phase cycling:* ϕ_1 *= x, -x;* ϕ_2 *= x;* ϕ_3 *= -x, -x, x, x, -y, -y, y, y;* ϕ_{rec} *= x, -x, -x, x, y, -y, -y, y; Pulsed field gradients:* G_1 *(1 ms) = 31%,* G_2 *(1 ms)= 11% ;* G_3 *(0.5 ms)= 23%,* G_4 *(0.5 ms) = 41% and* G_5 *(0.5 ms)= 60% (methyl region and the rest of the regions of Erythromycin-A;* $H\alpha+H\beta+H\gamma$ *region of ASAS),* G_5 *(0.5 ms)= 40% (*CH_2 *region of Erythromycin-A) and* G_5 *(0.5 ms) = 80% (NH region of ASAS), respectively of 53.5G/cm gradient strength. The pulsed field gradients are optimized for every experiment separately. The pulse sequences are developed and experimentally verified on Bruker Avance-III 700 MHz NMR spectrometer.*

VII.3.2. *Pure-shift HOBB and HOBS-decoupled* ^{1}*H spectra*

Figure VII.4 illustrates the comparison of the normal non-decoupled, pure-shift HOBB and HOBS-decoupled 1D ^{1}H spectra of Erythromycin-A and ASAS, under identical experimental conditions. A remarkable increase in the chemical shift resolution with complete collapse of scalar couplings is achieved for HOBB-decoupling. However the loss in the signal sensitivity is ~95 %, which is expected as the excitation and refocusing have been performed during the slice-selective gradients. In the Figure VII.4, the low intensity (4 to 8 %) HOBB-decoupled spectra of these samples are vertically magnified by a factor of 256, with respect to the corresponding conventional non-decoupled spectra. On the other hand, dramatic improvement in the sensitivity (106 to 210 %) of the pure-shift spectra has been obtained for the HOBS decoupling, which matches that of the conventional spectra (Figure VII.5). Further, it is noticed that both the HOBB and HOBS decoupled spectra exhibit low-intense side-bands **[17, 43]** (~6%) flanked on the either sides of the pure-shift resonances, separated by 2**n**/AQ = 66 Hz (Figure VII.6). These side-bands did not hamper the present analysis at any stage. However, intense side-bands may be of significant concern for accurate estimation of ROEs, particularly if they overlap with the pure-shift resonances.

In ASAS, the well dispersed downfield NH region represents the characteristic signature of a secondary folding and is consistent with their possible involvement in hydrogen bonding, akin to natural proteins. Nevertheless, though the HOBS spectra are sufficiently simplified with enhanced sensitivity, the regions correspond to non-methyl/CH_2 protons of Erythromycin-A and Hα/Hβ/Hγ protons of ASAS have still shown residual couplings due to the presence of their coupled partners *within* the selected band. The trade of sensitivity for selectivity or vice-versa cannot be avoided in the homodecoupling experiments. Overall, the complete and unambiguous spectral assignment has been accomplished with both the decoupling methods. As mentioned above, for specific cases, the application of both these techniques would be of exceptional advantage to resolve ambiguities, if any.

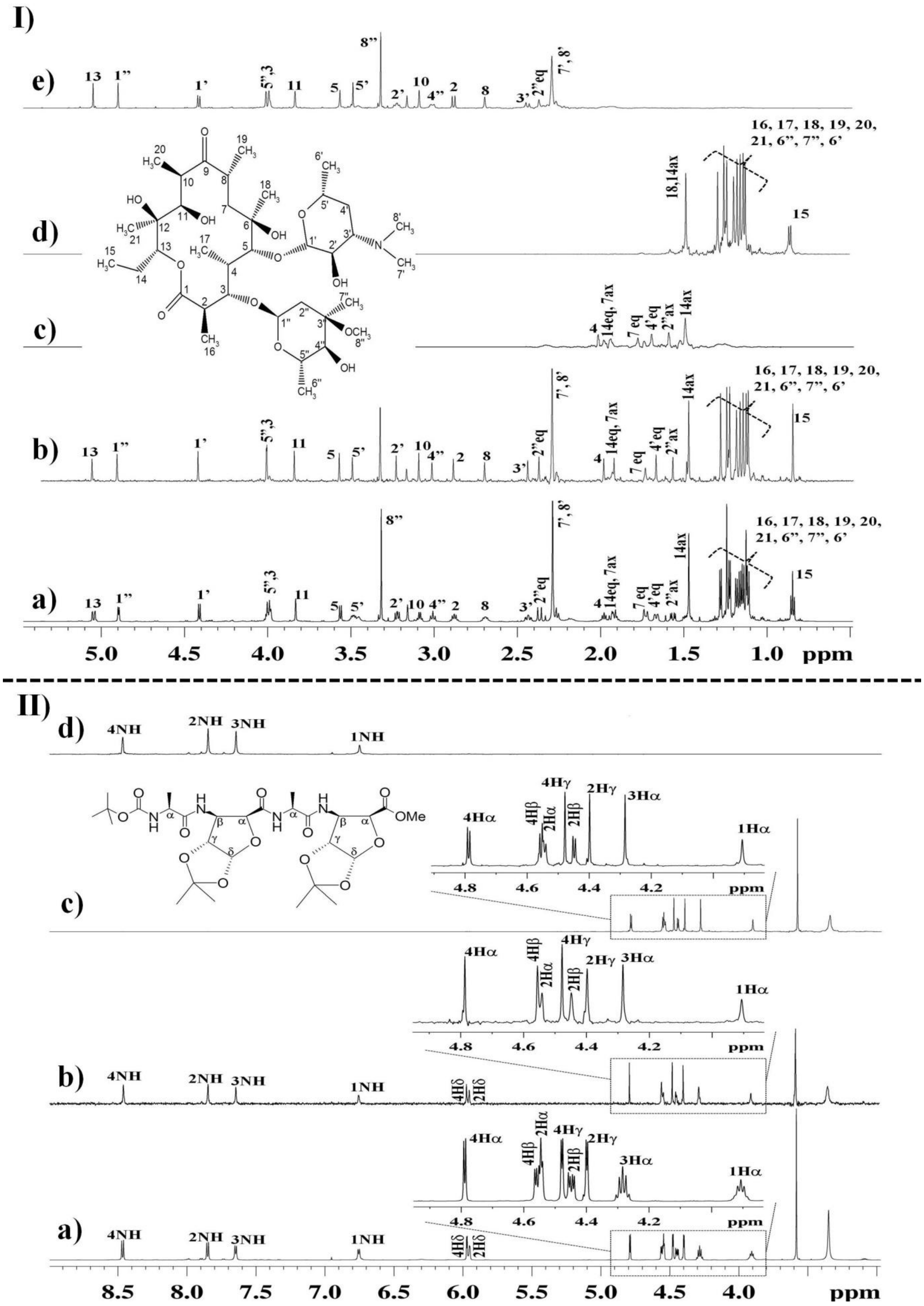

Figure VII.4: *Comparison of normal 1D (single 90^o pulse), homonuclear broadband (HOBB)-decoupled and homonuclear band-selective (HOBS)-decoupled ^{1}H spectra of*

Erythromycin-A (2.I) (50mM in $CDCl_3$) and ASAS (2.II) tetramer (30mM in DMSO-d_6). All the spectra are recorded at 300K with a same receiver gain and number of scans (4) and other experimental conditions at 700 MHz. The regular ^1H spectra of Erythromycin-A (I.a) and ASAA tetramer along with its expanded Hα/Hβ/Hγ region (II.a) show spectral complexity due to scalar couplings. The corresponding HOBB-decoupled spectra, I.b and II.b, respectively, show high-resolution spectra with complete collapse of scalar couplings. Due to the poor signal sensitivity, the intensity of these two HOBB spectra are vertically scaled up by a factor 256, with respect to the regular coupled-spectra (I a and II a). As explained in the text, the huge loss (~95%) in signal intensity is because of the signal originated from a thin slice (~100Hz) of the sample. On the other hand, in the case of HOBS, the signal is originated from the whole sample, due to which a dramatic increase in the signal intensity with respect to the HOBB decoupling, and comparable to that of the regular non-decoupled ^1H spectra, is evident. The HOBS-decoupled ^1H spectra corresponding to CH_2, methyl and the rest of the spectral regions of Erythromycin-A are shown in (I.c), (I.d) and (I.e), respectively. Similarly the HOBS-decoupled ^1H spectra of $H\alpha/H\beta/H\gamma$ (with expansion) and NH regions of ASAS are shown in (II.c) and (II.d), respectively.

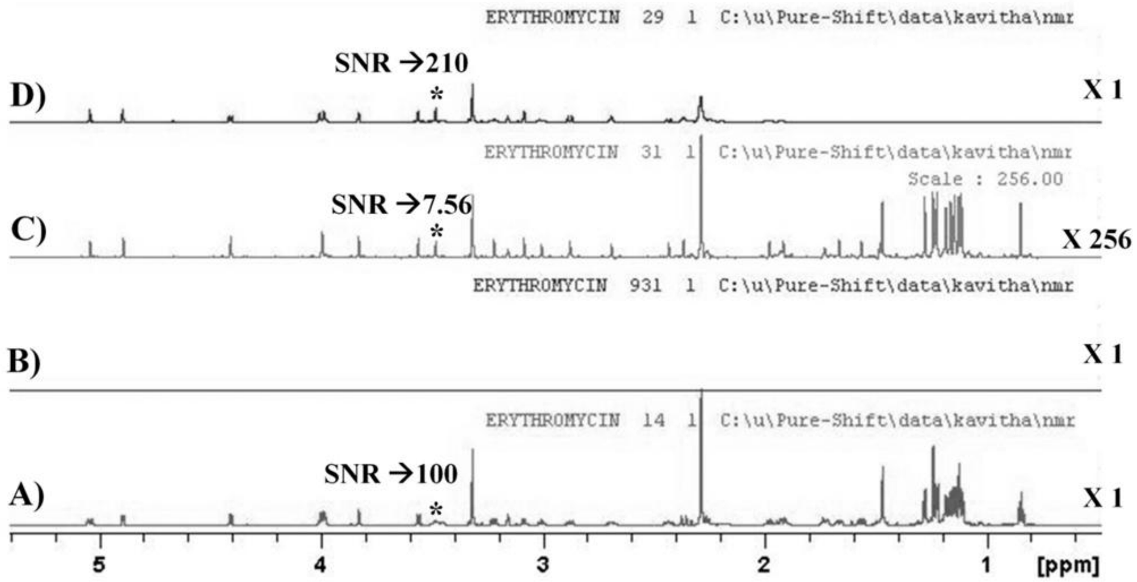

Figure VII.5: *Comparison of 1D conventional non-decoupled ^1H spectrum (A), HOBB-decoupled (B) &(C), and HOBS-decoupled (D) spectra of Erythromycin-A recorded at identical experimental conditions. The HOBB spectra are plotted at two different vertical scaling factors 1 (B) and 256 (C), with respect to the corresponding conventional spectrum (A). The HOBB provides high-resolution pure-shift spectra with complete suppression of multiplets spread over the entire spectral range, but suffers a heavy signal loss (~93%) in the signal intensity as explained in the main text. For HOBB, no signals are realized at the vertical scaling factor -1 (with reference to that of the conventional spectrum). The same spectrum is vertically magnified by a factor 256 (C) to realize all the pure-shift resonances.*

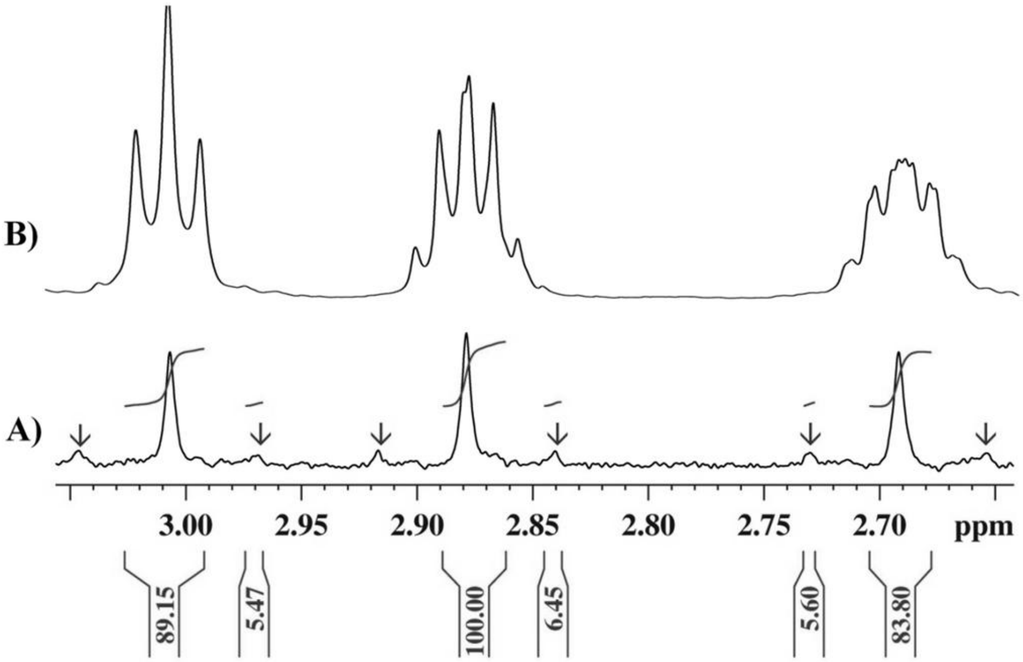

Figure VII.6: *Comparison of expanded regions of HOBB-decoupled spectrum along with the observed side-bands (A) and the corresponding conventional non-decoupled spectrum (B) of Erythromycin-A. The sideband intensities are ~6% of the corresponding pure-shift resonances and are positioned at 2n/AQ (Hz) where, n=20, AQ =0.585 s.*

VII.3.3. *2D Pure-shift HOBB-ROESY and HOBS-ROESY*

ROESY is specifically required for the analysis of mid-size molecules (ωτc~1, NOEs are close to zero or weak at typical high magnetic fields) such as Erythromycin-A and ASAS, which however is normally impeded by the TOCSY and offset interferences. It is important to eliminate these interferences in the pure-shift ROESY experiments, for accurate estimations of the cross-peak integrals. The pure-shift HOBB-ROESY and HOBS-ROESY schemes proposed herein demonstrate efficient suppression of these interferences and yield enhanced spectral resolution over the conventional ROESY (Figure VII.7 and Figure VII.8). The Figure VII.7 illustrates the expanded regions of regular ROESY (~1 hour/ 8 scans/ 256 increments), HOBB-ROESY (~15 hours/ 96 scans/ 256 increments) and HOBS-ROESY (~1 hour for each region / 8 scans/ 256 increments) for the Erythromycin-A. It can be seen in the regular ROESY (Figure VII.7a), the H11→H4 ROE, which is important to determine the conformation of the macrolide lactone ring, is severely overlapped with H14. On the other hand, a dramatic increase in the resolution has been obtained for the same by using HOBB-ROESY (Figure VII.7b) and HOBS-ROESY (Figure VII.7c). Similarly, the H10→ H19, H10→ H20 and H10→ H21 ROE cross-peaks are well resolved in HOBB (Figure VII.7e) and HOBS-ROESY (Figure VII.7f), whereas they are obscured in regular ROESY (Figure VII.7d). It implies that these pure-shift ROESY methods facilitate the measurement of more number of resolved ROE integrals (distance restraints), which aid the structural analysis with improved accuracy.

The structure/target-based design and development of small-molecular scaffolds is the central goal of foldamer research, which necessitates accurate estimation of ROE connectivities to establish the correct secondary folding and the resultant relative positioning of functional side-chains, so that they can be explored for specific molecular recognitions. The Figure VII.8 shows the expanded regions of regular ROESY (~2 hours /16 scans/ 256 increments), HOBB-ROESY (~65 hours /384 scans/ 256 increments) and HOBS-ROESY (2 hours /16 scans/ 256 increments), of four-residue ASAS foldamer molecule. In the regular ROESY (Figure VII.8a), the intra and inter-residue ROEs are poorly resolved due to the obscuring scalar-coupling multiplets. Particularly, the periodic inter-residue ROEs: 2NH→1Hα, 4NH→3Hα, 3NH→1Hα, 4NH→3NH, 3NH→2NH and 2NH→1NH, which are important for establishing the secondary folding for hybrid peptidic oligomers, are observed to be complex and ambiguous. However, the HOBB-ROESY and HOBS-ROESY schemes could greatly resolve these ambiguities and establish that the ASAS tetramer adopts helical folding with 11-membered NH_i-CO_{i+3} hydrogen bonding.

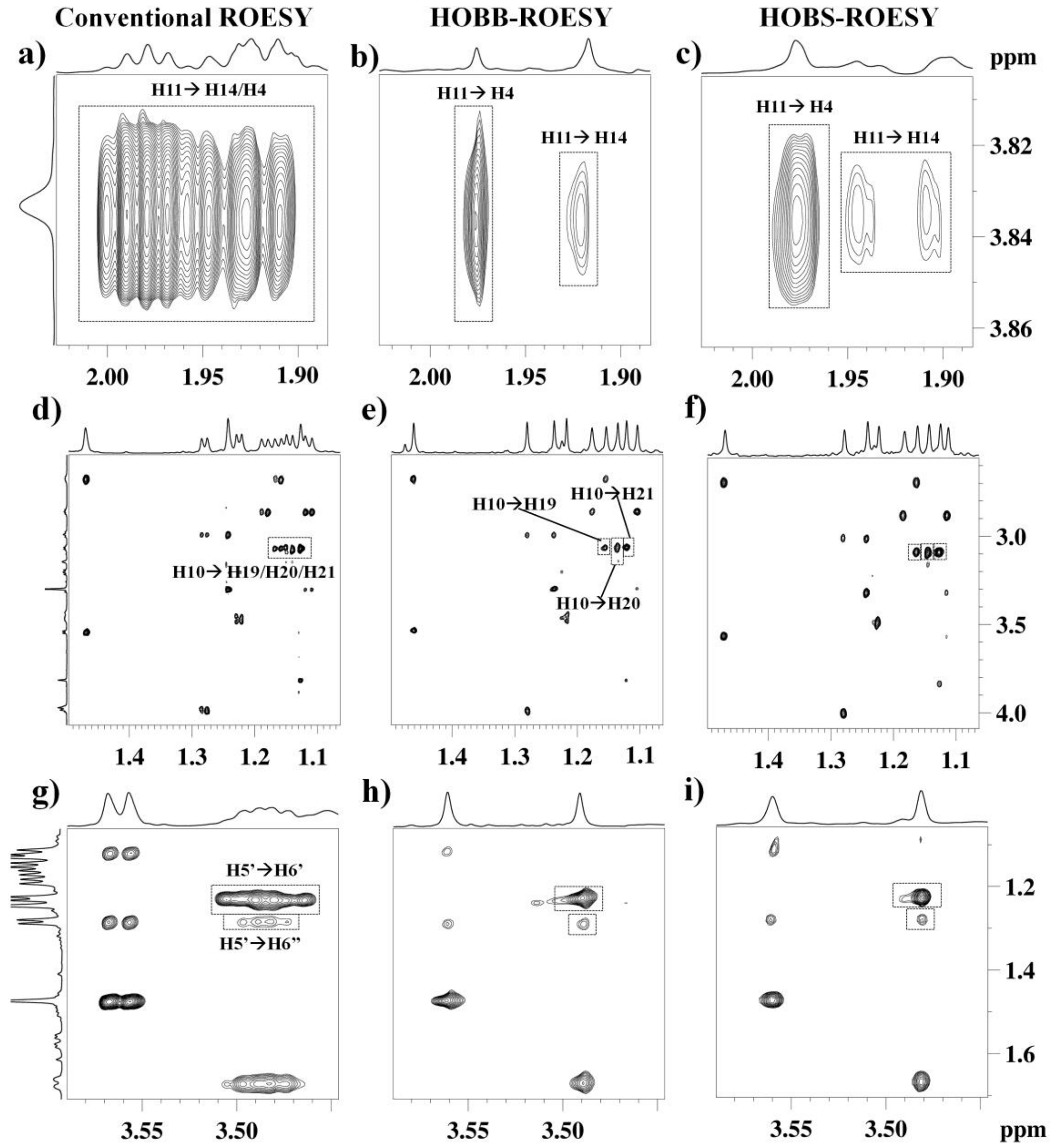

Figure VII.7: *Comparison of expanded regions of conventional, HOBB and HOBS-ROESY spectra of Erythromycin-A (50mM in $CDCl_3$ solvent), recorded at 700 MHz magnetic field with 300 ms of mixing time. The expanded regions of regular ROESY spectra are depicted in (a), (d) and (g). The corresponding expanded HOBB-ROESY spectra are shown in (b), (e) and (h), and the expanded HOBS-ROESY spectra for CH_2, CH_3 and the rest of the spectral regions, are shown in (c), (f) and (i), respectively. The comparison clearly highlights that the conventional ROESY shows completely overlapped cross-peaks for H11-14 and H11-H4 ROEs due to J-multiplicity (a). Whereas, this spectral complexity is greatly suppressed and significant enhancement in the resolution has been achieved for HOBB-ROESY (b) and HOBS-ROESY (c). The observed doublet like cross-peaks for H11-H14 in HOBS-ROESY is due to the residual J-coupling between axial and equatorial protons of H14, which cannot be suppressed within the band selection.*

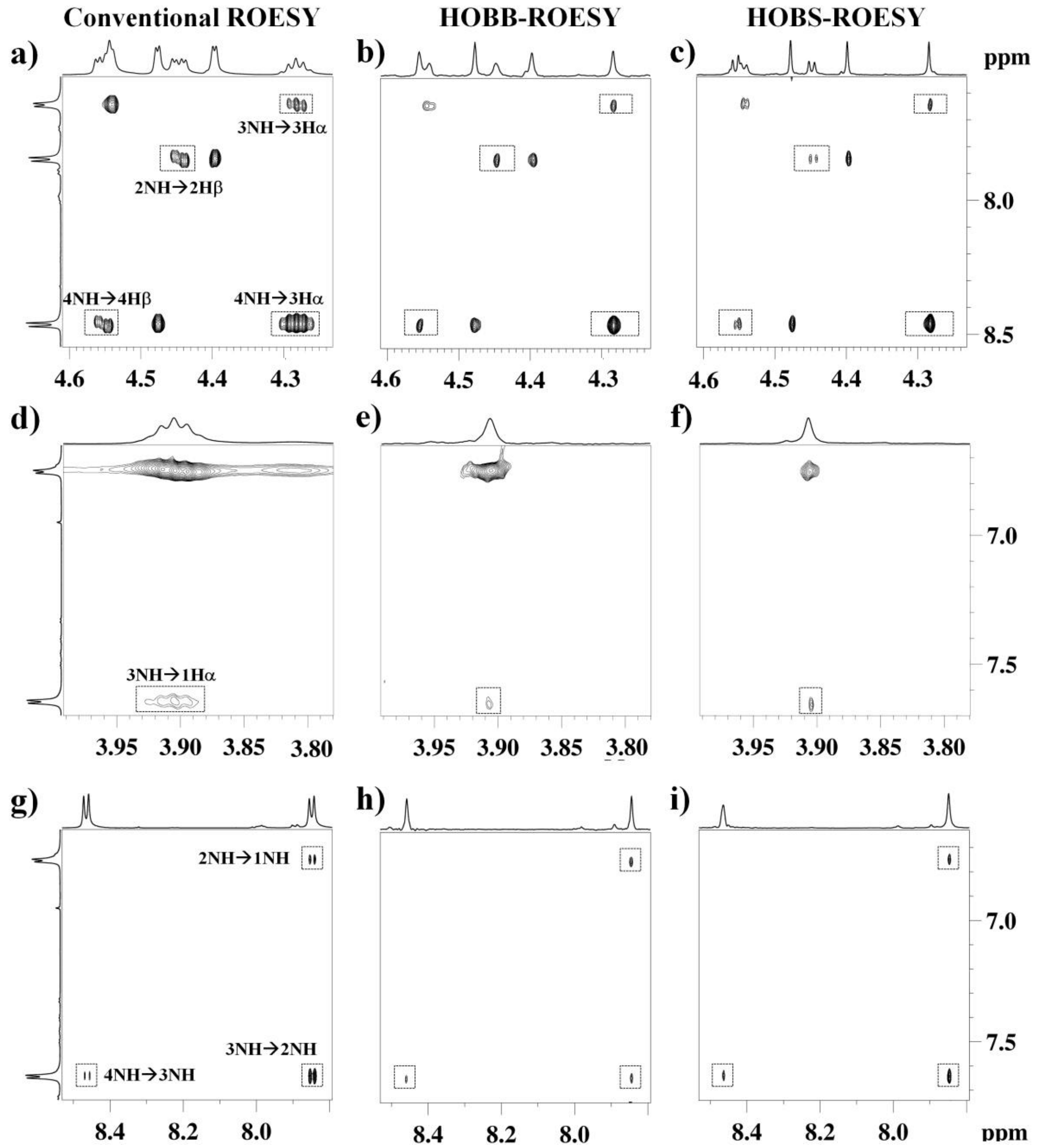

Figure VII.8: *Comparison of expanded ROESY NMR spectra of ASAS (30mM in DMSO-d_6 solvent) recorded at 700 MHz magnetic field with 300 ms of mixing time. The expanded regions of regular NH/Hα ROESY (a), (d) and (g) show poor resolution due to obscuring scalar couplings. The corresponding highly simplified HOBB-ROESY spectra are shown in (b), (e) and (h), and the HOBS-ROESY spectra are shown in (c), (f) and (i), respectively. The HOBS-ROESY spectra are recorded by selecting Hα/Hβ/Hγ and NH regions. It can be seen that these homodecoupled ROESY schemes provide high spectral resolution with respect to the regular ROESY. The sensitivity obtained for HOBS-ROESY is particularly remarkable and matches with that of regular ROESY.*

In both the examples, the spectra are free from the undesired TOCSY and offset interferences. It can be further seen that, expect for the signals those are scalarly coupled within the selected band, the HOBS-ROESY spectra are identical to those of HOBB-ROESY, in terms of enhanced-resolution.

VII.4. Conclusions

In conclusion, new homodecoupled broadband (HOBB) as well as band-selective (HOBS) pure-shift ROESY sequences have been demonstarted, which utilize the recently developed *real-time* ZS-based decoupling schemes for direct acquisition dimension, and experimentally demonstrated for medium-sized organic molecules. Furthermore, the JS-based mixing employed during the spin-lock periods of ROESY effectively suppresses the undesired resonance offsets and interferences of TOCSY cross-peaks in ROEs. These versatile pure-shift ROESY methods have been experimentally demonstrated for medium-sized organic molecules, which resulted in dramatic improvement in the ROE cross-peak resolution and hence its estimation, compared to the normal ROESY. From the conventional ROESY data, the estimation of specific ROE-integrals for the crowded regions (for example, Figure VII.7a) was not possible. Nevertheless, despite the HOBB-ROESY provides better resolution with complete suppression of multiplets, the penalty on the sensitivity is significantly high and the method demands more experimental time. The method is particularly useful for molecules that exhibit extensive scalar coupling network, spread over the entire chemical shift range. On the other hand, the HOBS-ROESY has provided simplified and full sensitive ROE cross-peaks comparable to that of conventional ROESY, for each selected band. However, the spectra may carry residual *J*-couplings among the protons within the selected band. These two experimental approaches are complimentary to each other and may offer new possibilities for unambiguous structural elucidations of, particularly, complex synthetic organic molecules and natural products. The application of distance restraints derived from pure-shift ROE integrals in isotropic medium along with the orientational restraints: heteronuclear RDCs, measured in appropriate orienting media, may further enhance the accuracy of determinations of conformations/configurations of complex molecules.

VII.5. References

[1] A. J. Shaka, J. Keeler and R. Freeman, Separation of chemical shifts and spin coupling in proton NMR. Elimination of dispersion signals from two-dimensional spectra, J. Magn. Reson, 56 (1984) 294 – 313.

[2] W. P. Aue, J. Karhan and R. R. Ernst, Homonuclear broadband decoupling and two dimensional J-resolved NMR spectroscopy, J. Chem. Phys, 64 (1976) 4226 – 4227.

[3] Ad. Bax, A. F. Mehlkopf and J. Smidt, Homonuclear broadband-decoupled absorption spectra, with linewidths which are independent of the transverse relaxation rate, J. Magn. Reson, 35 (1979) 167 –169.

[4] Ad. Bax and R. Freeman, Investigation of Complex Networks of Spin-Spin Coupling By Two- Dimensional NMR, J. Magn. Reson, 44 (1981) 542-561..

[5] O. W. Soerensen, C. Griesinger and R. R. Ernst, Time reversal of the evolution under scalar spin-spin interactions in NMR. Application for .omega.1 decoupling in two-dimensional NOE spectroscopy, J. Am. Chem. Soc, 107 (1985) 7778-7779.

[6] R. Bruschweiler, C Griesinger, O.W Sørensen and R.R Ernst, Combined use of hard and soft pulses for ω_1 decoupling in two-dimensional NMR spectroscopy, J. Magn. Reson, 78 (1988) 178-185.

[7] M. A. McCoy and L. Mueller, Selective shaped pulse decoupling in NMR: homonuclear [carbon-13] carbonyl decoupling, J. Am. Chem. Soc, 114 (1992) 2108-2112.

[8] M. Woodley and R. Freeman, Elimination of spin–spin splittings from high resolution proton NMR spectra, J. Magn. Reson, 111 (1994) 225–228.

[9] A. Hammarstrom and G. Otting, Improved Spectral Resolution in 'H NMR Spectroscopy by Homonuclear Semiselective Shaped Pulse Decoupling during Acquisition, J. Am. Chem. Soc, 116 (1994) 8847-8848.

[10] J. Nuzillard, Time-Reversal of NMR Signals by Linear Prediction. Application to Phase-Sensitive Homonuclear J-Resolved Spectroscopy, J. Magn. Reson, 118 (1996) 132 – 135.

[11] S. Simova, H. Sengstschmid and R. Freeman, Proton Chemical-Shift Spectra, J. Magn. Reson,124 (1997) 104-121.

[12] K. Zangger and H. Sterk, Homonuclear broadband-decoupled NMR spectra, J. Magn. Reson, 124 (1997) 486-489.

[13] J.C. Cobas and M. Martin-Pastor, A homodecoupled diffusion experiment for the analysis of complex mixtures by NMR, J. Magn. Reson, 171 (2004) 20–24.

[14] J.A. Aguilar, S. Faulkner, M. Nilsson and G.A. Morris, Pure Shift 1H NMR: A Resolution of the Resolution Problem?, Angew. Chem. Int. Ed, 49 (2010) 3901-3903.

[15] G.A. Morris, J.A. Aguilar, R. Evans, S. Haiber and M. Nilsson, True Chemical Shift Correlation Maps: A TOCSY Experiment with Pure Shifts in Both Dimensions, J. Am. Chem. Soc, 132 (2010) 12770-12772.

[16] J.A. Aguilar, A.A. Colbourne, J. Cassani, M. Nilsson and G.A. Morris, Decoupling Two-Dimensional NMR Spectroscopy in Both Dimensions: Pure Shift NOESY and COSY, Angew. Chem. Int. Ed, 51 (2012) 6460-6463.

[17] S. Islam, J. A. Aguilar, M. W. Powner, M. Nilsson, G. A. Morris and J. D. Sutherland, Detection of Potential TNA and RNA Nucleoside Precursors in a Prebiotic Mixture by Pure Shift Diffusion-Ordered NMR Spectroscopy, Chem. Eur. J, 19 (2013) 4586 – 4595.

[18] M. Nilsson and G. A. Morris, Pure shift proton DOSY: diffusion-ordered 1H spectra without multiplet structure, Chem. Comm, (2007) 933–935.

[19] J. J. Koivisto, Zero-quantum filtered pure shift TOCSY, Chem. Comm, 49 (2013) 96-98.

[20] J.R. Garbow, D.P. Weitekamp and A. Pines, Bilinear rotation decoupling of homonuclear scalar interactions, Chem. Phys. Lett, 93 (1982) 504–509.

[21] J.A. Aguilar, M. Nilsson and G.A. Morris, Simple Proton Spectra from Complex Spin Systems: Pure Shift NMR Spectroscopy Using BIRD, Angew. Chem. Int. Ed, 50 (2011) 9716-9717.

[22] A. Lupulescu, G.L. Olsen and L. Frydman, Toward single-shot pure-shift solution 1H NMR by trains of BIRD-based homonuclear decoupling. J. Magn. Reson. 218 (2012) 141-146.

[23] P. Sakhaii, B. Haase and W. Bermel, Experimental access to HSQC spectra decoupled in all frequency dimensions, J. Magn. Reson, 199 (2009) 192–198.

[24] L. Paudel, R.W. Adams, P. Király, J.A. Aguilar, M. Foroozandeh, M.J. Cliff, M. Nilsson, P. Sándor, J.P. Waltho and G.A. Morris, Simultaneously Enhancing Spectral

Resolution and Sensitivity in Heteronuclear Correlation NMR Spectroscopy, Angew. Chem. Int. Ed, 52 (2013) 1-5.

[25] I. Timári, L. Kaltschnee, A. Kolmer, R. W. Adams, M. Nilsson, C. M. Thiele, G. A. Morris and K. E. Kövér, Accurate determination of one-bond heteronuclear coupling constants with “pure shift” broadband proton-decoupled CLIP/CLAP-HSQC experiments, J. Magn. Reson, 239 (2013) 130-138.

[26] T. Reinsperger and B. Luy, Homonuclear BIRD-Decoupled Spectra for Measuring One-Bond Couplings with Highest Resolution: CLIP/CLAP-RESET and Constant-Time-CLIP/CLAP-RESET, J. Magn. Reson, 239 (2013) 110-120.

[27] A. J. Pell, R. A. E. Edden and J. Keeler, Broadband proton-decoupled proton spectra, Magn. Reson. Chem, 45 (2007) 296–316.

[28] A. J. Pell and J. Keeler, Two-dimensional J-spectra with absorption-mode lineshapes, J. Magn. Reson, 189 (2007) 293–299.

[29] B. Luy, Adiabatic z-filtered J-spectroscopy for absorptive homonuclear decoupled spectra, J. Magn. Reson, 201 (2009) 18–24.

[30] N.H. Meyer and K. Zangger, Simplifying proton NMR spectra by instant Homonuclear broadband decoupling, Angew. Chem. Int. Ed, 52 (2013) 7143-7146.

[31] P. Sakhaii, B. Haase, W. Bermel, R. Kerssebaum, G.E. Wagner and K. Zangger, Broadband homodecoupled NMR spectroscopy with enhanced sensitivity, J. Magn. Reson, 233 (2013) 92-95.

[32] L. Castanar, P. Nolis, A. Virgili and T. Parella, Full Sensitivity and Enhanced Resolution in Homodecoupled Band-Selective NMR Experiments, Chem. Eur. J, 19 (2013) 17283-17286.

[33] L. Castanar, J. Saurí, P. Nolis, A. Virgili and T. Parella, Implementing homo- and heterodecoupling in region-selective HSQMBC experiments, J. Magn. Reson, 238 (2013) 63-69.

[34] H. Geen and R. Freeman, Band-selective radiofrequency pulses, J. Magn. Reson, 93 (1991) 93 – 141.

[35] J. Ying, J. Roche and Ad Bax, Homonuclear decoupling for enhancing resolution and sensitivity in NOE and RDC measurements of peptides and proteins, J. Magn. Reson, (2013) http://dx.doi.org/10.1016/j.jmr.2013.11.006.

[36] T. Hwang and A. J. Shaka, Cross Relaxation without TOCSY: Transverse Rotating-Frame Overhauser Effect Spectroscopy, J. Am. Chem. Soc, 114 (1992) 3157–3159.

[37] J. Schleucher, J. Quant, S.J. Glaser and C. Griesinger, A Theorem Relating Cross-Relaxation and Hartmann-Hahn Transfer in Multiple-Pulse Sequences. Optimal Suppression of TOCSY Transfer in ROESY, J. Magn. Reson, 112 (1995) 144-151.

[38] C. M.Thiele, K. Petzold and J Schleucher, EASY ROESY: Reliable Cross-Peak Integration in Adiabatic Symmetrized ROESY, Chem. Eur. J, 15 (2009) 585 – 588.

[39] J. R. Everett and J. W. Tyler, An Analysis of the 1H and I3C N.m.r. Spectra of Erythromycin A using dimensional Methods, J. Chem. Soc., Perkin Trans, 1 (1985) 2599-2603.

[40] B. Jagadeesh, A. Prabhakar, G. D. Sarma, S. Chandrasekhar, G. Chandrashekar, M. S. Reddy and B. Jagannadh, Formation of left-handed helices in hybrid peptide oligomers with cis β-sugar amino acid and L-Ala as building blocks, Chem. Comm, (2007) 371–373.

[41] D. H. Appella, L. A. Christianson, D. Klein, D. R. Powell, X. Huang, J. J. Barchi and S. H. Gellman, Residue-Based Control of Helix Shape in β-Peptide Oligomers, Nature, 387 (1997) 381–384.

[42] W. S. Horne, L. M. Johnson, T. J. Ketas, P. J. Klasse, M. Lu, J. P. Moore and S. H. Gellman, Structural and biological mimicry of protein surface recognition by α/β-peptide foldamers, PNAS, 106 (2009) 14751–14756.

[43] L. Castanar, M. Perez-Trujillo, P. Nolis, E. Monteagudo, A. Virgili and T. Parella, Chem. Phys. Chem. (2014), DOI: 10.1002/cphc.201301130.

Chapter-VIII

Spectral simplifications in solution-state NMR

Real-time pure-shift adiabatic z-filtered spin-echo and constant time in-phase COSY

VIII.1. Introduction

As discussed in chapter-vii, the inherent rich structural information in ^{1}H NMR spectra is often obscured due to scalar multiplicity spread over the limited chemical shift range. The very recent methodological advances in homodecoupling, particularly the real-time pure-shift methods that effectively collapse the scalar multiplets to singlets, have added new dimension to the NMR spectroscopy. [1, 2] While the majority of real-time pure-shift methods reported so far by various research groups address the through-bond correlations with enhanced sensitivity, the chapter-vii provides through-space correlations: pure-shift ROESY with HOBB as well as HOBS decoupling. In the light of these developments, there is an immense scope to extend these real-time pure-shift homodecoupling strategies to the other basic/routine pulse schemes to enhance the capabilities of structural elucidation of complex organic molecules. The present chapter brings out real-time pure-shift 2D adiabatic z-filtered spin-echo and constant time in-phase COSY for organic molecules.

Spin-echo based experiments are of fundamental importance in NMR spectroscopy: for example, (i) they are widely used to refocus chemical shift information along the indirect dimension (ii) for suppressing inhomogeneous line-broadening and undesirable protein backgrounds in the analysis of metabolite samples.[3] Conventional 2D spin-echo (*J*-spectra) facilitates the observation of scalar couplings along the indirect dimensions, but suffers from poor resolution along the direct dimensions due to the conversion of phase twisted dispersive line shapes to amplitude mode lines. Many 2D spin echo approaches for measuring the scalar couplings have been reported,[4-8] which involve resolution enhancement either by mathematical manipulations or special type of spectral processing/reconstruction, of the data. However, they exhibit artefacts at the feet of the spectra and may cause significant distortions in the signal intensity and / or suffer from poor sensitivity.

Recently, adiabatic z-filter spin-echo has been reported [8] for collapsing the multiplets, which involves processing the data by symmetry based pattern reconstruction algorithms. This approach is useful to generate fully homodecoupled spectra even in the presence of very strong couplings. Conversely, it is not helpful for scalar coupling measurements.

In section-A, the pulse sequence that is a hybrid of both two-dimensional adiabatic z-filtered spin-echo[8] and the real-time ZS decoupling block[1]: i.e., homonuclear broadband decoupled z-filtered spin echo (HOBBZFSE), has been developed to accomplish pure absorptive mode *J*-spectra, which suppresses the scalar coupling multiplets along the direct dimensions, without the need of any special processing methods.

Similarly, homonuclear correlation spectroscopy (COSY) is an important experiment for routine small molecular characterizations. Several variants of COSY pulse sequences, DQF-COSY (Double Quantum Filtered COSY),[9] P.COSY (purged COSY),[10] P.E. COSY (primitive exclusive COSY) [11] and CT-COSY (constant time COSY),[12] which are useful for identification of chemical shifts and measurement of $^{n}J_{HH}$ scalar couplings from the anti-phase multiplets, are known. However, the anti-phase multiplets along the F1 and F2 dimensions reduce the cross-peak sensitivity, which is almost to zero for the broad multiplets. The improvised version of E.COSY (exclusive COSY) [13] pulse sequence is useful to monitor the spin-spin correlation as well as measurement of small $^{n}J_{HH}$ from the anti-phase multiplets with better sensitivity than that of DQF-COSY.

Some efforts to convert the anti-phase magnetization into in-phase magnetization in the COSY sequences are reported earlier. Amongst these, one of the promising approaches is based on the insertion of a 180^{o} refocusing pulses[14] such as in SUPER-COSY,[15] ISECR-COSY and DQF-ISECR-COSY (ISECR: in-phase cross-peaks).[16] In SUPER-COSY, the cross-peak signals are observed in-phase while the diagonal signals are observed in dispersive mode. However, in the case of ISECR-COSY, complete in-phase spectra are observed only for longer refocusing periods, which compromises with the sensitivity considerably. Further, the sensitivity of DQF-ISECR-COSY is even lower than the ISECR-COSY due to the double quantum filter.

Subsequently, an advanced version of CT-COSY with z-filter (IP-COSY) [17] has been reported, which generates fairly strong in-phase signals in both the dimensions and still retain some residual anti-phase components. It is shown in the section-B of this chapter, that the retained anti-phase components of COSY can be suppressed by using the versatile adiabatic zero quantum filter (z-filter) blocks, which relies on the spatial encoding z-gradient during the adiabatic inversion pulse followed by a homo-spoil gradient.[18] The real-time HOBB decoupling block discussed in chapter-vii can be conveniently added to the fully in-phase adiabatic z-filtered COSY NMR (HOBBIPZF-COSY) pulse sequences. This method allows to record pure-shift COSY NMR spectra in a short time, which is much more efficient compared to the known full-sensitive pure-shift nQF-CT- COSY sequences.[19]

Section-A

VIII.A.1. Results and discussion

VIII.A.1.1. *Real-time adiabatic z-filtered HOBB spin-echo pulse scheme (HOBBZFSE)*

Figure VIII.A.1 depicts the pulse sequence used for 2D real-time homodecoupled broadband adiabatic z-filtered spin-echo (HOBBZFSE), which operates in an instantaneous mode (no additional pseudo dimensions are required) and provide simplified spectra with enhanced resolution along with the coupling information. The initial part of the sequence uses the adiabatic chirp shaped inversion pulses during the spatial encoding gradient (G1), which, significantly averages out the zero-quantum magnetization. At the end of the adiabatic z- filtered spin-echo, the conventional 90^o pulse is replaced by HOBB decoupling block for accomplishing high resolution. Herein, the zero quantum filtered magnetization is subjected to slice-selective excitation by 90° EBURP (e) in the presence of gradient G2. The broadband decoupling is accomplished through interrupting the acquisition in ‘n’ number of intervals (~20) with a combination of hard 180° and soft 180°slice-selective Gaussian (g) refocusing pulses.

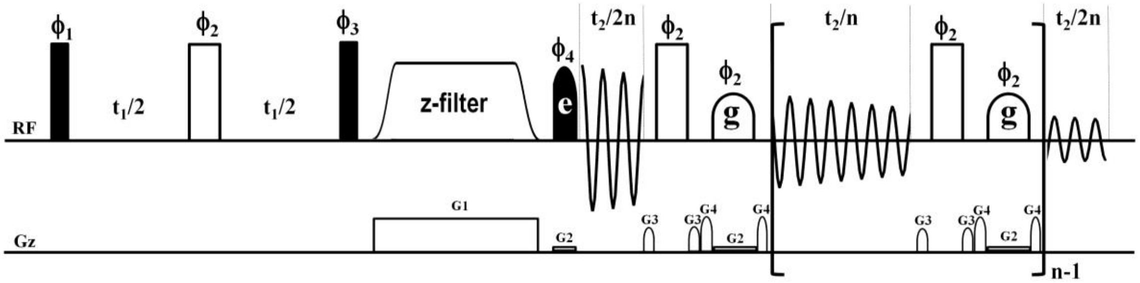

Figure VIII.A.1: *HOBBZFSE: Schematic diagram of real-time adiabatic z-filtered spin-echo pulse sequence with Homonuclear Broadband decoupling (HOBB) decoupling during the direct acquisition dimension. The filled and open rectangles represent the 90° and 180° pulses, respectively. The chirp shaped inversion pulse of 20 ms length is applied during the spatial encoding gradient (G1), which suppresses the zero quantum magnetization and yields only in-phase signals. The filled semi ellipsoid, '**e**', represents the 90° EBURP shape pulse (53.5 ms) applied during the slice- selective gradient that corresponds to 100 Hz bandwidth. The open semi ellipsoid, '**g**' represents the Gaussian shape, respectively. Herein, Gaussian 180° pulse of 8.8 ms is applied during slice-selection gradient. The number of dwelling points/sweep-width along the direct and indirect dimensions is equal to 4096/3.5 kHz and 128/50 Hz, respectively. The corresponding acquisition time is ~585 ms and the number of decoupling interruptions is equal to 20. Specific parameters for the present pulse sequence: phase cycling:* $\phi_1 = x$; $\phi_2 = x, -x$; $\phi_3 = -x$; $\phi_4 = x$; $\phi_{rec} = x$; *pulsed field gradients:* $G_{1,2,3,4}$ *= 11%, 1-2%, 11% and 11-31%, respectively at 53.5G/cm gradient strength in 1 ms duration. The pulse sequence is developed and experimentally verified on Bruker Avance-III 700 MHz NMR spectrometer.*

VIII.A.1.2. *2D Pure-shift HOBBZF-SE of Erythromycin-A*

The Figure VIII.A.2 compares the expanded regions of conventional adiabatic z-filtered spin- echo (~18 min/ 4 scans/ 128 increments) and HOBBZFSE (~21 min/ 4 scans/ 128 increments) for the Erythromycin-A. It is evident from the results that the crowded methyl region of the conventional spin-echo spectra (Figure. VIII.A.2a) is dramatically simplified in HOBBZFSE to clear singlets along the direct dimension and nice doublets are observed along the indirect dimension of HOBBZFSE (Figure. VIII.A.2b). Similarly, the H7ax, H14eq (Figure.VIII.A.2d) H3, H5" (Figure.VIII.A.2g) are clearly resolved in HOBBZFSE and allows to quantify the scalar coupling as shown in Figure. VIII.A.2h. All the HOBBZFSE spectra are free from multiplets and other artefacts due to zero-quantum magnetization, thereby facilitates to measure the scalar couplings in complex organic natural products as evidenced here.

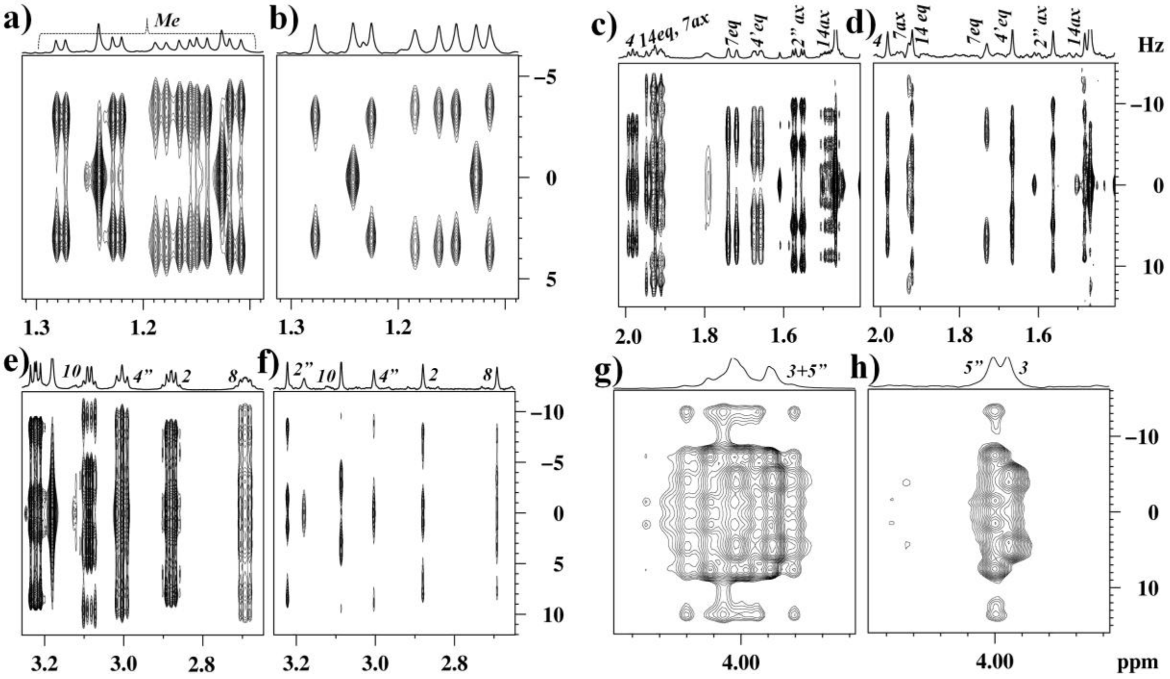

Figure VIII.A.2: *Comparison of expanded regions of conventional 2D spin-echo and 2D HOBBZFSE spectra of Erythromycin-A (50mM in $CDCl_3$ solvent), recorded at 700 MHz magnet. The expanded regions of conventional 2D spin-echo spectra are depicted in (a), (c), (e) and (g). The corresponding expanded HOBBZFSE spectra are shown in (b), (d), (f) and (h). Herein, one dimensional projections are externally added and the numbering in italic nearby projections depicts the protons of Erythromycin-A. The comparison clearly highlights that the conventional spin-echo shows fully overlapped spectral peaks due to J-multiplicity, whereas, this spectral complexity is greatly suppressed and significant enhancement in the resolution has been achieved for HOBBZFSE.*

VIII.A.2. Conclusions

In summary, a homodecoupled broadband adiabatic z-filtered spin-echo pulse sequence, HOBBZF-***SE*** is developed, which utilizes the real-time ZS-based decoupling scheme for direct acquisition dimension. Furthermore, the adiabatic chirp inversion pulses employed during the spatial encoded gradients effectively suppresses the undesired anti-phase magnetization and generates pure in-phase spin-echo spectra. These versatile pure-shift HOBBZFSE methods have been experimentally demonstrated for organic natural product Erythromycin-A, which resulted in dramatic improvement in resolution along the direct dimension, compared to the normal spin-echo. This method is particularly useful for molecules that exhibit extensive scalar coupling network, spread over the entire chemical shift range. The application of scalar couplings measured from the present method, may further simplify the determinations of conformations/configurations of small synthetic organic molecules/ natural products.

Section-B

VIII.B.1. Results and discussion

VIII.B.1.1. *Real-time adiabatic z-filtered HOBB COSY pulse scheme (HOBBIPZF-COSY)*

Figure VIII.B.1 depicts the pulse sequences used for recording the two-dimensional in-phase COSY spectra. The conventional IPCOSY sequence that employs only homo-spoil gradients and the IPZF-COSY that utilizes adiabatic z-filer along with the homo-spoil gradients are shown in Figures VIII.B.1a and 1b, respectively. The real-time Homonuclear broadband decoupled adiabatic z-filter COSY (HOBBIPZF-COSY) developed in the present work and is shown in Figure VIII.B.1c. The HOBBIPZF-COSY operates in an instantaneous mode (no additional pseudo dimensions are required) and provide simplified completely COSY spectra with enhanced resolution. The initial part of the IPZF-COSY sequence uses the constant time version during the t1 evolution, one more 180° pulse along the direct dimensions followed by adiabatic chirp shaped inversion pulses during the spatial encoding gradient (G4); which significantly removes the zero quantum-magnetization. At the end of the IPZF-COSY, the conventional 90^{o} pulse is replaced by HOBB decoupling block for accomplishing high resolution. Herein, the zero quantum filtered magnetization is subjected to slice-selective excitation by 90° EBURP (e) in the presence of gradient G5. The broadband decoupling is accomplished through interrupting the acquisition in ‘n’ number of intervals (~20) with a combination of hard 180° and soft 180°slice-selective Gaussian (g) refocusing pulses.

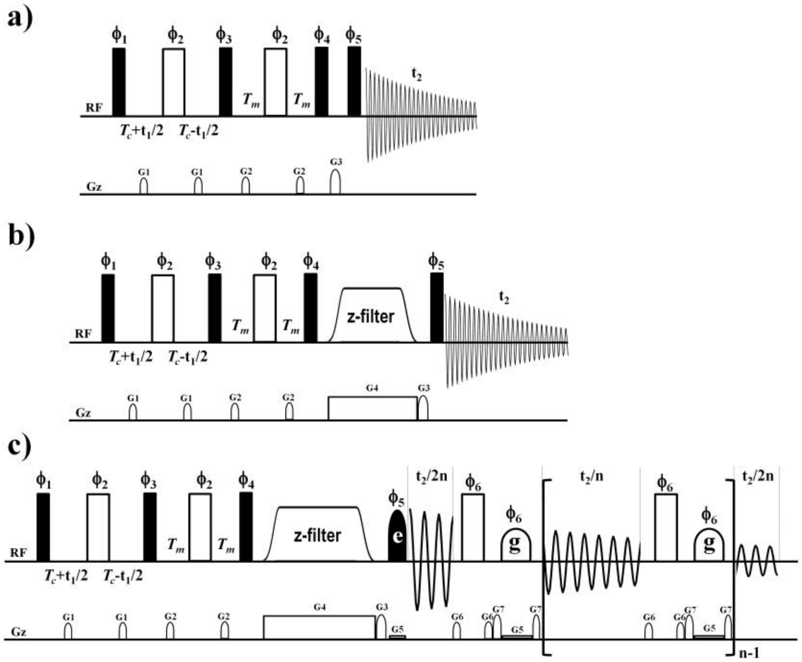

Figure VIII.B.1: *Schematic block diagram of z-filtered spin-echo pulse sequences (a) IP-COSY, (b) IPZF-COSY and (c) HOBBIPZF-COSY with Homonuclear Broadband decoupling (HOBB) decoupling during the direct acquisition dimension. The filled and open rectangles represent the 90° and 180° pulses, respectively. The chirp shaped inversion pulse of 20 ms length is applied during the spatial encoding gradient (G4), which suppresses the zero quantum magnetization and yields only in-phase signals. The filled semi ellipsoid, '**e**', represents the 90° EBURP shape pulse (53.5 ms) applied during the slice- selective gradient that corresponds to 100 Hz bandwidth. The open semi ellipsoid, '**g**' represents the Gaussian shape, respectively. Herein, Gaussian 180° pulse of 8.8 ms, is applied during slice-selection gradient. The refocusing periods Tc and Tm of 13 ms is used. The number of dwelling points/sweep-width along the direct dimensions are equal to 4096/3.5 kHz, 8192/7.0 kHz are used for Erythromycin-A and quinine+quinidine mixture, respectively. The corresponding acquisition time is ~585 ms. The number of decoupling interruptions **n** equals to 30 and 20 for quinine+quinidine and Erythromycin-A, respectively. Specific parameters for the present pulse sequence: phase cycling: ϕ_1 = x, x,_x,_x, y, y,_y,_y; ϕ_2 = x; ϕ_3 = y, y, y, y, x, x, x, x; ϕ_4 = x, x, x, x, y, y, y, y; ϕ_5= 4 (x,-x), 4 (y,-y); ϕ_6= x, -x; ϕ_{rec} = 2 (x,-x,-x, x), 2 (y,-y,-y, y); pulsed field gradients: $G_{1,2,3,4,5,6,7}$ = 11%, 11%, 31%, 11%, 1-2%, 11% and 11-31%, respectively at 53.5G/cm gradient strength in 1 ms duration.*

VIII.B.1.2. *Comparison of DQF-COSY, IP-COSY, IPZF-COSY and HOBBIPZF-COSY spectra of Erythromycin-A*

The Figure VIII.B.2 compares the expanded regions of DQF-COSY (~7 min / 4 scans/ 64 increments), IP-COSY (~7 min/ 4 scans/ 64 increments), IPZF-COSY (~7 min hours/ 4 scans/ 64 increments) and HOBBIPZF-COSY (~8 min/ 4 scans/ 64 increments) for the Erythromycin-A. All the peaks of DQF-COSY are appeared as anti-phase contours (Figure VIII.B.2a, Figure VIII.B.2e, and the traces of diagonal peaks and cross-peaks are taken at the dotted line and highlighted by dotted squares and circles, respectively). Similarly, residual anti-phase traces are retained for both diagonal and cross-peaks in IP-COSY spectrum (Figure VIII.B.2b and Figure VIII.B.2f). However, they are completely suppressed in IPZF-COSY spectrum, at the cost of bit sensitivity (Figure VIII.B.2c and Figure VIII.B.2g). Thus, IPZF-COSY allows measuring the required scalar coupling with better accuracy, when compared with the DQF-COSY and IP-COSY. On the other hand, in the HOBBIPZF-COSY, the scalar multiplets of all the peaks (Figure VIII.B.2d) are dramatically simplified to clear singlets along the direct dimension (Figure VIII.B.2h) and all the correlated cross-peaks are observed.

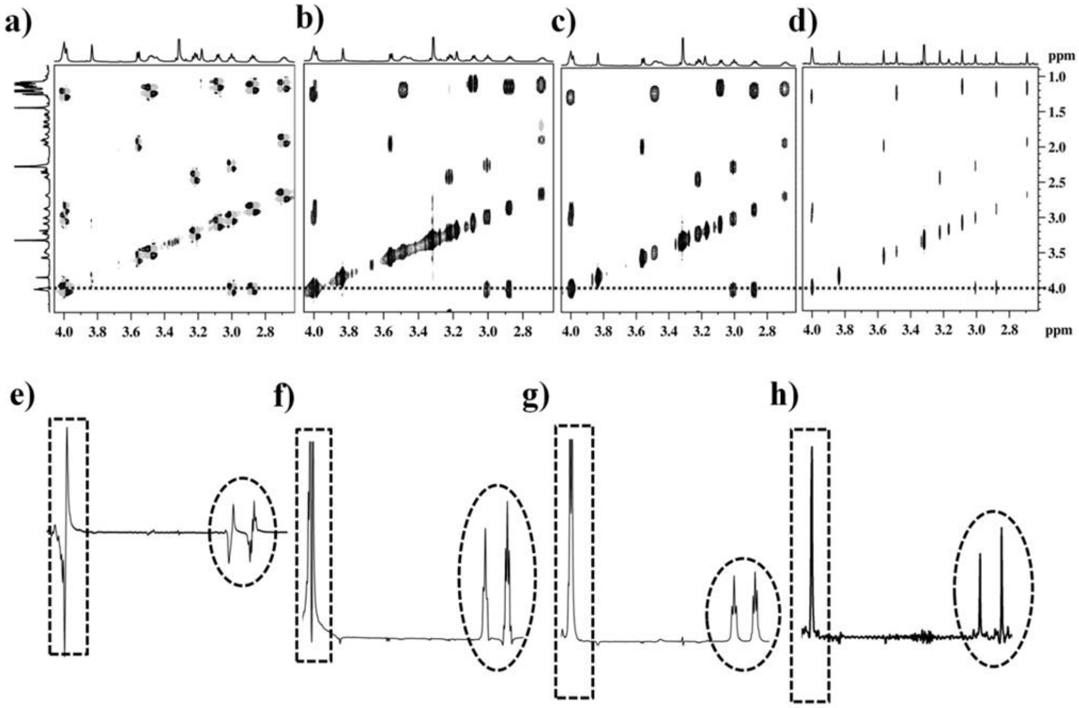

Figure VIII.B.2: *Comparison of expanded regions of DQF-COSY, IP-COSY, IPZF-COSY and HOBBIPZF-COSY of Erythromycin-A (50mM in $CDCl_3$ solvent), recorded at 700 MHz field strength are depicted in (a), (b), (c) and (d), respectively. The corresponding traces are shown in (e), (f), (g) and (h), respectively. The respective traces of diagonal and cross-peaks are taken at blue dotted line and highlighted by dotted square and dotted circles, respectively. The comparison clearly highlights that the spectral complexity is greatly suppressed and significant enhancement in the resolution has been achieved for HOBBIPZF-COSY.*

VIII.B.1.3. *2D Pure-shift HOBBIPZF-COSY of mixture of Quinine and Quinidine*

Figure VIII.B.3 compares the expanded regions of DQF-COSY, IP-COSY, IPZF-COSY and HOBBIPZF-COSY (~14 min/ 4 scans/ 128 increments) for the mixture of Quinine + Quinidine. The multiplets of all the peaks, (Figure VIII.B.3a, VIII.B.3b, and VIII.B.3c) are dramatically simplified to clear singlets along the direct dimension (Figure VIII.B.3d) and unambiguous correlated cross-peaks are observed in HOBBIPZF-COSY.

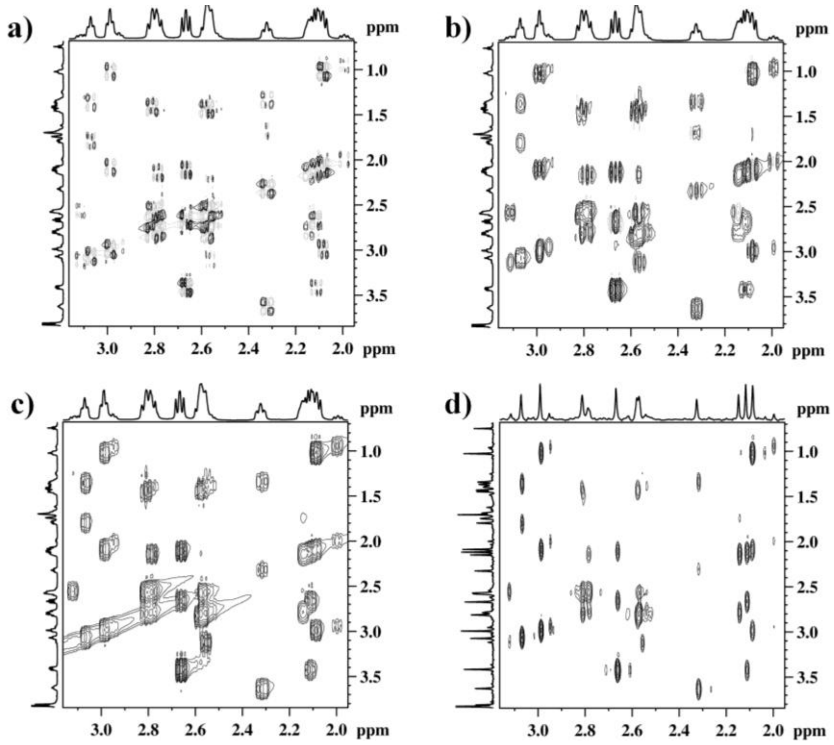

Figure.VIII.B.3: *Comparison of expanded regions of DQF-COSY, IP-COSY, IPZF-COSY and HOBBIPZF-COSY spectra of mixture of Quinine + Quinidine (30mM in $CDCl_3$ solvent), recorded at 700 MHz are depicted in (a), (b), (c) and (d), respectively. The comparison clearly highlights that the spectral complexity is greatly suppressed and significant enhancement in the resolution has been achieved for HOBBIPZF-COSY.*

VIII.B.2. Conclusions

In summary, an improved version of in-phase adiabatic z-filtered COSY (IPZF-COSY) pulse sequence and its real-time pure-shift homodecoupling (direct detection) analogue HOBBIPZF-COSY have been developed. In contrast to IP-COSY, the adiabatic chirp inversion pulses employed during the spatial encoded gradients effectively suppress the undesired anti-phase magnetization, thereby the cross-peaks of IPZF-COSY allows to measure the accurate scalar couplings. Furthermore, the versatile pure-shift HOBBIPZF-COSY methods have been experimentally demonstrated on Erythromycin-A and a mixture of Quinine + Quinidine, which resulted in dramatic improvement in resolution along the direct dimension, compared to the normal DQF-COSY, IP-COSY and IPZF-COSY. This method is particularly useful for molecules that exhibit extensive scalar coupling network, spread over the entire chemical shift range. These developments are expected open new possibilities for unambiguous structural characterizations of small and medium size complex organic molecules.

VIII.2. References

[1] N.H. Meyer and K. Zangger, Simplifying proton NMR spectra by instant Homonuclear broadband decoupling, Angew. Chem. Int. Ed, 52 (2013) 7143-7146.

[2] L. Castanar, P. Nolis, A. Virgili and T. Parella, Full Sensitivity and Enhanced Resolution in Homodecoupled Band-Selective NMR Experiments, Chem. Eur. J, 19 (2013) 17283-17286.

[3] O. Beckonert, H. C. Keun, T.M. D. Ebbels, J. Bundy, E. Holmes, J. C. Lindon and J. K. Nicholson, Metabolic profiling, metabolomic and metabonomic procedures for NMR spectroscopy of urine, plasma, serum and tissue extracts, Nature Protocols, 11 (2007) 2692-2703.

[4] Ad. Bax, R. Freeman and G. A. Morris, A Simple Method for Suppressing Dispersion-Mode Contributions in NMR Spectra: The “Pseudo Echo”, J. Magn. Reson, 43 (1981) 333-338.

[5] W.P. Aue, J. Karhan and R.R. Ernst, Homonuclear broad band decoupling and two-dimensional J-resolved NMR spectroscopy, J. Chem. Phys, 64 (1976) 4226–4227.

[6] S. Simova, H. Sengstschmid and R. Freeman, Proton Chemical-Shift Spectra, J. Magn. Reson, 124 (1997) 104-121.

[7] A. J. Pell, and J. Keeler, Two-dimensional J-spectra with absorption-mode lineshapes, J. Magn. Reson, 189 (2007) 293–299.

[8] B. Luy, Adiabatic z-filtered J-spectroscopy for absorptive homonuclear decoupled spectra, J. Magn. Reson, 201 (2009) 18–24.

[9] A. E. Derome and M. P. Williamson, Rapid-pulsing artefacts in double-quantum-filtered COSY. J. Magn. Reson. 88 (1980) 177-185.

[10] D. Marion and Ad. Bax, P.COSY, a sensitive alternative for double-quantum-filtered COSY, J. Magn. Reson, 80 (1988) 528-533.

[11] L. Mueller, P.E.COSY, a simple alternative to E.COSY, J. Magn. Reson, 72 (1987) 191-196.

[12] Z. Wu and Ad. Bax, Measurement of Homonuclear Proton Couplings Based on Cross-Peak Nulling in CT-COSY, J. Magn. Reson, 151 (2001) 242-252.

[13] C. Griesinger, O. W. Soerensen and R. R. Ernst, Two-dimensional correlation of connected NMR transitions, J. Am. Chem. Soc, 107 (1985) 6394–6396.

[14] O.W Sørensen, M. H Levitt and R. R Ernst, Uniform excitation of multiple-quantum coherence: Application to multiple quantum filtering, J. Magn. Reson, 55 (1983) 104-113.

[15] A. Kumar, R. V. Hosur and K. Chandrasekhar, A superior pulse scheme for homonuclear two-dimensional correlated spectroscopy, J. Magn. Reson, 60 (1984) 143-148.

[16] S. Talluri and H. A. Scheraga, COSY with in-phase cross peaks, J. Magn. Reson, 86 (1990) 1-10.

[17] Y. Xia, G. Legge, K. Jun, Y. Qi, H. Lee and X. Gao, IP-COSY, a totally in-phase and sensitive COSY experiment, Magn. Reson. Chem, 43 (2005) 372–379.

[18] M. J. Thrippleton and J. Keeler, Elimination of Zero-Quantum Interference in Two-Dimensional NMR Spectra, Angew. Chem. Int. Ed, 42 (2003) 3938 –3941.

[19] J. A. Aguilar, A. A. Colbourne, J. Cassani, M. Nilsson and G. A. Morris, Decoupling Two-Dimensional NMR Spectroscopy in Both Dimensions: Pure Shift NOESY and COSY, Angew. Chem. Int. Ed, 51 (2012) 6460-6463.

List of Publications

[1] A short and common stereoselective approach to 5/6, 6/6, 6/7 bicyclic aza sugar, B. Chandrasekhar, B. V. Rao, **K. Veera Mohana Rao** and B. Jagadeesh, *Tetra. Asym*, **2009**, 20, 1217

[2] Enantiopure cycloalkane fused tetrahydropyrans through domino Michael–ketalizations with organocatalysis, S. Chandrasekhar, K. Mallikarjun, G. P. K. Reddy, ***K. Veera Mohana Rao*** and B. Jagadeesh, *Chem.Comm.* **2009**, 4985.

[3] Intramolecular Thiopalladation of Thioanisole-Substituted Propargyl Imines: Synthesis of Benzothiophene-Based Palladacycles, P. R. Likhar, S. M. Salian, S. Roy, M. L. Kantam, B. Sridhar, ***K. Veera Mohana Rao*** and B. Jagadeesh, *Organometallics,* **2009**, 28, 3966.

[4] Uridate/pyridyl Pd(II) complexes: Phosphine-free high turnover catalysts for the Heck reaction of deactivated aryl bromides, P. Srinivas, K. Srinivas, P. R. Likhar, B. Sridhar, ***K. Veera Mohana Rao***, S. Bhargava, M. L. Kantam, *J. Organometallic. Chem*, **2011**, 696, 795.

[5] Short and efficient total synthesis of (+)-deoxoprosopinine *via* diastereoselective allylation of the *in situ* formed bicyclic *N*-acyl iminium ion with π-nucleophile, P. R. Krishna, P. Srinivas, B. K.Reddy, **K. Veera Mohana Rao** and B. Jagadeesh, *Syn. lettt,* **2012,** 23**,** 2814**.**

[6] Total Synthesis of a 6,6-Spiroketal Metabolite, Dinemasone A, C. R. Reddy, B. Srikanth, U. Dilipkumar, ***K. Veera Mohana Rao*** and B. Jagadeesh, *Eur. J. Org. Chem*, **2013**, 525.

[7] Monodispersed and Stable Nano Copper(0) from Copper- Aluminium Hydrotalcite: Importance in C=C Couplings of Deactivated Aryl Chlorides, R. Arundhathi, D. Damodara, ***K. Veera Mohana Rao***, M. L. Kantam and P. R. Likhar, *Adva. Synth & Catal,* **2013**, 355, 751.

[8] Unambiguous determination of conformation and relative configuration of a multiple stereo-centre molecule Rifamycin-S by using scaled residual dipolar couplings: A case study, ***K. Veera Mohana Rao***, R. Kavitha and B. Jagadeesh, *J. Mole. Stru*, **2013**, 1053, 122.

[9] Formation of periodic γ-turns in α/β-hybrid peptides: DFT and NMR experimental evidences, S. Chandrasekhar, ***K. Veera Mohana Rao***, M. Seenaiah, P. Naresh, A. S. Devi and B. Jagadeesh, *Chem. Asian. J*, **2014**, 9, 457.

[10] Real-time Homonuclear broadband and band-selective decoupled pure-shift ROESY, ***K. Veera Mohana Rao*** and B. Jagadeesh (in press, *Magnetic Resonance in Chemistry*)

[11] Hadamard encoded spin-echo modulations: scalar coupling measurements in uniformly labelled organic solids, ***K. Veera Mohana Rao*** and B. Jagadeesh (*Manuscript under preparation*)

List of presentations / participation in workshops and symposia

[1] Attended workshop on **“Homi Bhabha Centenary School on Relaxation in NMR and Related Aspects”**, Tata Institute of Fundamental Research, Mumbai, India, February-2009.

[2] Attended “**National Symposium on Magnetic Resonance**” at Indian Institute of chemical Technology, Hyderabad, India, February-2009.

[3] Attended “**National Symposium on Magnetic Resonance**” at CBMR, Lucknow, India, February-2010. (**Presented a poster**)

[4] Attended “**International Conference and Humboldt Kolleg**” at Indian Institute of chemical Technology, Hyderabad, India, September-2010. (**Presented a poster**)

[5] Attended workshop on **“Recent Advances in NMR Spectroscopy”**, Tata Institute of Fundamental Research, Hyderabad, India, December-2011.

[6] Attended “**National Symposium on Magnetic Resonance**” at IISC, Bangalore, India, February 2012. (**Oral presentation**)

[7] Attended “**ENC Symposium”** at Miami, USA, April, 2012. (**Presented a poster**)